UNIVERSITÉ DU LUXEMBOURG

PhD-FSTM-2021-002
The Faculty of Science, Technology and Medicine

DISSERTATION

Defence held on 14/01/2021 in Luxembourg

to obtain the degree of

DOCTEUR DE L'UNIVERSITÉ DU LUXEMBOURG

EN SCIENCE DE L'INGÉNIEUR

by

Valentino VIGNERI
Born on 5 November 1992 in Galatina, (Italy)

LOAD BEARING MECHANISMS OF HEADED STUD SHEAR CONNECTIONS IN PROFILED STEEL SHEETING TRANSVERSE TO THE BEAM

Dissertation defence committee

Prof. Dr.-Ing. Christoph Odenbreit, Dissertation Supervisor
Professor, University of Luxembourg, Faculty of Science, Technology and Medicine

Prof. Dr.-Ing Markus Schäfer, Chairman
Professor, University of Luxembourg, Faculty of Science, Technology and Medicine

Prof. Dr. Dennis Lam, Vice-chairman
Professor, University of Bradford, Faculty of Engineering and Informatics

Prof. Dr. Stephen Hicks
Professor, University of Warwick, School of Engineering

Dr. François Hanus
Head of Steligence Engineering, ArcelorMittal

Declaration of Authorship

I, Valentino VIGNERI, declare that this thesis titled, "Load Bearing Mechanisms of Headed Stud Shear Connections in Profiled Steel Sheeting Transverse to the Beam" and the work presented in it are my own. I confirm that:

- This work was done wholly or mainly while in candidature for a research degree at this University.
- Where any part of this thesis has previously been submitted for a degree or any other qualification at this University or any other institution, this has been clearly stated.
- Where I have consulted the published work of others, this is always clearly attributed.
- Where I have quoted from the work of others, the source is always given. With the exception of such quotations, this thesis is entirely my own work.
- I have acknowledged all main sources of help.
- Where the thesis is based on work done by myself jointly with others, I have made clear exactly what was done by others and what I have contributed myself.

Signed: _____

Date: _____

Acknowledgements

This thesis was realised during my time as a doctoral researcher at the ArcelorMittal Chair of Steel Construction, University of Luxembourg. The work presented was financially supported by Arcelormittal Global R&D Long Products Luxembourg in the scope of the research project ShearCON under the grant agreement UL-E-AGR-0022-10-C. I hereby express my gratitude to all the members of ArcelorMittal with whom I have had the pleasure to collaborate. Furthermore, I would like to acknowledge HPC for providing support to the numerical study presented. All the simulations were carried out using the HPC facilities of the University of Luxembourg, https://hpc.uni.lu (Varrette et al., 2014).

I am very grateful to my supervisor *Prof. Christoph Odenbreit*, whose advices, open-mindedness and constructive criticism guided me through this research work. Besides his professional support, I would like to thank him for being such a patient and kind person. It has been a great pleasure working with him.

Many thanks are due to my thesis supervision committee, *Prof. Dennis Lam* and *Dr. François Hanus*, for the valuable remarks provided during these years. Their expertise and knowledge have been of importance for accomplishing the results shown in this thesis. I have also had the great opportunity to work closely with *Prof. Stephen Hicks* and to discuss with *Prof. Markus Schäfer* in several occasions, especially in the context of the revision of EN 1994-1-1. Their help is highly appreciated.

I would like to thank all my colleagues for their friendly cooperation, in particular: *Andras Kozma*, *Alfredo Romero*, *Matthias Braun*, *Renata Obiala*, *Job Duarte da Costa*, *Maciej Chrzanowski*, *Yves Staudt*, *Ali Azim Azary*, *Jie Yang*, *Sebastian Latz* and *Steffen Betchel*. Thanks are extended to the laboratory staff who supported all the experimental tests conducted at the University of Luxembourg: *Marc Seil*, *Gilbert Klein*, *Claude Collé*, *Vincent Reis Adonis*, *Logan Freitas*, *Ed Weyer*, *Ken Adam*, *Cédric Bruyère*, *Ralph Reiter* and many others. Sincere thanks to *Kristian Bracaj* and *Lorik Rugova* who helped me in the preparation of the specimens.

Finally, I would like to express my immense gratitude to my mother *Miranda*, my father *Francesco* and my brother *Luigi* whose tireless support and encouragement during my entire life made it all possible. And, I would like to give special thanks to my beloved fiancé *Federica* for her invaluable help and understanding throughout my studies. I take the opportunity to thank my old friends *Marco* and *Simone* for being always supportive and open to all kinds of discussion. Amongst all the people I have met in the last years, a particular mention goes to *Khachatur*, *Seif* and *Surena* with whom I have enjoyed spending my lunch breaks and free time during my stay in Luxembourg.

Trier, December 2020

Valentino Vigneri

Abstract

Composite steel-concrete floor solutions have become popular in the design of buildings thanks to the efficient combination of high tensile strength and ductility of steel with reinforced concrete elements in compression. To ensure the longitudinal shear transfer between the downstand steel beam and the concrete slab in composite beams, headed stud shear connections are generally employed with profiled steel sheeting transverse to the supporting beam. However, whilst the steel deck enhances the bending resistance of the slab, the performance of the shear connection decreases. Based on the evaluation of a large database of push-out tests carried out in the last 40 years, several design models have been proposed in the last decades to predict the resistance of studs but none of them provides safe and reliable results. This is related to the fact that the proposed design equations do not always consider appropriately the actual resistance mechanisms activated in the shear connection. Also, as the failure modes are typically observed at high displacements, no information on the resistance components at lower displacements is given. Therefore, a deep investigation on the sequence of the load bearing resistance mechanisms of headed stud shear connections was performed with the support of an experimental campaign of 21 full scale push-out tests and numerical simulations. From the analysis of the experimental results, it was seen that all the samples experienced rib punching at low displacements followed by concrete pull-out failure or stud rupture. The influence of several structural parameters was also assessed by comparing different test series. It was found that 200 mm wide recess and slab depth have a minor impact on the performance of the connection. Instead, the addition of waveform rebars increased the resistance by 26% as well as the slip capacity whereas the different position of the wire mesh did not show an important influence. To investigate specifically the behaviour of the shear connections, the distribution of the compressive stresses in the rib and the plastic hinges developed in the stud connector were evaluated by means of a validated finite element model. From the outcomes of the experimental and numerical study, three main load bearing phases were distinguished. At low displacements (Phase 1), the concrete is not damaged until the typical cone crack initiates at the edge of the rib and the stud deforms in bending. Subsequently (Phase 2), while the cracks propagate, the internal forces in the rib redistribute and the resistance is governed by the bearing stresses of the concrete in front of the connector. At large displacements (Phase 3), the front side of the concrete rib is highly damaged whereas the tension stresses in the stud increases significantly due to pulling forces. For further slips, this can lead to concrete pull-out or stud rupture as confirmed by the experimental studies. These insights were taken as a basis for the development of three respective mechanical models: cantilever model, modified strut and tie model (MSTM), and strut and tie model (STM). Whilst the first considers the system as a cantilever beam, the other two reproduce the concrete as a system of compression struts and the steel sheeting was modelled as tie

elements. All the resistance functions were analytically derived in consideration of the experimental and numerical results in order to estimate the capacity of the shear connection at different displacements. As the STM focuses on the behaviour at large deformations, only the first two models were considered to predict the actual capacity of the shear connection. The design resistance of these two proposed models was finally calibrated according to the statistical procedure of EN 1990 (BSI, 2002).

Keywords: Composite beams, Shear connections, Headed studs, Push-out tests, Finite element modelling, Load bearing mechanisms, Analytical modelling, Statistical analysis, Design models

---

Contents

List of Figures

List of Tables

List of Abbreviations

3D	**3**-**D**imensional
ALLIE	**I**nternal **E**nergy output
ALLKE	**K**inetic **E**nergy output
B31	2-node linear **B**eam elements in the space
C3D8R	**8**-Node brick element with **R**educed integration
CDP	**C**oncrete **D**amaged **P**lasticity
CV	**C**oefficient of **V**ariation
CPO	**C**oncrete **P**ull-**O**ut
DoF	**D**egree **o**f **F**reedom
FE	**F**inite **E**lement
HPC	**H**igh-**P**erformance **C**omputing
LI	**L**oad **I**ntroduction
LVDT	**L**inear **V**ariable **D**ifferential **T**ransformer
MSTM	**M**odified **S**trut and **T**ie **M**odel
PDF	**P**robability **D**ensity **F**unction
RC	**R**einforced **C**oncrete
RP	**R**ib **P**unching
S4R	**4**-node quadrilateral **S**hell element with **R**educed integration
SR	**S**tud **R**upture
STM	**S**trut and **T**ie **M**odel
TL	**T**ransversal **L**oad

List of Symbols

Displacements and Rotations

s	Longitudinal slip of the shear connection
α	Rotation angle of the stud head
α_s	Inclination angle of the concrete slab
$\delta_{u,B2}$	Slip capacity according to EN 1994-1-1 B.2.5 (BSI, 2004b)
$\delta_{uk,B2}$	Characteristic slip capacity according to EN 1994-1-1 B.2.5 (BSI, 2004b)
ϕ	Inclination angle of the stud

Forces and Moments

C_i	Compressive force in the strut i
D_i	Tensile force in the tie element i
g_{rt}	Resistance function used as design model
$M_{\cdot}$	Bending moment at the section/node $\cdot$
M_y	Bending moment around the y axis
M_{pl}	Plastic bending resistance of the cross-section of the stud
$N_{\cdot}$	Axial force at the section/node $\cdot$
N_{pl}	Plastic resistance of the cross-section of the stud
P	Load per stud
P_1	Analytically predicted load per stud in phase 1
P_2	Analytically predicted load per stud in phase 2
P_3	Analytically predicted load per stud in phase 3
P_c	Load taken by the concrete cone in bending in phase 1
P_e	Experimental resistance of the stud
$P_{e,1}$	Maximum experimental resistance of the stud between 1 and 3 mm slip
$P_{e,2}$	Maximum experimental resistance of the stud between 3 and 10 mm slip
$P_{e,3}$	Maximum experimental resistance of the stud at ca. 25 mm slip
$P_{e,norm}$	Experimental resistance of the stud normalized on the concrete strength
$P_{Rd,\cdot}$	Proposed design resistance according to $\cdot$ model
$P_{Rk,B2}$	Estimated characteristic resistance according to EN 1994-1-1 B.2.5 (BSI, 2004b)
P_s	Load taken by the stud in bending in phase 1
T	Total force in the tie bars used in push-out tests
r_e	Experimental resistance value
$r_{t,\cdot}$	Theoretical resistance value according to $\cdot$ model

r_d	Design value of the resistance
r_k	Characteristic value of the resistance
r_n	Nominal value of the resistance
$V.$	Shear force at the section/node ·

GEOMETRY

A_{col}	Effective lateral surface area of the weld collar
$A_{col,nom}$	Nominal effective lateral surface area of the weld collar
A_{ce}	Effective area of the concrete cone according to Lloyd and Wright (1990)
A_{cem}	Mean effective area of the concrete cone according to Lloyd and Wright (1990)
A_s	Cross-sectional area of the stud
b_0	Effective width of the rib according to EN 1994-1-1 (BSI, 2004b)
b_{bot}	Bottom width of the rib of the profiled steel sheeting
$b_{bot,nom}$	Nominal bottom width of the rib of the profiled steel sheeting
b_{top}	Top width of the rib of the profiled steel sheeting
$b_{top,nom}$	Nominal top width of the rib of the profiled steel sheeting
c	Depth of the strut C_1
d_{col}	Diameter of the weld collar (ISO/TC44/SC10, 2017)
$d_{col,nom}$	Nominal diameter of the weld collar (ISO/TC44/SC10, 2017)
d	Diameter of the shank of the stud
d_m	Mean diameter of the shank of the stud
d_{nom}	Nominal diameter of the shank of the stud
e_f	Effective concrete cover in front of the stud according to Johnson and Yuan (1998)
e_k	Effective concrete cover in front of the stud according to Konrad (2011)
e_L	Longitudinal distance between the stud and the mid of the trough (+: Favourable position; -: Unfavourable position)
e_s	Effective concrete cover in front of the stud according to Johnson and Yuan (1998) for studs in staggered position
e_t	Transversal spacing between the studs in the trough
h_{col}	Height of the weld collar (ISO/TC44/SC10, 2017)
$h_{col,nom}$	Nominal height of the weld collar (ISO/TC44/SC10, 2017)
h_h	Height of the stud head
h_p	Height of the profiled steel sheeting
$h_{p,nom}$	Nominal height of the profiled steel sheeting
h_s	Distance from the upper plastic hinge to the base of the stud
h_{sc}	Length of the stud after welding
$h_{sc,meas}$	Measured length of the stud after welding
h_{scm}	Mean length of the stud after welding
$h_{sc,nom}$	Nominal length of the stud after welding

h_{slab}	Overall depth of the slab
l	Width of the strut C_1
n_r	Number of studs per rib
s_t	Longitudinal spacing between the studs in the trough according to Johnson and Yuan (1998)
t	Thickness of the profiled steel sheeting
t_{nom}	Nominal thickness of the profiled steel sheeting
w	Distance between the centroid of the connector and the edge of the trough at the rib-slab interface (on the favourable side)
w_c	Crack opening
$w_{c,crit}$	Critical value of the crack opening
W	Sectional modulus of the concrete cone failure surface
θ	Inclination angle of the concrete cone surface
θ_N	Angle for spreading the load from the stud in specimens without recess
θ_R	Angle for spreading the load from the stud in specimens with recess

MATERIALS

e	Eccentricity parameter that defines the rate at which the flow potential function (Simulia, 2014) approaches to the asymptote
E_c	Secant elastic modulus of concrete
E_{cm}	Mean secant elastic modulus of concrete
E_s	Elastic modulus of the stud material
E_{sm}	Mean elastic modulus of the stud material
f_{bc}	Equibiaxial compressive strength of concrete
f_c	Compressive cylinder strength of concrete
$f_{c,meas}$	Measured compressive cylinder strength of concrete
f_{ck}	Characteristic compressive cylinder strength of concrete
f_{cm}	Mean compressive cylinder strength of concrete
$f_{c,cube}$	Compressive cube strength of concrete
$f_{ck,cube}$	Characteristic compressive cube strength of concrete
$f_{cm,cube}$	Mean compressive cube strength of concrete
f_{ct}	Tensile strength of concrete
f_{ctm}	Mean tensile strength of concrete
f_{ctk}	Characteristic tensile strength of concrete
f_y	Yield strength of the material
f_{yp}	Yield strength of the sheeting material
f_{ypm}	Mean yield strength of the sheeting material
$f_{yp,nom}$	Nominal yield strength of the sheeting material
f_u	Ultimate tensile strength of the stud material
$f_{u,meas}$	Measured ultimate tensile strength of the stud material
f_{um}	Mean ultimate tensile strength of the stud material

$f_{u,nom}$	Nominal ultimate tensile strength of the stud material
G_f	Fracture energy
K_c	Ratio of the second stress invariant on the tensile meridian to that on the compressive meridian for any given value of p such that the maximum principal stress is negative (Simulia, 2014)
Ψ	Dilation angle of the concrete in the p-q plane

STATISTICAL PARAMETERS

b	Mean correction factor
D	Deviation from the mean
$k_{d,n}$	Design fractile factor
$k_{d,\infty}$	Design fractile factor for $n \to \infty$
k_n	Characteristic fractile factor
k_∞	Characteristic fractile factor for $n \to \infty$
n	Number of test results
s^2_Δ	Estimated value for the variance of Δ
V_δ	Estimator for the coefficient of variation of the error term δ
V_r	Coefficient of variation of the design model
V_{rt}	Coefficient of variation of the theoretical resistance r_t from uncertainties in the basic variables
$\underline{X}$	Array of the basic variables
$\underline{X}_m$	Array of the mean values of the basic variables
$\underline{X}_n$	Array of the nominal values of the basic variables
δ	Error term
δ_i	Observed error term for the test specimen i
Δ	Logarithm of the error term δ
Δ_i	Logarithm of the error term δ_i
$\overline{\Delta}$	Estimated value for the mean of Δ
γ_M	Partial safety factor for the resistance
γ^*_M	Corrected partial safety factor for the resistance
γ_V	Proposed partial safety factor for the resistance
μ	Mean value
ρ	Linear correlation coefficient

STRESSES AND STRAINS

p	Hydrostatic pressure stress
q	Von Mises equivalent stress
ε_c	Compressive strain
ε_{c0}	Compressive strain at the maximum stress
ε_c^{pl}	Plastic compressive strain
ε_s	Tensile strain of steel

ε_t	Tensile strain
ε_u	Ultimate strain
σ_c	Compressive stress
σ_{eff}	Effective stress of the concrete strut
σ_t	Tensile stress

OTHERS

c_w	Stiffness of the horizontal springs
d_c	Compressive damage parameter
d_t	Tensile damage parameter
N	Number of members
M	Mass scaling factor
n_s	Degree of statical indeterminacy
n_y	Degree of activation of the plastic hinges in the stud
r_i	Number of restrained degrees of freedom relative to the i^{th} joint

Alla mia Famiglia

Chapter 1

Introduction

1.1 General

Starting from the 1960s, composite steel-concrete structures have become a world-wide popular solution that exploits the benefits of structural steel and reinforced concrete elements. Steel-concrete members combine the compressive strength of concrete with high yield strength of steel resulting in a efficient system perfectly suitable for the design of multi-storey buildings. Furthermore, the concrete can provide fire protection if the steel elements are embedded as in the case of fully or partially encased composite beams. However, a typical composite steel-concrete beam consist of a downstand steel beam connected to a concrete slab which can be pre-cast (generally with hollow-core geometry) or cast in situ. In the latter case, the concrete slab can be solid or cast onto a profiled steel sheeting resulting in a composite slab. Modern steel-concrete industry favours the use of the profiled sheeting transverse to the supporting beams where the deck enhances the bending resistance of the slab.

The aforementioned configurations refer to secondary beam applications where the load is spread uniformly along the steel profile. To ensure the composite action of the steel beam and the slab, shear connections shall be adequately dimensioned. These elements aim to transfer the longitudinal shear force at the beam-slab interface along the length limiting the slip displacements. There are several types of shear connectors which can be employed while novel demountable connectors have been recently investigated in several research projects. However, headed studs directly welded to the steel beam top flange are the most used shear connectors in steel-concrete beams. Their good structural performance as well as the ease of installation ensure a cost-effective solution. In the current work, two typical steel-concrete beam configurations are firstly considered: steel beam with (i) solid reinforced concrete slab and (ii) with composite concrete slab using profiled steel sheeting transverse to the supporting beam. Generally, in both configurations, the headed stud shear connection exhibits sufficient slip capacity allowing for the use of plastic design with partial shear connection according to EN 1994-1-1 (BSI, 2004b): this represent a further reason behind the widespread use of these design solutions.

1.2 Motivation

Numerous experimental push-out tests have been carried out since 1950s to assess the performance of headed stud shear connections. In parallel, several analytical and empirical approaches have been proposed to predict the load bearing resistance of studs in solid slabs and in profiled steel sheeting. However, design rules for headed

studs in profiled decks are not always appropriate when novel profiled sheeting are employed. Based on the evaluation of push-out tests carried out in the last 40 years, recent studies found out that current EN 1994-1-1 rules overestimate the design resistance of headed stud shear connectors placed in open trough steel sheeting, especially in case of slender troughs (Lawson et al., 2017). The aim of these geometries is to optimize the design of composite steel-concrete floors by reducing the self-weight of the slab and increasing the bending resistance of the slab. Currently, the analytical expressions in EN 1994-1-1 for the strength of headed studs is based on the calibration of the resistance in solid slabs by including an empirical reduction factor k_t, as explained in Section 2.4. Therefore, they do not account for the real failure modes occurring when the headed studs are placed in profiled steel sheeting. This would explain the reason behind the inadequacy of current EN 1994-1-1 rules for the calculation of the design resistance of headed stud shear connections in open trough steel sheeting. Further studies investigated the failure mechanisms of studs in steel sheeting and they provided some alternative mechanical models. However, failure modes are typically observed after testing at relatively high displacements. In most of the cases, they do not give a comprehensive picture of the different resistance components involved due to the complex interaction between stud, concrete and steel sheeting. For this reason, a deep investigation on the sequence of the different load bearing mechanisms of headed stud shear connections in profiled steel sheeting was undertaken in this thesis with the support of experimental, numerical and analytical results.

1.3 Objectives

As discussed in the previous section, it is acknowledged that the resistance of headed stud shear connectors according to current rules of EN 1994-1-1 (BSI, 2004b) does not conservatively predict the experimental resistance of shear connections using open trough steel sheeting. To overcome the issue related to this unsatisfactory prediction of the resistance, it is of crucial importance to have a deep understanding of the actual bearing mechanisms activated in the shear connection. It is therefore vital to identify the resistance components that govern the capacity of the shear connection throughout the test. Furthermore, the analytical characterisation of the connection system is necessary to establish reliable mechanical models. On that basis, more optimized analytical equations for predicting the design resistance of studs can be derived while supporting the development of novel and efficient steel sheeting products in the future.

1.4 Outline

The structure of this thesis is given in Figure 1.1. Chapter 1 consists in a general introduction on headed stud shear connections including the description of the issues related to the use of novel types of profiled steel sheeting transverse to the supporting beam. The relevant past research studies and design models are provided and discussed in Chapter 2 while the methodology followed in this work is defined in Chapter 3. Chapter 4 presents the conducted experimental study on headed studs in open trough profiled sheeting where several design parameters are investigated by performing a total of 21 push-out tests. The experimentally obtained results were used for the validation of a non linear finite element (FE) model described in Chapter 5 in order to investigate the bending behaviour of the stud as well as the stresses and

damage in the concrete. Based on the experimental and numerical outcomes, three main phases characterizing the load bearing behaviour of the shear connection were identified and discussed in Chapter 6. The understanding of the load bearing mechanisms was translated into ad-hoc mechanical models in Chapter 7. The respective analytical equations were derived and two design proposals were statistically calibrated in Chapter 8 in accordance with the standard procedure of EN 1990 (BSI, 2002) . Finally, Chapter 9 summarizes the key points of the thesis and it provides outlook on future research.

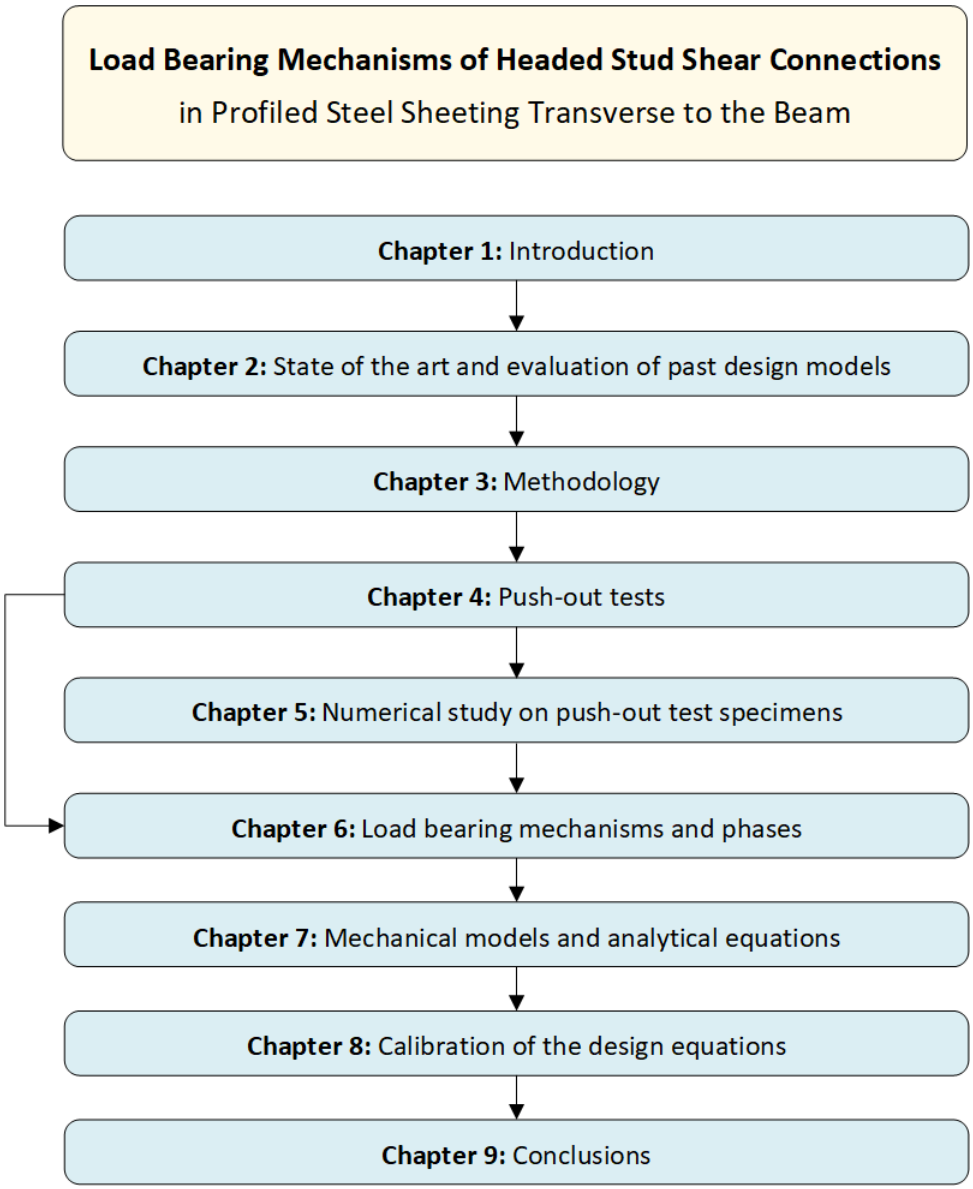

FIGURE 1.1: Outline of the thesis

Chapter 2

State of the art and evaluation of past design models

2.1 Shear connectors in composite beams

As already mentioned, composite steel-concrete elements have been widely used, especially in building and bridge applications. In case of composite beams, appropriate shear connectors are adopted to ensure the transfer of the longitudinal shear along the span. Notwithstanding the variety of shear connectors, headed studs (Figure 2.1) represent the most common design solution adopted in the last decades. One of the reasons lie in the installation process that is quick and easy. The studs are automatically welded directly to the top of the steel flange by a welding gun and they can be used in combination with profiled steel sheeting (composite slab). In this case, the studs can be placed in pre-punched holes of the steel sheeting or they can be through-deck welded. Additionally, they do not obstruct the placement of the reinforcement in the concrete slab and they preserve the shear resistance in all the directions.

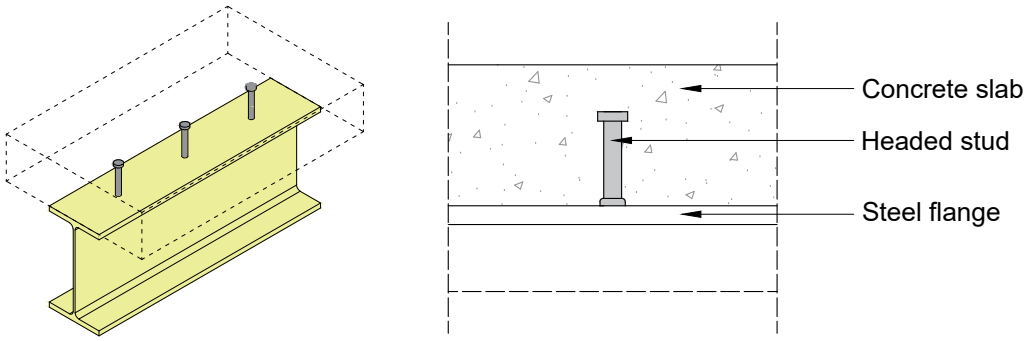

FIGURE 2.1: Isometric view and detail of headed stud connectors

Whilst the mechanical performance of headed studs have been investigated since 1950s, experimental studies and design recommendations for bolted shear connectors, shown in Figure 2.2, were first published by Dallam (1968) to support their use. Nevertheless, bolts are not frequently used in steel-concrete beams as shear connections compared to headed studs. However, an advantage of these connectors consist in the lack of weld that reduces the issues related to fatigue. Although the mechanical performance of bolted shear connectors is generally comparable with headed stud configurations (Pavlović et al., 2013), there are several types of bolted

connections which have been investigated, such as: friction grip, single or double embedded nut with or without preloading.

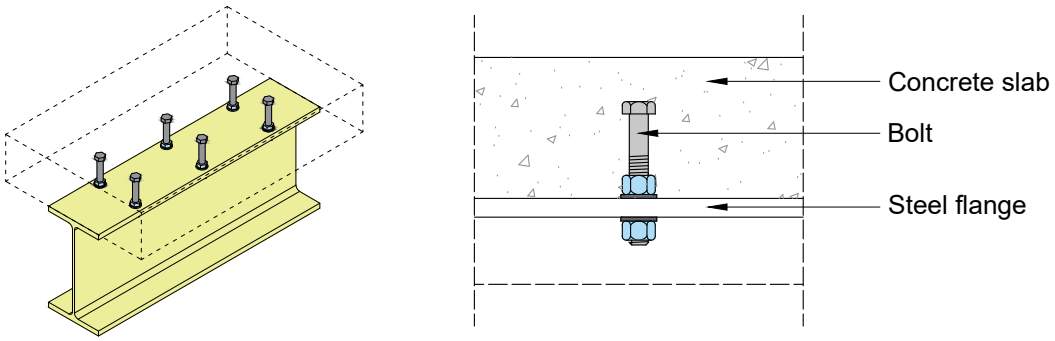

FIGURE 2.2: Isometric view and detail of bolted shear connectors

Another type of shear connector is the so called "Channel connector". It consists of a C-shape steel profile that is welded directly on the top flange of the steel beam, see Figure 2.3. The first experimental studies were presented by Viest (1951) and Slutter and Driscoll (1963) to check their performance in steel-concrete beam applications. In general, these connectors have relatively high resistance that can potentially replace groups of headed studs (Maleki and Bagheri, 2008). To support their use in practice, ad-hoc analytical equations for calculating their shear capacity in solid slabs were recently included in Canadian (NRC, 2005) and American (AISC, 2005) design codes. Further to the literature available, most of the current research on channel connectors is heading towards the use of these profiles in combination with high strength concrete in order to obtain a more effective design solution.

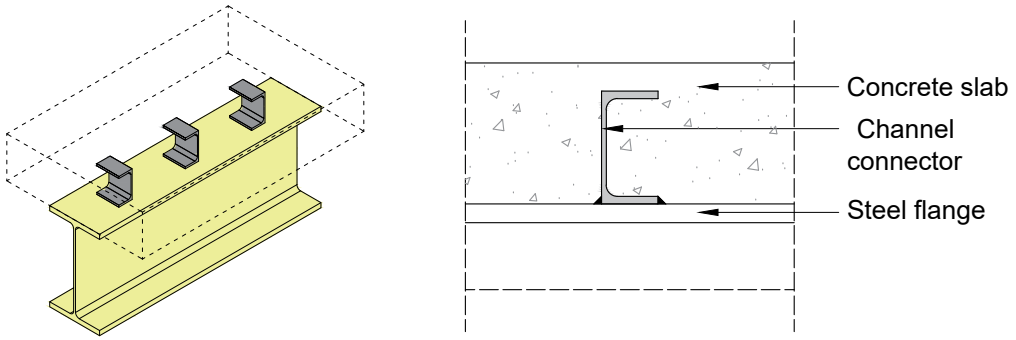

FIGURE 2.3: Isometric view and detail of channel connectors

In Figure 2.4, it is shown a shear connector which is formed by a flat holed steel plate welded on the top flange of the beam along its longitudinal direction. These types of connectors are called "Perfobond". They were firstly developed in the 1980s (Zellner, 1988) with the aim of creating a connection system easy to install with high fatigue strength as an alternative to typical headed studs. Additionally, the concrete dowels and the transverse reinforcement bars normally placed through the rib holes ensure high longitudinal shear capacity, the transfer of uplift forces (Leonhardt et al., 1987) and a ductile behaviour. The robust research studies carried out in the last years have supported the increasing use of these connectors, especially in bridge applications.

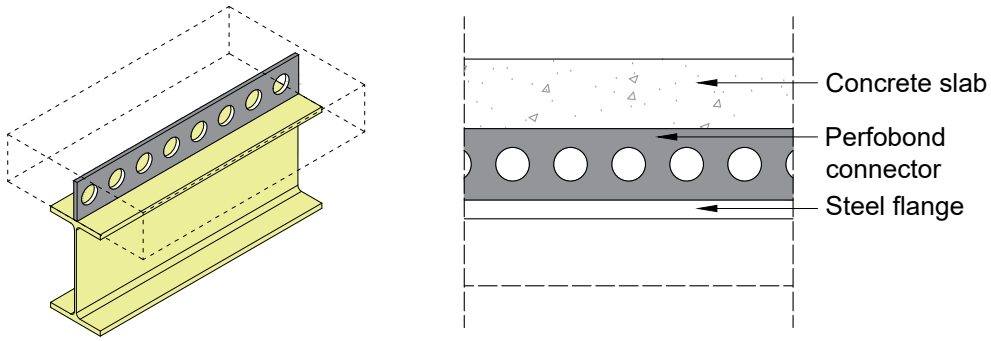

FIGURE 2.4: Isometric view and detail of perfobond shear connectors

2.2 Headed stud shear connections

2.2.1 Overview

Notwithstanding all the possible types of shear connectors available on the market, headed studs represent the traditional way to ensure the composite action between the steel beam and the concrete slab in building applications. As already mentioned, they are typically employed along with reinforced concrete slabs (Figure 2.5a) or composite slabs with profiled steel sheeting transverse to the beam (Figure 2.5b).

This particular orientation of the profiled decks improves significantly the bending resistance of the slab while reducing the structural performance of the shear connection along the longitudinal direction of the beam. The load bearing capacity of studs in transverse profiled sheeting varies between 40% and 70% of the respective capacity in solid slabs whereas the ductility increases. However, headed studs in profiled sheeting are sensitive to a wide range of parameters, such as: geometry of the trough, length of the connector, welding procedure, position of the stud in the trough, number of studs per rib. For this reason, after describing the most common testing procedures in Section 2.2.2, the available experimental studies are considered separately in Section 2.2.3 and Section 2.2.4 for studs in solid slabs and in transverse profiled sheeting, separately. In parallel with the experimental studies, more and more refined models have been developed over the years to predict the shear resistance of stud and to support the development of novel products. In order to assess the suitability of the proposed design models, statistical analyses were performed and the results are discussed in Section 2.3 for solid slabs and in Section 2.4 for composite slabs, respectively.

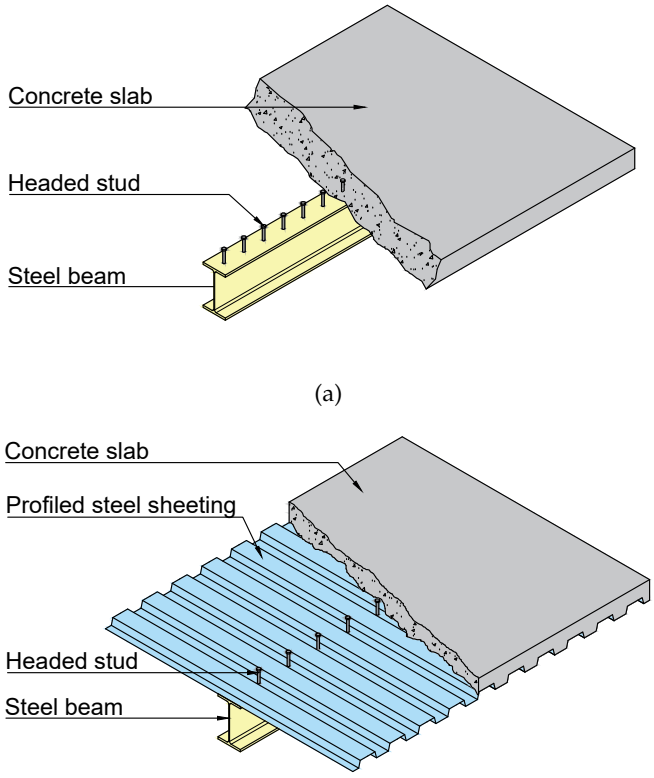

FIGURE 2.5: Composite beam with headed studs in (a) solid and in (b) composite slab with profiled steel sheeting transverse to the beam

2.2.2 Testing procedure

Two main experimental approaches can be followed to assess the mechanical performance of headed studs (and shear connections in general): (i) full-scale beam tests or (ii) push-out tests. Whilst the beam tests can potentially reproduce the actual structural conditions of the entire composite beam in the building, the push-out test represents a more convenient solution. First of all, a push test specimen is easy to manufacture and it does not require special measurement tools: the shear load and the corresponding slip of each connector can be directly computed from the applied push force and linear variable differential transformer (LVDT) sensors. To ease the visualization of the sample, the standard push-out test specimen recommended by EN 1994-1-1 (BSI, 2004b) for studs in solid slabs is given in Figure 2.6 including the distribution of the forces suggested by Roik and Hanswille (1987).

Conversely, in beam tests, extensive strain and slip measurements are needed to account for the distribution of the slip along the span. Despite the advantages of push-out tests, the load bearing behaviour of shear connections observed in these tests may differ from the respective beam. For example, Hicks (2009) showed that the performance of headed studs in profiled sheeting observed in push test specimens (with normal load applied on the slabs) were lower than the companion beam tests with a resistance reduction of ca. 30% and a lower slip capacity. This difference is the consequence of the lack of standardized push test specimens. Although it seems that push-out tests provide conservative estimation of the performance of the connectors, there are various setup parameters that influence the behaviour of stud connectors

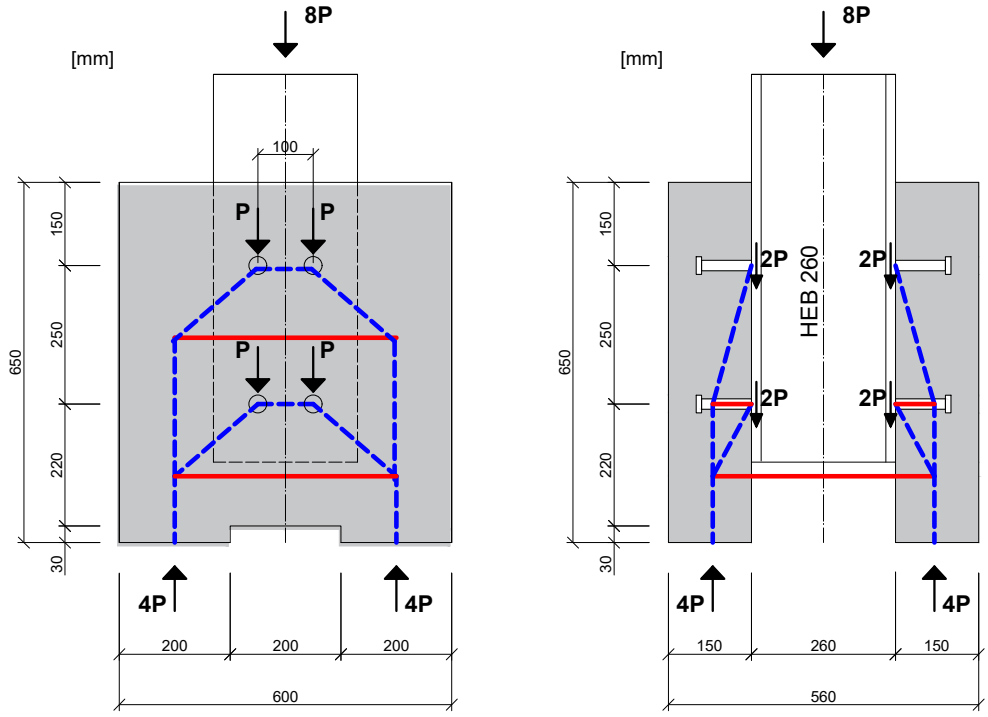

FIGURE 2.6: Standard push-out test specimen recommended by EN 1994-1-1 (BSI, 2004b) including the distribution of the forces according to Roik and Hanswille (1987)

in push tests. Sliding bearings at the base may underestimate the capacity of the connector (Hicks and McConnel, 1997) whereas stiff lateral restrains increases their performance (Döinghaus, 2001; Ernst, 2006). Another parameter is the transverse load that would replace the vertical load acting the real composite beam. As pointed out by Rambo-Roddenberry (2002) and Nellinger et al. (2017), the application of transversal load (normal to the slab) on push-out test specimens with profiled steel sheeting enhances the performance leading to a relative increase of ca. 10%-30% in resistance. To ensure the consistency of the push-out test results, an alternative push test rig allowing for a controlled application of transversal load was also calibrated against beams tests (Hicks and Smith, 2014). However, it is still under discussion whether this load would be safely representative of the real conditions in buildings.

For push-out test specimens, it was also found that the slab width is a key parameter that can change the failure mode from rib shearing to concrete pull-out (Lloyd and Wright, 1990). Hence, narrow slabs shall be avoided because they induce rib shearing failure which does not normally occur in composite beams. Owing to the eccentricity of the load created by the profiled sheeting, vertical cracks may propagate on the cover part of the slab (Kemp and Trinchero, 1997) leading to a premature "back-breaking" failure which can be prevented by placing sufficient longitudinal reinforcement in the slab.

In view of all the considerations made on standard push-out test specimens, alternative testing methods and set-ups have been developed over the years to appropriately reflect the failure modes of the connectors in composite beams, such as single-sided push-out test (Döinghaus, 2001), horizontal push-off test (Lam, 1998; Ernst, 2006) and other modified setups (Shen and Chung, 2017).

2.2.3 Experimental studies on headed studs in solid slabs

The first experimental study on headed studs in solid slabs was conducted by Viest (1956), where the diameter of the shank of the stud varied from 13 mm to 32 mm. The tested specimens experienced stud shearing or concrete bearing failure. Similar studies have been performed in that decade to investigate the potential of such connectors by varying the geometry of the stud (Yamamoto and Nakamura, 1962; Sattler, 1962). A few years later, Mainstone and Menzies (1967) conducted an extensive experimental campaign including push-out tests to check the performance of studs under static and fatigue load. Ollgaard et al. (1971) carried out 48 push-out tests using normal weight and lightweight concrete while changing several material properties of the concrete (compressive and splitting strength, modulus of elasticity, density, aggregate type) as well as the diameter and the number of studs per slab. This study highlighted the importance of the concrete compressive strength and modulus of elasticity of concrete on the capacity of the shear connection. Similarly, in the same year, Menzies (1971) presented the results of further push-out tests with particular focus on the influence of the concrete strength. In the 1980s, many push tests were carried out (Oehlers, 1981; Hiragi et al., 1981; Roik and Hanswille, 1983) increasing the robustness of the database which was used to calibrate the equations proposed in the draft of EN 1994-1-1 design rules (Roik et al., 1988). In the 1990s, several research works started to include specimens with high strength concrete, such as Bullo and Di Marco (1995), and An and Cederwall (1996). The former study consists of 18 push-out tests prepared with three different concrete classes corresponding to a characteristic cylinder strength of 30 MPa, 60 MPa and 80 MPa in combination with a stud diameter of 19 or 25 mm. In the latter, the results of 8 push-out tests using high strength and normal strength concrete, and different amount of transversal reinforcement were presented. Hicks (1997) highlighted the importance of the frictional forces developed at the beam-floor interface which affects the apparent shear capacity of the connection. The impact of the friction on the stud strength was also confirmed by Rambo-Roddenberry (2002) who presented the results of 24 push-out tests on headed studs in solid slabs. Hanswille et al. (1998) carried out 10 push-out tests on 25 mm diameter studs showing that the connectors achieve sufficient slip capacity to be considered as ductile according to EN 1994-1-1 (BSI, 2004b). 62 tests on studs in high strength concrete slabs were analysed by Döinghaus (2001), including single-sided push-out tests. Several test series were also dedicated to the investigation of unconventional enhancement devices. A few years later, several push-out and beam test specimens with 25, 27 and 30 mm diameter studs were manufactured and tested by Lee et al. (2005) under static and fatigue load and it was seen that the diameter of the stud has a negative impact on the fatigue strength. In 2007, a broad experimental study on headed studs including push-out test and full scale beam tests under static and cyclic load was conducted (Feldmann, 2007). From the static push-out tests, it was seen that studs in high strength concrete did not meet the ductility criterion of EN 1994-1-1 (BSI, 2004b). Another large test program was presented by Jähring (2007) with particular emphasis on specimens with high performance concrete. In addition to concrete strength, shank diameter and spacing between the studs, the effect of the weld and the head was also investigated. To encourage the implementation of high strength materials in practice, high strength studs with different diameters have been tested in recent expertimental studies (Wang et al., 2011).

2.2.4 Experimental studies on headed studs in profiled steel sheeting

In the 1980s, several experimental investigations were undertaken for evaluating the behaviour of studs welded in open trough profiled sheeting via push-out tests (Roik and Bürkner, 1980; Roik and Bürkner, 1981; Roik and Hanswille, 1983). Compared to solid slabs, additional parameters are of importance for the performance of the shear connection such as the relative position of the stud in the trough, the welding procedure as well as the geometry of the rib. In consideration of the economical benefit given by the application of the profiled steel sheeting on the design of composite floors, further tests were carried out in combination with several types of decks, including re-entrant profiles (Bode and Künzel, 1987) and different stud heights (Roik and Lungershausen, 1988). In their study, Roik and Lungershausen (1988) pointed out that a sufficient embedment depth (i.e. the difference between the height of the stud and the rib) prevents the concrete pull-out failure resulting in a highly ductile behaviour where the studs develop two full plastic hinges. In the same period, Jayas and Hosain (1987) conducted 8 tests with 76 mm long stud where different stud arrangements were checked. Most of them showed concrete pull-out while one test experienced unwanted rib shearing failure owing to the reduced width of the rib. Based on the results available, it was evident that the geometry of the rib affects the strength of the connection by changing from concrete related failures to stud shearing (or rupture). Robinson (1988) carried out several push-out tests and two parallel full-scale beam tests on different types of shear connections with transverse steel sheeting. It was seen that the use of the mean strength of the push-out specimens in the calculation of the bending resistance of the composite beam leads to a good estimation. However, it does not necessarily mean that the push-out test reflects accurately the behaviour of the shear connections in composite beams. In view of the positive influence of the through-deck welding procedure on the resistance of the stud, more and more researchers focused on specimens with through-deck welded studs by performing numerous push-out tests (Lloyd and Wright, 1990; Mottram and Johnson, 1990; Sublett, 1992; Lyons, 1994). In particular, the experimental investigation of Lloyd and Wright (1990) consisted of 42 push-out tests on studs in trapezoidal profiled steel sheeting where most of the samples exhibited concrete pull-out failure. Based on the observation of the wedged cone after demounting, the authors proposed an analytical formulation of the failure surface of the cone. A few years later, Yuan (1996) presented a study on through-deck welded studs and it was found that the existing methods for predicting their resistance give unsatisfactory results as they do not distinguish the different failure modes. To address this issue, they identified several types of failure by performing 16 new tests: stud shearing, rib punching and concrete pull-out including mixed combinations. To compensate for the reduced performance of shear connections in profiled sheeting, the implementation of special reinforcement bars and enhancement devices were discussed in a novel experimental investigation performed by Ernst (2006). In this work, a special single-sided push test rig was developed and used to prevent unwanted failures. It was found that the use of waveform reinforcement elements can prevent premature concrete pull-out failures while stud performance-enhancing devices increased the resistance up to 30% by ensuring a local high confinement around the base of the connector. In parallel with the increasing research on headed studs in profiled sheeting, new deck profiles have been developed. However, because of their relatively slender geometry, they may not always fulfil the resistance and ductility requirements of EN 1994-1-1 (BSI, 2004b). On the other hand, notwithstanding the potential unsafety of some configurations, Hicks (2009) showed that headed studs placed in a

full-scale composite beam have higher resistance and slip capacity than the companion push test. Recently, Shen and Chung (2017) carried out several push-out tests on various headed stud shear connections using a modified test setup. Unlike in standard push test specimens, the beam-slab elements were inclined by an angle of 15° leading to shear and tension force acting in parallel. This modification was applied to reproduce the mechanical conditions of headed studs employed in steel-concrete beams with large web openings. In this case, the shear connectors undergo high pulling forces that may limit the bending resistance (Lawson et al., 2013) of the composite beam. In the last years, within the scope of the project DISCCO (Lawson et al., 2017), an extensive experimental study including push-out and full scale beam tests were carried out. The specimens used modern forms of steel sheeting highlighted the deficiency of the EN 1994-1-1 design rules in the prediction of the capacity of the shear connection. Currently, the experimental research has been focusing on the evaluation of the shear connection performance under extreme conditions such as cyclic load (Sun et al., 2019), impact load (Huo et al., 2019) and fire conditions (Lim et al., 2020).

2.3 Prediction of the resistance of studs in solid slabs

On the basis of the extensive literature available, different analytical approaches have been proposed to predict the resistance of headed studs shear connections in solid slabs. In the following sections, three design models are evaluated statistically in accordance with the standard procedure of EN 1990 detailed in Appendix A against a representative database of push-out tests defined in Section 2.3.1.

The results of the statistical analysis for each design model (BSI, 2004b; Oehlers and Johnson, 1987; Konrad, 2011) are given in Section 2.3.2, 2.3.3 and 2.3.4. Then, their performance are compared and discussed in Section 2.3.5.

2.3.1 Representative database

A representative database of 274 push-out tests using headed stud shear connectors in solid slabs was considered and it is given in Appendix B.1. The tests cover a wide range of application: the minimum and maximum values of the basic variables are shown in Table 2.1.

TABLE 2.1: Limits of the basic variables in the representative database for headed studs in solid slabs

Variable	Min	Max
Nominal diameter of the stud - d_{nom}	13 mm	32 mm
Mean length of the stud (after welding) - h_{scm}	70 mm	200 mm
Mean compressive cylinder strength of concrete - f_{cm}	16.6 MPa	112.7 MPa
Mean ultimate tensile strength of stud material - f_{um}	392 MPa	675 MPa

Since the elastic modulus of concrete was not always reported, it was calculated according to Eq.(2.1) recommended by EN 1992-1-1 (BSI, 2004a):

$$E_c = 22000 \left[\left(\frac{f_c[\text{MPa}]}{10} \right) \right]^{0.3} \text{[MPa]} \tag{2.1}$$

2.3.2 EN 1994-1-1 (2004b) design model

According to EN 1994-1-1 (BSI, 2004b), the resistance function in Eq.(2.2) for predicting the capacity of headed stud shear connections in solid slabs is the minimum between Eq.(2.3) and Eq.(2.4). The former is related to the yield strength of the stud shank under shear and tension forces while the latter considers the bearing resistance of the concrete at the base of the stud (i.e. in proximity of the weld collar).

$$r_{t,EC4,ss} = \min\{r_{t1,EC4,ss}, r_{t2,EC4,ss}\} \tag{2.2}$$

and

$$r_{t1,EC4,ss} = 0.8 f_u \frac{\pi d^2}{4} \tag{2.3}$$

$$r_{t2,EC4,ss} = 0.29\ \alpha\ d^2 \sqrt{f_c E_c} \tag{2.4}$$

With:

$$\alpha = \begin{cases} 0.2\left(\frac{h_{sc}}{d} + 1\right) & \text{for } h_{sc}/d \leq 4 \\ 1 & \text{for } h_{sc}/d > 4 \end{cases} \tag{2.5}$$

Where:

f_u	is the ultimate tensile strength of the stud material
f_c	is the cylinder compressive strength of concrete
E_c	is the modulus of elasticity of concrete
h_{sc}	is the length of the stud after welding
d	is the diameter of the shank of the stud

The corresponding design equations using nominal properties are:

$$P_{Rd,EC4,ss} = \min\{P_{Rd1,EC4,ss}, P_{Rd2,EC4,ss}\} \tag{2.6}$$

and

$$P_{Rd1,EC4,ss} = \left(0.8 f_{u,nom} \frac{\pi d_{nom}^2}{4}\right) \cdot \frac{1}{\gamma_V} \tag{2.7}$$

$$P_{Rd2,EC4,ss} = \left(0.29\ \alpha\ d_{nom}^2 \sqrt{f_{ck} E_{cm}}\right) \cdot \frac{1}{\gamma_V} \tag{2.8}$$

With:

$\gamma_V = 1.25$ (recommended)

Where:

$f_{u,nom}$ is the nominal ultimate tensile strength of the material of the stud, not greater than 500 MPa in computation

f_{ck} is the characteristic cylinder compressive strength of concrete

E_{cm} is the mean modulus of elasticity of concrete

d_{nom} is the nominal diameter of the shank of the stud

The equations defined above were statistically evaluated against the entire representative database of 274 push-out tests and the results are displayed in the plot in Figure 2.7. 204 tests fall within the domain of Eq.(2.3), see Figure 2.7a, with a coefficient of variation V_r of 13.6%. Instead, Eq.(2.4) representing concrete related failures, exhibits relatively higher dispersion owing to the variability of the basic variables, see Figure 2.7b. The linear correlation factor $\rho = 0.908$ was calculated by considering both resistance equations. The corrected partial safety factor γ_M^* is equal to 1.064 and 1.274 while the recommended value γ_V is 1.25. Although these equations show a good statistical correlation and safe results, they are not optimized for configurations with high strength concrete causing an underestimation of the design resistance given by Eq.(2.3) of ca. 15%.

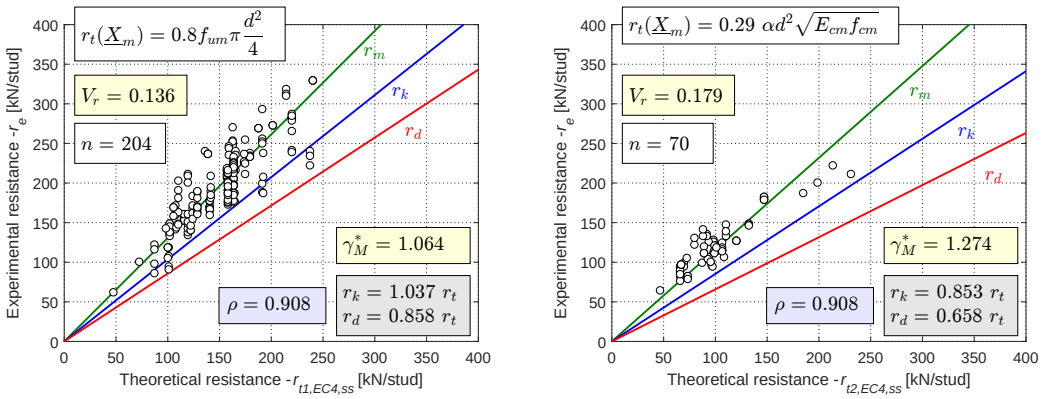

(a) (b)

FIGURE 2.7: Comparison between experimental and theoretical resistance according to EN 1994-1-1 (2004b) design model for studs in solid slabs

2.3.3 Oehlers and Johnson (1987) design model

Oehlers and Johnson (1987) proposed a simple design model that considers a mixed failure of concrete and stud in a single expression. The corresponding equation was empirically obtained and it is given by:

$$r_{t,Oeh,ss} = 3.66\ \frac{\pi d^2}{4} \left(\frac{E_c}{E_s}\right)^{0.4} \left(\frac{f_c}{f_u}\right)^{0.35} \tag{2.9}$$

Where:

E_s is the modulus of elasticity of the material of the stud

The corresponding design equation using nominal variables is:

$$P_{Rd,Oeh,ss} = \left[3.66\ \frac{\pi d_{nom}^2}{4}\left(\frac{E_{cm}}{E_{sm}}\right)^{0.4}\left(\frac{f_{ck}}{f_{u,nom}}\right)^{0.35}\right]\cdot\frac{1}{\gamma_V} \tag{2.10}$$

With:

$\gamma_V = 1.10$ (recommended)

Where:

$f_{u,nom}$ is the nominal ultimate tensile strength of the material of the stud

E_{sm} is the mean modulus of elasticity of the material of the stud

The result of the statistical evaluation of Eq.(2.10) is visualized in Figure 2.8. A linear correlation coefficient $\rho = 0.897$ is achieved whereas a relatively high variability is observed with $V_r = 18.3\%$. In the initial calibration of the equation, a partial safety factor $\gamma_V = 1.10$ was proposed even though the corrected partial safety factor $\gamma_M^* = 1.305$. Notwithstanding the ease of use, the application of the design resistance of Eq.(2.10) leads to an overestimation of ca. 18%.

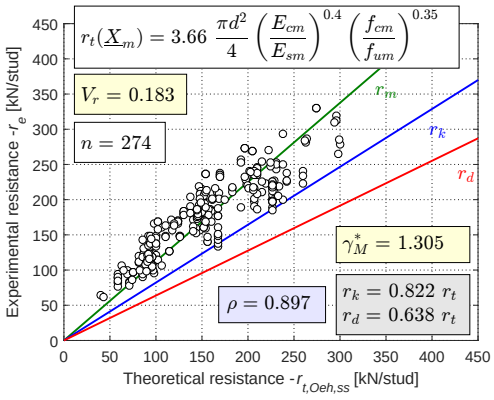

FIGURE 2.8: Comparison between experimental and theoretical resistance according to Oehlers and Johnson (1987) design model for studs in solid slabs

2.3.4 Konrad (2011) design model

Although the equations proposed by Konrad (2011) rely on the resistance mechanisms activated around the stud, the final expressions were statistically derived. The respective resistance of the stud is calculated by Eq.(2.11) as the minimum between Eq.(2.12) and Eq.(2.13). The values f_c and f_u must be taken in MPa. Unlike in previous models, the dimensions of the weld collar are also required, see Figure 2.9.

$$r_{t,Kon,ss} = \min\{r_{t1,Kon,ss}, r_{t2,Kon,ss}\} \tag{2.11}$$

and

$$r_{t1,Kon,ss} = 313 A_{col}\left(\frac{f_c}{30}\right)^{\frac{2}{3}} + 240\left(\frac{f_u}{500}\right)d^2 \tag{2.12}$$

$$r_{t2,Kon,ss} = 326 A_{col} \left(\frac{f_c}{30}\right)^{\frac{2}{3}} + 220 \left(\frac{f_c}{30}\right)^{\frac{1}{3}} \left(\frac{f_u}{500}\right)^{\frac{1}{2}} d^2 \tag{2.13}$$

With:

$$A_{col} = 0.5\, d_{col}\, h_{col} \tag{2.14}$$

Where:

A_{col}	is the effective lateral surface area of the weld collar
d_{col}	is the diameter of the weld collar
h_{col}	is the height of the weld collar

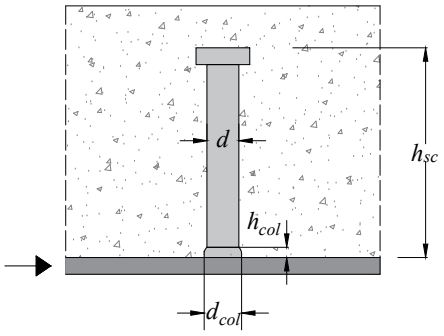

FIGURE 2.9: Dimensions of headed stud shear connections in solid slabs according to Konrad (2011) design model

The respective design equations using nominal values of the variables are given by:

$$P_{Rd,Kon,ss} = \min\{P_{Rd1,Kon,ss}, P_{Rd2,Kon,ss}\} \tag{2.15}$$

$$P_{Rd1,Kon,ss} = \left[313 A_{col,nom} \left(\frac{f_{ck}}{30}\right)^{\frac{2}{3}} + 240 \left(\frac{f_{u,nom}}{500}\right) d_{nom}^2\right] \cdot \frac{1}{\gamma_V} \tag{2.16}$$

$$P_{Rd2,Kon,ss} = \left[326 A_{col,nom} \left(\frac{f_{ck}}{30}\right)^{\frac{2}{3}} + 220 \left(\frac{f_{ck}}{30}\right)^{\frac{1}{3}} \left(\frac{f_{u,nom}}{500}\right)^{\frac{1}{2}} d_{nom}^2\right] \cdot \frac{1}{\gamma_V} \tag{2.17}$$

With:

$$A_{col,nom} = 0.5\, d_{col,nom}\, h_{col,nom} \tag{2.18}$$

$\gamma_V = 1.25$ (recommended)

Where:

$A_{col,nom}$ is the nominal effective lateral surface area of the weld collar

$d_{col,nom}$ is the nominal diameter of the weld collar (ISO/TC44/SC10, 2017)

$h_{col,nom}$ is the nominal height of the weld collar (ISO/TC44/SC10, 2017)

The comparison between theoretical resistance values and test results is visualized in Figure 2.10a and Figure 2.10b. A good statistical correlation is observed in both equations with a maximum coefficient of variation $V_r = 16.5\%$ and a linear correlation factor $\rho = 0.915$. The recommended partial safety factor of 1.25 is on the safe side with a maximum underestimation of ca. 8%.

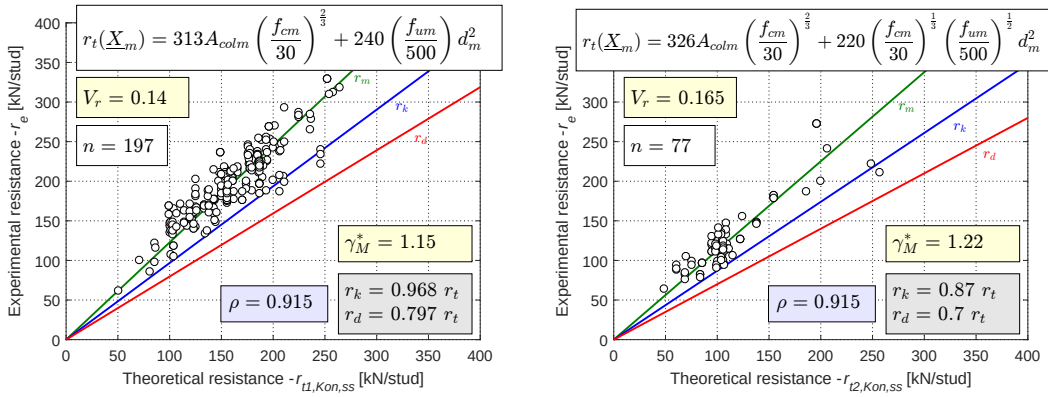

(a) (b)

FIGURE 2.10: Comparison between experimental and theoretical resistance according to Konrad (2011) design model for studs in solid slabs

2.3.5 Comparison between different design models

To have a consistent comparison between the design models considered in the previous sections, the key results of the statistical analyses are summarized in Table 2.2.

It can be said that the simple design approach proposed by Oehlers and Johnson (1987) leads to an unconservative estimation of the capacity with a relatively high coefficient of variation. On the other hand, the design models of EN 1994-1-1 (BSI, 2004b) and Konrad (2011) provide a more satisfactory prediction of the resistance of headed studs in solid slabs with a lower dispersion. These results may be explained by the use of two equations that account for steel and concrete related failure modes separately. In consideration of the field of application shown Table 2.1, these two design models are both suitable for practical use. However, whilst EN 1994-1-1 design equations (BSI, 2004b) were initially calibrated against normal strength concrete specimens, the model of Konrad (2011) supports better the use of headed studs shear connections with high strength materials. The advantages and disadvantages of the design models considered are finally shown in Table 2.3.

TABLE 2.2: Results of the statistical evaluation of the design models for the resistance of studs in solid slabs

	EN 1994-1-1 (2004b)		Oehlers (1987)	Konrad (2011)	
	Eq. (2.3)	Eq. (2.4)	Eq. (2.9)	Eq. (2.12)	Eq. (2.13)
n	204	70	274	197	77
b	1.307	1.159	1.125	1.228	1.126
ρ	0.908		0.897	0.915	
V_r	0.136	0.179	0.183	0.140	0.165
γ_M^*	1.064	1.274	1.305	1.150	1.220
γ_V	1.25	1.25	1.10	1.25	1.25

TABLE 2.3: Comparison between different design models for the resistance of studs in solid slabs

	Advantages	Disadvantages
EN 1994-1-1 (2004b)	+ Good statistical correlation with low scatter + Conservative	- Not optimized for high strength materials
Oehlers and Johnson (1987)	+ Easy-to-use: only one equation	- Unconservative
Konrad (2011)	+ Good statistical correlation with low scatter + Conservative + Calibrated against tests including high strength materials	- Nominal weld collar dimensions are not always available and may differ from ISO/TC44/SC10 (2017)

2.4 Prediction of the resistance of studs in profiled steel sheeting

Similarly to what has been done for studs in solid slabs, several analytical methods have been proposed over the years to predict the resistance of headed stud shear connections in composite slabs with transverse profiled steel sheeting. Because of the variety of test setup and loading procedures used in different experimental studies, only the representative tests were considered from the initial database, as detailed in Section 2.4.1.

From all the analytical approaches developed in the past, five design models were analysed according to the statistical procedure of EN 1990 (Appendix A) from Section 2.4.2 to Section 2.4.6. Finally, an overall comparison between these proposals is provided in Section 2.4.7.

2.4.1 Representative database

The initial test database counts a total of 587 push-out tests using headed stud shear connections in profiled sheeting transverse to the beam. Only those push-out tests which are representative of the actual resistance of the shear connection in composite beams were considered according to the following constraints:

- No tests with reported weld seam faults: Such type failure are caused by poor welding of studs that compromises the performance of the shear connection;

- No tests with transversal load applied: It is still under discussion whether the vertical load always applies at any point of the slab in building applications as local uplift may occur (Chapman, 1964; Chapman and Balakrishnan, 1964);
- No tests with more than 2 studs per rib;
- No tests with Light Weight or Low Strength Concrete (f_{cm} <24 MPa).

241 push-out tests fell within these limits. Although low strength concrete specimens were not considered in most of the past reliability analyses, it could be discussed whether the push-out test specimens with $f_{cm} < 24$ MPa should be included in the representative database. If no limitation of the concrete strength is considered, 19 tests should be added resulting in a total of 260 tests and the detailed list is given in Appendix B.2. All the analyses of the design models presented in this chapter were also carried out including cases with $f_{cm} < 24$ MPa and the results are given in Appendix C.1.

The short-term relaxation effects (Hanswille and Porsch, 2007) were not taken into account for the determination of the experimental value of the resistance r_e. However, some of the push-out tests considered in the database used dial gauges where the influence of short-term relaxation would already have been implicitly included in the data.

TABLE 2.4: Limits of the basic variables in the representative database for headed studs in profiled steel sheeting

Variable	Min	Max
Nominal diameter of the stud - d_{nom}	19 mm	22 mm
Mean length of the stud (after welding) - h_{scm}	70 mm	200 mm
Nominal height of the deck - $h_{p,nom}$	40 mm	136 mm
Nominal bottom width of the deck - $b_{bot,nom}$	40 mm	160 mm
Nominal top width of the deck – $b_{top,nom}$	101 mm	240 mm
Nominal thickness of the sheeting – t_{nom}	0.6 mm	1.2 mm
Mean compressive cylinder strength of concrete - f_{cm}	24 MPa	58.1 MPa
Mean ultimate tensile strength of stud material - f_{um}	417 MPa	570 MPa

2.4.2 EN 1994-1-1 (2004b) design model

The design resistance of studs in composite slabs with transverse profiled sheeting proposed in EN 1994-1-1 (BSI, 2004b) is the result of the combination of several contributions (Grant et al., 1977; Roik et al., 1988; Stark and Hove, 1991). The design approach is empirical and it considers a reduction factor k_t that applies to the respective resistance of studs in solid slabs (see Section 2.3.2). The resistance function is given in Eq.(2.19) while the geometrical properties required are shown in Figure 2.11.

$$r_{t,EC4,ps} = \min\{r_{t1,EC4,ps}, r_{t2,EC4,ps}\} \tag{2.19}$$

and

$$r_{t1,EC4,ps} = k_t \cdot 0.8 f_u \frac{\pi d^2}{4} \tag{2.20}$$

$$r_{t2,EC4,ss} = k_t \cdot 0.29\ \alpha\ d^2 \sqrt{f_c E_c} \tag{2.21}$$

With:

$$\alpha = \begin{cases} 0.2\left(\frac{h_{sc}}{d} + 1\right) & \text{for } h_{sc}/d \leq 4 \\ 1 & \text{for } h_{sc}/d > 4 \end{cases} \tag{2.22}$$

$$k_t = \frac{0.7}{\sqrt{n_r}} \frac{b_0}{h_p} \left(\frac{h_{sc}}{h_p} - 1\right) \leq k_{t,max} \tag{2.23}$$

Where:

$f_{u,nom}$ is the nominal ultimate tensile strength of the material of the stud, not greater than 450 MPa in computation

n_r is the number of studs per rib

TABLE 2.5: Upper limits $k_{t,max}$ for the reduction factor k_t

Number of studs per rib	Thickness t of the sheet [mm]	Through-deck welded studs and $d \leq$20 mm	Profiled sheeting with holes and $d \leq$22 mm
$n_r = 1$	≤ 1.0	0.85	0.75
	> 1.0	1.0	0.75
$n_r = 2$	≤ 1.0	0.70	0.60
	> 1.0	0.80	0.60

The corresponding design equations using nominal properties are:

$$P_{Rd,EC4,ps} = \min\{P_{Rd1,EC4,ps}, P_{Rd2,EC4,ps}\} \tag{2.24}$$

and

$$P_{Rd1,EC4,ps} = k_t \cdot \left(0.8 f_{u,nom} \frac{\pi d_{nom}^2}{4}\right) \cdot \frac{1}{\gamma_V} \tag{2.25}$$

$$P_{Rd2,EC4,ps} = k_t \cdot \left(0.29\ \alpha\ d_{nom}^2 \sqrt{f_{ck} E_{cm}}\right) \cdot \frac{1}{\gamma_V} \tag{2.26}$$

With:

$\gamma_V = 1.25$ (recommended)

Based on the results of the entire representative database in Figure 2.12, the design rules of EN 1994-1-1 are on the unsafe side where γ_M^* is even higher than 2.0 and the coefficient of variation V_r is 24.2% for Eq.(2.20) and 32.6% for Eq.(2.21). The statistical performance was also assessed in the recommended field of application considering the following limits:

- $h_{sc} - h_p \geq 2d$

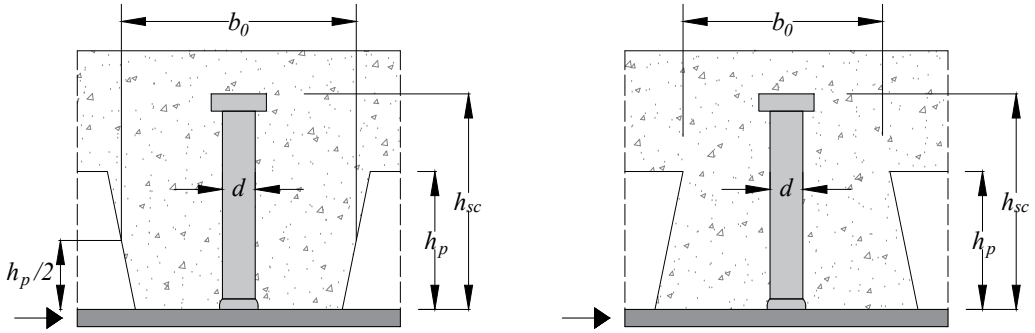

(a) (b)

FIGURE 2.11: Dimensions of headed stud shear connections with (a) open trough and (b) re-entrant sheeting according to EN 1994-1-1 (BSI, 2004b) design model

- $h_p \leq 85$ mm
- $b_0 \geq h_p$
- $d < 20$ mm for through-deck welded studs
- $e_t > 2.5d$

Where:

e_t is the transversal spacing between the studs in the trough

As shown in Table 2.6, while the scattering reduces to ca. 20%, the results are still unsatisfactory as confirmed by recent studies (Lawson et al., 2017). This is caused by the nature of the actual failure modes which are different from those occurring in studs placed in solid slabs. Nevertheless, based on the evaluation of different subsets, it was found that these design rules are suitable for studs placed in re-entrant profiled sheeting. However, they shall be applied only to those re-entrant profiles considered in the evaluation as newly developed products should be tested.

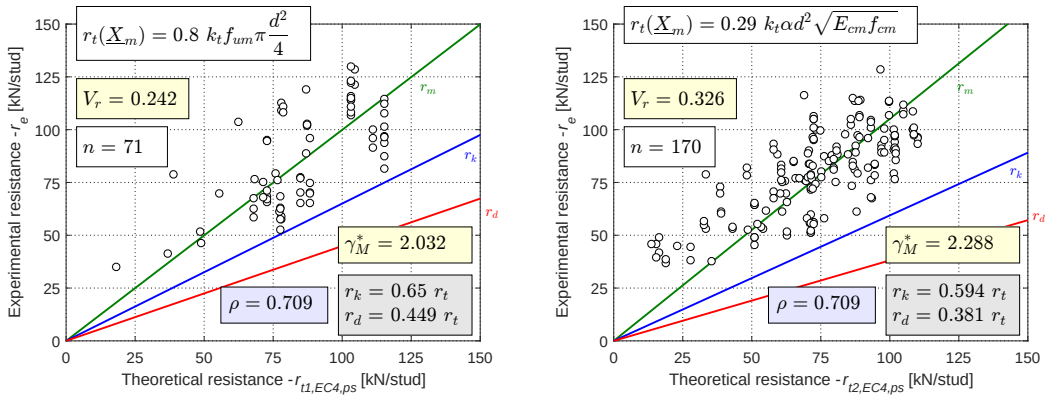

(a) (b)

FIGURE 2.12: Comparison between experimental and theoretical resistance according to EN 1994-1-1 (BSI, 2004b) design model for studs in profiled steel sheeting

TABLE 2.6: Results of the statistical evaluation of the EN 1994-1-1 (BSI, 2004b) design model for the resistance of studs in profiled steel sheeting

	All (Figure 2.12)		Field of application		Open trough decks		Re-entrant decks	
	Eq.(2.20)	Eq.(2.21)	Eq.(2.20)	Eq.(2.21)	Eq.(2.20)	Eq.(2.21)	Eq.(2.20)	Eq.(2.21)
n	71	170	59	100	50	137	21	33
ρ	0.709		0.625		0.695		0.798	
b	0.999	1.051	1.006	1.016	0.907	1.027	1.179	1.130
V_r	0.242	0.326	0.222	0.197	0.241	0.358	0.129	0.138
γ_M^*	2.032	2.288	1.902	1.623	2.256	2.596	1.237	1.195
γ_V	1.25	1.25	1.25	1.25	1.25	1.25	1.25	1.25

2.4.3 Lungershausen (1988) design model

The design model proposed by Lungershausen (1988) is a simple mechanical-based approach to predict the capacity of studs. The resistance value was considered to be a function of the geometrical and mechanical properties of the stud and the concrete related component was neglected. Lungershausen (1988) assumed that the stud develops a double curvature with two full plastic hinges with a lever arm equal to $\alpha_L d$. The resulting analytical resistance is given by:

$$r_{t,Lun,ps} = 0.8 \frac{\beta}{\sqrt{n_r}} \frac{2(f_u d^3/6)}{\alpha_L d} \tag{2.27}$$

With:

$$\alpha_L = 0.8 \left(\frac{h_p}{b_0}\right)^2 + 0.6 \tag{2.28}$$

$$\beta = \begin{cases} 1.0 & \text{for open trough profiles} \\ 1.1 & \text{for re-entrant profiles} \end{cases} \tag{2.29}$$

Instead, the design resistance using nominal variables is equal to:

$$P_{Rd,Lun,ps} = \left(0.8 \frac{\beta}{\sqrt{n_r}} \frac{2(f_{u,nom} d_{nom}^3/6)}{\alpha_L d_{nom}}\right) \cdot \frac{1}{\gamma_V} \tag{2.30}$$

With:

$$\gamma_V = 1.20 \text{ (recommended)}$$

The results displayed in Figure 2.13 show a relatively good agreement between experimental and analytical values of the resistance according to Eq. (2.27): the coefficient of variation V_r is 17.9% while the correlation factor ρ is equal to 0.786.

Although the approach is simple, the equation can conservatively predict the capacity of the shear connection using the recommended value of the partial safety factor

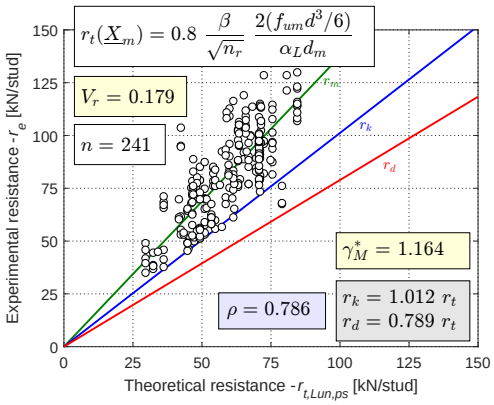

FIGURE 2.13: Comparison between experimental and theoretical resistance according to Lungershausen (1988) design model for studs in profiled steel sheeting

$\gamma_V = 1.20$ with an underestimation of ca. 4%. However, the design model was limited to shear connections with high embedment length $(h_{sc} - h_p)$ which prevents concrete pull-out failure allowing the development of two plastic hinges in the stud. The recommended field of application of the equations is defined by the following limitations:

- $h_{sc} - h_p \geq 2dn_r$
- $h_p \leq 140$ mm

As shown in the results of Table 2.7 the equation becomes more efficient with V_r=16% within these limits. It is therefore clear that the equation is not optimized for the headed studs with reduced embedment length which might be limiting for supporting the development of novel profiled decks in the future.

TABLE 2.7: Results of the statistical evaluation of Lungershausen (1988) design model for the resistance of studs in profiled steel sheeting

	All (Figure 2.13)	Field of application	Open trough decks	Re-entrant decks
n	241	171	187	54
ρ	0.786	0.775	0.791	0.649
b	1.375	1.368	1.337	1.474
V_r	0.179	0.160	0.172	0.169
γ_M^*	1.164	1.191	1.172	1.093
γ_V	1.20	1.20	1.20	1.20

2.4.4 Lloyd and Wright (1990) design model

The model proposed by Lloyd and Wright (1990) is based on the observation of the samples tested in their study. All the configurations considered experienced rib shearing and pull-out failure leading to the typical concrete cones around the studs. The resulting failure surfaces were carefully analysed and a geometrical formulation

was provided to estimate the area of concrete subjected to pulling forces. With reference to the proposed expression in Eq.(2.31), $f_{c,cube}$ and A_{ce} must be indicated in MPa and mm^2 to obtain the resistance value in kN.

$$r_{t,LW,ps} = (A_{ce}\sqrt{f_{c,cube}})^{0.34} \tag{2.31}$$

With:

$$A_{ce} = 2b_{top}\sqrt{\frac{b_{top}^2}{4} + (h_{sc} - h_p)^2} + b_{top}\sqrt{b_{top}^2 + 2(h_{sc} - h_p)^2} + 2b_{bot}\sqrt{3h_p^2} + \\ + 2e_t\sqrt{\frac{b_{top}^2}{4} + (h_{sc} - h_p)^2} \tag{2.32}$$

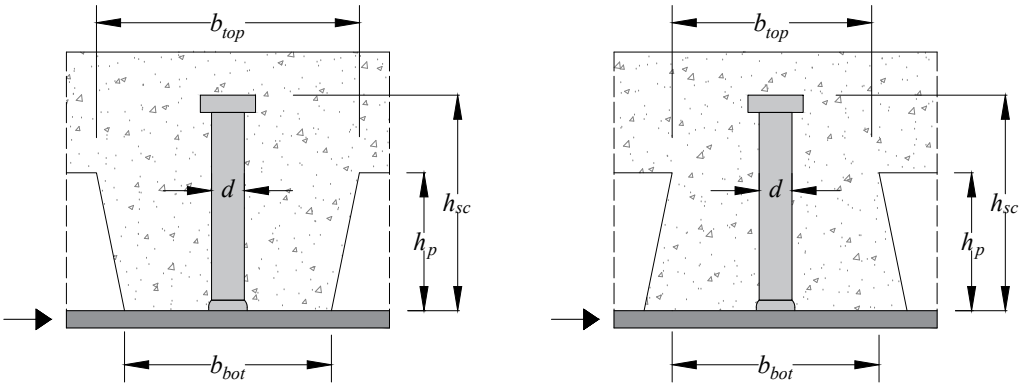

FIGURE 2.14: Dimensions of headed stud shear connections with (a) open trough and (b) re-entrant sheeting according to Lloyd and Wright (1990) design model

The respective design resistance using nominal variables is:

$$P_{Rd,LW,ps} = (A_{ce}\sqrt{f_{ck,cube}})^{0.34} \cdot \frac{1}{\gamma_V} \tag{2.33}$$

Where no value of the partial safety factor γ_V was recommended.

The theoretical resistance according to Eq.(2.31) shows a low correlation with the entire representative database where the coefficient of variation V_r exceeds 30%, as shown in Figure 2.15.

The inaccuracy of the prediction is due to the fact that the model was estimated against a limited set of push-out tests presented by the same authors (Lloyd and Wright, 1990). Thus, these tests were considered as the recommended field of application of Eq.(2.31). In this case, the design model delivers satisfactory results with a coefficient of variation of only 9.5%, see Table 2.8. However, the scope is very limited and it cannot be extended without including other types of failure modes as well as the properties of the stud material.

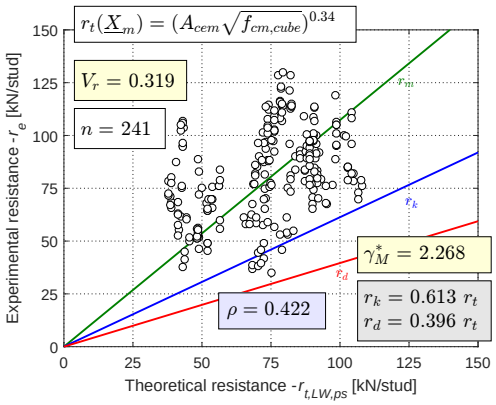

FIGURE 2.15: Comparison between experimental and theoretical resistance according to Lloyd and Wright (1990) design model for studs in profiled steel sheeting

TABLE 2.8: Results of the statistical evaluation of Lloyd and Wright (1990) design model for the resistance of studs in profiled steel sheeting

	All (Figure 2.15)	Field of application	Open trough decks	Re-entrant decks
n	241	33	187	54
ρ	0.422	0.584	0.590	0.467
b	1.073	1.060	0.992	1.554
V_r	0.319	0.095	0.273	0.251
γ^*_M	2.401	1.242	2.245	1.424
γ_V	-	-	-	-

2.4.5 Johnson and Yuan (1998) design model

To account for the actual failure modes occurring in headed stud shear connections in profiled steel sheeting, Johnson and Yuan (1998) proposed a design model that differentiates all the possible combinations of failure: shank failure (due to shear and tension), rib punching, concrete pull-out, combined rib punching and concrete pull-out, and combined rib punching and shank failure. These types of failure were considered separately according to different mechanical modes. Finally, to ease the practical use of the model, all the resistance functions were condensed in Eq.(2.34) recalling the reduction factor approach of EN 1994-1-1 (BSI, 2004b). All the required geometrical dimensions are given in Figure 2.16 and Figure 2.17.

$$r_{t,Joh,ps} = k^\star \cdot \min\left\{0.8 f_u \frac{\pi d^2}{4}, 0.37 d^2 \sqrt{f_c E_c}\right\} \tag{2.34}$$

With:

$$k^{\star} = \begin{cases} k_{11} = \dfrac{h_{sc}t + 4.3e_f}{4h_p + 3e_f} \leq 1.0 & n_r = 1 \text{ and } k_{11} \leq k_{12} \quad (2.35) \\ k_{12} = \dfrac{0.02(e_f + 6h_{sc})}{h_p} + 0.7 \leq 1.0 & n_r = 1 \text{ and } k_{11} > k_{12} \quad (2.36) \\ k_2 = \dfrac{0.25(4s_t + 3h_{sc}t)}{2h_p + 3e_s} \leq 1.0 & n_r = 2 \text{ and staggered} \quad (2.37) \\ k_3 = \dfrac{0.018(e_f + 4.24h_{sc})}{h_p} \leq 1.0 & \text{otherwise} \quad (2.38) \end{cases}$$

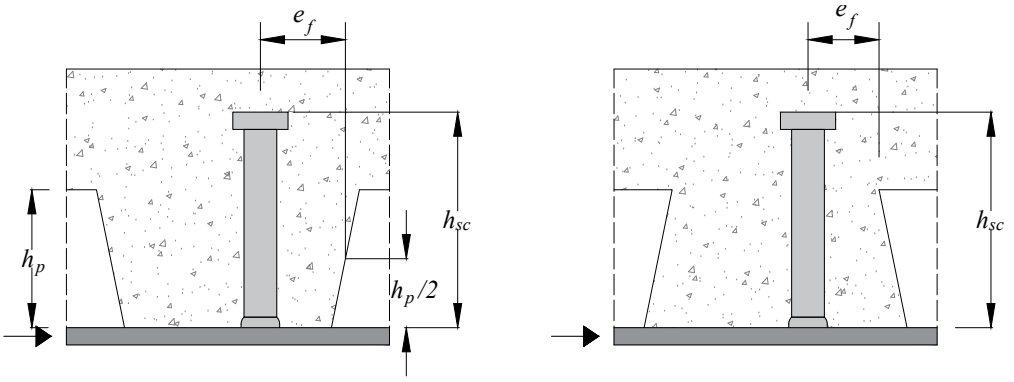

FIGURE 2.16: Dimensions of headed stud shear connections with (a) open trough and (b) re-entrant sheeting according to Johnson and Yuan (1998) design model

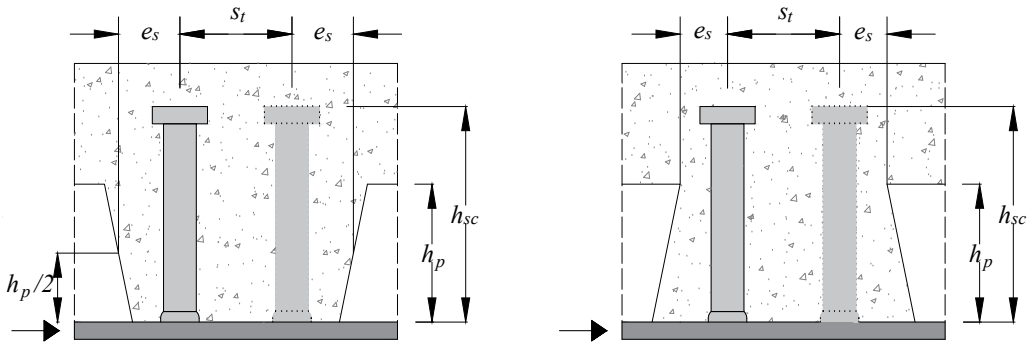

FIGURE 2.17: Dimensions of headed stud shear connections in staggered position with (a) open trough and (b) re-entrant sheeting according to Johnson and Yuan (1998) design model

The corresponding design resistance is given by:

$$P_{Rd,Joh,ps} = k^{\star} \cdot \min \left\{ 0.8 f_{u,nom} \frac{\pi d_{nom}^2}{4},\ 0.37 d_{nom}^2 \sqrt{f_{ck} E_{cm}} \right\} \cdot \frac{1}{\gamma_V} \quad (2.39)$$

With:

$$\gamma_V = 1.25 \text{ (recommended)}$$

The four subcases corresponding to a reduction factor of k_{11}, k_{12}, k_2 and k_3 were considered separately in the reliability analyses as they are related to different failure modes. The results against the entire database are visualized in Figure 2.18.

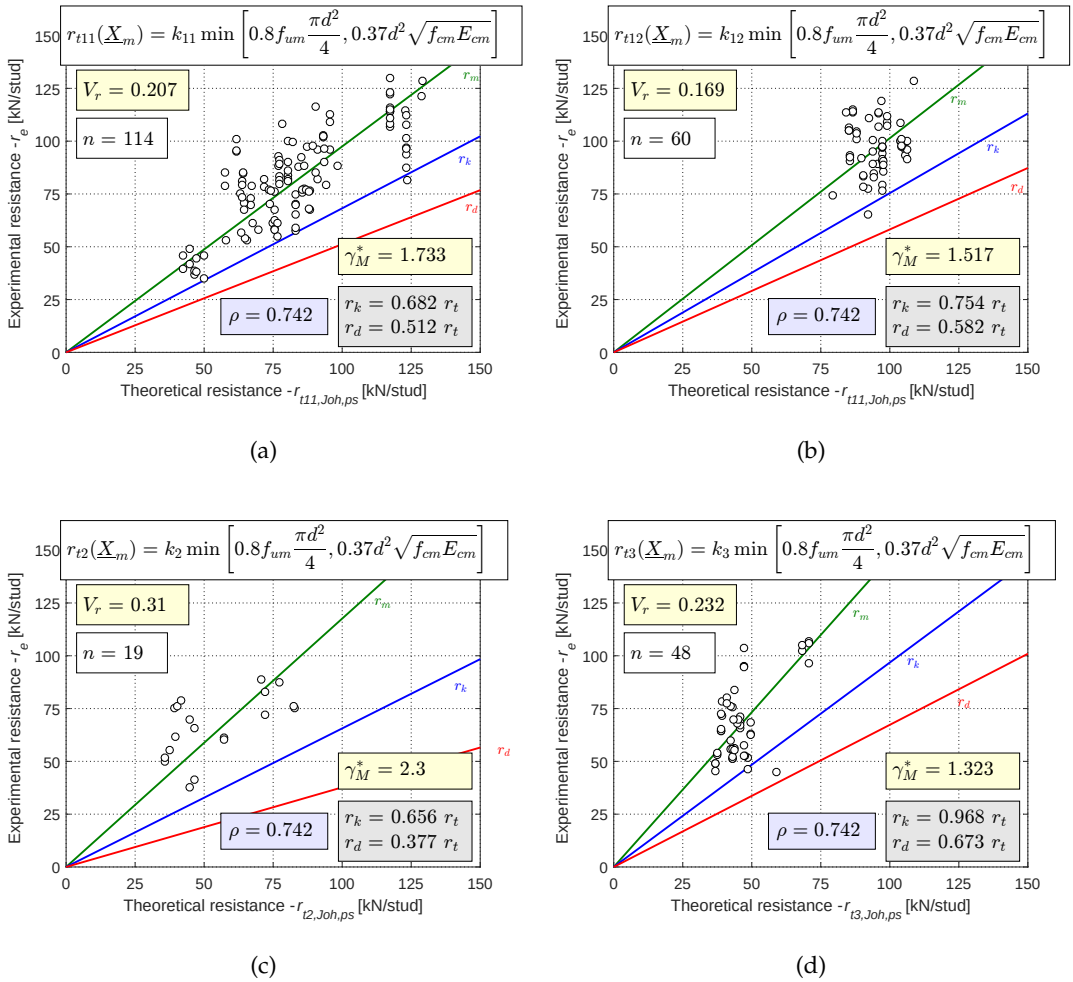

FIGURE 2.18: Comparison between experimental and theoretical resistance according to Johnson and Yuan (1998) design model for studs in profiled steel sheeting

As can be seen, the performance of the model is highly dependent on the subcase considered: the coefficient of variation V_r ranges between 16.9% and 31% whereas the linear correlation coefficient ρ of the entire design model is 0.779. In all four cases, the application of the design model leads to an unsafe prediction of the resistance with a target partial safety factor between 1.323 and 2.3 whereas a value of 1.25 was recommended. However, based on the original evaluation made by Johnson and Yuan (1998), the model is considered to be applicable within the following constraints:

- $h_{sc} - h_p > 35$ mm
- $0.8 \leq b_0/h_p < 3.2$
- d<20 mm for through-deck welded studs

- $2.8 \leq e_t \leq 5d$
- The strength class of the concrete is not higher than C35/45

The evaluations were re-performed within the field of application defined but the results do not change significantly, see Table 2.9. This might also be influenced by the reduced sample size of the subset considered. Slightly better performance are observed in case of re-entrant decks with a coefficient of variation of 10-18% but the prediction remains unconservative by around 14%.

TABLE 2.9: Results of the statistical evaluation of Johnson and Yuan (1998) design model for the resistance of studs in profiled steel sheeting

	All (Figure 2.18)				Field of application			
	Eq. (2.35)	Eq. (2.36)	Eq. (2.37)	Eq. (2.38)	Eq. (2.35)	Eq. (2.36)	Eq. (2.37)	Eq. (2.38)
n	114	60	19	48	98	59	12	19
ρ	0.742				0.668			
b	0.975	1.014	1.176	1.465	0.974	1.012	1.196	1.495
V_r	0.207	0.169	0.310	0.232	0.206	0.169	0.355	0.184
γ_M^*	1.733	1.517	2.300	1.323	1.785	1.519	3.156	1.168
γ_V	1.25	1.25	1.25	1.25	1.25	1.25	1.25	1.25
	Open trough decks				Re-entrant decks			
	Eq. (2.35)	Eq. (2.36)	Eq. (2.37)	Eq. (2.38)	Eq. (2.35)	Eq. (2.36)	Eq. (2.37)	Eq. (2.38)
n	82	52	18	35	32	8	1	13
ρ	0.744				0.683			
b	0.958	0.992	1.181	1.349	1.001	1.162	1.133	1.670
V_r	0.233	0.166	0.317	0.205	0.120	0.117	-	0.181
γ_M^*	1.982	1.539	2.373	1.336	1.330	1.173	-	1.065
γ_V	1.25	1.25	1.25	1.25	1.25	1.25	1.25	1.25

2.4.6 Konrad (2011) design model

Further to the design model proposed for studs in solid slabs, Konrad (2011) included a reduction factor for extending the scope to headed studs in composite slabs with profiled steel sheeting. Unlike EN 1994-1-1 (BSI, 2004b), this empirical reduction factor applies only to the equation considering concrete-related failures. The initial proposal included 6 different subcases depending on the ratio h_{sc}/h_p and the concrete spacing in front of the stud e_k defined in Figure 2.19. Then, the final expression was simplified as follows:

$$r_{t,Kon,ss} = \min\{r_{t1,Kon,ps}, r_{t2,Kon,ps}\} \tag{2.40}$$

and

$$r_{t1,Kon,ps} = 313 A_{col} \left(\frac{f_c}{30}\right)^{\frac{2}{3}} + 240 \left(\frac{f_u}{500}\right) d^2 \tag{2.41}$$

$$r_{t2,Kon,ps} = k_{\perp} \cdot \left[326 A_{col} \left(\frac{f_c}{30} \right)^{\frac{2}{3}} + 220 \left(\frac{f_c}{30} \right)^{\frac{1}{3}} \left(\frac{f_u}{500} \right)^{\frac{1}{2}} d^2 \right] \tag{2.42}$$

With:

$$k_{\perp} = \begin{cases} k_n \cdot \left[0.038 k_e \frac{b_0}{h_p} + 0.597 \right] \leq 1.0 & \begin{cases} \text{Pre-punched sheeting; and} \\ e_k > 55 \text{ mm} \end{cases} \quad (2.43) \\ k_n k_{Tr} \cdot \left[0.042 k_e \frac{b_0}{h_p} + 0.663 \right] \leq 1.0 & \begin{cases} \text{Through-deck welding; and} \\ e_k > 55 \text{ mm} \end{cases} \quad (2.44) \\ k_n \cdot \left[0.317 k_e \frac{b_0}{h_p} + 0.06 \right] \leq 0.8 & e_k \leq 55 \text{ mm} \quad (2.45) \end{cases}$$

$$k_n = \begin{cases} 1.0 & n_r = 1 \\ 0.8 & n_r = 2 \end{cases} \tag{2.46}$$

$$k_e = \begin{cases} 1 & 55 \text{ mm} < e_k \leq 100 \text{ mm} \\ 2 & e_k > 100 \text{ mm} \end{cases} \tag{2.47}$$

$$k_{Tr} = \begin{cases} 1.25 & \text{Re-entrant profiles} \\ 1.0 & \text{Open trough profiles} \end{cases} \tag{2.48}$$

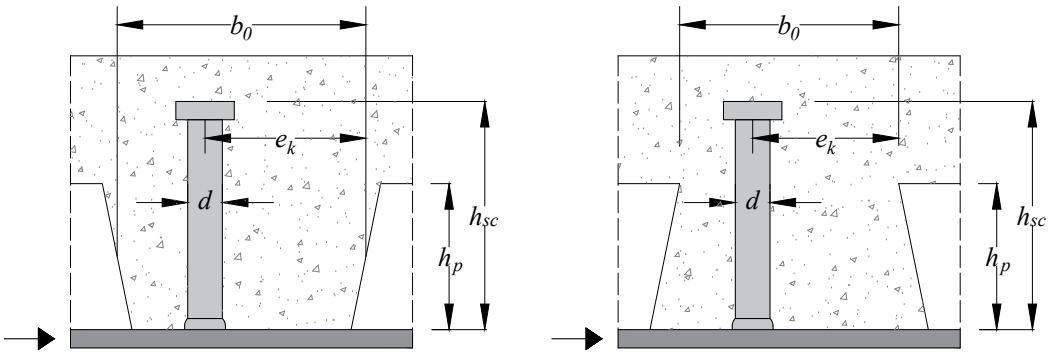

(a) (b)

FIGURE 2.19: Dimensions of headed stud shear connections with (a) open trough and (b) re-entrant sheeting according to Konrad (2011) design model

The proposed design resistance is equal to:

$$P_{Rd,Kon,ps} = \min\{P_{Rd1,Kon,ps}, P_{Rd2,Kon,ps}\} \tag{2.49}$$

and

$$P_{Rd1,Kon,ps} = \left[313 A_{col} \left(\frac{f_c}{30}\right)^{\frac{2}{3}} + 240 \left(\frac{f_u}{500}\right) d^2\right] \cdot \frac{1}{\gamma_V} \tag{2.50}$$

$$P_{Rd2,Kon,ps} = k_\perp \cdot \left[326 A_{col} \left(\frac{f_c}{30}\right)^{\frac{2}{3}} + 220 \left(\frac{f_c}{30}\right)^{\frac{1}{3}} \left(\frac{f_u}{500}\right)^{\frac{1}{2}} d^2\right] \cdot \frac{1}{\gamma_V} \tag{2.51}$$

With:

$\gamma_V = 1.25$ (recommended)

Only one of the tests fell within the domain of Eq.(2.41) while all the others are plotted in Figure 2.10. A good statistical correlation is found ($\rho = 0.795$) while the coefficient of variation is 21%. This model delivers a corrected partial safety factor γ_V^* of 1.48 which is ca. 18% higher than the proposed value $\gamma_V = 1.25$. The evaluation was also carried out in the recommended field of application defined by the following geometrical limits:

- $d \leq 20$ mm for through-deck welded studs
- $h_{sc}/h_p \geq 1.56$

In consideration of the conditions above, the remaining 191 tests were evaluated. As can be seen in Table 2.10, whilst the dispersion reduces slightly, the resistance equations are still unsatisfactory with an overprediction of 11%. However, this design model could be safely adopted for configurations with re-entrant profiled sheeting.

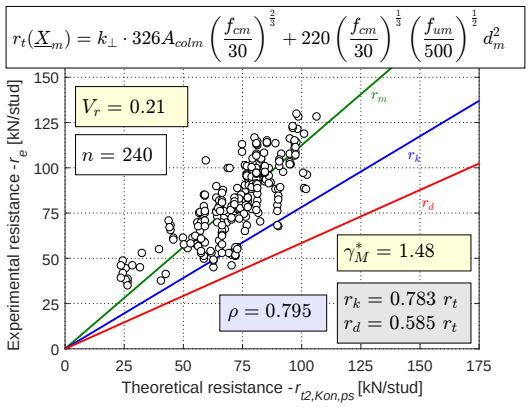

FIGURE 2.20: Comparison between experimental and theoretical resistance according to Konrad (2011) design model for studs in profiled steel sheeting

TABLE 2.10: Results of the statistical evaluation of Konrad (2011) design model for the resistance of studs in profiled steel sheeting

	All (Figure 2.20)		Field of application		Open trough decks		Re-entrant decks	
	Eq. (2.41)	Eq. (2.42)	Eq. (2.41)	Eq. (2.42)	Eq. (2.41)	Eq. (2.42)	Eq. (2.41)	Eq. (2.42)
n	1	240	1	190	1	186	0	54
ρ	0.795		0.754		0.756		0.695	
b	1.106	1.125	1.106	1.130	1.106	1.110	-	1.160
V_r	-	0.210	-	0.193	-	0.224	-	0.151
γ_M^*	-	1.480	-	1.399	-	1.566	-	1.228
γ_V	1.25	1.25	1.25	1.25	1.25	1.25	1.25	1.25

2.4.7 Comparison between different design models

The main results of the statistical evaluation for each design model in its field of application are summarized in Table 2.11, and the list of the main advantages and disadvantages is given in Table 2.12.

TABLE 2.11: Statistical evaluation of the design models for the resistance of studs in profiled steel sheeting in the respective field of application

	EN 1994-1-1 (2004b)		Lungershausen (1988)	Lloyd and Wright (1990)
	Eq. (2.20)	Eq. (2.21)	Eq. (2.27)	Eq. (2.31)
n	59	100	171	33
ρ	0.625		0.775	0.584
b	1.006	1.016	1.368	1.060
V_r	0.222	0.197	0.160	0.095
γ_M^*	1.902	1.623	1.191	1.242
γ_V	1.25	1.25	1.20	-

	Johnson and Yuan (1998)				Konrad (2011)	
	Eq. (2.35)	Eq. (2.36)	Eq. (2.37)	Eq. (2.38)	Eq. (2.41)	Eq. (2.42)
n	98	59	12	19	1	190
ρ	0.668				0.754	
b	0.974	1.012	1.196	1.495	1.106	1.130
V_r	0.206	0.169	0.355	0.184	-	0.193
γ_M^*	1.785	1.519	3.156	1.168	-	1.399
γ_V	1.25	1.25	1.25	1.25	1.25	1.25

It can be concluded that only Eq.(2.27) provides a conservative estimation of the design resistance of studs in profiled sheeting. Although this model represents a simple way to predict the capacity of the shear connection, it neglects the influence of several key variables that are acknowledged to have a considerable impact on the behaviour of the shear connection such as: concrete strength, through-deck welding and the position of the stud. It is also confirmed that the design model of EN 1994-1-1 (BSI, 2004b) is not adequately calibrated but it remains applicable to configurations with re-entrant decks. The more complex approach proposed by Johnson and Yuan

TABLE 2.12: Comparison between different design models for the resistance of studs in profiled steel sheeting

Design model	Advantages	Disadvantages
EN 1994-1-1 (2004b)	+ Good correlation and safe prediction in case of re-entrant sheeting + Easy-to-use: reduction factor to be added to the resistance of solid slabs	- Poor statistical fitting and unconservative for open trough sheeting - Eccentric position of the studs in the trough is not accounted - Actual failure modes of the studs in profiled sheeting are not considered
Lungershausen (1988)	+ Easy-to-use: only one equation + Low scattering and conservative prediction in its field of application	- Limited scope to studs with high embedment length - Several key variables are neglected
Lloyd and Wright (1990)	+ Easy-to-use: only one equation + Analytical definition of the concrete cone failure surface	- Poor statistical correlation with high scattering - Limited field of application - Ultimate strength of the stud material is neglected
Johnson and Yuan (1998)	+ All combination of failure modes are accounted	- Complex for practical use: 4 subcases to compute the reduction factor - Unconservative prediction
Konrad (2011)	+ Good statistical correlation with limited dispersion + Safe prediction in case of re-entrant sheeting	- Unconservative prediction - Actual failure modes are not considered

(1998) accounts for the influence of several parameters and failure modes without reaching fully satisfactory results. Lloyd and Wright (1990) design model shows a good agreement with the actual resistance only within a very limited scope of application defined by their own push-out test specimens. The approach of Konrad (2011) shows better correlation with test results with relatively low scattering and broad scope. However, the design equations are on the unsafe side as the corrected partial safety factor $\gamma_M^* = 1.399$ is higher than the recommended value of 1.25. Furthermore, the empirical nature of the model does not support the development of novel products where the failure modes may not be appropriately considered.

Chapter 3

Methodology

To reach the objectives fixed in Section 1.3, 21 experimental push-out tests on headed studs in profiled sheeting (Chapter 4) were designed and performed to check the influence of different parameters. Also, to evaluate the load bearing mechanisms activated in the shear connections in detail, some of the specimens were longitudinally cut at different displacements. In this way, the crack pattern developed in the concrete rib and the deformation of the studs can be studied in detail. In parallel, an extensive numerical study using a validated non-linear FE model was undertaken and presented in Chapter 5 to support the experimentally obtained results. Both experimental and numerical outcomes represent the basis for the development of the sequence of load bearing mechanisms described in Chapter 6. The mechanical models and the respective analytical equations were finally derived (Chapter 7) and statistically calibrated according to EN 1990 (BSI, 2002) for design applications (Chapter 8). A summary of the methodology followed in the current work is visualized in the flow chart in Figure 3.1.

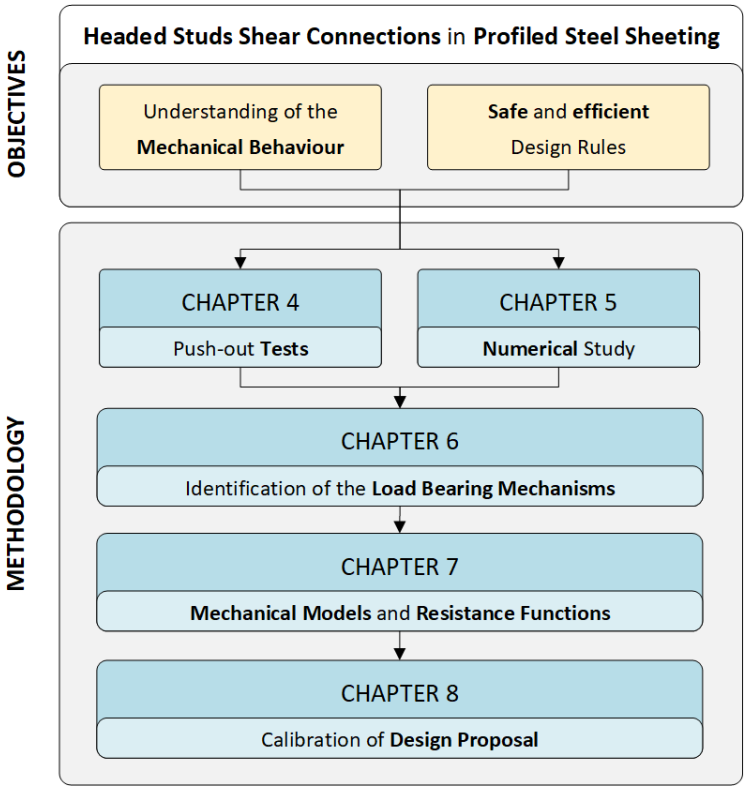

FIGURE 3.1: Methodology and objectives of the thesis

Chapter 4

Push-out tests

As discussed in Chapter 2, the push-out test represents the most convenient procedure to evaluate the structural performance of shear connectors used in composite beams without carrying out more time consuming beam tests. Moreover, according to previous experimental studies (Rambo-Roddenberry, 2002; Hicks, 2009; Nellinger, 2015), push-out tests without the application of the transversal load on the slab delivers conservative values of the resistance of the headed stud shear connections compared to the respective beam test configuration.

Based on the previous considerations, to assess the performance of novel products appearing on the market, a set of 21 push-out tests was performed at University of Luxembourg using the open trough steel sheeting ArcelorMittal Cofraplus® 60. To comprehend the actual bearing mechanisms activated in the shear connections, especially at low slips, some tests were intentionally stopped at certain displacements and longitudinally cut.

In addition, the influence of the following design parameters on the performance of the connection was investigated:

- Recess
- Waveform rebar
- Welding type
- Position of the wire mesh
- Stud height
- Slab depth

After describing the preparation and the execution of the tests from Section 4.1 to 4.5, the results are presented and discussed in Section 4.6 and 4.7, respectively. Finally a summary is provided in Section 4.8

4.1 Preparation of the test specimen

All the push-out specimens consist of two headed studs welded onto each of the flanges of a HE 260 B steel beam embedded in composite slabs using the profiled sheeting ArcelorMittal Cofraplus® 60 (ArcelorMittal-Construction, 2015) shown in Figure 4.1.

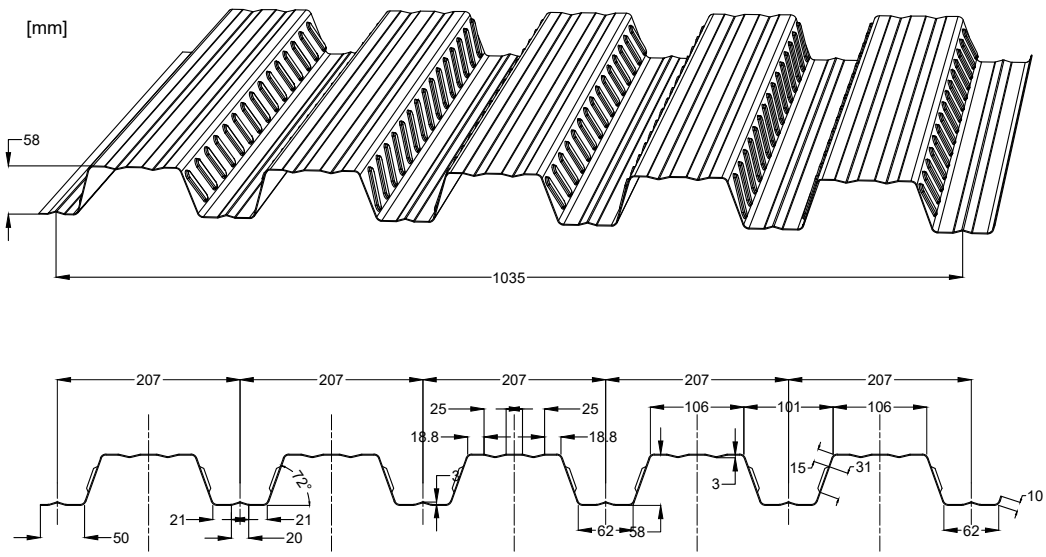

FIGURE 4.1: Dimensions of the profiled sheeting ArcelorMittal Cofraplus® 60

Both concrete slabs were cast horizontally as shown in Figure 4.2. Four polypropylene tubes were included in each slab in correspondence with four additional prepunched holes to accommodate the tension bars through the slabs, as explained later in Section 4.2. In addition to the wire mesh layer, local reinforcement was added to prevent back-breaking failure as well as local crushing failure at the slab foot.

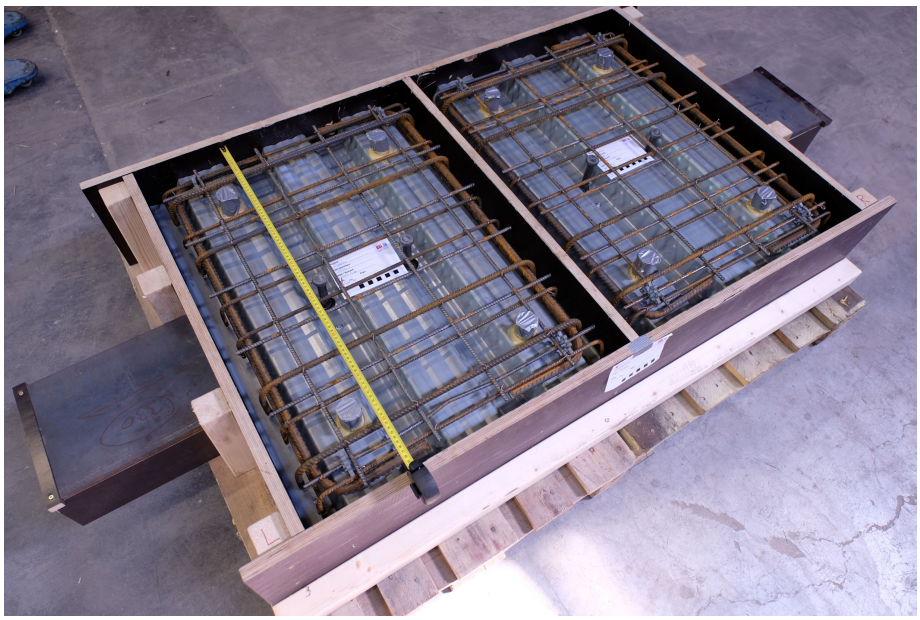

FIGURE 4.2: Test specimen before concreting

After casting both half specimens, the two parts were welded together before being placed into the testing frame. While the slab dimensions were kept constant, see Figure 4.3, their depth was 120 mm or 140 mm depending on the configuration.

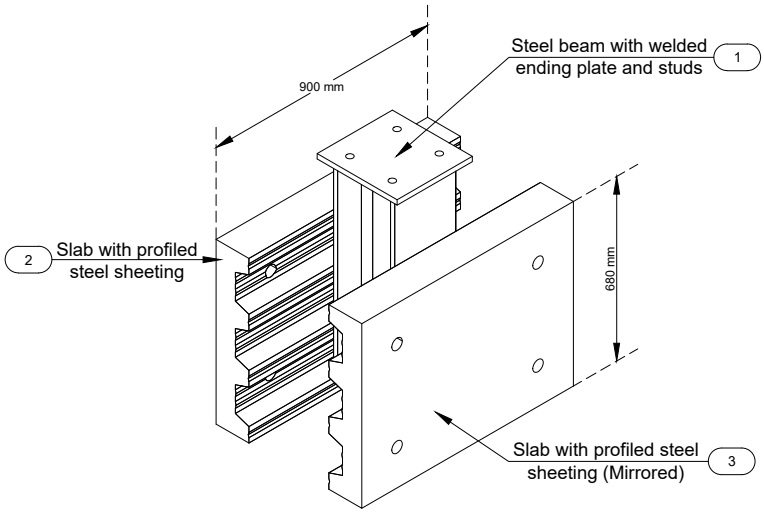

FIGURE 4.3: Isometric view of the test specimen

4.2 Setup and instrumentation

Once the test specimens were assembled, they were moved into the testing frame under a 1MN capacity hydraulic jack available in the Laboratory of steel structures at University of Luxembourg. The specimens were bedded on a mortar layer. However, owing to the eccentricity of the reaction forces caused by the depth of the steel sheeting, the base of the slab may undergo unwanted lateral movements if the frictional resistance at the base is exceeded. In this case, some uplift occurred between the slab and the steel beam inducing additional tensile forces in the stud. In order to prevent this phenomenon, the base of the specimens was restrained by means of two threaded tie bars. These were fixed by nuts which were tightened by hand. The setup of the specimen in the frame is shown in Figure 4.4.

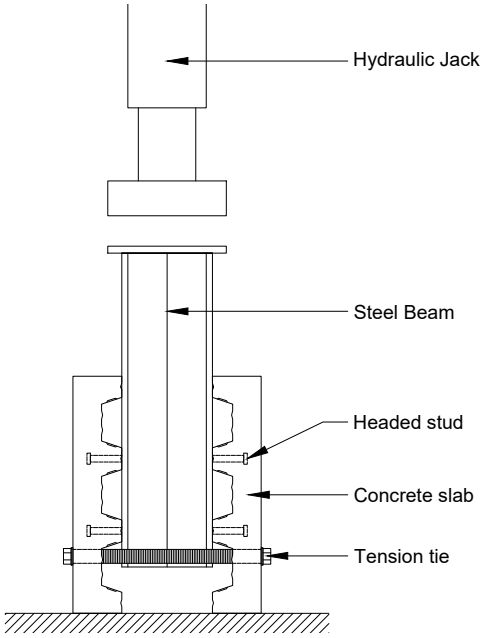

FIGURE 4.4: Side view of the test setup of the experimental study

A total of 12 linear variable displacement transducers (LVDT) were used for each specimen to measure the displacements of different parts throughout the testing procedure. The location and the respective ID number of each LVDT is shown in Figure 4.5. The longitudinal slip between the concrete slab and the steel beam was detected continuously during the entire test by six LVDTs. Two of them (01, 02) measured the relative displacement between the beam and the upper surface of the slab while four sensors (11, 12, 13, 14) were attached to the inner side of the specimen to detect the relative slip at a lower location. Because of the tension ties fixed at the bottom of the slabs, the upper part of the specimen may undergo outward deformations, especially at high slips. For this reason, three more LVDTs were fixed to an ad-hoc aluminium frame to measure the lateral movement of the concrete slabs (21, 22, 23 and 24, 25, 26).

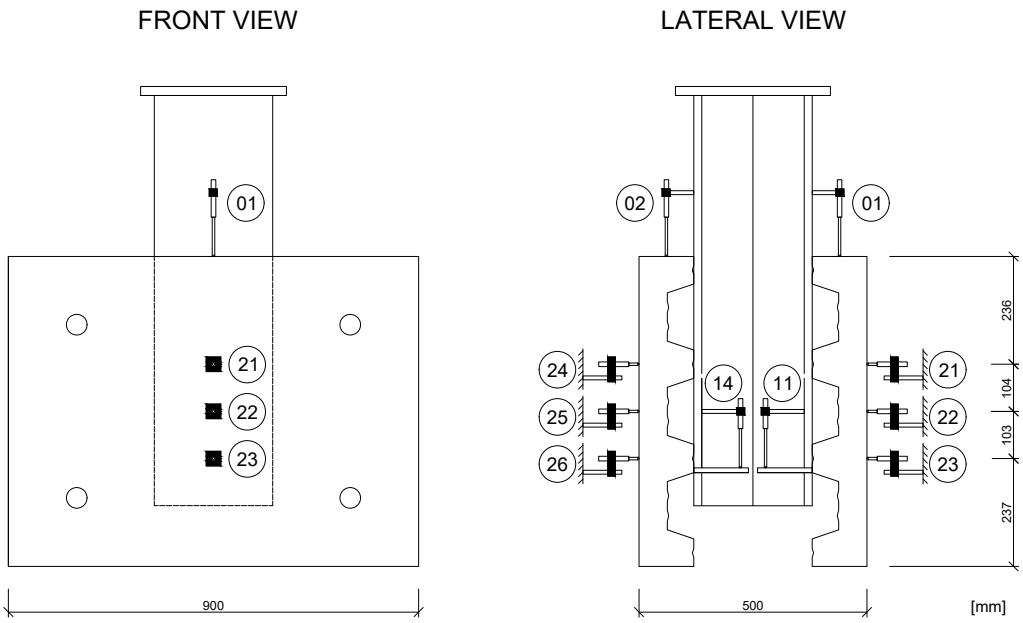

FIGURE 4.5: Position of the LVDT sensors

The transverse displacement between the beam and the profiled steel sheeting in proximity of the connector (uplift) was not measured because it was thought that the rotation of the rib affect the results. Starting from test CP12C-2, the force taken by the bottom tension ties was included in the measurements via two load cells placed between the nut and the slab, see Figure 4.6a. Only the test series using waveform reinforcement bars was instrumented with additional strain gauges as seen in Figure 4.6b. Such devices were used to measure the tensile strain of the rebar at the expected location of the crack.

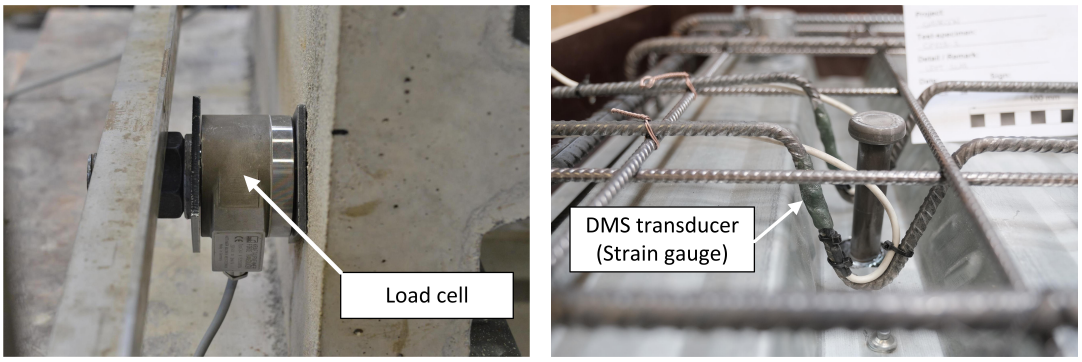

(a) (b)

FIGURE 4.6: (a) Load cell installed at the bottom tension ties and (b) strain gauge glued on the waveform rebar

4.3 Testing procedure

All tests were conducted in accordance with the guidelines provided by EN 1994-1-1 B.2.4 (BSI, 2004b). The load was first applied up to 40% of the expected peak. Then, 25 load cycles between 5% and 20% of the predicted failure load were introduced at a frequency of 0.011 cycles per second. After that, the hydraulic jack was switched to displacement-controlled mode with a constant speed of 0.4 mm/min. To identify the stiffness of the shear connection at different stages, the load was increased gradually. The specimen was completely unloaded at a load level of 60% of the predicted resistance and at the slip displacement of ca. 6 mm, 10 mm and 25 mm. 5-minute pauses were also introduced at ca. 2 mm, 4 mm 8 mm and 15 mm slip to check the load reduction caused by the short-term relaxation of the concrete.

4.4 Test program

A summary of the nominal properties of all the test series is given in Table 4.1. The impact of the investigated parameters on the behaviour of the shear connection was assessed by comparing tests where only the considered variable differs. The paired test series relative to each variable are indicated in Table 4.2.

TABLE 4.1: Data of the test series

Test series	Sheeting product	d [mm]	h_{sc}[a] [mm]	n_r [-]	Weld [-]	h_{slab}[b] [mm]	Concrete class	Recess	Wire mesh	Waveform rebar
CP12A	Cofraplus 60	19	100	1	PP	120	C35/45	No	Low	No
CP12B	Cofraplus 60	19	100	1	PP	120	C35/45	No	Low	Yes
CP12C	Cofraplus 60	19	100	1	PP	120	C35/45	Yes	Low	No
CP14A	Cofraplus 60	19	100	1	PP	140	C40/50[c]	No	Low	No
CP14B	Cofraplus 60	19	100	1	PP	140	C40/50[c]	No	High	No
CP14C	Cofraplus 60	19	100	1	TD	140	C40/50[c]	No	High	No
CP14D	Cofraplus 60	19	125	1	PP	140	C35/45	No	Low	No

[a] h_{sc} is the nominal as-welded length of the stud
[b] h_{slab} is the overall depth of the slab
[c] The concrete class was supposed to be C35/45. To have a consistent comparison, the results will be normalized on the measured concrete strength

TABLE 4.2: Investigated parameters of the experimental study

Parameters \ Series	CP12A	CP12B	CP12C	CP14A	CP14B	CP14C	CP14D
Recess	A		A				
Waveform rebar	B	B					
Welding type					C	C	
Position of wire mesh				D	D		
Height of the stud				E			E
Slab depth	F			F			

4.5 Material properties

The compressive strength of concrete was measured by testing 150 mm cubes and 150x300 mm cylinders, shown in Figure 4.7. For each mixture, 15 cylinder specimens and 6 cubes were prepared and tested in parallel with the push-out tests. To evaluate the mean compressive cylinder strength f_{cm} at the exact date of testing, the results were interpolated using the exponential function recommended by EN 1992-1-1 (BSI, 2004a). All the concrete samples were air-cured alongside the push-out specimens in compliance with EN 1994-1-1 B.2.3 (BSI, 2004b).

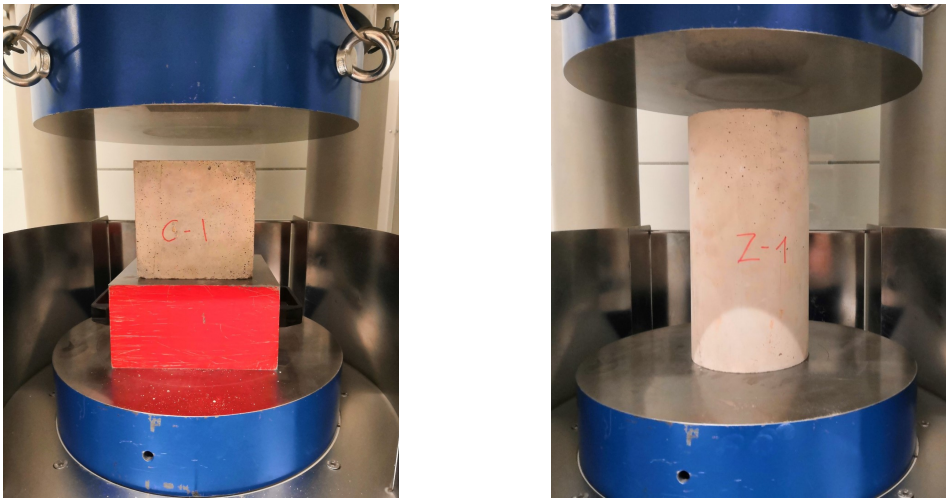

(a) (b)

FIGURE 4.7: Concrete (a) cube and (b) cylinder before testing

All the headed stud shear connectors considered in this study belong to the type "SD1" according to ISO/TC44/SC10 (2017) , with a minimum (specified) ultimate tensile strength of 470 MPa. As given by ArcelorMittal-Construction (2015), the steel of the profiled sheeting Cofraplus® 60 is S350GD+ZM175.

The properties of the stud and profiled sheeting material employed in this experimental campaign were determined via tensile tests. The specimens were prepared in accordance with the guidelines of ISO 6892-1(ISO/TC164/SC1, 2019), see Figure 4.8. The average measured material properties of each specimen are listed in Table 4.3. Further details of all tests conducted on the materials are provided in Appendix D.1.

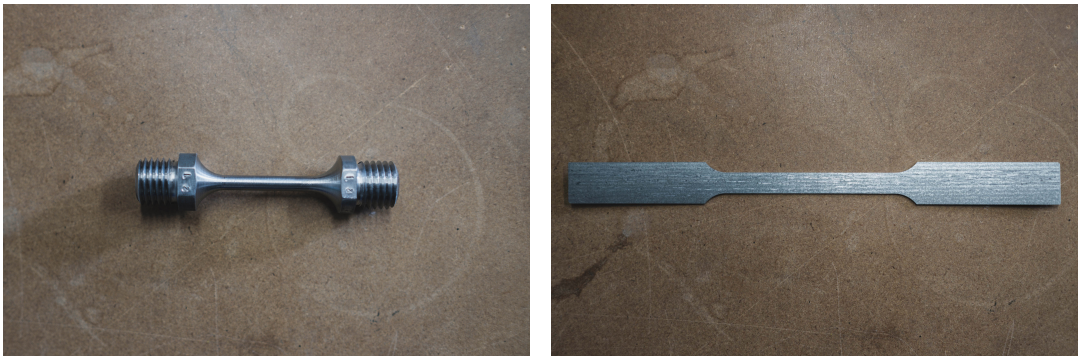

(a) (b)

FIGURE 4.8: Machined tensile test specimens of (a) headed stud and (b) profiled steel sheeting

TABLE 4.3: Summary of the measured material properties

Test series	Concrete Cylinder strength - f_c [MPa]	Headed stud Tensile strength - f_u [MPa]	Profiled sheeting Yielding strength - f_{yp} [MPa]
CP12A-1	42.2		
CP12A-2	42.9	551.0	385.0
CP12A-3	44.0		
CP12B-1	42.2		
CP12B-2	42.6	551.0	385.0
CP12B-3	43.2		
CP12C-1	45.7		
CP12C-2	46.0	551.0	385.0
CP12C-3	46.5		
CP14A-1	49.3		
CP14A-2	49.7	551.0	385.0
CP14A-3	50.2		
CP14B-1	50.7		
CP14B-2	50.8	551.0	385.0
CP14B-3	51.1		
CP14C-1	51.8		
CP14C-2	51.9	551.0	385.0
CP14C-3	52.0		
CP14D-1	43.5		
CP14D-2	43.7	504.3	385.0
CP14D-3	44.2		

4.6 Test results

The results of the conducted push-out tests are presented in this section for each series with particular emphasis on the load-slip curves and the observed failure modes. In all the experimental curves, the slip displacement was taken as an average of the measurements detected by the LVDT 01 and 02 as the data of 11, 12, 13 and 14 was not always available. Since the minimum characteristic slip capacity for ductile connectors is 6 mm according to EN 1994-1-1 (BSI, 2004b), the experimental resistance of the connector P_e was taken as the maximum load within the first 6 mm of slip. The ductility of each push test series was always defined in terms of characteristic slip capacity in accordance with EN 1994-1-1, as detailed in Section 4.7.1. The properties and the results of each test are detailed in Appendix D.2.

4.6.1 CP12A series

In this test series, a single 19 mm diameter headed stud with the nominal height of 100 mm was welded directly on the beam top flange through pre-punched holes in each rib. One Q188A wire mesh was placed at ca. 20 mm above the deck rib. The geometry of the configuration CP12A is provided in Figure 4.9 while Table 4.4 summarizes the main measured data of each push-out test, including the measured as-welded length of the stud h_{scm}. The experimental load-slip curves obtained from the tests are given in Figure 4.10.

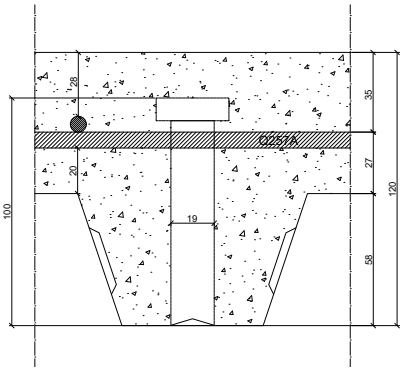

FIGURE 4.9: Detail of the configuration CP12A

CP12A	-1	-2	-3
f_{cm} [MPa]	42.2	42.9	44.0
f_{um} [MPa]	551.0	551.0	551.0
n_r [-]	1	1	1
d [mm]	19	19	19
h_{scm} [mm]	98	98	98
P_e [kN/stud]	68.31	65.25	69.48
Failure mode(s)	RP CPO	RP CPO	RP CPO

TABLE 4.4: Main measured data of the test series CP12A

For all tests, the maximum load was achieved at ca. 2-6 mm followed by a smooth softening branch. The tests were finally stopped at ca. 25 mm where the load reduced by around 40% compared to the peak. The average experimental resistance is 67.7 kN/stud with a maximum deviation from the mean of 3.6%. From the observation of the longitudinal cut of the specimen CP12A-3 in Figure 4.11, it can be seen that the failure occurs gradually due to the progressive crushing of the concrete in front of the stud leading to the bulging of the steel deck: this is the so called "rib punching" (RP) failure. It could be assumed that at higher displacements, owing to the higher tensile forces in the stud, the concrete cone underneath the connector is pulled out of the slab resulting in the "concrete pull-out" (CPO) failure.

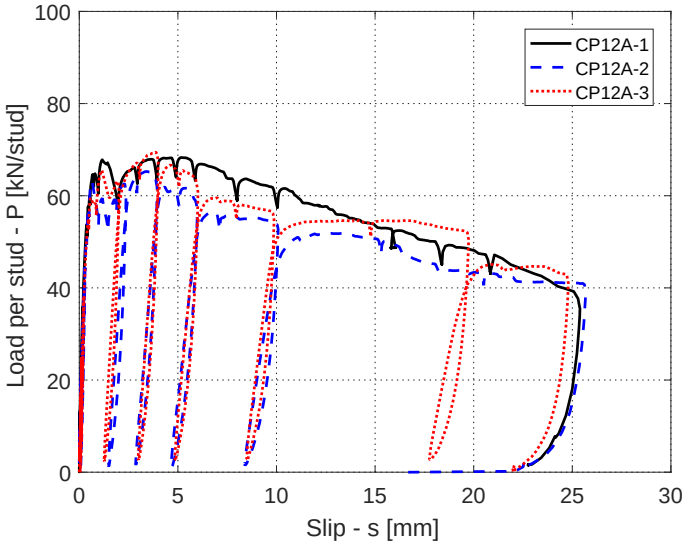

FIGURE 4.10: Experimental load-slip curve of the test series CP12A

FIGURE 4.11: Cut section of the CP12A-1 specimen after testing at a slip of ca. 25 mm

4.6.2 CP12B series

From the collaboration with "Arcelormittal Global R&D Long Products Luxembourg" and Prof. Schäfer, waveform reinforcement bars were proposed and included in the specimens of this series. The target is to enhance the performance of the stud connector employed in this type of profiled sheeting with particularly narrow troughs.

The test series CP12B aims to check the influence of the waveform rebars on the performance of the shear connection. This additional rebars were included in the rib as shown in Figure 4.12 and the main measured properties are provided in Table 4.5. The load-slip curves in Figure 4.13 shows an average resistance of ca. 85.27 kN/stud with a maximum deviation of 5.4% from the mean. As can be seen, the addition of these special rebars enhances also the ductility of the shear connection.

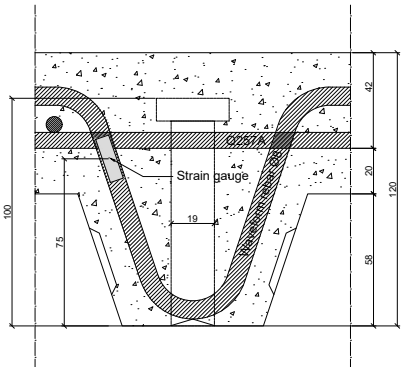

FIGURE 4.12: Detail of the configuration CP12B

CP12B	-1	-2	-3
f_{cm} [MPa]	42.2	42.6	43.2
f_{um} [MPa]	551.0	551.0	551.0
n_r [-]	1	1	1
d [mm]	19	19	19
h_{scm} [mm]	98	98	98
P_e [kN/stud]	81.28	83.74	90.66
Failure mode(s)	RP CPO	RP CPO	RP CPO

TABLE 4.5: Main measured data of the test series CP12B

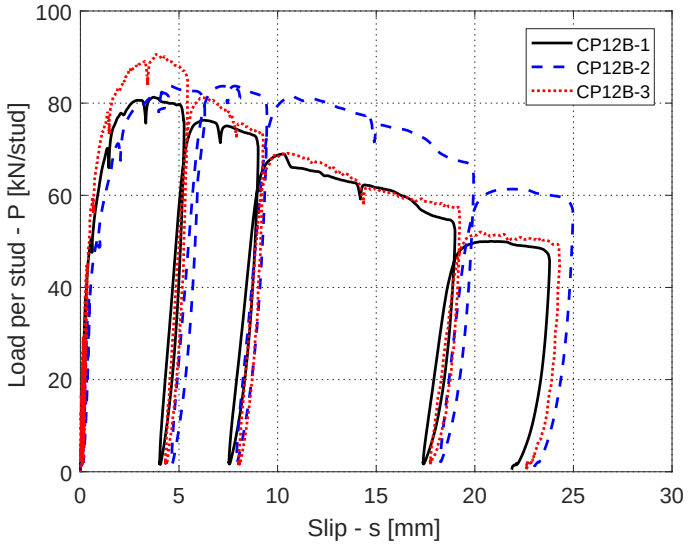

FIGURE 4.13: Experimental load-slip curve of the test series CP12B

The positive influence of these special bars is confirmed by the measurements of the strain gauges (SG2, SG3 and SG4) acquired during the test CP12B-1, see Figure 4.14. At ca. 1-2 mm slip the tensile strain starts to increase linearly until a slip displacement of up to around 10-15 mm. All tests experienced rib punching at low slips while the concrete pull-out failure occurred at higher displacements.

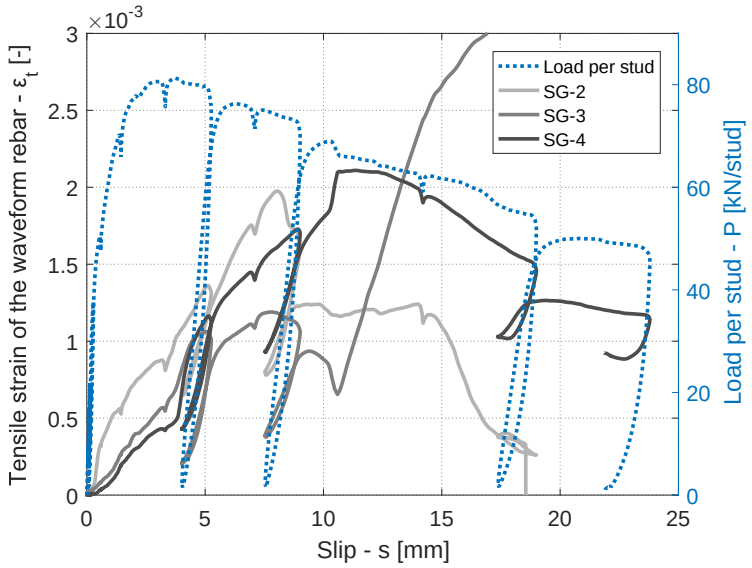

FIGURE 4.14: Measured tensile strain of the waveform rebar and load-slip curve of the CP12B-1

4.6.3 CP12C series

The specimens of the CP12C series are nominally identical to tests CP12A with the exception of the 200 mm wide recess introduced at the base of both slabs. To avoid any modification of the geometry of the specimens, the recess was created through the mortar bed. The detail of the geometry is given in Figure 4.15 and the main measured properties are provided in Table 4.6. The load-slip measurements in Figure 4.16 shows an average experimental resistance of 71.6 kN/stud with a maximum deviation of 5.4%. Tests CP12C-1 and CP12C-2 experienced rib punching at low displacements followed by concrete pull-out failure.

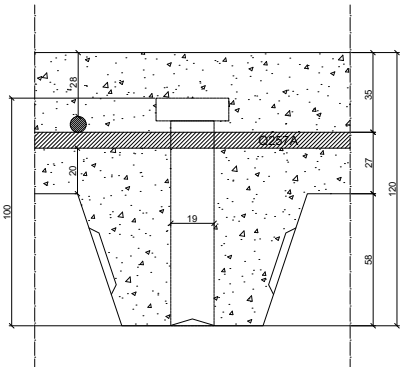

FIGURE 4.15: Detail of the configuration CP12C

CP12C	-1	-2	-3[a]
f_{cm} [MPa]	45.7	46.0	46.5
f_{um} [MPa]	551.0	551.0	551.0
n_r [-]	1	1	1
d [mm]	19	19	19
h_{scm} [mm]	98	98	98
P_e [kN/stud]	69.27	75.53	70.09
Failure mode(s)	RP CPO	RP CPO	-

TABLE 4.6: Main measured data of the test series CP12C

[a]The specimen CP12C-3 was intentionally stopped at ca. 2 mm slip

From the test CP12C-2, the tensile forces activated in the bottom bars were measured by means of load cells and the resulting total force T (acting on each slab) is plotted

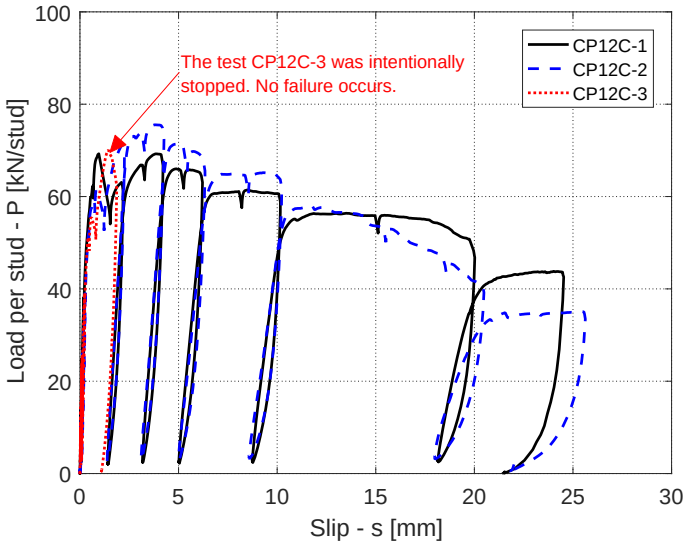

FIGURE 4.16: Experimental load-slip curve of the test series CP12C

in Figure 4.17 together with the outward inclination angle α_s of the slab measured by the lateral LVTDs. It is clear that the angle α_s is proportional to the forces T that prevent the lateral sliding at the base owing to the eccentricity of the load. At higher displacements, this phenomenon induces further pulling forces in the upper row of studs.

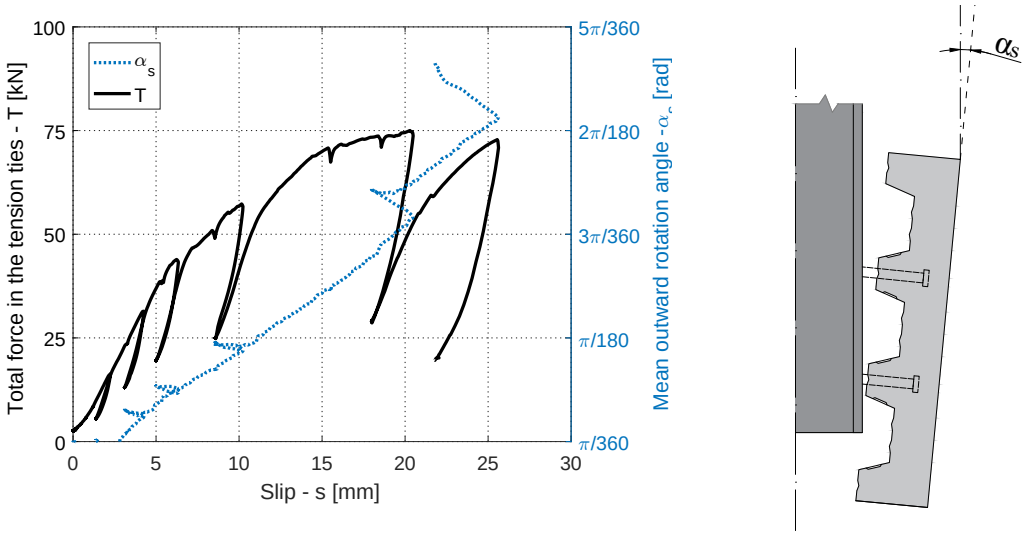

FIGURE 4.17: Total forces in the tension ties T and outward rotation angle α_s of the specimen CP12C-2

The test CP12C-3 was intentionally stopped at a slip of ca. 2 mm to investigate the damage of the concrete around the stud. After testing, the specimen was longitudinally cut as displayed in Figure 4.18. The typical concrete cone crack path is clearly visible but it is not fully developed. On the other hand, the concrete rib is almost intact and it seems that rib punching failure has not occurred yet. Therefore, based on the respective load-slip curve in Figure 4.16, it can be preliminarily stated that the first peak load at ca. 1-2 mm is governed by the cracking of the concrete cone.

FIGURE 4.18: Cut section of the specimen CP12C-3 at a slip of ca. 2 mm

4.6.4 CP14A series

In this test series, the slab depth was increased to 140 mm while the position of the Q188A wire mesh was kept 20 mm above the deck as in the previous tests. The respective geometry is given in Figure 4.19 and the key test results are shown in Table 4.7. The load-slip curve of each specimen is provided in Figure 4.20. The test specimen CP14A-1 was accidentally loaded at high displacement rate from ca. 0.6 mm up to around 5 mm slip. Therefore, this test was not considered in the evaluation of the results. Considering the other two tests (CP14A-2 and CP14A-3) a first local peak was reached at 1-2 mm slip followed by a second higher peak within 3-6 mm. The average experimental resistance is 77.4 kN/stud with a maximum deviation of 6.5%. Both tests exhibited a ductile behaviour and they were stopped after a load reduction of 40-50% at around 25 mm slip.

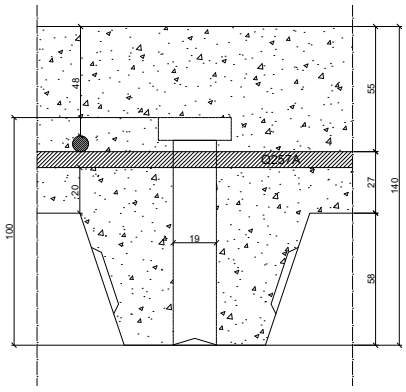

FIGURE 4.19: Detail of the configuration CP14A

CP14A	-1[a]	-2	-3
f_{cm} [MPa]	49.3	49.7	50.2
f_{um} [MPa]	551.0	551.0	551.0
n_r [-]	1	1	1
d [mm]	19	19	19
h_{scm} [mm]	98	98	98
P_e [kN/stud]	85.66	72.35	82.47
Failure mode(s)	RP CPO	RP CPO	RP CPO

TABLE 4.7: Main measured data of the test series CP14A

[a]The specimen CP14A-1 was accidentally loaded at high displacement rate up to 5 mm slip

In all three specimens, the cone failure surface was clearly visible after demounting, as shown in Figure 4.21a. Notwithstanding that only one plastic hinge was observed in the studs after demounting, see Figure 4.21b, the double curvature may develop at lower displacements. This aspect was investigated numerically and discussed in Chapter 5.

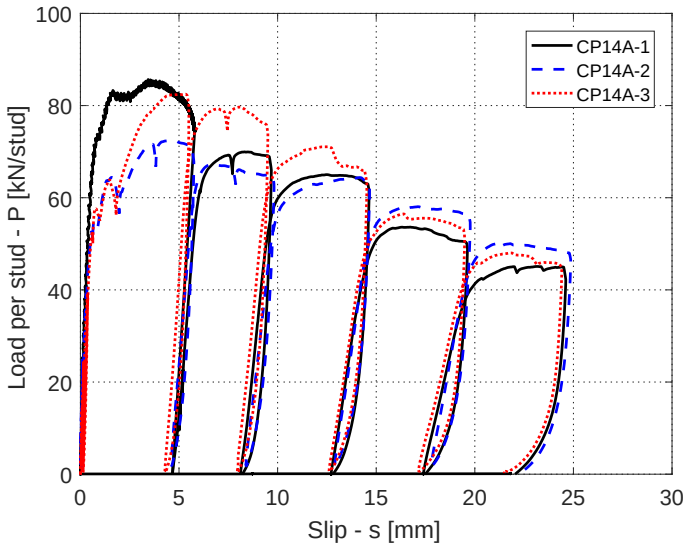

FIGURE 4.20: Experimental load-slip curve of the test series CP14A

(a) (b)

FIGURE 4.21: (a) Cone failure surface and (b) stud deformation after demounting the specimen of the series CP14A

4.6.5 CP14B series

The samples of these series are nominally identical to the test series CP14A with the exception of the position of the reinforcement mesh layer: the Q188A wire mesh was moved 40 mm above the deck. In this way, the longitudinal reinforcing bars should not prevent or delay the propagation of the concrete cone cracks. The geometry of the specimen is shown in Figure 4.22 and the main measured parameters are given in Table 4.8. Figure 4.23 shows the load-slip curves of each specimens: the average measured resistance is 84.9 kN/stud with a maximum deviation of 5.2% from the mean. Again, the failure modes observed were rib punching followed by concrete pull-out at higher displacements.

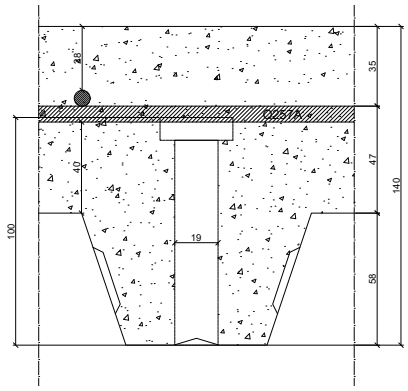

FIGURE 4.22: Detail of the configuration CP14B

CP14B	-1	-2	-3
f_{cm} [MPa]	50.7	50.8	51.1
f_{um} [MPa]	551.0	551.0	551.0
n_r [-]	1	1	1
d [mm]	19	19	19
h_{scm} [mm]	98	98	98
P_e [kN/stud]	85.46	80.45	88.70
Failure mode(s)	RP CPO	RP CPO	RP

TABLE 4.8: Main measured data of the test series CP14B

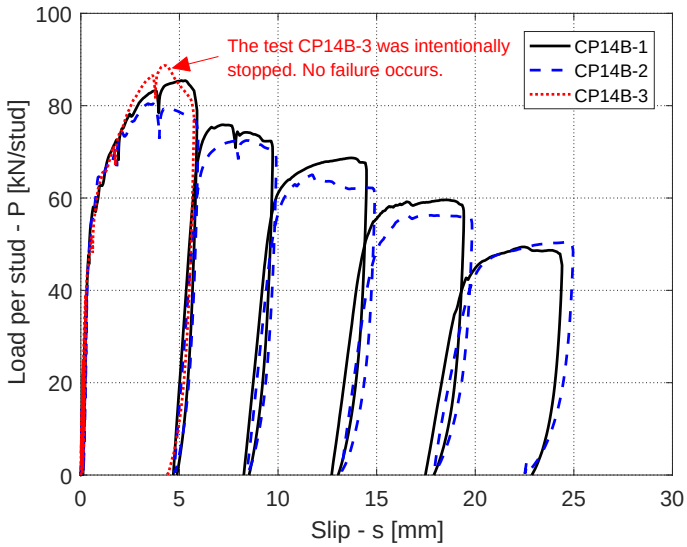

FIGURE 4.23: Experimental load-slip curve of the test series CP14B

To identify the evolution of the damage pattern around the stud throughout the tests, the test CP14B-3 was stopped at ca. 6 mm slip and longitudinally cut, as can be seen in Figure 4.24. At this stage, the concrete cone crack pattern is fully developed and one of the concrete ribs is importantly damaged owing to the rib punching (RP) failure.

FIGURE 4.24: Cut section of the specimen CP14B-3 after testing at a slip of ca. 6 mm

4.6.6 CP14C series

The headed studs of the specimens CP14C were welded through the profiled sheeting while the location of the wire mesh was kept 40 mm above the rib as in the series CP14B, see Figure 4.25. In order to accommodate for through-deck welded studs, the profiled steel sheeting used in this series does not have the central stiffener in the trough (Cofraplus 60® C). The main measured data is provided in Table 4.7 and the load-slip plots are shown in in Figure 4.26. CP14C-2 and CP14C-3 behaved similarly with a mean experimental resistance of 85.24 kN/stud and a deviation of only 0.2%. Compared to CP14B test series, the peak load is slightly delayed at ca. 5-8 mm.

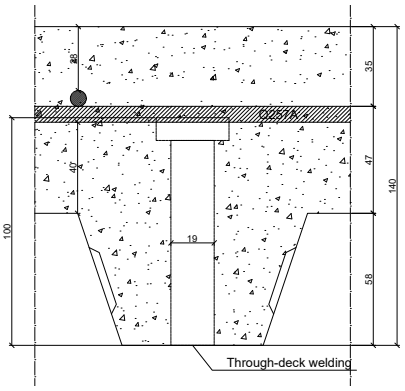

FIGURE 4.25: Detail of the configuration CP14C

CP14C	-1	-2	-3
f_{cm} [MPa]	51.8	51.9	52.0
f_{um} [MPa]	551.0	551.0	551.0
n_r [-]	1	1	1
d [mm]	19	19	19
h_{scm} [mm]	94	94	94
P_e [kN/stud]	66.56	83.54	85.08
Failure mode(s)	RP CPO	RP CPO	RP CPO

TABLE 4.9: Main measured data of the test series CP14C

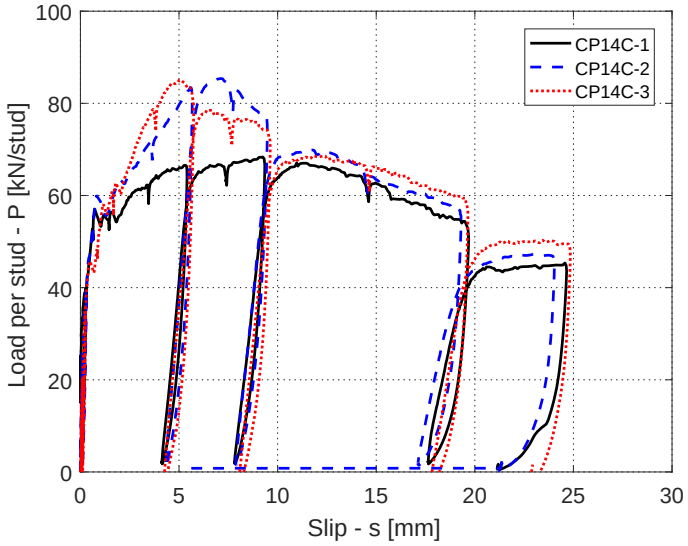

FIGURE 4.26: Experimental load-slip curve of the test series CP14C

As the test CP14C-1 delivers an unexpected low resistance which can be explained by the weld quality of one of the studs. It was observed that, compared to a standard through-deck welded stud, the weld fillet at the base of the connector of the specimen CP14C-1 was only partially formed, as shown in Figure 4.27a. After demounting the sample and removing the steel sheeting, it was confirmed that the stud base was not perfectly welded to the beam as shown in 4.27b.

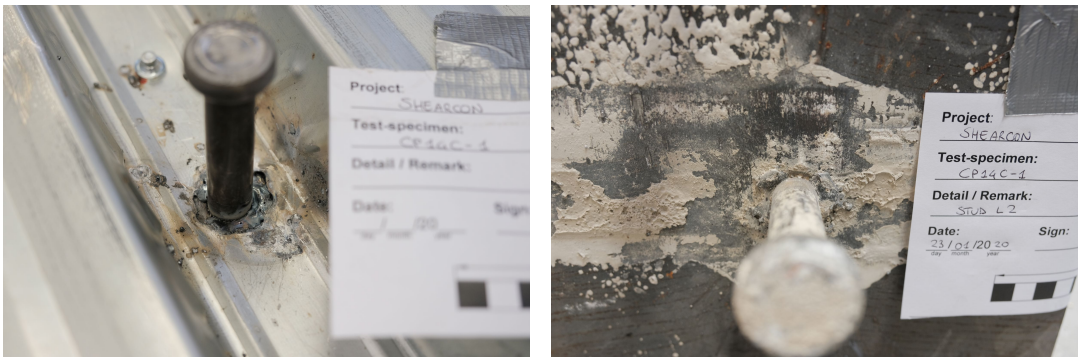

(a) (b)

FIGURE 4.27: Weld fillet of the through-deck welded stud of the specimen CP14C-1: (a) before and (b) after testing

4.6.7 CP14D series

Unlike all the previous tests, the series CP14D uses 125mm long headed studs. The wire mesh was placed on the lower position, i.e. 20 mm above the rib, which corresponds to exactly 30 mm below the head of the stud, see Figure 4.28. The main test results are shown in Table 4.10 while the full load-slip measurements are given in Figure 4.29. The average maximum capacity was 84.28 kN/stud with a deviation of less than 5%. After demounting the specimens, most of the studs were fully ruptured as shown in Figure 4.30: this explains the sudden load reduction observed in the load-slip curves at ca. 18-23 mm slip. Also, the higher embedment length of the stud allowed the development of a double plastic curvature of the connector that was still visible at high displacements.

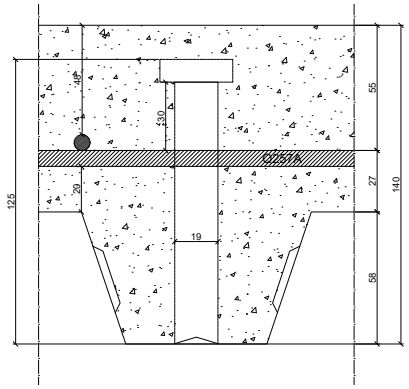

FIGURE 4.28: Detail of the configuration CP14D

CP14D	-1	-2	-3
f_{cm} [MPa]	43.5	43.7	44.2
f_{um} [MPa]	504.3	504.3	504.3
n_r [-]	1	1	1
d [mm]	19	19	19
h_{scm} [mm]	94	94	94
P_e [kN/stud]	80.33	87.31	85.19
Failure mode(s)	RP CPO, SR	RP CPO, SR	RP CPO, SR

TABLE 4.10: Main measured data of the test series CP14D

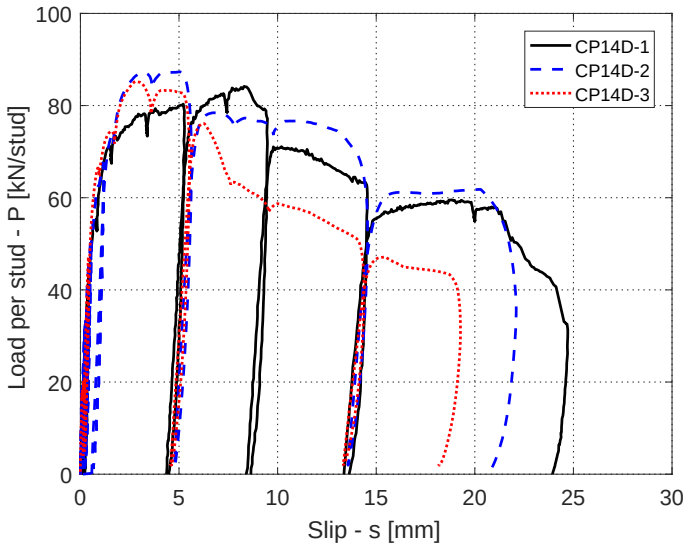

FIGURE 4.29: Experimental load-slip curve of the test series CP14D

FIGURE 4.30: Headed studs of the specimen CP14D-1 after rupture

4.7 Discussion of test results

4.7.1 Test assessment according to EN 1994-1-1 B.2.5 (BSI, 2004b)

As alternative to the statistical procedure described in Appendix A, EN 1994-1-1 B.2 (BSI, 2004b) allows to estimate the characteristic resistance and slip capacity of each test series using an easier procedure. Hence, considering the value $P_{e,i}$ as the resistance of the i^{th} test of the series, the respective characteristic resistance can be taken as:

$$P_{Rk,B2} = 0.9 \min_i \{P_{e,i}\} \tag{4.1}$$

The corresponding slip capacity $\delta_{u,B2}$ of each specimen can be calculated as the maximum slip value at which the load is equal to $P_{Rk,B2}$, as shown in Figure 4.31.

The characteristic value $\delta_{uk,B2}$ shall be taken as the minimum of the slip capacity values $\delta_{ui,B2}$ reduced by 10%:

$$\delta_{uk,B2} = 0.9 \min_i \{\delta_{ui,B2}\} \tag{4.2}$$

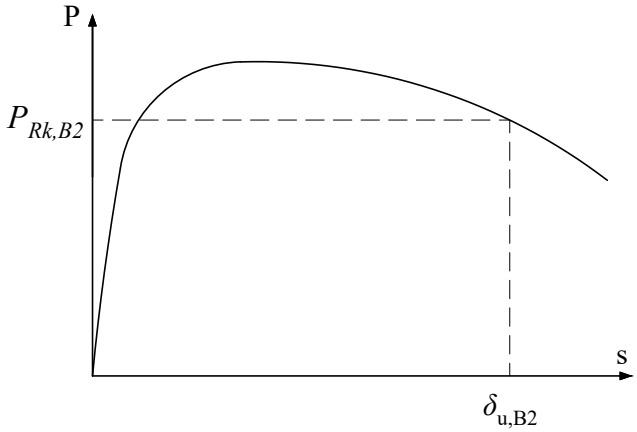

FIGURE 4.31: Definition of the slip capacity according to EN 1994-1-1 B.2.5 (BSI, 2004b)

However, in order to apply this simplified procedure, the test series shall satisfy the following requirements:

- At least three nominally identical specimens are tested
- The deviation D from the mean value of the resistance of each test shall not exceeed 10%

Although some of the tests performed do not have the entire load-slip curve, the procedure was applied to all the test series. The characteristic values of the resistance as well as slip capacity were plotted in Figure 4.32a and Figure 4.32b while all the details are given in Table 4.11.

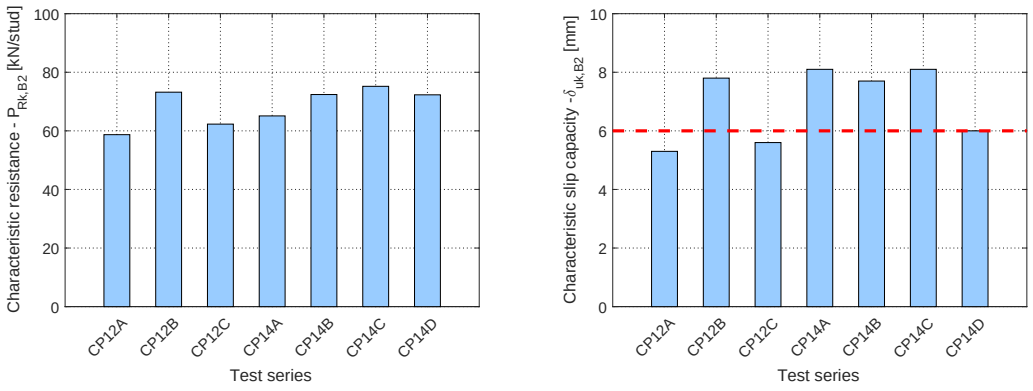

(a) (b)

FIGURE 4.32: Characteristic resistance $P_{Rk,B2}$ and (b) slip capacity $\delta_{uk,B2}$ for each test series according to EN 1994-1-1 B.2.5 (BSI, 2004b)

According to EN 1994-1-1, all the shear connections tested can be considered as ductile because the characteristic slip is at least 6 mm. Only series CP12A and CP12C had a value of $\delta_{uk,B2}$ slightly below this threshold. All these values were finally used to quantify the impact of the variables on the performance of the shear connection which is discussed in the next sections.

TABLE 4.11: Results of the push-out tests evaluated according to EN 1994-1-1 B.2.5 (BSI, 2004b)

Test Specimen	d [mm]	h_{sc} [mm]	n_r [-]	f_{cm} [MPa]	P_e [kN/stud]	D [-]	$P_{e,mean}$ [kN/stud]	$P_{Rk,B2}$ [kN/stud]	$\delta_{u,B2}$ [mm]	$\delta_{uk,B2}$ [mm]
CP12A-1	19	98	1	42.2	68.3	0.9%			11.3	
CP12A-2	19	98	1	42.9	65.3	-3.6%	67.7	58.7	5.9	5.3
CP12A-3	19	98	1	44.0	69.5	2.7%			7.7	
CP12B-1	19	98	1	42.2	81.3	-4.6%			8.6	
CP12B-2	19	98	1	42.6	83.7	-1.7%	85.2	73.2	17.0	7.8
CP12B-3	19	98	1	43.2	90.7	6.4%			9.2	
CP12C-1	19	98	1	45.7	69.3	-3.3%			6.2	
CP12C-2	19	98	1	46.0	75.5	5.4%	71.6	62.3	10.2	5.6
CP12C-3	19	98	1	46.5	70.1	-2.2%			-	
CP14A-1[a]	19	98	1	49.3	85.7	-			-	
CP14A-2	19	98	1	49.7	72.4	-6.5%	77.4	65.1	9.0	8.1
CP14A-3	19	98	1	50.2	82.5	6.5%			14.4	
CP14B-1	19	98	1	50.7	85.5	0.7%			9.1	
CP14B-2	19	98	1	50.8	80.6	-5.2%	84.9	72.4	8.5	7.7
CP14B-3	19	98	1	51.1	88.7	4.5%			-	
CP14C-1[a]	19	94	1	51.8	66.6	-			-	
CP14C-2	19	94	1	51.9	83.5	-0.9%	84.3	75.2	9.5	8.1
CP14C-3	19	94	1	52.0	85.1	0.9%			9.0	
CP14D-1	19	124	1	43.5	80.3	-4.7%			9.5	
CP14D-2	19	124	1	43.7	87.3	3.6%	84.3	72.3	13.5	6.0
CP14D-3	19	124	1	44.2	85.2	1.1%			6.7	

[a] Not considered in the evaluation

4.7.2 Influence of the recess

The recess of the concrete slab represents one the parameters which is optional in the standard push-out test specimen indicated in the current version of EN 1994-1-1 Annex B.2 (BSI, 2004b). The idea behind the use of recess is that it allows a wider distribution of the compressive forces over the width of the slab which would be more representative of the actual stress distribution in composite beam applications. However, this results in higher splitting forces that may induce cracks along the longitudinal direction which should be restrained by the transversal reinforcement bars. A simplified strut and tie model representing the distribution of the forces in the specimens is given in Figure 4.33a and 4.33b for slabs without and with recess, respectively.

Based on this model, the inclination of the compression struts θ_R (which is always higher than θ_N) is proportional to the width of the recess. In the presented experimental study, all the specimens had one layer of Q188A wire mesh and a 16-mm-diameter U-rebar placed at the bottom of the slabs to transfer the transversal splitting forces. From the load-slip curves obtained in series CP12A (without recess) and CP12C (with 200 mm wide recess) in Figure 4.34, no significant changes can be observed. The only difference was that the slabs of the samples without recess exhibited less vertical (i.e. longitudinal) cracks than the ones with recess, as shown in Figure 4.35. From these results, it appears that the 200 mm wide recess affects neither

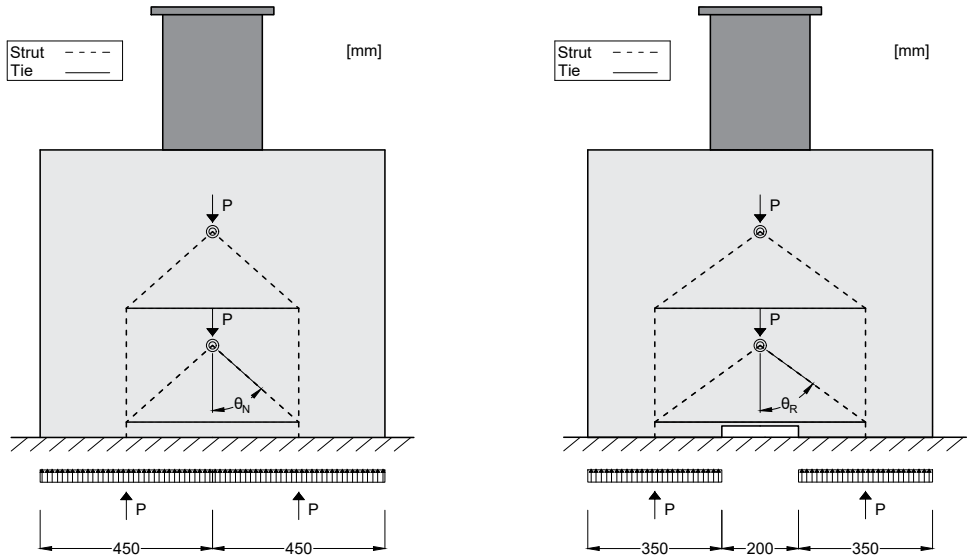

FIGURE 4.33: Simplified distribution of the forces in push-out tests (a) without and (b) with 200 mm wide recess

the resistance nor the slip capacity of the shear connection if adequate transversal reinforcement is provided.

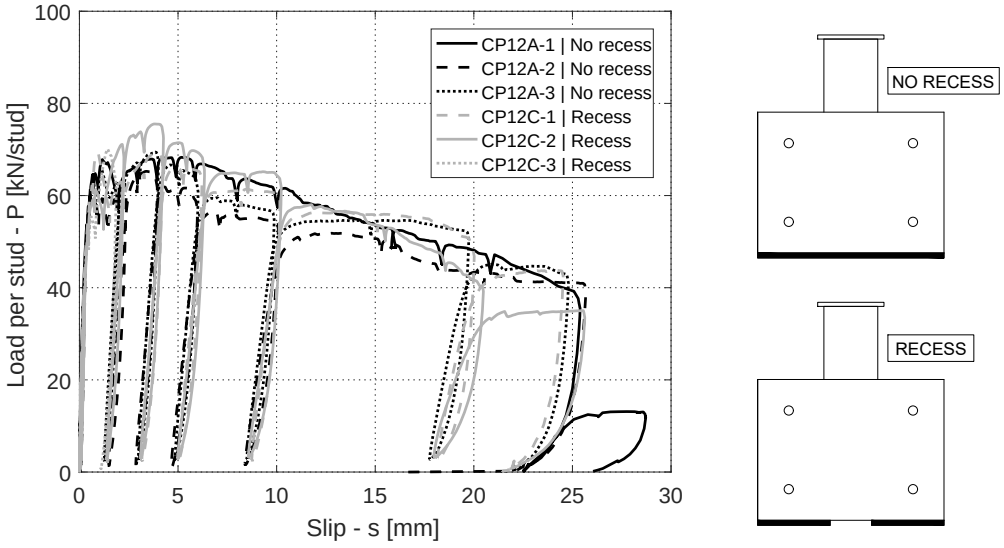

FIGURE 4.34: Load-slip curve for specimens without and with recess

(a) (b)

FIGURE 4.35: Crack pattern after test (a) without and (b) with recess

4.7.3 Influence of the waveform rebar

The influence of the waveform rebar was investigated by comparing the results of the test series CP12A and CP12B. These special reinforcement bars were designed to be perpendicular to the expected concrete cone cracks that develops at the edge of the rib. From the load-slip curve of Figure 4.36, a significant rise in resistance is observed at early stages as soon as the concrete cone cracks initiate (at ca. 1-2 mm) leading to an increase of the peak load by ca. 26% which is in line with the findings of Ernst (2006). These results are supported by the measurements of the strain of the waveform rebars shown in Figure 4.14. The ductility was also improved with a characteristic slip capacity increasing from 5.3 mm to 7.8 mm.

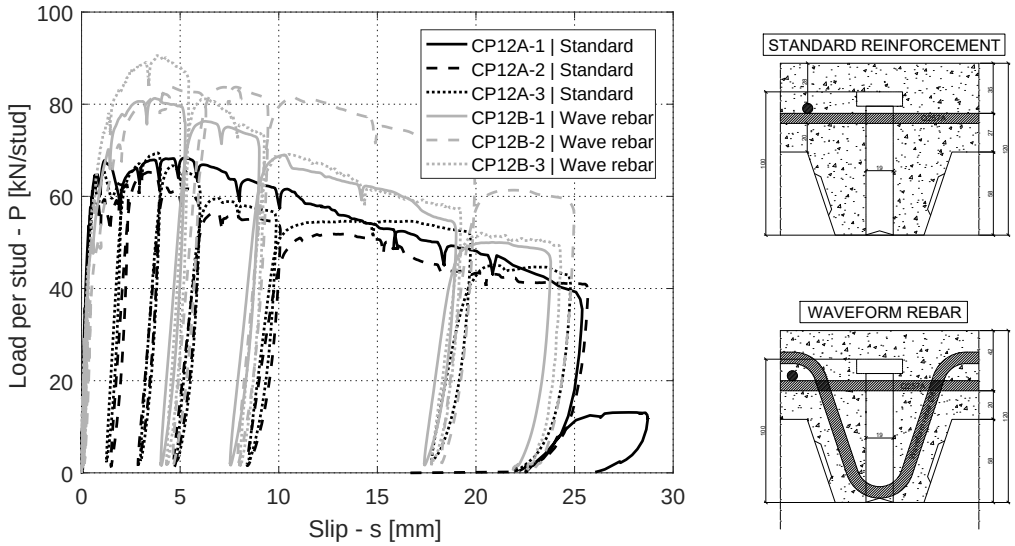

FIGURE 4.36: Load-slip curve for specimens without and with waveform rebar

4.7.4 Influence of the welding type

Unlike in past studies where through-deck welded studs exhibited an increase in resistance by ca. 10% using the same sheeting (Cashell and Baddoo, 2014), the specimens of the series CP14C did not show better performance than the configurations with studs placed in pre-punched holes. The test specimen CP14C-1 was not considered in this evaluation due to the welding quality, see Figure 4.27. As confirmed by Figure 4.37 all the load-slips curves almost overlap leading to similar values of the resistance and slip capacity.

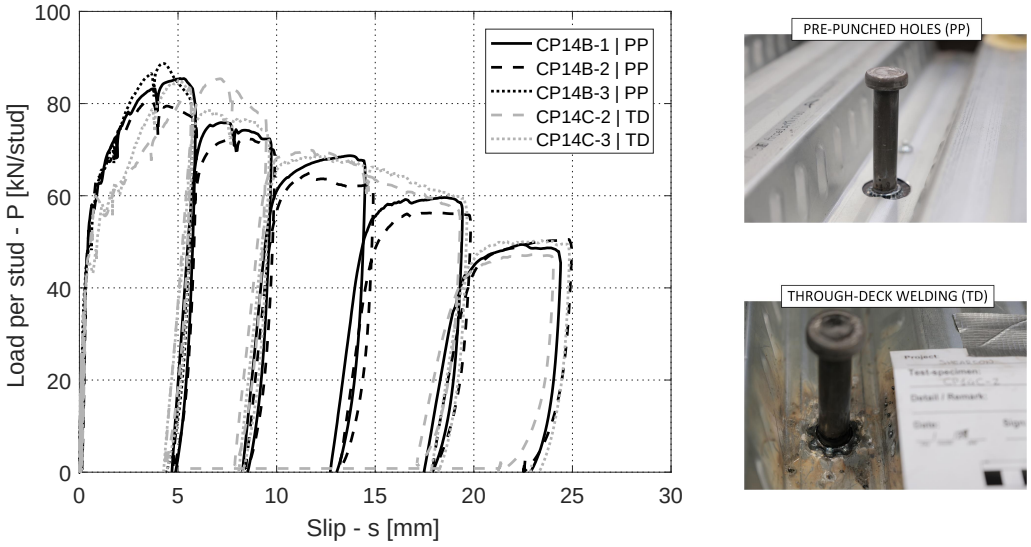

FIGURE 4.37: Load-slip curve for specimens with pre-punched holes and with through-deck welded studs

4.7.5 Influence of the position of wire mesh

From Figure 4.38, it appears that the higher position of the wire mesh leads to an increase of the average peak load from 77.4 kN/stud to 84.9kN/stud while the slip capacity was 8.1mm and 7.1 mm, respectively. Although it seems that the higher position of the wire mesh enhances the resistance of the shear connection, it might be that such difference fall within the variability of the experimental results. In any case, it can be concluded that the higher position of the wire mesh did not reduce the performance of the shear connection considered.

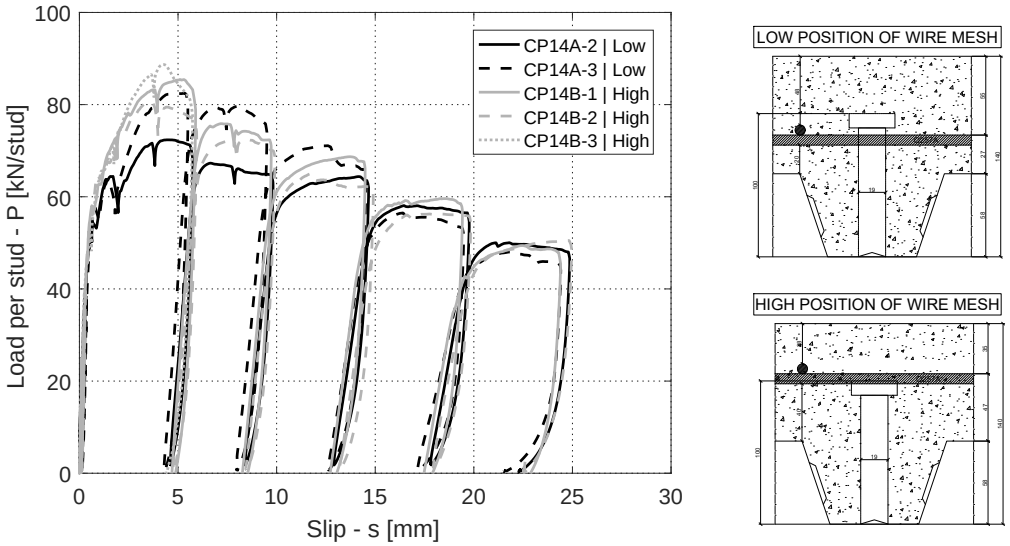

FIGURE 4.38: Load-slip curve for specimens with low and high position of the wire mesh using 100 mm high studs

No difference in the mechanical behaviour was observed: in all cases the failure occurred due to the gradual crushing of the rib followed by the pull-out of the concrete cone. This can be explained by the fact that the longitudinal reinforcement bar

of the wire mesh is not perpendicular to the concrete cone cracks as in the series with waveform reinforcement bars (CP12B) where the impact was significant.

4.7.6 Influence of the stud height

The influence of the stud length was checked by comparing the series CP14A (100 mm stud) with CP14D (125 mm stud) where the wire mesh was placed 20 mm above the rib (low position) in both cases. Although the compressive concrete strength in CP14D was lower, the specimens with 125 mm studs exhibited slightly higher strength, see Figure 4.39.

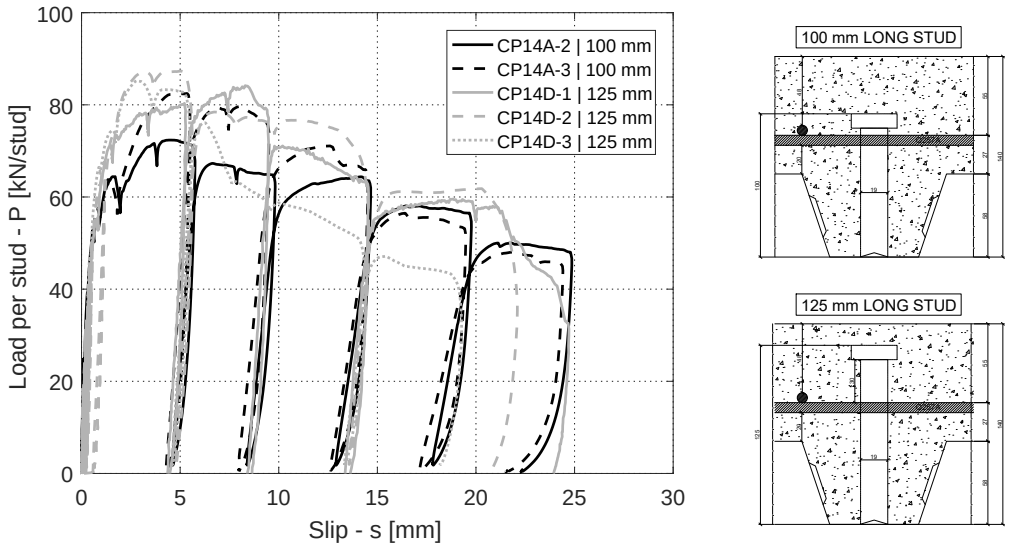

FIGURE 4.39: Load-slip curve for specimens with 100 and 125 mm high studs

Since the resistance of the specimens considered is related to the material strength, the mean experimental resistance of the connector was normalized on the concrete strength (Shen, 2014) using an exponential factor of 2/3 (Lawson et al., 2017). Considering the mean resistance of the test series $P_{e,mean}$, the corresponding value normalized on a concrete strength of 43 MPa $P_{e,Norm}$ will be equal to:

$$P_{e,Norm} = P_e \cdot \left(\frac{43}{f_{cm}}\right)^{2/3} \tag{4.3}$$

After normalization, the resistance for 100 and 125 mm studs were 70.25 kN/stud and 83.26 kN/stud respectively, leading to a 18.5% increase. Conversely, the slip capacity reduces slightly from 8.1 mm to 6.0 mm. Whilst the load-slip behaviour was comparable at low displacements, stud fracture occurred only in 125 mm stud samples at ca. 15-25 mm slip.

4.7.7 Influence of the slab depth

In general, the total slab depth does not affect the resistance of the headed studs in profiled sheeting as the failure modes are localized within the through or at the shank of the stud. From the load-slip curves obtained in the tests, the series CP14A with a slab depth of 14 cm exhibited higher resistance than the series CP12A that has 12 cm deep slab, see Figure 4.40. The mean resistance increased from 67.7 kN/stud

to 77.4 kN/stud. However, such discrepancy is mitigated by the different measured concrete strength. The average cylinder compressive strength in the series CP12A was 43.0 MPa and the respective value in the series CP14A was 50.0 MPa.

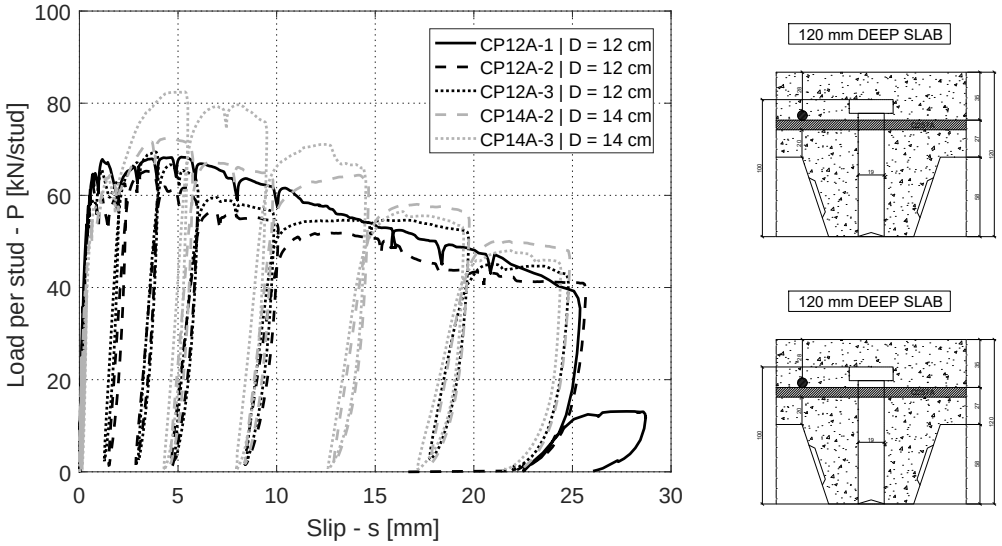

FIGURE 4.40: Load-slip curve for specimens with 12 cm and 14 cm deep concrete slab

As done in the previous section, the mean experimental resistance was normalized on the concrete strength $f_c = 43$ MPa. The corresponding normalized resistance values are 67.7 kN/stud and 69.9 kN/stud for the test series CP12A and CP14A, resulting in an increase of only +3%. Therefore, the slab depth shows a positive but minor impact on the capacity of the shear connection. On the other hand, a beneficial effect of the slab depth on the ductility was found: the characteristic slip capacity increases from 5.3 mm to 8.1 mm as the top concrete cover might help to delay the rotation of the stud head.

4.7.8 Observed failure modes

In all the conducted tests, rib punching (RP) failure occurs due to the high bearing stresses and the limited concrete cover in the front side of the trough. This "intermediate" failure occurs at relatively low displacement (from ca. 4 mm slip) in a ductile manner. The increasing displacement leads to the bulging of the steel sheeting and concrete pull-out (CPO) failure as shown in Figure 4.41a and Figure 4.41b. In case of 125 mm long studs, owing to the longer embedment depth provided by the slab, the concrete pull-out failure is slightly "delayed" and the rupture of the shank of the stud (combined shear and tension) occurred in the range of 15-25 mm of slip. In parallel, the headed stud deforms in bending developing a single or double curvature depending on the geometry. Unlike in 100 mm high stud configurations, 125 mm studs showed a double bending curvature which is still visible after rupture. The detailed list of all the failure modes observed in each push-out test is provided in Table 4.12.

(a) (b)

FIGURE 4.41: (a) Damage of the concrete in front of the stud due to rib punching at ca. 6 mm slip and (b) concrete cones due to pull-out observed after testing

TABLE 4.12: Failure modes observed in the conducted push-out tests

Test Specimen	Failure modes			Test Specimen	Failure modes		
CP12A-1	RP	CPO	-	CP14B-1	RP	CPO	-
CP12A-2	RP	CPO	-	CP14B-2	RP	CPO	-
CP12A-3	RP	CPO	-	CP14B-3	RP	CPO	-
CP12B-1	RP	CPO	-	CP14C-1	RP	CPO	-
CP12B-2	RP	CPO	-	CP14C-2	RP	CPO	-
CP12B-3	RP	CPO	-	CP14C-3	RP	CPO	-
CP12C-1	RP	CPO	-	CP14D-1	RP	CPO	SR
CP12C-2	RP	CPO	-	CP14D-2	RP	CPO	SR
CP12C-3	RP	CPO	-	CP14D-3	RP	CPO	SR
CP14A-1	RP	CPO	-				
CP14A-2	RP	CPO	-				
CP14A-3	RP	CPO					

RP: Rib punching | CPO: Concrete Pull-Out | SR: Stud Rupture

4.8 Summary

A total of 21 push-out tests on conventional 19mm diameter headed studs placed in the profiled steel sheeting ArcelorMittal Cofraplus® 60 were carried out and presented in this chapter. In order to guarantee the robustness of the results, 3 nominally identical samples were prepared and tested in each series. From a general evaluation of the entire set of tests, all specimens behave ductile reaching a peak load at ca. 2-6 mm followed by a smooth load reduction. Based on the evaluations according to EN 1994-1-1 B.2 (BSI, 2004b), all the specimens showed a characteristic slip capacity $\delta_{uk,B2}$ higher than 6 mm, while CP12A and CP12C series delivered a $\delta_{uk,B2}$ between 5 and 6 mm.

All the configurations experienced rib punching at around 2-6 mm slip. This type of failure occured in a ductile manner while the concrete rib was gradually damaged due to the increasing bearing stresses. In parallel, the headed studs deform in bending with single or double curvature, depending on its length. At higher displacements, the concrete cone cracks observed at earlier stages propagate until the cones were fully detached from the slab (Concrete pull-out). Unlike 100 mm long studs, 125 mm studs were fully ruptured owing to the high shear and tensile stresses arising at large deformations. Several parameters were also investigated in

this experimental study. On that basis, the following considerations can be made:

1. The 200 mm wide recess applied to the base of the specimen has a minor beneficial impact on the performance of the connectors.
2. The addition of a waveform rebar increases the resistance by 26% and it improves its ductility by delaying the propagation of the concrete cone cracks.
3. The test specimens with through-deck welding studs did not show any evident improvement compared to the configurations with studs placed in prepunched holes.
4. The higher location of the wire mesh does not reduce the resistance of the shear connection.
5. By varying the length of the stud from 100 mm to 125 mm, the performance of the connection improves with a relative increase of the resistance of approximately 18.5%.
6. The depth of the slab has a positive but negligible impact on the capacity of the shear connection.

Chapter 5

Numerical study on push-out test specimens

To extend the findings of the push-out tests presented in Chapter 4, a non linear 3D finite element (FE) model was developed using the commercial software ABAQUS 6.14 (Simulia, 2014). The numerical model was firstly validated against different push-out test results using measured material properties and nominal geometrical dimensions of the corresponding specimens. The validated FE model was finally used to carry out a parametric investigation aiming to analyse the response of the shear connection in detail by changing several properties. The key objective is to comprehend how the stresses and internal forces are distributed in the shear connection during the testing process. For this purpose, the damage pattern in the concrete as well as the bending deformation of the stud connector were evaluated at different displacements. The general modelling and solving approach was kept constant throughout the entire parametric study where more than 20 cores were simultaneously used for running each numerical simulation thanks to High-Performance Computing (HPC) facilities avaliable at University of Luxembourg (Varrette et al., 2014).

5.1 Description of the numerical model

5.1.1 Geometry, model assembly and boundary conditions

Based on the outcomes of several studies on refined numerical modelling of shear connections in composite structures (El-Lobody and Lam, 2002; Qureshi et al., 2011; Spremic et al., 2018), the dynamic-explicit solver was chosen to perform the numerical study with a quasi-static application of the load by inputting the displacement in a smooth manner. Such solving procedure was preferred in order to overcome convergence issues which may arise in the post-cracking stage. In addition, to reduce the modelling and computational time, only a quarter of the test sample was reproduced in the FE model with the double-symmetry boundary conditions.

Due the complexity of the 3D model, a key role was assigned to the size and the pattern of the mesh. For brick elements, the adopted mesh pattern consisted of a regular scheme of 8-node solid elements. Based on a preliminary mesh sensitivity analysis, the reference edge size was assessed to be approximately 5-10 mm. A certain mesh refinement was accounted in the proximity of any geometrical irregularities (i.e. discontinuities and joint details) to ensure the accuracy of the results during the simulations. A relatively coarse mesh pattern was used for the regions that are not directly involved in key mechanical interactions.

The FE model of the push-out test specimens consists of four main assembly elements:

- Steel beam with headed studs
- Profiled steel sheeting
- Reinforced concrete slab
- Base steel plate

The choice of the mesh element type aimed to maximize the computational efficiency of the FE model as well as ensuring a reliable simulation of the mechanical interaction between the model components. Based on the available ABAQUS element library (Simulia, 2014), 8-node brick elements with reduced integration (C3D8R) were selected for the steel beam, the studs and the concrete slab. 2-node linear beam elements (B31) were used for the steel reinforcement bars which were embedded in the slab. Finally, 4-node quadrilateral shell elements with reduced integration (S4R) were chosen for the profiled steel decking. The final FE assembly resulted in a total number of about 110'000 solid elements, 192 beam elements and 6'590 shell elements, with ca. 400'000 DOFs. The meshed instances of the FE model are shown in Figure 5.1. Notwithstanding that the headed studs and the steel beam were considered as one whole assembly element, they were characterized by different material properties as explained later in Section 5.1.2.

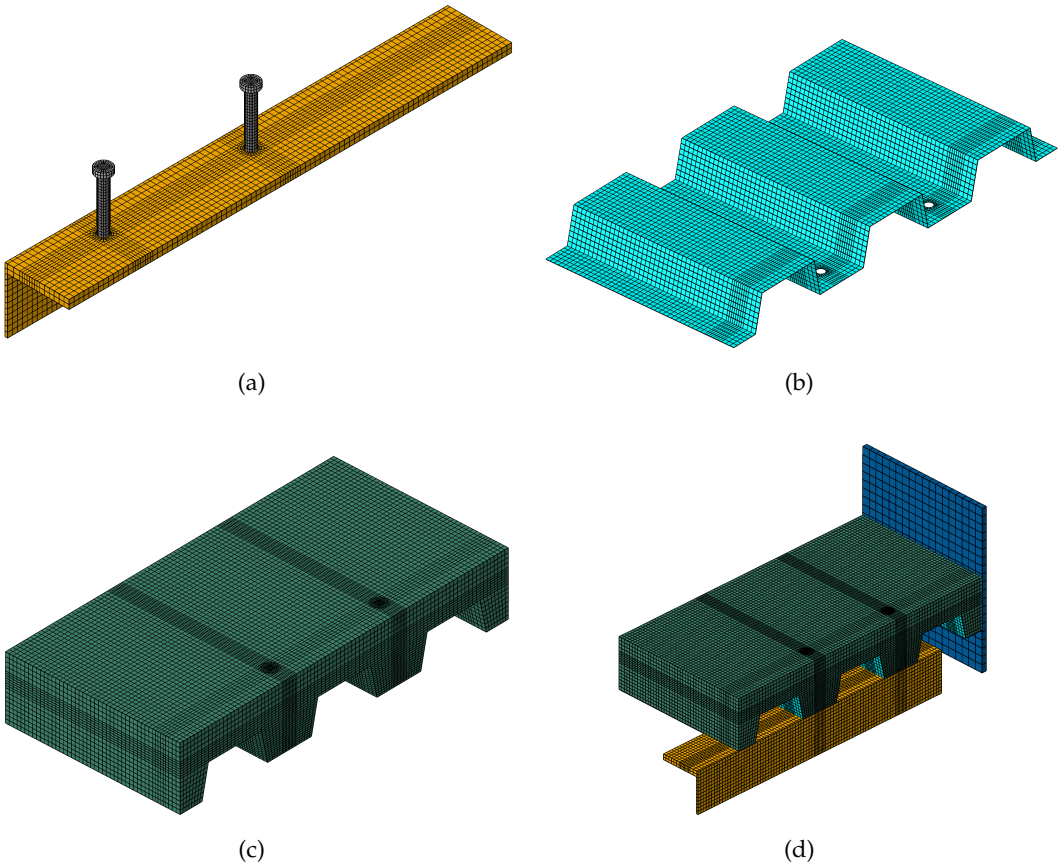

FIGURE 5.1: Meshed instances of the finite element model: (a) Beam and studs, (b) profiled steel deck, (c) concrete slab and (d) full setup

Careful considerations were made especially for the regions of contact between the steel and concrete components (i.e. where damage initiation and propagation is expected) to ensure a reliable estimation of the load-slip response in the post-elastic stage. The set of surface-to-surface contact interactions was defined with the general contact algorithm, including normal and tangential behaviour (Zhang et al., 2008). The hard contact formulation was used to characterize the normal behaviour of two FE instances in contact. This means that a possible separation between the involved surfaces without transferring tensile stresses was allowed. Conversely, the full transmission of compressive stresses was ensured in order to avoid possible overlapping or penetration throughout the simulations. For the input variables of the tangential behaviour, the static friction coefficient was set to 0.5 for all the steel-to-concrete contact surfaces and 0.3 for steel-to-steel surfaces (Zhang et al., 2008). To take into account the through-deck welding process, a tie constraint was enforced between the nodes at the base of the studs and the sheeting. On the other hand, for pre-punched hole configurations, no interaction was considered due to the negligible resistance provided by the steel sheeting on the stud base. To implement a fully rigid interaction between the bars and the surrounding concrete slab, the embedded constraint was assigned to the steel reinforcement bars, as conventionally used for the numerical modelling of steel-concrete or timber-concrete composite systems (Amadio et al., 2017).

5.1.2 Material properties

The characterization of the materials was carried out on the basis of the available experimental data. The steel of the beam, sheeting, studs and reinforcement bars was modelled via a bilinear stress-strain law and Von Mises failure criteria. The material of the base plate was assumed linear-elastic as no plastic deformation is expected to occur. The data of the material modelling of the steel elements is summarized in Table 5.1.

TABLE 5.1: Data of material of the steel elements used in the FE model

Part	Failure criterion	Elastic modulus E [MPa]	Yield strength f_y [MPa]	Ultimate strength f_u [MPa]	Ultimate strain ε_u [MPa]
Beam	Von Mises	210000	424	525	0.16
Profiled deck	Von Mises	210000	350	420	0.16
Headed studs	Von Mises	210000	470 (500)	500 (550)	0.075
Reinforcement bars	Von Mises	210000	500	550	0.20
Base plate	-	210000	-	-	-

As done in recent numerical studies on headed stud shear connections (Qureshi, 2010), the concrete damaged plasticity (CDP) model was used to account for the tensile and compressive damage propagation in the concrete slab. The respective plasticity parameters are given in Table 5.2 and they are defined below.

TABLE 5.2: Plasticity parameters of the CDP model

Ψ [°]	e [-]	f_{b0}/f_{c0} [-]	K_c [-]
38	0.1	1.16	0.67

Ψ is the dilation angle of the concrete in the p–q plane

p is the hydrostatic pressure stress

q is the Von Mises equivalent stress

e is the eccentricity parameter that defines the rate at which the flow potential function (Simulia, 2014) approaches to the asymptote (recommended value of 0.1)

f_{bc}/f_c is the ratio of equibiaxial-to-uniaxial compressive strength (recommended value of 1.16)

K_c is the ratio of the second stress invariant on the tensile meridian, to that on the compressive meridian for any given value of p such that the maximum principal stress is negative (recommended value of 0.67) (Simulia, 2014)

With the exception of the dilation angle Ψ taken as 38° (Vigneri et al., 2019a), the default recommended values of the plasticity parameters were chosen.

The calibration of the compressive constitutive behaviour was performed in accordance with Popovics (1973) and Thorenfeldt et al. (1987). The respective uniaxial stress-strain function is shown in Figure 5.2a and defined by the following equation:

$$\sigma_c = f_c \frac{\left(\frac{\varepsilon_c}{\varepsilon_{c0}}\right)}{(n-1) + \left(\frac{\varepsilon_c}{\varepsilon_{c0}}\right)^n} \tag{5.1}$$

Where:

f_c is the uniaxial compressive strength of concrete

ε_c is the compressive strain

ε_{c0} is the compressive strain at which the maximum stress f_c is reached.

The parameter n was estimated by Thorenfeldt et al. (1987) as follows:

$$n = 1.25 \cdot [0.058 f_c[\text{MPa}] + 1] \tag{5.2}$$

The compression damage parameter d_c was calculated according to:

$$d_c = 1 - \frac{\left(\frac{\sigma_c}{E_c}\right)}{\varepsilon_c^{pl}\left(\frac{1}{b_c} - 1\right) + \left(\frac{\sigma_c}{E_c}\right)} \tag{5.3}$$

Where:

E_c is the elastic modulus of concrete

ε_c^{pl} is the uniaxial plastic compressive strain

b_c is a parameter taken as 0.7 (Birtel and Mark, 2006)

The uniaxial post-crack behaviour of the concrete was implemented by using the exponential tensile stress-crack opening $\sigma_t - w_c$ function proposed by Cornelissen

et al. (1986), shown in Figure 5.2b and given by:

$$\sigma_t = f_{ct}\left[g(w_c) - \left(\frac{w_c}{w_{c,crit}}\right) g(w_{c,crit})\right] \tag{5.4}$$

With:

$$g(w_c) = \left[1 + \left(\frac{3w_c}{w_{c,crit}}\right)^3\right] \exp\left(-\frac{6.93w_c}{w_{c,crit}}\right) \tag{5.5}$$

and

$$w_{c,crit} = 5.14\frac{G_f}{f_{ct}} \tag{5.6}$$

Where:

f_{ct}	is the uniaxial tensile strength of concrete
w_c	is the crack opening
$w_{c,crit}$	is the critical value of w_c at which no tensile stress can be transferred
G_f	is the fracture energy, taken according to FIB (2010)

The tensile damage parameter d_t was assumed linearly proportional to the tensile stress reduction after cracking as given in Eq.(5.7).

$$d_t = \begin{cases} 0 & w = 0 \\ 1 - \frac{\sigma_t}{f_{ct}} & w > 0 \end{cases} \tag{5.7}$$

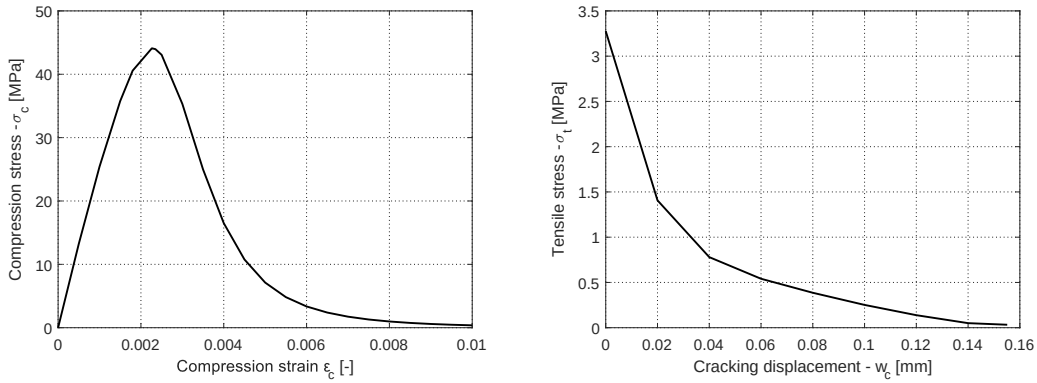

(a) (b)

FIGURE 5.2: Example of constitutive uniaxial law used in the FE model for concrete in (a) compression and (b) tension

5.1.3 Mass scaling factor sensitivity analysis

The dynamic-explicit solver allows the use of a mass scaling factor M which increases the density of the elements. In this case, M increases the minimum time increment while minimizing the computation time. However, it is essential to limit the value of M in order to keep the process quasi-static. This was made by checking the global response and the ratio between the kinetic energy (ALLKE) and the

internal energy (ALLIE) of the whole system. It is recommended that the ratio ALLKE/ALLIE lies below 5% (Simulia, 2014). Based on these considerations, a sensitivity analysis of the mass scaling factor M was carried out to assess its influence on the mechanical response a push-out test specimen. The corresponding load-slip curves are plotted in Figure 5.3a. In parallel, the relative amount of kinetic energy throughout the simulation was extracted and displayed in Figure 5.3b respectively. Based on the evaluation of these results, a mass scaling factor M of 10^2 was finally chosen for the numerical study.

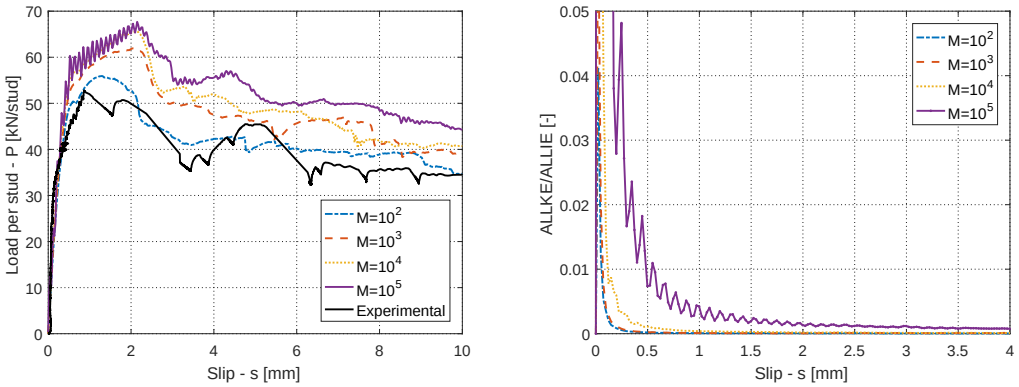

(a) (b)

FIGURE 5.3: (a) Load-slip curves and (b) Kinetic-Internal energy ratio (ALLKE/ALLIE) for different values of mass scale factor M relative to DISCCO push-out test 3-01-3 (Lawson et al., 2017)

5.2 Validation against test data

In order to validate the numerical model herein described, one push-out test (3-01-3) from the project DISCCO (Lawson et al., 2017) and another one from the conducted tests (CP12A) presented in chapter 4 were considered, see Table 5.3. In the latter case, the constraint provided by the bottom tie bars was also included in the model by fixing the outward displacement of the respective portion of the slab surface.

TABLE 5.3: Data of the configurations considered for the validation

Configuration	h_p [mm]	b_{bot} [mm]	b_{top} [mm]	t [mm]	d [mm]	h_{sc} [mm]	n_r [-]	Weld [-]	e_t [mm]	f_c [MPa]	f_u [MPa]
3-01-3	80	120	155	0.9	19	118	2	TD[a]	100	40.4	500
CP12A	58	62	101	0.88	19	98	1	PP[b]	-	43.0	550

[a]TD: Through-deck welding
[b]PP: Pre-punched sheeting

Where:

t is the thickness of the sheeting
n_r is the number of studs per rib
e_t is the transversal spacing between the studs
f_u is the ultimate strength of the stud material

The other geometrical variables are shown in 5.4.

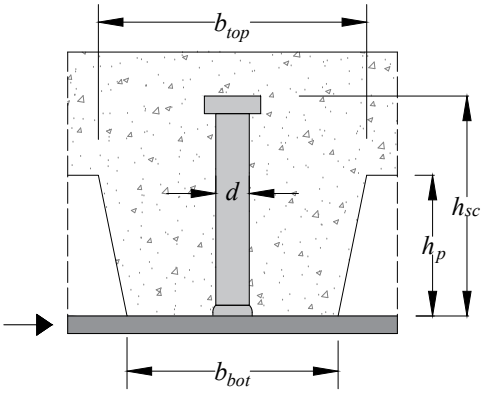

FIGURE 5.4: Geometrical dimensions of the shear connection

As can be seen from the load-slip curves in Figure 5.5, a good correlation between experimental and numerical curves was achieved for both configurations given in Table 5.3. The relative difference in terms of maximum load between the experimental tests and the numerical simulations does not exceed 6%.

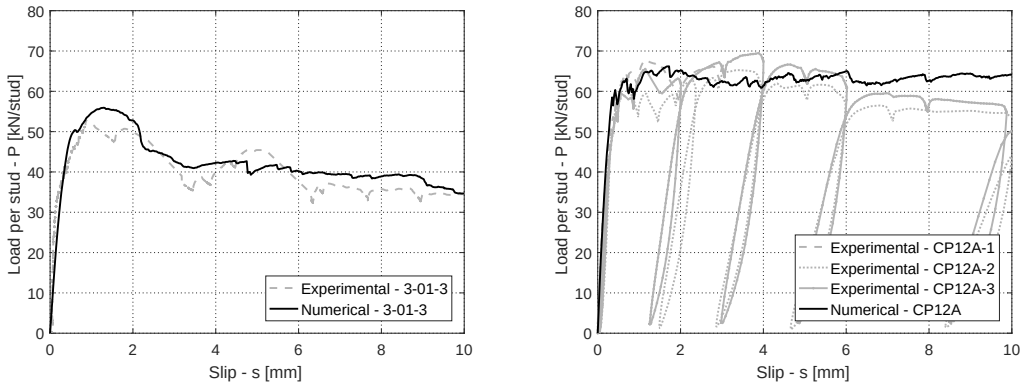

(a) (b)

FIGURE 5.5: Experimental and numerically obtained load-slip curves

Besides, the experimental and numerically obtained results were compared in terms of concrete damage pattern. The tensile damage contour for the configuration CP12A was extracted at 6 mm and plotted in Figure 5.6a including the distribution of the maximum principal stresses (in absolute value). By observing the longitudinal cut of the respective test specimen at the same displacement in Figure 5.6b, the concrete cone crack pattern as well as the crushing of the concrete rib occurred in front of the stud are captured by the numerical model.

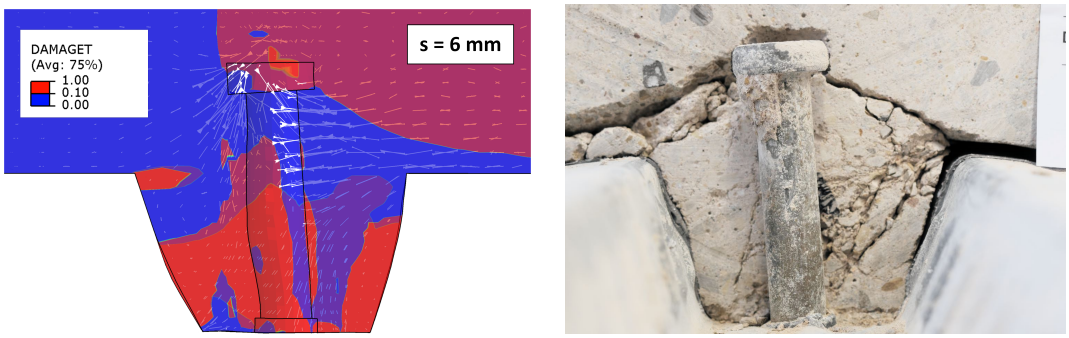

(a) (b)

FIGURE 5.6: (a) Tensile damage contour with the maximum principal stresses in the FE model and (b) cut section of the respective test specimen at 6 mm of slip

5.3 Parametric study

Given the good agreement between experimental tests and numerical simulations, the FE model was further extended to assess the impact of several properties on the behaviour of the connection. In particular, the parametric study focuses on the influence of the following variables:

- Embedment length of the stud above the rib $(h_{sc} - h_p)$
- Number of studs per rib n_r
- Stud diameter size d
- Transversal distance between the studs e_t
- Type of welding

The data of the numerical simulations is finally summarized in Table 5.4.

TABLE 5.4: Data of the parametric numerical study

Configuration	h_p [mm]	b_{bot} [mm]	b_{top} [mm]	t [mm]	d [mm]	h_{sc} [mm]	n_r [-]	Weld [-]	e_t [mm]	f_c [MPa]	f_u [MPa]
CP12A	58	62	101	0.88	19	98	1	PP	-	43.0	550
NR1-1-h110	80	120	155	0.9	19	110	1	TD	-	44.1	500
NR1-1	80	120	155	0.9	19	121	1	TD	-	44.1	500
NR1-h130	80	120	155	0.9	19	130	1	TD	-	44.1	500
3-02-h110	80	120	155	0.9	19	110	2	PP	100	42.6	500
3-02	80	120	155	0.9	19	123	2	PP	100	42.6	500
3-02-h130	80	120	155	0.9	19	130	2	PP	100	42.6	500
3-02-d22	80	120	155	0.9	22	123	2	PP	100	42.6	500
3-01-3-h110	80	120	155	0.9	19	110	2	TD	100	40.4	500
3-01-3	80	120	155	0.9	19	118	2	TD	100	40.4	500
3-01-3-h130	80	120	155	0.9	19	130	2	TD	100	40.4	500
3-01-3-e150	80	120	155	0.9	19	118	2	TD	150	40.4	500
3-01-3-e70	80	120	155	0.9	19	118	2	TD	70	40.4	500

5.4 Damage and stresses in the concrete rib

In all the simulations run in the numerical study, a common damage pattern was observed in the concrete between 0 and 10 mm of slip displacements. Owing to the high bending stiffness of the concrete rib, the tensile stresses on the edge of the rib reaches the tensile strength of the material at small slips. This is highlighted by the contour plot of the tensile damage parameter extracted by the FE simulations at 1 mm slip, see Figure 5.7. On the same plot, the distribution of the maximum principal tensile stresses is also included.

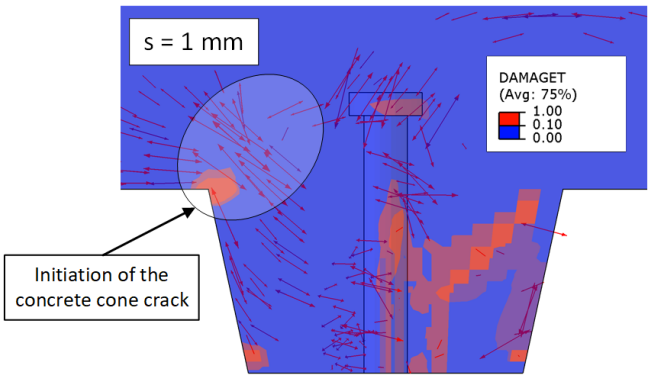

FIGURE 5.7: Contour plot of the tensile damage parameter including the distribution of the maximum tensile principal stresses at 1 mm slip displacement

Due to the initiation of this crack, the spread of the stresses in the concrete drastically change and the forces are gradually redirected to the undamaged part of the rib. Thanks to the analysis of the maximum principal stresses shown in Figure 5.8, the location and direction of the internal forces in the concrete was identified. It shall be noted that as the crushing of the concrete around the shank of the stud increases, the centre of stiffness moves up as well as the bearing forces. This phenomenon is also related to the plastic hinges activated in the stud which are evaluated in the next section.

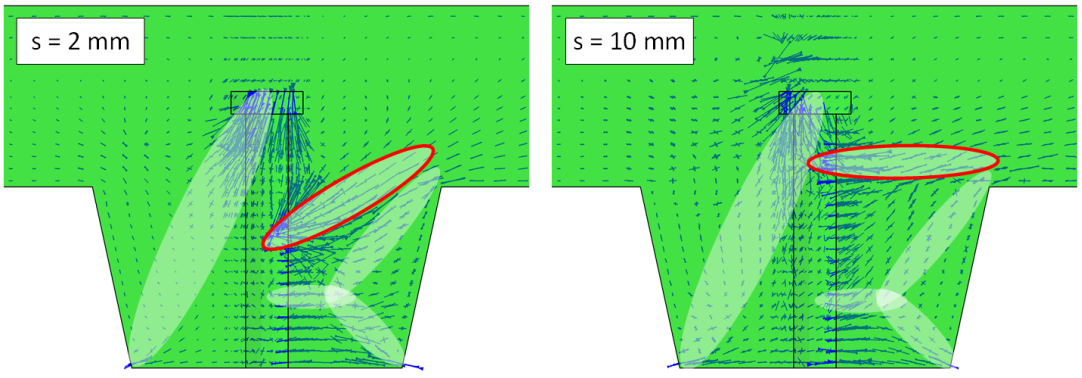

(a) (b)

FIGURE 5.8: Distribution of the compressive principal stresses in the concrete at (a) 2 mm and (b) 10 mm slip

5.5 Development of plastic hinges in the stud

5.5.1 Stress-based method

The experimental results showed that a "plastic hinge" is always activated at the base of the shear stud where it is welded to the steel beam top flange. On the other hand, a second upper plastic hinge may (partially or fully) develop in the stud at a certain height. Since the observation of the headed stud after testing provides a rough estimation of the bending stresses developed at early stages, the stress distribution at the critical cross-sections of the stud was carefully evaluated in the numerical model through a stress-based method which is herein described. First, the normal stresses were extracted at the cross-section where they reach a local maximum, see Figure 5.9. Whilst the bottom hinge was considered fixed at ca. $d/2$ above the base of the stud, the vertical coordinate of the upper hinge was defined at the distance h_s. Since Von Mises failure criteria was used for the stud material, the normal stress (S22) may reach values even higher than the uniaxial strength of the material f_u because of the tri-axiality of the stress field.

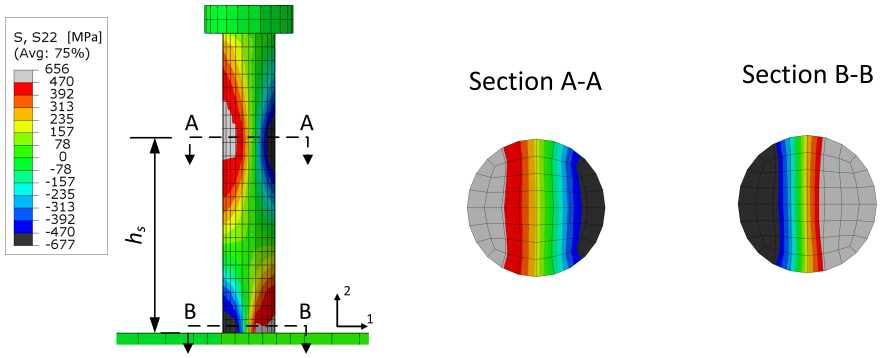

FIGURE 5.9: Normal stress (S22) contour of the headed stud: (a) side and (b) sectional view at the height of the upper and (c) bottom plastic hinge

Once the normal stress distribution was determined, the cross-sectional bending moment M_y at section A-A was extracted by means of the feature *FREE BODY CUT available in Abaqus (Simulia, 2014).

To compute the degree of activation of the second plastic hinge in the stud, the acting bending moment M_y was finally compared with the cross-sectional plastic bending resistance of the stud M_{pl} defined as:

$$M_{pl} = \frac{1}{6} f_u d^3 \tag{5.8}$$

Assuming that the plastic bending resistance is always exploited at the base, the number of plastic hinges for each stud is equal to:

$$n_y = 1 + \frac{M_y}{M_{pl}} \leq 2 \tag{5.9}$$

5.5.2 Results

From the procedure described in the previous section, the number of plastic hinges n_y were computed at 2, 4 and 6 mm slip values. The reason is that the value of 6 mm corresponds to the minimum characteristic slip to ensure the ductility of the shear connections according to EN 1994-1-1 (BSI, 2004b). The resulting number of plastic hinges n_y as well as the vertical coordinate of the upper hinge h_s were taken as the mean value of the two studs. In all simulations, it was observed that, by increasing the slip, the concrete surrounding the stud underwent progressive damage until the rotation of the head occurs. Beyond a certain slip value, the concrete damage becomes important, so that the head of the stud starts to rotate and the degree of activation of the plastic hinge reduces.

At relatively low slip displacements, the degree of activation of the plastic hinges remains stable and the position of the upper hinge moves upwards until the stud head rotates, see Figure 5.10.

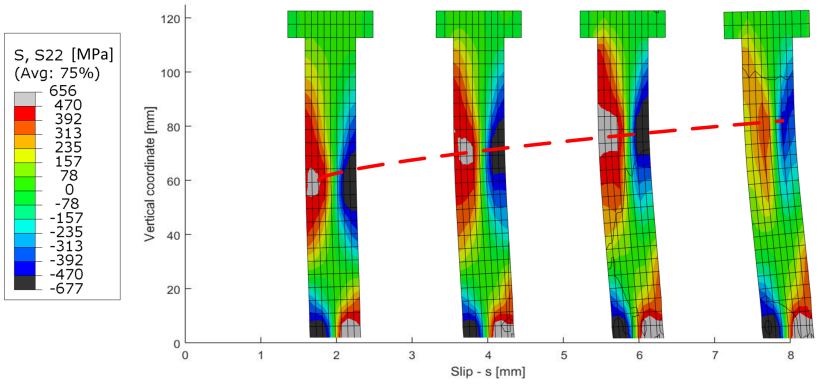

FIGURE 5.10: Vertical stress contour of the stud at 2, 4, 6 and 8 mm of slip displacement

Figure 5.11 shows the relation between (i) the slip displacement s, (ii) the rotation angle α of the stud head and (iii) the number of activated plastic hinges n_y. When the angle α starts to increase significantly, the degree of activation of the upper plastic hinge reduces drastically. All the results of the simulations are listed in Table 5.5.

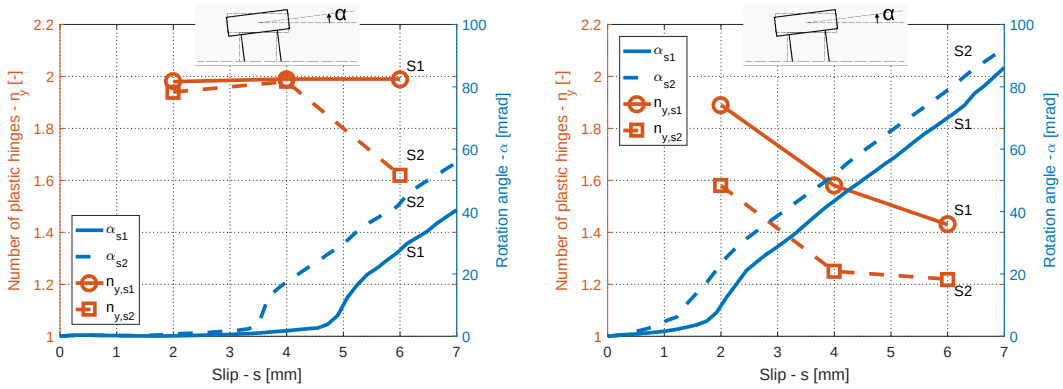

(a) (b)

FIGURE 5.11: Number of plastic hinges n_y and rotation angle of the stud head (a) for pre-punched sheeting and (b) for through-deck welded studs

TABLE 5.5: Number and position of the plastic hinges in the stud evaluated in the numerical study

Ref. Name	s [mm]	$n_{y,s1}$ [a] [-]	$n_{y,s2}$ [b] [-]	n_y [-]	h_{s1} [c] [mm]	h_{s2} [d] [mm]	h_s [mm]
CP12A	2	1.97	1.74	1.85	58	61	60
	4	1.98	1.93	1.96	63	71	67
	6	1.89	1.96	1.92	71	71	71
NR1-1_h110	2	1.95	1.92	1.94	55	55	55
	4	1.97	1.93	1.95	60	60	60
	6	1.86	1.55	1.71	75	75	75
NR1-1	2	2.00	1.94	1.97	45	50	48
	4	2.00	2.00	2.00	55	55	55
	6	2.00	1.94	1.97	60	65	63
NR1-1_h130	2	2.00	1.89	1.95	50	50	50
	4	2.00	1.97	1.99	55	60	58
	6	1.99	1.96	1.97	65	65	65
3-02_h110	2	1.98	1.92	1.95	60	60	60
	4	1.92	1.59	1.75	75	80	78
	6	1.50	1.32	1.41	90	90	90
3-02	2	1.98	1.94	1.96	59	59	59
	4	1.99	1.98	1.98	69	74	72
	6	1.99	1.62	1.81	80	80	80
3-02_d22	2	1.95	1.80	1.88	69	74	72
	4	1.65	1.45	1.55	84	84	84
	6	1.51	1.52	1.52	84	84	84
3-02_h130	2	1.97	1.94	1.96	60	60	60
	4	2.02	1.97	2.00	65	75	70
	6	2.00	1.97	1.99	75	80	78
3-01-3_h110	2	1.61	1.23	1.42	75	75	75
	4	1.32	1.01	1.17	85	85	85
	6	1.16	1.00	1.08	90	90	90
3-01-3_e70	2	1.85	1.44	1.65	74	79	77
	4	1.46	1.20	1.33	88	98	93
	6	1.32	1.18	1.25	88	98	93
3-01-3	2	1.89	1.58	1.73	69	75	72
	4	1.58	1.25	1.41	88	88	88
	6	1.43	1.22	1.33	98	93	96
3-01-3_e150	2	1.86	1.41	1.63	69	74	72
	4	1.44	1.12	1.28	94	98	96
	6	1.40	1.05	1.22	94	98	96
3-01-3_h130	2	1.91	1.81	1.86	70	70	70
	4	1.96	1.62	1.79	80	95	88
	6	1.44	1.49	1.46	90	100	95

[a] $n_{y,s1}$: Number of plastic hinges in the stud on the top row
[b] $n_{y,s2}$: Number of plastic hinges in the stud on the bottom row
[c] $h_{y,s1}$: Vertical coordinate of the upper plastic hinge in the stud on the top row
[d] $h_{y,s2}$: Vertical coordinate of the upper plastic hinge in the stud on the bottom row

5.5.3 Influence of the parameters

Number of studs per rib: All configurations analysed with one stud per rib showed the development of nearly 2 full plastic hinges disregarding the value of the slip s, see Figure 5.12. Conversely, if two studs are placed in the rib, the concrete between the studs carries more load and the local crushing may occur at earlier stages. This leads to a loss of the flexural stiffness provided by the concrete surrounding the stud heads resulting in lower values of n_y which are discussed in the next paragraphs.

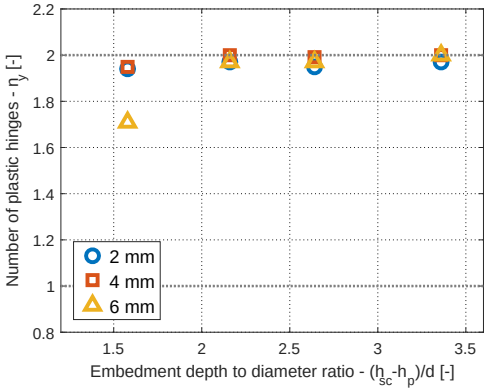

FIGURE 5.12: Number of plastic hinge for one stud per rib ($n_r = 1$) at 2, 4 and 6 mm of slip

Length of the studs: The parametric study shows that a longer length of the connector leads to higher values of n_y, as confirmed by Figure 5.13. This is a direct consequence of the increased flexural stiffness provided by the slab on the stud head as a result of the higher embedment length $(h_{sc} - h_p)$.

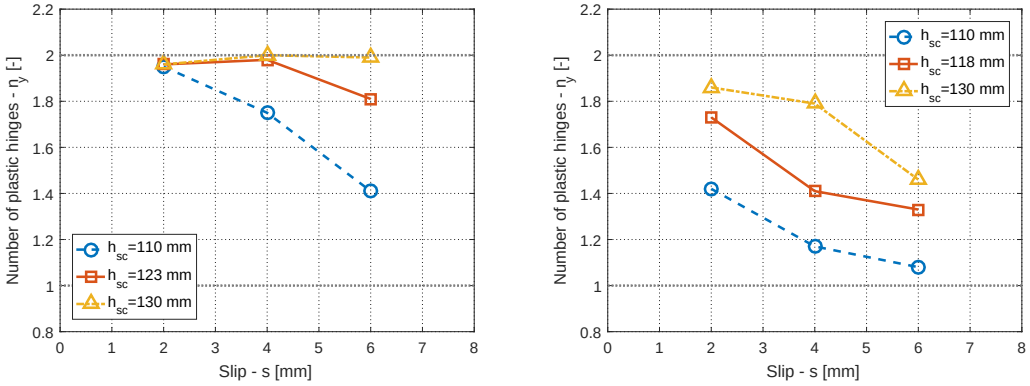

(a) (b)

FIGURE 5.13: Evolution of the number of plastic hinges with different stud heights (a) for pre-punched sheeting and (b) for through-deck welding specimen

Type of welding: By changing the type of welding from pre-punched hole sheeting (Figure 5.13a) to through-deck welded studs (Figure 5.13b), the plastic hinges reduces by around 10-20%. In consideration of the tie constraint used for through-deck welding, these configurations carry a relatively higher amount of the load by the sheeting in tension which is back-anchored to the rear side of the trough. This leads to an increase of the compressive stresses behind the connector which cause the premature rotation of the stud head reducing n_y.

Diameter of the stud: The plastic bending capacity of the stud M_{pl} is cubically proportional to the diameter of the studs d and, as a result, it is proportional to the shear force that can be transferred in the slab through the stud. However, for larger diameters, the concrete around the stud head has to bear higher stresses in order to exploit the plastic bending resistance of the stud. Therefore, increasing the shank diameter d reduces significantly the degree of activation of the plastic hinges n_y, as seen in Figure 5.14.

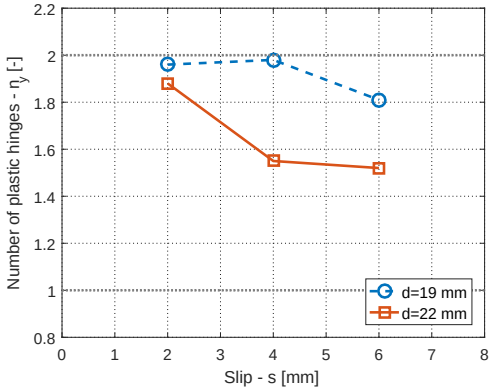

FIGURE 5.14: Number of plastic hinges for 19mm and 22 mm diameter studs

Transversal spacing between the studs: The influence of the transversal spacing e_t between the studs was also investigated for 70, 100 and 150 mm. The results summarized in Figure 5.15 shows that this parameter has a minor impact on the bending moment capacity of the studs. However, it should be noted that due to the geometric limitations of the steel beam flange, e_t cannot significantly vary. Therefore, it is thought that the mutual interaction between the studs would reduce for larger spacing, until each connector would behave as in the case of n_r=1.

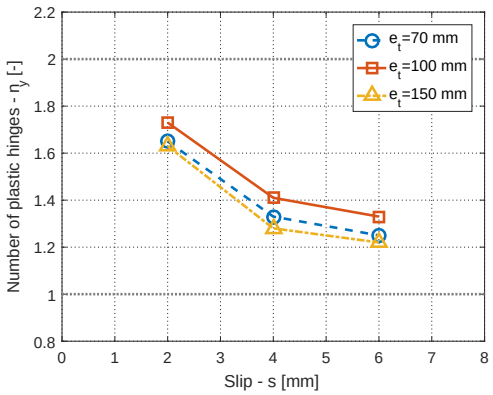

FIGURE 5.15: Number of plastic hinges for different values of transversal spacing

Chapter 6

Load bearing mechanisms and phases

From the observation of the longitudinal cut of the test specimens at different slip displacements in Chapter 4, the load bearing mechanisms activated in the shear connection were determined with the additional support of the numerical study presented in Chapter 5. Only one bearing mechanism and the respective model are not sufficient to outline the non-linear behaviour of the shear connection during the entire push-out test. Hence, three main phases were distinguished and presented in this chapter corresponding to a slip displacement of ca. 2, 6 and 25 mm where:

1. Phase 1 (Section 6.1) corresponds to the pre-cracking stage where the concrete cone crack initiates;
2. Phase 2 (Section 6.2) indicates the post-cracking stage;
3. Phase 3 (Section 6.3) focuses on the behaviour of the connection at large displacements.

The transition between the identified load bearing mechanisms is summarized in Section 6.4. However, although the failure mechanisms outline the global behaviour of the connection, the distribution of the internal forces remains unknown. Therefore, the resistance components were determined and defined in Section 6.5. Such components are necessary for the development of the mechanical models presented in Chapter 7. Finally, relevant considerations are included in Section 6.6 to define the boundary conditions within which the presented resistance mechanisms are still applicable.

6.1 Phase 1: Initiation of the concrete cone failure

In the first phase (1-3 mm slip), the stud starts to deform in bending and the concrete rib behaves elastically until the first crack appears on the edge of the rib. With reference to the cut section of the specimen CP12C-3 in Figure 6.1 after ca. 2 mm of slip displacement, the following considerations can be made:

(i) Owing to the high bending stiffness of the rib, the crack at the edge of the rib occurs. The typical concrete cone crack pattern is not fully complete at this stage.

(ii) The rib punching diagonal crack is already visible in the rib: at this point, the bearing forces acting at the shank of the stud start to split between the slab and the sheeting while no evident damage of the concrete can be seen.

FIGURE 6.1: Cut section of the test specimen CP12-3 at ca. 2 mm slip highlighting the visibly damaged parts

Although no clear curvature can be distinguished along the stud, on the basis of the numerical investigations, it can be assumed that the headed stud develops a double curvature.

6.2 Phase 2: Rib punching

Once the concrete rib is cracked, all the internal forces redistribute as pointed out in Section 5.4. In this phase, a significant part of the load is transferred by the concrete in front of the stud that gradually crushes because of the high local bearing stresses. Similarly to what is shown in the previous section, the analysis of the longitudinal cut of the specimen CP14B-3 in Figure 6.2 after ca. 6 mm of slip allows to identify the following bearing mechanisms:

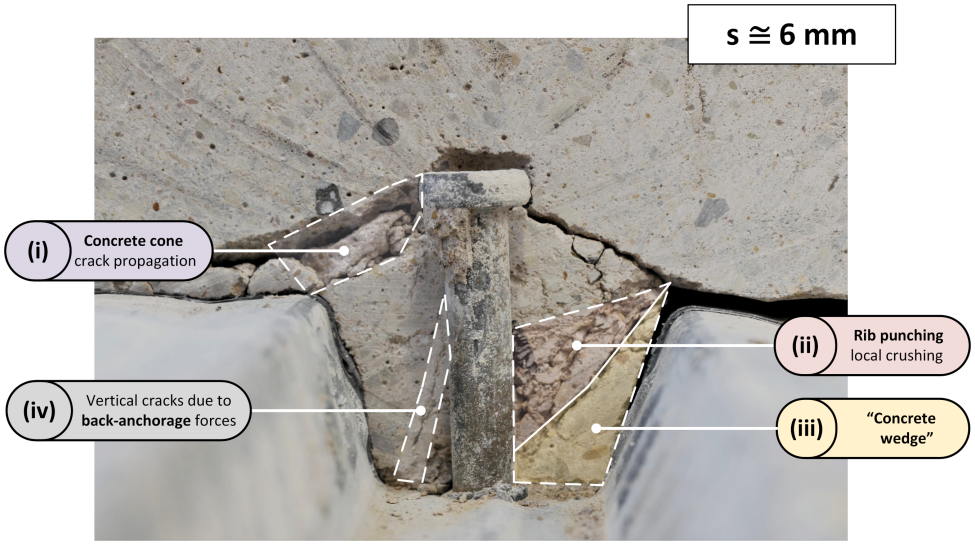

FIGURE 6.2: Cut section of the test specimen CP14B-3 at ca. 6 mm slip highlighting the visibly damaged parts

(i) The concrete cone crack pattern propagates across the rib. This occurs in a ductile manner allowing for the redistribution of the forces in the trough.

(ii) The bearing stresses significantly increase and the localized damage of the concrete in front of the stud is clearly visible as a consequence of the rib punching failure.

(iii) Part of the bearing forces is transferred to the steel sheeting through the so called "concrete wedge" (Ernst, 2006) which forms at the right corner.

(iv) In parallel, the stud induces high compression forces into the rear side of the concrete rib leading to the vertical crack appearing underneath the head of the connector.

The plastic curvature developed at the base of the stud is visible at this stage. The position of the upper plastic hinge follows the location at which the concrete remains undamaged. The gradual crushing of the concrete moves the upper hinge towards the head of the stud as long as its rotation is restrained, as confirmed by the numerically obtained results in Figure 5.11.

6.3 Phase 3: Stud pulling

At higher displacements, the concrete rib crushes while the shear connection capacity reduces gradually. In consideration of the higher slips, a considerable part of the load is carried by the stud through tension forces. Owing to the high shear and tensile stresses acting at the shank of the stud, the connector may also fracture as seen in the conducted push-out tests with 125 mm long studs. From the analysis of the cut section of the specimen CP12A-3 after testing (at ca. 25 mm) given in Figure 6.3, the following considerations can be made:

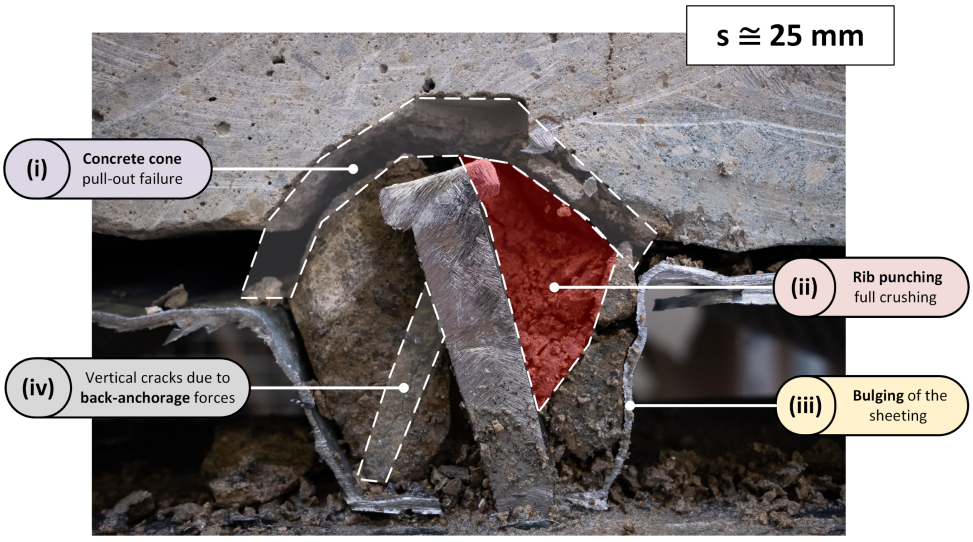

FIGURE 6.3: Cut section of the test specimen CP12A-3 at ca. 25 mm slip highlighting the visibly damaged parts

(i) Failure occurs gradually due to concrete pull-out where the cone detaches from the slab as a consequence of the increasing pulling forces.

(ii) The front side of the rib is fully damaged and the bearing forces along the length of the stud reduce drastically.

(iii) The pulling action of the concrete "wedge" against the sheeting results in the bulging of the profiled sheeting. For further displacements, the steel deck may torn completely as observed in similar configurations (Lawson et al., 2017).

(iv) As a result of the increasing tension in the stud, the rear side of the concrete rib undergo further damage as confirmed by the propagation of the vertical crack.

At this stage, the plastic hinge formed at the base is evident. Depending on the degree of restrain provided by the slab, the head of the stud grdually rotates. However, in case of higher embedment length, such rotation can be prevented up to higher displacements.

6.4 Transition between the load bearing mechanisms

The load bearing mechanisms identified in the previous sections take places at different displacements corresponding to three separate phases. The transition between these phases occurs in a smooth manner in consideration of the gradual propagation of the concrete cone cracks and the progressive crushing of the concrete around the stud. These mechanisms justify the non-linear behaviour of headed stud shear connections observed in push-out tests while the resistance components, defined in the next section, indicate exactly how the force is transferred from the steel beam to the concrete slab.

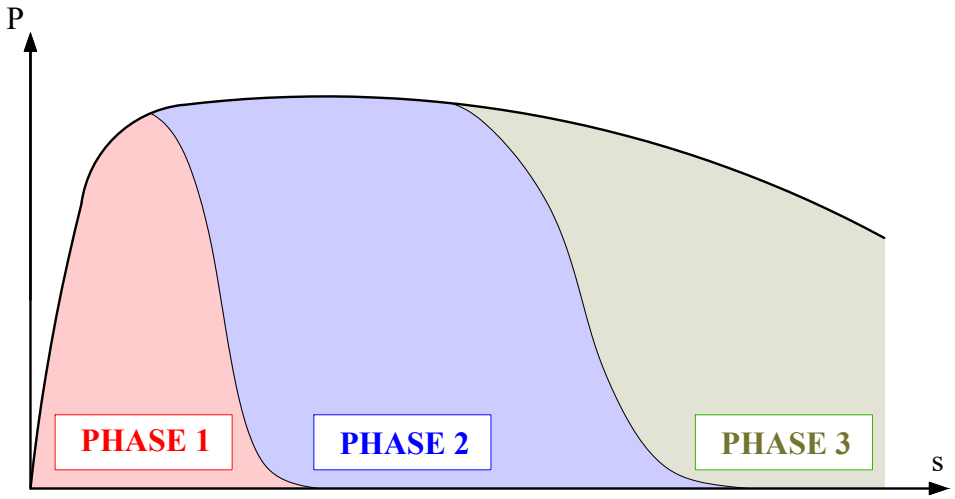

FIGURE 6.4: Transition between the three load bearing mechanisms presented

6.5 Resistance components

Based on the load bearing resistance mechanisms defined, the shear connection can be considered as a structural system where:

- First, the concrete rib acts as a cantilever in beam in bending (Phase 1) until the first cracks appear at the edge of the trough. After the redistribution of the internal forces, the undamaged part of the concrete is modelled as an equivalent system of compression struts (Phase 2 and 3);

- Owing to the high bending and axial stiffness of the stud, it is assumed that the connector is able to transfer a considerable part of the load through axial, bending and shear (beam element);
- The steel sheeting brings part of the punching forces through tension and it also restrains the horizontal slip of the connector, especially in case of through deck welding. All the horizontal tension forces are back-anchored to the rear side of the trough.

From the additional analysis of the compressive stresses in the concrete in Section 5.4 and the bending deformation of the stud in Section 5.5, the different resistance components were determined and summarized in Table 6.1, Table 6.2 and Table 6.3 for Phase 1,2, and 3, respectively.

TABLE 6.1: Resistance components in phase 1

PHASE 1		
Component	**Description**	**Sketch**
A	Concrete cone in bending	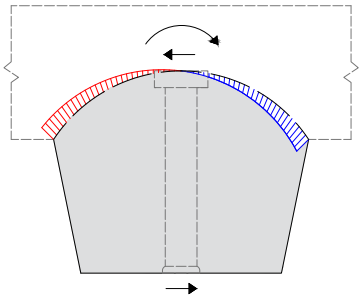
S1	Stud in bending at bottom location	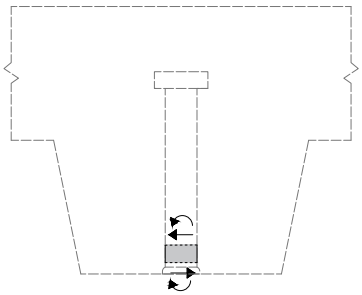
S2	Stud in bending at upper location	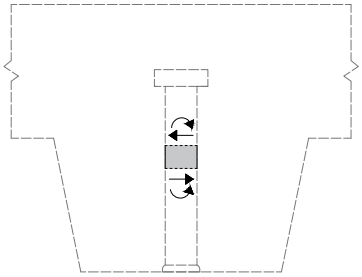

TABLE 6.2: Resistance components in phase 2

PHASE 2		
Component	**Description**	**Sketch**
C1	Concrete cover in front of the stud in compression	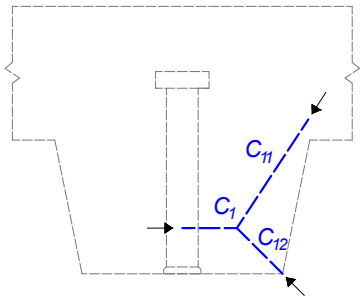
C2	Concrete in compression at the location of the upper hinge	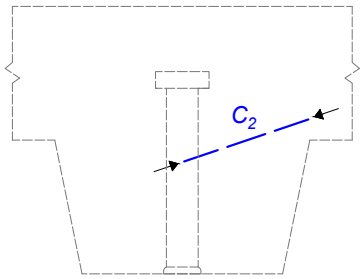
C3	Concrete rib in compression due to shear in the rib	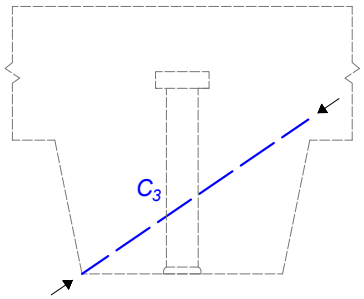
C4	Concrete behind the stud in compression	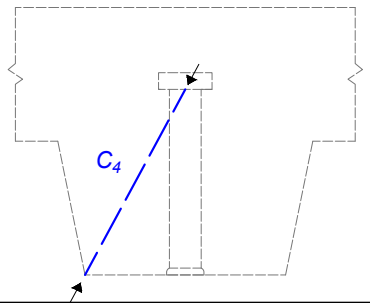
S1	Stud in bending at bottom location	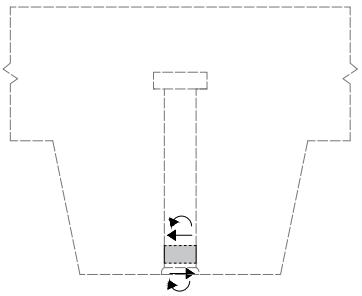

Continue on the next page

Table 6.2 - *continued from previous page*

PHASE 2		
Component	**Description**	**Sketch**
S2	Stud in bending at upper location	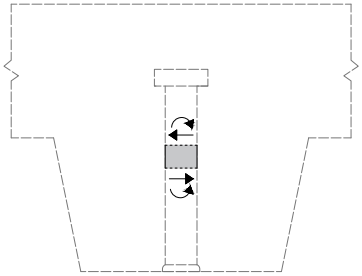
ST	Stud in tension	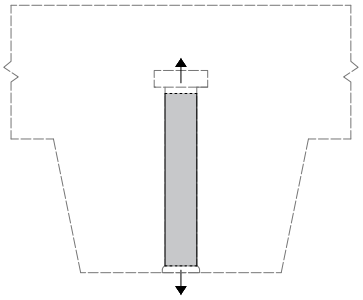
D1	Steel sheeting in tension due to punching forces	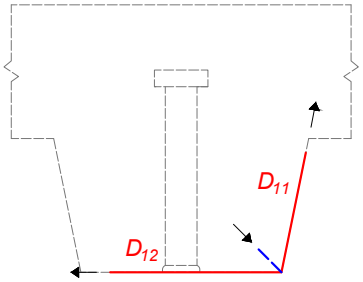
D2	Steel sheeting in tension on the rear side of the shear connection	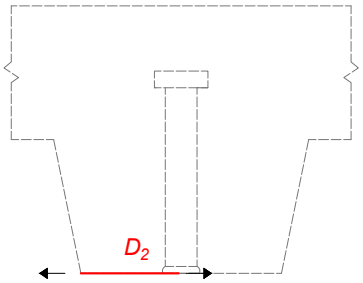

TABLE 6.3: Resistance components in phase 3

PHASE 3		
Component	**Description**	**Sketch**
C2	Concrete in compression at the location of the upper hinge	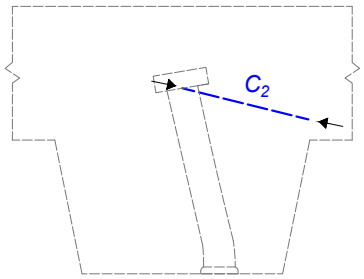
C3	Concrete rib in compression due to shear	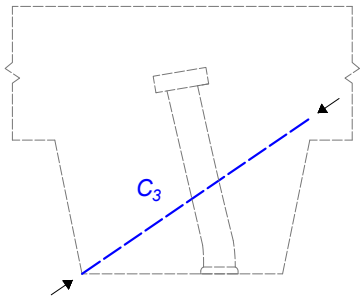
C4	Concrete behind the stud in compression	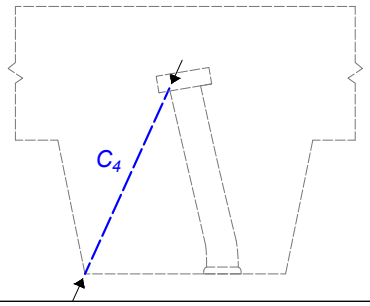
S1	Stud in bending at bottom location	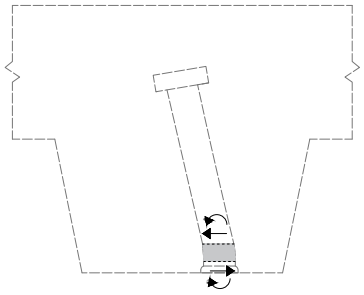
ST	Stud in tension	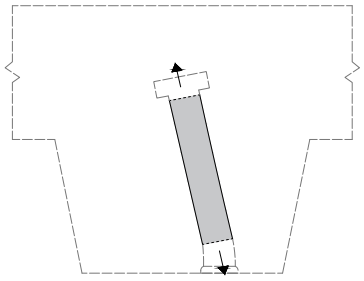

Continue on the next page

Table 6.3 - *continued from previous page*

PHASE 3		
Component	**Description**	**Sketch**
D2	Steel sheeting in tension on the rear side of the shear connection	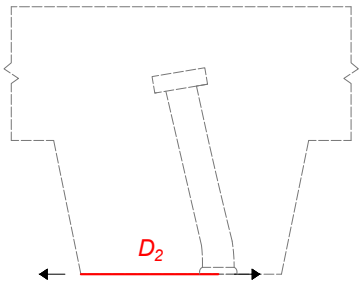

6.6 Limits of application

All the contents of this chapter refer to the analysis of headed stud shear connections centrally placed in the profiled steel sheeting Cofraplus 60 (ArcelorMittal-Construction, 2015). Compared to the common products used in the last decades, the trough of this steel sheeting is relatively narrow and the sequence of the load bearing mechanisms proposed might not be extended to further configurations. For example, in case of headed stud welded in favourable position or with insufficient anchorage length, the pull-out failure appears prematurely at lower displacements because of the reduced portion of concrete in the rear side of the trough that prevent the rotation of the connector. This has been observed in several experimental studies (Yuan, 1996; Lim et al., 2020; Shen and Chung, 2017) where the concrete pull-out occurs prior to the rib punching without any visible damage of the rib due to bearing stresses. Therefore, the sequence of the resistance mechanisms in Figure 6.4 was assumed to be different for such cases where phase 2 or 3 is not fully activated as shown in Figure 6.5.

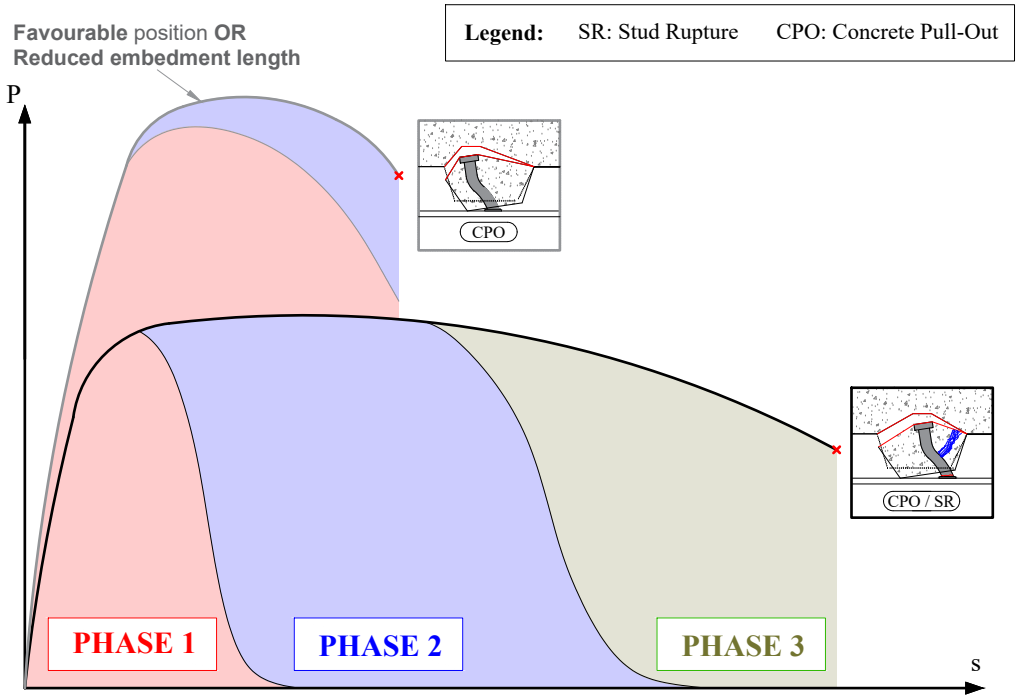

FIGURE 6.5: Typical load-slip curve for headed stud shear connector including the load bearing phases

It was considered that the three main load bearing mechanisms outlined in this chapter are suitable within a specific field of application. However, the exact boundary conditions can be hardly determined by using the outcomes of the tests presented. Hence, the respective mechanical models and analytical equations to predict the resistance of the shear connection were firstly defined in Chapter 7 and the corresponding scope of application was statistically investigated in Chapter 8.

Chapter 7

Mechanical models and analytical equations

Based on the sequence of the load bearing mechanisms described in Chapter 6, three mechanical models were developed and presented in this chapter. In the first phase, the resistance of the shear connection is related to the initiation of concrete cone failure in combination with the bending capacity developed in the studs, as suggested by Nellinger (2015). Until this point, it is assumed that the concrete is uncracked and the whole rib is considered as a linear-elastic cantilever according to Euler-Bernoulli beam theory (Phase 1). By increasing the slip displacement, the concrete cone cracks propagate and the activated load bearing mechanisms change (Phase 2). To model such condition, a new modified strut and tie model is presented. At very large displacements (Phase 3), a considerable part of the load is transferred to the slab through tensile forces in the studs. Similarly, an ad-hoc strut and tie model is proposed. These analytical models refer to conventionally reinforced shear connections without accounting for the effect of waveform reinforcement bars or enhancement devices (Ernst, 2006). Finally, the mechanical-based analytical equations were derived and compared to the push-out test results.

7.1 Phase 1: Cantilever model for uncracked concrete

7.1.1 Structural system

The cantilever model considered in Phase 1 is based on the contribution of Nellinger (2015) where the system was assumed to be the sum of the concrete cone and stud in bending. However, in the current work, the results on the bending component of the stud given in Chapter 5 were also implemented in the analytical equations for predicting the resistance of the shear connection. The model includes two parallel acting systems: the linear-elastic concrete cone and the stud in bending, see Figure 7.1.

From the stress distribution of a linear elastic cantilever beam subjected to the load given in Figure 7.1a, the crack is expected to initiate at the edge where the normal stress reaches the tensile strength of the material f_{ct}. Although the transversal load applied on the slab is not considered in the analytical modelling, its positive effect shown by Lawson et al. (2017) may be accounted in this mechanical model as an equivalent stabilizing moment which prevents the rotation of the concrete rib. As a result, the resistance as well as the ductility of the shear connection would increase.

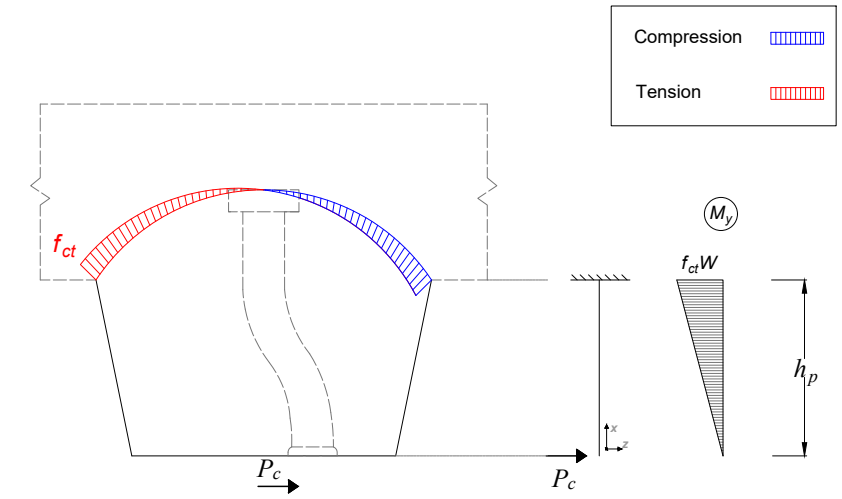

(a)

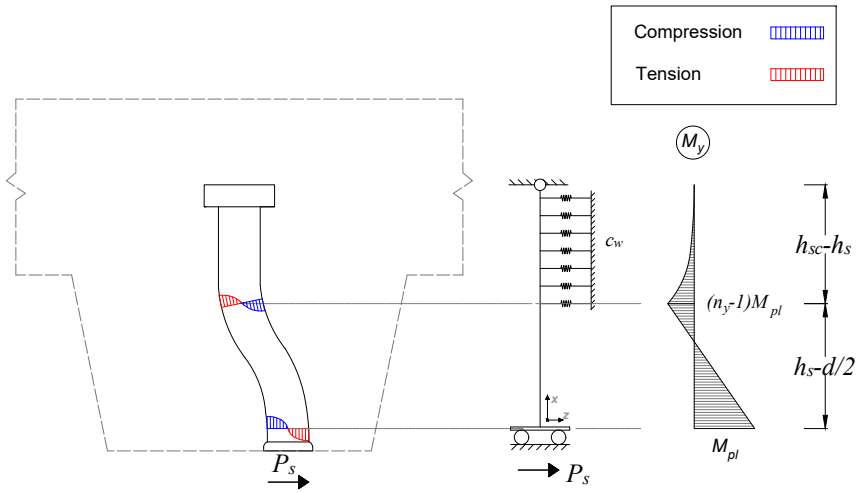

(b)

FIGURE 7.1: Cantilever model of (a) concrete cone and (b) headed stud

Concurrently, the double bending deformation of the stud induces high normal stresses. It was assumed that the bending moment at the a height of $d/2$ reaches the plastic bending resistance of the cross section (i.e. full plastic hinge). The upper plastic hinge may develop at a arbitrary location with a vertical coordinate h_s while the upper side of the connector was considered embedded in concrete by means of a system of linear springs. These horizontal springs with stiffness c_w reproduce the bearing forces of the concrete which restrain the upper part of the stud, as shown in Figure 7.1b. The value of the stiffness c_w is very sensitive to the geometry of the shear connection and two extreme cases can potentially occur. If $c_w \to 0$, no restraint is provided and the upper hinge does not develop. In this case, only one plastic hinge is activated at the base, i.e. $n_y = 1$, see Figure 7.2a. Conversely, if the stiffness of the springs is relatively high, the second plastic hinge is fully activated at the vertical coordinate h_s, as shown in Figure 7.2b. Although the value c_w is highly dependent on the embedment depth $(h_{sc} - h_p)$ as well as the diameter of the stud d, it can be hardly defined by analytical equations. Therefore, the values were implicitly calculated via

the equivalent parameters n_y and h_s, as described in Section 7.1.4.

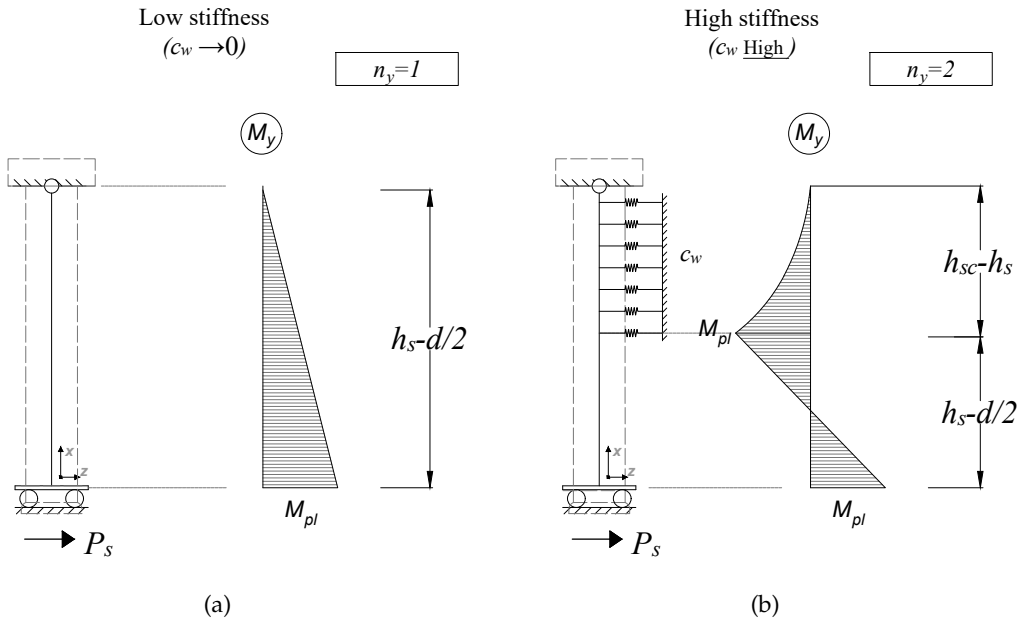

FIGURE 7.2: Equivalent static scheme of the stud for (a) low and (b) high stiffness c_w of the linear elastic springs

7.1.2 Static analysis and assumptions

The cantilever system for the concrete cone in Figure 7.1a is statically determined with a maximum bending moment acting at the rib-slab interface. Instead, the stud is represented by a beam element in Figure 7.1b that comply with the following assumptions: (i) the length of the beam is equal to the distance between the local maximum bending moments; (ii) the bottom plastic hinge always develops at a distance of ca. $d/2$ from the base; (iii) the location where the second plastic hinge develops is considered at a height of h_s. Under such conditions, both systems can be solved and the respective equilibrium equations are given in the following section.

7.1.3 Equilibrium equations

With reference to the system in Figure 7.1a, the load per stud which can be withstood by the uncracked concrete cone P_c, namely component (A), is equal to:

$$P_c = \frac{f_{ct} W}{n_r h_p} \tag{7.1}$$

Where:

f_{ct}	is the tensile strength of concrete
n_r	is the number of studs per rib
W	is the section modulus of the concrete cone surface

The geometry of the concrete cone surface was already evaluated in previous studies (Hawkins and Mitchell, 1984; Lloyd and Wright, 1990). However, based on the

observation of the samples after testing, the geometry identified by Nellinger (2015) was considered, see Figure 7.3.

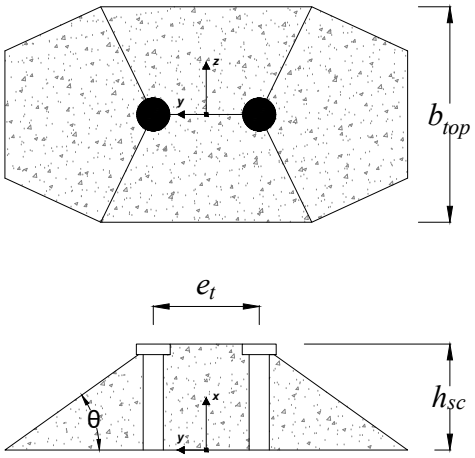

FIGURE 7.3: Geometry of the concrete cone failure surface (Nellinger, 2015)

Assuming that $\cot\theta$ is equal to 1.2 (Nellinger, 2015), the section modulus of the simplified concrete cone surface is:

$$W = [2.4h_{sc} + (n_r - 1)e_t]\frac{b_{max}^3}{6b_{top}} \tag{7.2}$$

With:

$$b_{max} = \max(b_{top}, b_{bot}) \tag{7.3}$$

In parallel, the headed stud deforms in bending developing one or two full plastic hinges (Lungershausen, 1988).From the mechanical model in Figure 7.1b, the part of the load taken by each stud corresponds to the components (S1)+(S2) defined in Chapter 6 and it is given by:

$$P_s = \frac{n_y M_{pl}}{h_s - d/2} \tag{7.4}$$

With:

$$M_{pl} = \frac{f_u d^3}{6} \tag{7.5}$$

The degree of activation n_y as well as the location of the upper plastic hinge h_s remain unknown and they are evaluated in the following section on the basis of the numerical study presented in Chapter 5. Finally, based on the co-existing resistance components of the concrete cone and the stud in bending, the resulting capacity of the shear connection is given by the sum of Eq.(7.1) and Eq.(7.4):

$$P = \frac{f_{ct}W}{n_r h_p} + \frac{n_y M_{pl}}{h_s - d/2} \tag{7.6}$$

7.1.4 Bending capacity of the stud

The values n_y and h_s adopted in Eq.(7.4) were estimated from the numerical results shown in Section 5.5. As the embedment length $(h_{sc} - h_p)$ and the diameter of the stud d represent the key parameters that influence the development of the plastic hinges, n_y was considered proportional to $(h_{sc} - h_p)$ and inversely proportional to d at this stage. However, in case of one stud per rib, it was assumed that the stud always develops two full plastic hinges, as confirmed by the results in Figure 5.12. The relationship in Eq.(7.7) was preliminarily defined and finally checked against the numerical results for two studs per rib $n_r = 2$, see Figure 7.4. As can be seen, the prediction is conservative at 2 mm slip but it is slightly more accurate at 4 or 6 mm slip.

$$n_y = \begin{cases} 2 & n_r = 1 \\ 1.92\frac{(h_{sc}-h_p)}{2d} - 2.84 & n_r = 2 \end{cases} \tag{7.7}$$

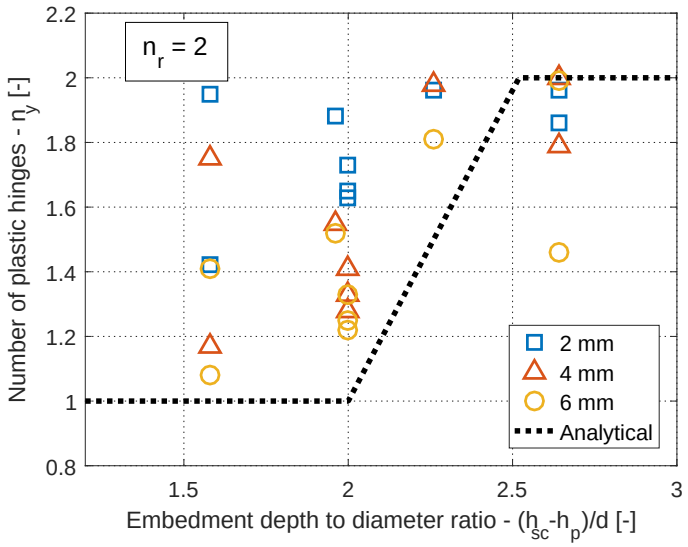

FIGURE 7.4: Numerical and analytical values of n_y in phase 1 for $n_r = 2$

Based on the evaluation of the numerically obtained results at 2 mm slip, the analytical value of the vertical coordinate of the upper plastic hinge h_s was considered equal to 0.82 h_p. The comparison between numerical and analytical predictions is given in the bar chart in Figure 7.5. Although the analytical expression of h_s is simple and it neglects several parameters, the analytical-to-numerical ratio of h_s values has an average of $\mu = 1.03$ with a coefficient of variation CV of approximately 16%.

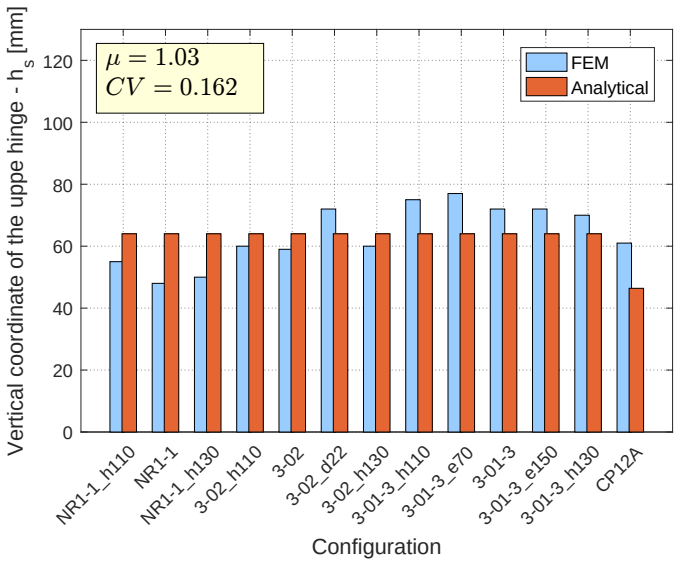

FIGURE 7.5: Numerical and analytical values of h_s at a slip displacement of 2 mm

7.1.5 Resistance function

To account for the effect of the thickness of the steel sheeting, the welding type and the eccentric position of the stud, the correction factor k_u was included in the final expression of the resistance. Furthermore, a coefficient C was added on the basis of preliminary statistical evaluations which will be verified in the next chapter. The resulting resistance function for phase 1 was also proposed for the revised version of EN 1994-1-1 by CEN/TC250/SC4 (2020) and it is equal to:

$$P_1 = C \cdot k_u \cdot \left(\frac{f_{ct} W}{n_r h_p} + \frac{n_y f_u d^3/6}{0.82 h_p - d/2} \right) \tag{7.8}$$

$\frac{f_{ct}W}{n_r h_p}$	Component (A)	Concrete cone in bending
$\frac{n_y M_{pl}}{h_s - d/2}$	Component (S1)+(S2)	Stud in bending

With:

$$C = 1.85 \frac{h_p}{b_0}, \quad 1.0 \leq C \leq 1.35$$

$$W = [2.4 h_{sc} + (n_r - 1) e_t] \frac{{b_{max}}^3}{6 b_{top}}$$

$$n_y = \begin{cases} 2 & n_r = 1 \\ 1.92 \frac{h_{sc} - h_p}{2d} - 2.84 & n_r = 2 \end{cases}$$

TABLE 7.1: Values of the correction factor k_u

	Profiled sheeting with pre-punched holes	Through-deck welded studs $t < 1$ mm	Through-deck welded studs $t \geq 1$ mm
Centred or staggered position	1.0	1.05	1.25
Favourable position	1.1	1.16	1.38
Unfavourable position	0.8	0.95	1.0

Where:

f_{ct} is the tensile strength of concrete

f_u is the ultimate tensile strength of the stud material

n_r is the number of stud connectors per rib

e_t is the transversal spacing between the studs

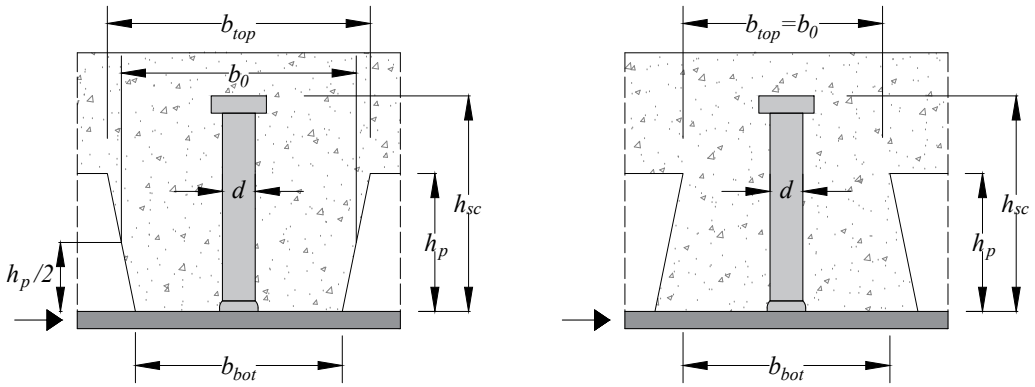

FIGURE 7.6: Geometrical dimensions of headed stud shear connections with (a) open trough and (b) re-entrant sheeting according to the cantilever model presented

7.2 Phase 2: Modified strut and tie model for cracked concrete

7.2.1 Structural system

Based on the considerations made in Chapter 6, once the concrete cone crack starts to propagate, the whole rib is replaced by a complex system of struts. Unlike past strut and tie models (Johnson and Yuan, 1998; Jenisch, 2000; Ernst, 2006), in this case, the proposed "modified" strut and tie model (MSTM) includes the compression struts together with the tension and bending components of the stud. The steel sheeting is assumed to transfer the forces through tension. Finally, the structural system of the MSTM for headed stud shear connections is given in Figure 7.7 where the following components can be distinguished:

(C1) The three struts C_1, C_{11} and C_{12} replace the rib punching compressive stresses. The forces in the strut C_1 are assumed to spread in the struts C_{11} and C_{12} following the direction of the principal compressive stresses observed in the FE model.

(C2) Compressive forces at location of the upper plastic hinge.

(C3) Diagonal strut as a result of the shear in the whole concrete rib.

(C4) Compression forces in the rear side of the trough that prevent the rotation of the connector.

(S1) Plastic bending moment and shear at the base of the connector (node B).

(S2) Bending moment at the upper location of the stud (node A) where a second plastic hinge may develop.

(D1) Tension in the profiled steel sheeting subjected to punching forces by the concrete strut C_{12}. The forces are transferred to the slab by the element D_{11} while the element D_{12} is anchored at the rear side of the connection (node R).

(D2) Tension force in the steel sheeting acting at the base of the stud, especially in case of through-deck welded studs.

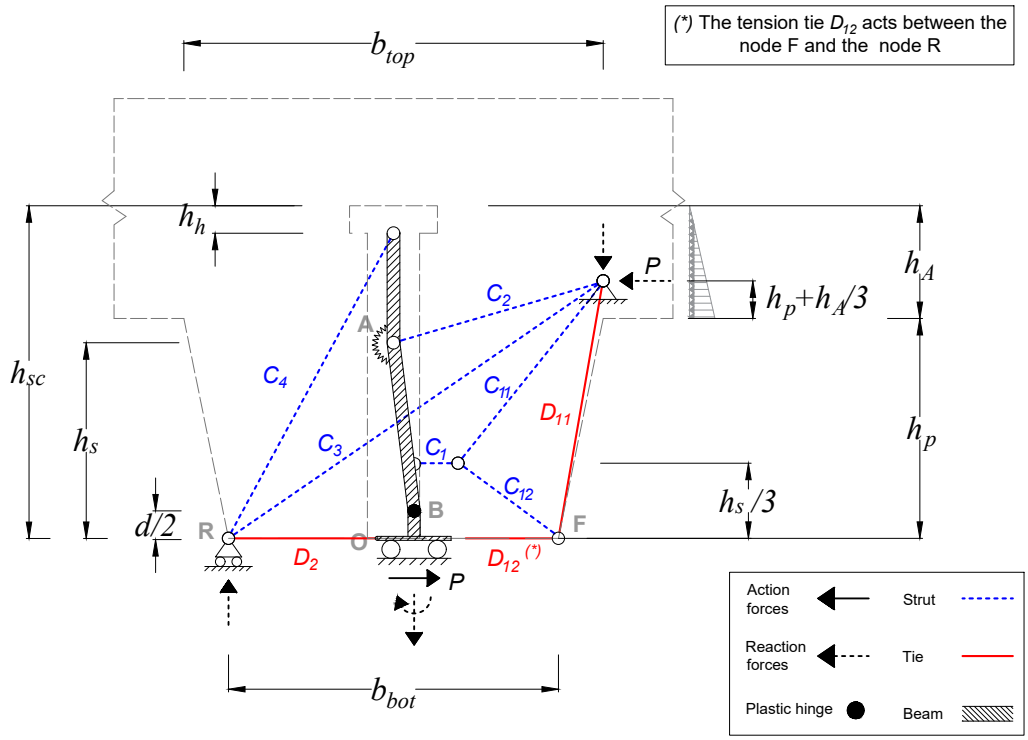

FIGURE 7.7: Modified strut and tie model

As shown in Chapter 5 and confirmed by recent numerical studies on headed studs in profiled sheeting (Shen, 2014), the bearing forces acting on the stud decrease approximately linearly along the height of the stud. Assuming that these stresses are localized up to the height h_s (i.e. between O and A), the resultant force C_1 applies at a height $h_s/3$. As assumed in Phase 1, the lower plastic hinge forms at a fixed distance of $0.5d$ (i.e. node B) from the base of the connector (Nellinger, 2015).

7.2.2 Static analysis and assumptions

The three external equilibrium equations might not be sufficient to calculate all the internal forces of the system. To assess whether the model is statically determined,

the degree of statical indeterminacy n_s was calculated and it is defined as:

$$n_s = \sum_i r_i - 3N \tag{7.9}$$

Where:

N	is the number of the members
r_i	is the number of restrained degrees of freedom (DOFs) of the joint i

In the system shown in Figure 7.7, the total number of members N is 12 while the restrained external DoFs are 5. As already discussed, the bending moment of the stud at the base reaches the sectional plastic bending resistance while the upper hinge may partially develops without reaching the full plastic bending resistance. In consideration of the numerical results in Section 5.5, the DoFs were released at the nodes A and B, and the respective bending moments were estimated using the numerically obtained values of n_y. Additionally, based on experimental observations, it was assumed that the sheeting locally yields and the tie element D_2 reaches its plastic resistance. From these assumptions, 3 DoFs relative to the internal restraints were released resulting in a total of 31. Finally, the degree of statical indeterminacy n_s of the MSTM in this phase is given by:

$$n_s = (31 + 5) - 3 \cdot 12 = 0 \tag{7.10}$$

Considering that all the kinematic constraints are necessary, the structural system in Figure 7.7 is statically determinate and the equilibrium equations are sufficient to calculate the internal forces.

7.2.3 Equilibrium equations

Given the bottom part of the stud (node O) up to the node B shown in Figure 7.8a, from the horizontal equilibrium equation, the following relationship was obtained:

$$V_B + P - D_2 = 0 \tag{7.11}$$

According to the assumptions made, the bending moment at the node B is equal to the plastic bending resistance of the circular cross section M_{pl}:

$$M_B = +M_{pl} \tag{7.12}$$

With:

$$M_{pl} = \frac{f_u d^3}{6} \tag{7.13}$$

If the segment AB in Figure 7.8b is considered, from the rotational equilibrium equation around the node A, the following expression can be obtained:

$$M_A - M_B - C_1 \cdot \frac{2}{3} h_s - V_B \cdot \left(h_s - \frac{d}{2} \right) = 0 \tag{7.14}$$

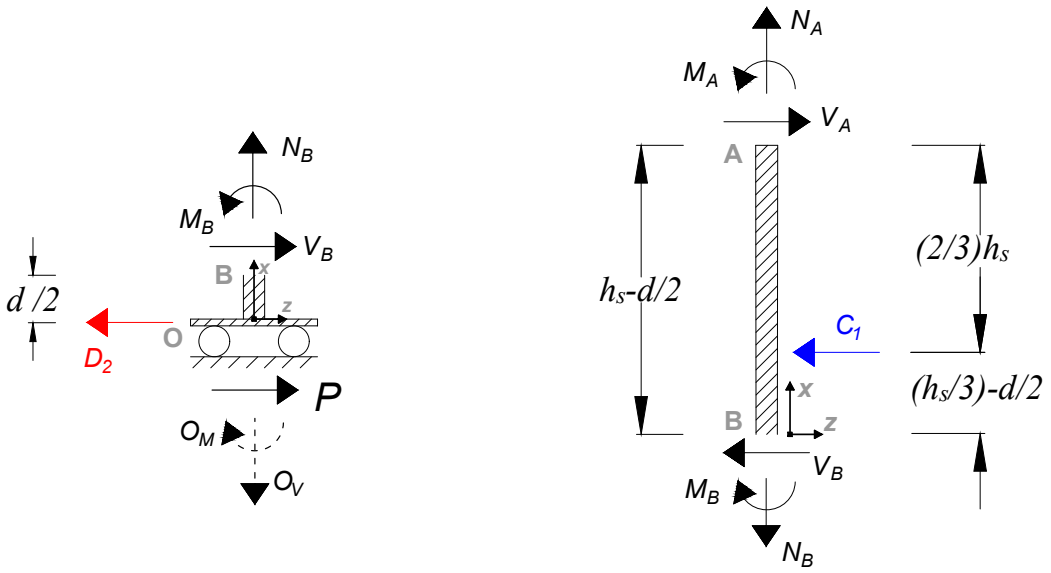

(a) (b)

FIGURE 7.8: Internal forces and reaction forces of the segment (a) BO and (b) AB of the modified strut and tie model

Where the bending moment M_A is not necessarily equal to $-M_{pl}$ in case of partial development of the plastic hinge. Based on the definition of n_y as the "number of plastic hinges" in the stud, M_A can be written as:

$$M_A = -(n_y - 1)M_{pl} \tag{7.15}$$

By substituting Eqs. (7.11) (7.12) and (7.15) in Eq. (7.14), the resulting force P is given by:

$$P = C_1 \cdot \frac{2h_s}{3(h_s - d/2)} + \frac{n_y M_{pl}}{h_s - d/2} + D_2 \tag{7.16}$$

7.2.4 Bending capacity of the stud

The values n_y and h_s were estimated in this section with the support of the numerical results presented in Section 5.5. Similarly to the expression provided in the mechanical model of Phase 1, the "number" of plastic hinges n_y activated in the stud for $n_r = 2$ was considered proportional to the embedment length of the stud $(h_{sc} - h_p)$ and inversely proportional to the diameter of the stud d. Finally, the numerically obtained values of n_y were considered for estimating the following analytical expression:

$$n_y = \begin{cases} 2 & n_r = 1 \\ 1.67\frac{(h_{sc}-h_p)}{2d} - 0.17 & n_r = 2 \end{cases} \tag{7.17}$$

Figure 7.9 confirms that there is a good agreement between numerical and analytically predicted values of n_y, especially for s=4 mm.

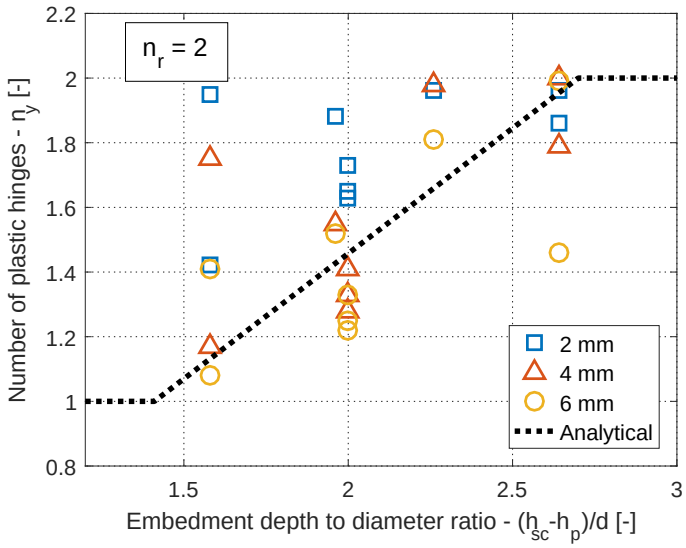

FIGURE 7.9: Numerical and analytical values of n_y in phase 2 for $n_r = 2$

The vertical coordinate of the upper plastic hinge h_s was assessed numerically and the following key parameters were identified: number of studs per rib n_r, height of the stud h_{sc} and slenderness of the sheeting (h_p/b_{top}) which was already considered by Lungershausen (1988) in its design model. Finally, the proposed analytical expression of h_s is given by:

$$h_s = 110\alpha_E \cdot (0.4n_r + 0.2)\left[0.8\left(\frac{h_p}{b_{top}}\right)^2 + 0.6\right][mm] \leq 1.1h_p \tag{7.18}$$

but not higher than $2d$ in computation

With:

$$\alpha_E = \frac{2.7d}{h_{sc} - h_p} \leq 1.0 \tag{7.19}$$

From the comparison between numerically obtained and predicted values of h_s at a slip of 4 mm, a good correlation can be seen in Figure 7.10: the mean value μ of the analytical-to-numerical ratio of h_s is 1.01 with a coefficient of variation CV of ca. 10%.

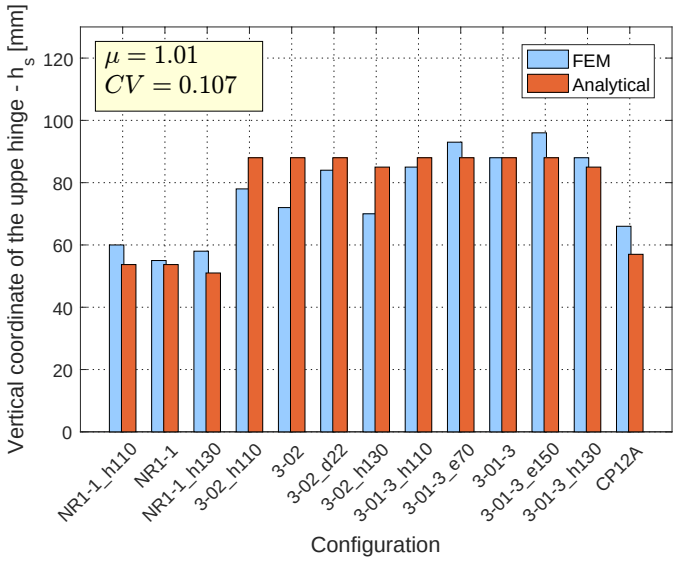

FIGURE 7.10: Numerical and analytical values of h_s at a slip displacement of 4 mm

7.2.5 Condition of failure

As pointed out in Chapter 6, the resistance of the shear connection in the post-cracking stage (i.e. Phase 2) is mostly governed by the local crushing of the concrete in front of the stud where rib punching failure occurs. However, past experimental studies (Yuan, 1996; Shen, 2014; Lim et al., 2020) showed that "concrete pull-out" failure may occur at early stages in case of studs placed on the favourable side or when the length of the stud is limited. To better predict the resistance of such configurations, an alternative failure condition may be implemented in the proposed analytical model. Besides rib punching and concrete pull-out, none of the reported push-out tests on headed studs with profiled sheeting exhibits premature shear failure of the stud shank within the first 6 mm of slip displacement. Thus, the shear failure is not considered in the equations of the proposed mechanical model.

In consideration of the damage observed in the specimens due to rib punching failure, it was assumed that the resistance of the MSTM is achieved when the capacity of the strut C_1, namely $C_{1,max}$, is exploited. The load C_1 is spread between the slab and the sheeting via the struts C_{11} and C_{12}, respectively. The latter corresponds to the portion of concrete named "wedge" which pushes against the steel deck resulting in outwards deformations (bulging). This represents the reason behind the ductility of the push-out test specimens (Chapter 4). In parallel, it was considered that all the other members of the model behave sufficiently ductile to allow the exploitation of the capacity $C_{1,max}$. A schematic representation of the elements involved in the failure is displayed in Figure 7.11.

This condition leads to the load P_2 given by Eq.(7.20) where the value of $C_{1,max}$ remains unknown and it is estimated in the next section.

$$P_2 = P(C_1 = C_{1,max}) \tag{7.20}$$

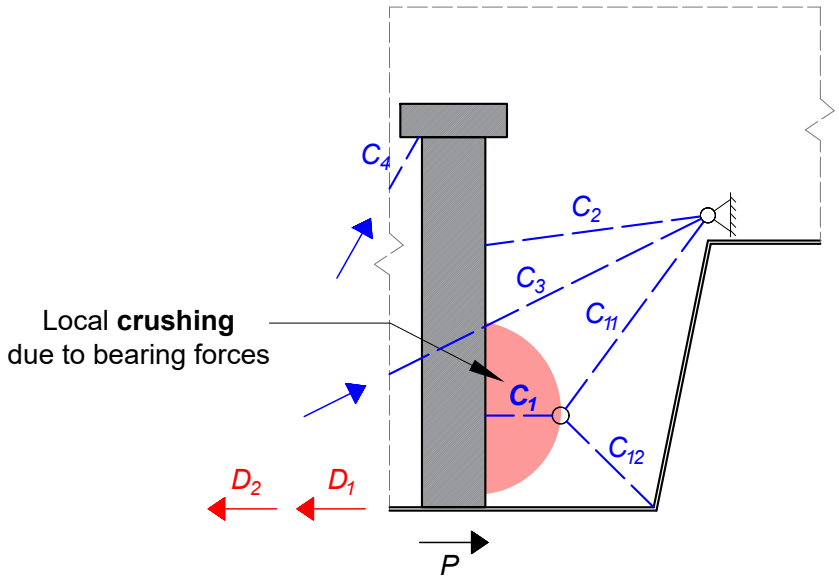

FIGURE 7.11: Detail of the concrete struts involved in the rib punching failure

7.2.6 Analogy with RC corbels

The typical crack pattern of RC corbels at failure is similar to what was observed in the concrete rib of headed stud shear connections in the post-cracking stage (Phase 2). Also, RC corbels are well represented by a simple "strut and tie" model where the tension is taken by the reinforcement bars and the vertical load is transferred to the column via a diagonal concrete strut which can be compared with the strut C_1. From these considerations, the force in the strut is taken as:

$$C_1 = \sigma_{eff} \cdot l \cdot c \tag{7.21}$$

Where:

σ_{eff}	is the effective stress of the concrete
l	is the width of the strut C_1
c	is the depth of the strut C_1

With reference to the analogy between headed stud shear connection and RC corbel in Figure 7.12, the effective width l of the compressed strut C_1 was considered equal to the depth of the compressive zone at the rib-slab interface (Section A-A) as typically done in the strut and tie modelling of RC corbels (Hwang et al., 2000; Russo et al., 2006) at the respective beam-column interface. As the concrete cone cracks developed on the rear side of the stud in Phase 1, the effective section of the rib was simplified as the front part with an height equal to w, as shown in Figure 7.13. On the other hand, the depth of the strut c was assumed equal to $2d$ as a result of a preliminary evaluation of the compressive stresses in the FE model in the transversal direction. However, further investigations are recommended to accurately calibrate this variable for different configurations.

Although it is acknowledged that the headed stud transfers also bending moment and shear, in this specific case the connector was considered as an equivalent reinforcement bar in tension with the cross sectional area A_s. This procedure was followed only to estimate the capacity of the strut C_1 as well as the corresponding

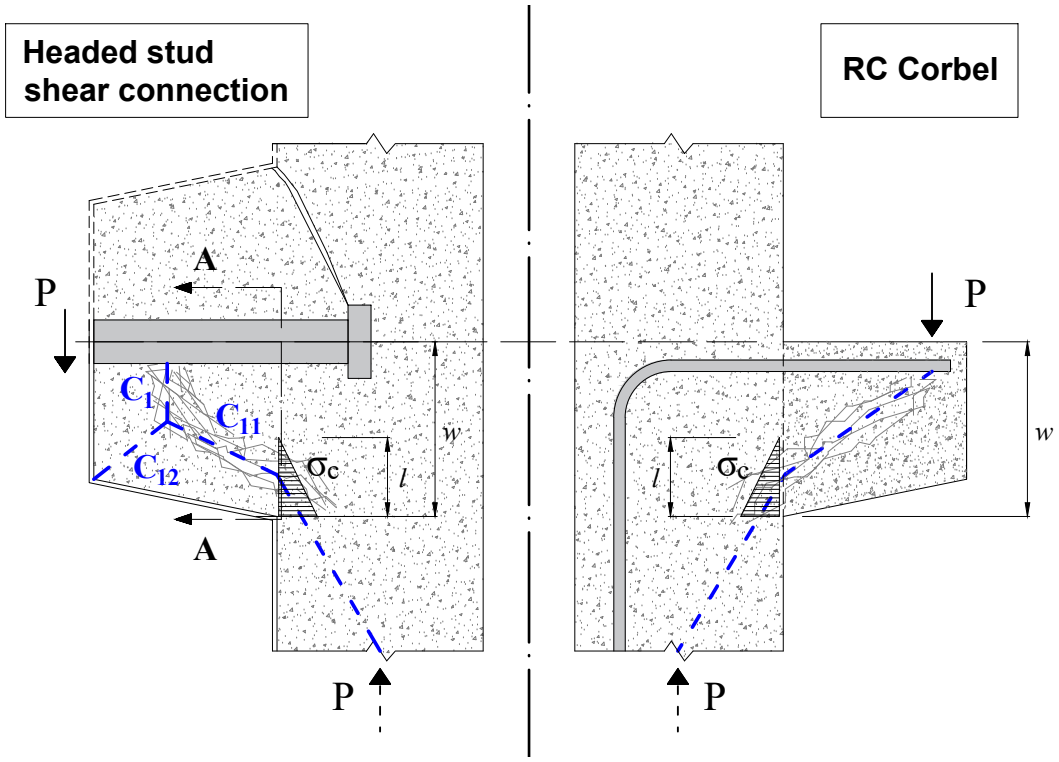

FIGURE 7.12: Analogy between headed stud shear connection in profiled steel sheeting in the post-cracking stage (Phase 2) and RC corbel

key variables. Therefore, it does not accurately reproduce the real distribution of the stresses at the rib-slab interface.

From these considerations, section A-A was taken as a cross section of a single layer reinforced concrete beam subjected to hogging moment. The corresponding elastic distribution of the axial strain and compression stresses can be derived in accordance with Euler-Bernoulli beam theory, as displayed in Figure 7.13. The horizontal equilibrium equation gives the following relationship:

$$-\frac{1}{2}\sigma_{c,max} \cdot c \cdot l + \sigma_s \cdot A_s = 0 \tag{7.22}$$

In addition, from the elastic distribution of the axial strains, it can be found:

$$\frac{\varepsilon_{c,max}}{l} = \frac{\varepsilon_s}{w - l} \tag{7.23}$$

Considering the materials as linear elastic, Eq.(7.23) can be written as:

$$\frac{\sigma_{c,max}}{E_c l} = \frac{\sigma_s}{E_s(w - l)} \tag{7.24}$$

From Eq.(7.22) and Eq.(7.24), the quadratic equation with the unknown l was obtained:

$$l^2 + 2xw \cdot l - 2xw^2 = 0 \tag{7.25}$$

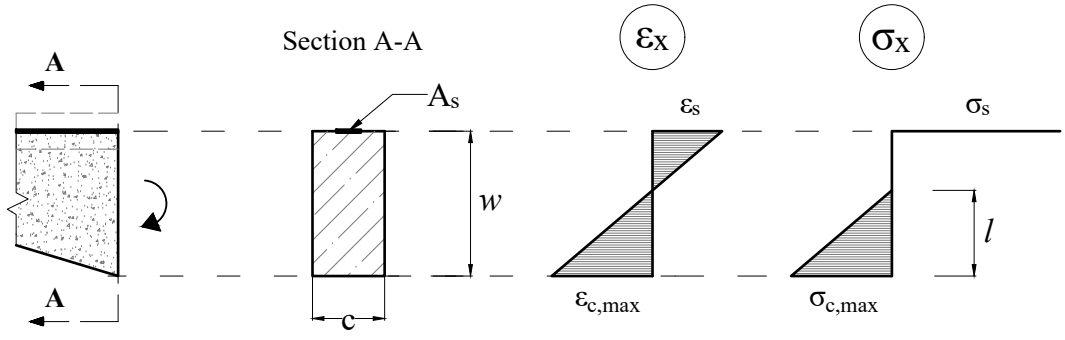

FIGURE 7.13: Simplified effective section at the rib-slab interface subjected to hogging bending moment and distribution of the axial strains and stresses

With:

$$x = \frac{E_s}{E_c}\frac{A_s}{c \cdot w} \tag{7.26}$$

l was finally calculated by solving Eq.(7.25) and considering only the positive value which gives:

$$l = (\sqrt{x^2 + 2x} - x) \cdot w \tag{7.27}$$

Finally, Eq.(7.27) can be further condensed as follows:

$$l = k \cdot w \tag{7.28}$$

With:

$$k = \sqrt{x^2 + 2x} - x \tag{7.29}$$

The resistance of the strut C_1 is exploited when the effective compressive stress σ_d reaches its maximum value $\sigma_{d,max}$. As already confirmed by experimental evidences, the concrete portion replaced by the struts C_1 and C_{11} undergoes splitting tensile stresses (in the transversal direction) as shown in Figure 6.2. EN 1992-1-1 (BSI, 2004a) gives as recommended value of the compression strength of the cracked strut $0.6f_c$. Therefore, the estimated value of the capacity of the strut $C_{1,max}$ is equal to:

$$C_{1,max} = 0.6f_c \cdot k \cdot w \cdot 2d \tag{7.30}$$

7.2.7 Resistance function

If two studs are placed in the same rib, part of the concrete between the connectors is subjected to higher stresses due to their interaction. To solve this issue, a reduction factor $k_n = 0.8$ applied to $C_{1,max}$ was preliminarily proposed for $n_r = 2$. In order to include cases with re-entrant profiled sheeting, an amplification factor $k_s = 1.7$ was finally added to the concrete component while the load taken by the steel deck was

simplified as follows:

$$D_2 = k_w \cdot f_{yp} \pi t d \tag{7.31}$$

Where:

f_{yp}	is the yield strength of the steel sheeting material
t	is the thickness of the steel sheeting

From a preliminary statistical evaluation of different subsets, a reduction factor $k_w = 0.7$ was introduced for pre-punched hole configurations while no reduction ($k_w = 1.0$) was considered for through-deck welded studs where the tension tie D_2 is supposed to transfer more force. To verify the suitability of the previous assumptions and simplifications, further evaluations were carried out and detailed in Chapter 8.

Based on the procedure described, the final expression for predicting the post-cracking (Phase 2) resistance P_2 of headed stud connections in profiled steel sheeting is:

$$P_2 = k_s k_n (1.2 f_c \cdot d \cdot k \cdot w) \cdot \zeta + \frac{n_y f_u d^3/6}{h_s - d/2} + k_w \cdot f_{yp} \pi t d \tag{7.32}$$

$k_s k_n (1.2 f_c \cdot d \cdot k \cdot w) \cdot \zeta$	Component (C1)	Rib punching
$\frac{n_y f_u d^3/6}{h_s - d/2}$	Component (S1)+(S2)	Stud in bending
$k_w \cdot f_{yp} \pi t d$	Component (D2)	Steel sheeting in tension

With:

$$k_s = \begin{cases} 1.0 & \text{Open trough profiles} \\ 1.7 & \text{Re-entrant profiles} \end{cases} \tag{7.33}$$

$$k_n = \begin{cases} 1.0 & n_r = 1 \\ 0.8 & n_r = 2 \end{cases} \tag{7.34}$$

$$k = \sqrt{x^2 + 2x} - x \tag{7.35}$$

$$x = \frac{E_s}{E_c} \frac{\pi d}{8w} \tag{7.36}$$

$$\zeta = \frac{2 h_s}{3(h_s - d/2)} \tag{7.37}$$

$$n_y = \begin{cases} 2 & n_r = 1 \\ 1.67\frac{(h_{sc}-h_p)}{2d} - 0.17 & n_r = 2 \end{cases} \tag{7.38}$$

$$h_s = 110\alpha_E \cdot (0.4n_r + 0.2)\left[0.8\left(\frac{h_p}{b_{top}}\right)^2 + 0.6\right][mm] \leq 1.1h_p \tag{7.39}$$

but not lower than $2d$ in computation

With:

$$\alpha_E = \frac{2.7d}{h_{sc} - h_p} \leq 1.0 \tag{7.40}$$

$$k_w = \begin{cases} 0.7 & \text{Pre-punched holes} \\ 1.0 & \text{Through-deck welding} \end{cases} \tag{7.41}$$

Where:

E_c	is the modulus of elasticity of concrete
E_s	is the modulus of elasticity of the stud material
n_r	is the number of stud connectors per rib
f_c	is the compressive strength of concrete
f_u	is the ultimate tensile strength of the stud material
f_{yp}	is the yield strength of the material of the sheeting
t	is the thickness of the steel sheeting

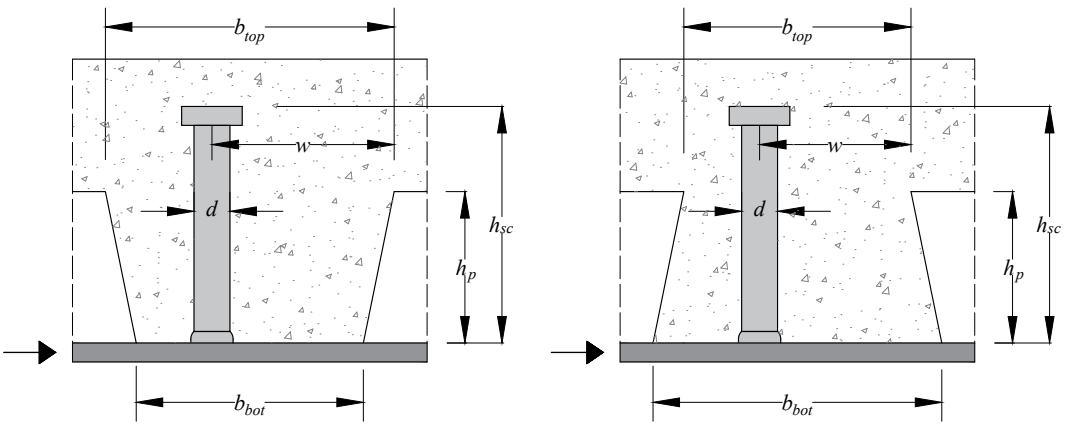

FIGURE 7.14: Geometrical dimensions of headed stud shear connections with (a) open trough and (b) re-entrant sheeting according to the MSTM

7.3 Phase 3: Strut and tie model

7.3.1 Structural system

Providing that concrete pull-out and stud rupture do not occur, second-order geometric effects become predominant at higher slip displacements where the connector transfers a considerable part of the shear load by tensile stresses (Lungershausen, 1988). As discussed in Chapter 6, these resistance mechanisms can be activated only if enough embedment depth is ensured. In this phase, the portion of the concrete rib in front of the stud is fully crushed and it is not able to transfer significant compressive stresses. Because of the rotation of the head of the connector, the second curvature (together with the upper plastic hinge) gradually vanishes while the centre of stiffness moves towards the slab. The "strut and tie" model representing these conditions is finally illustrated in Figure 7.15.

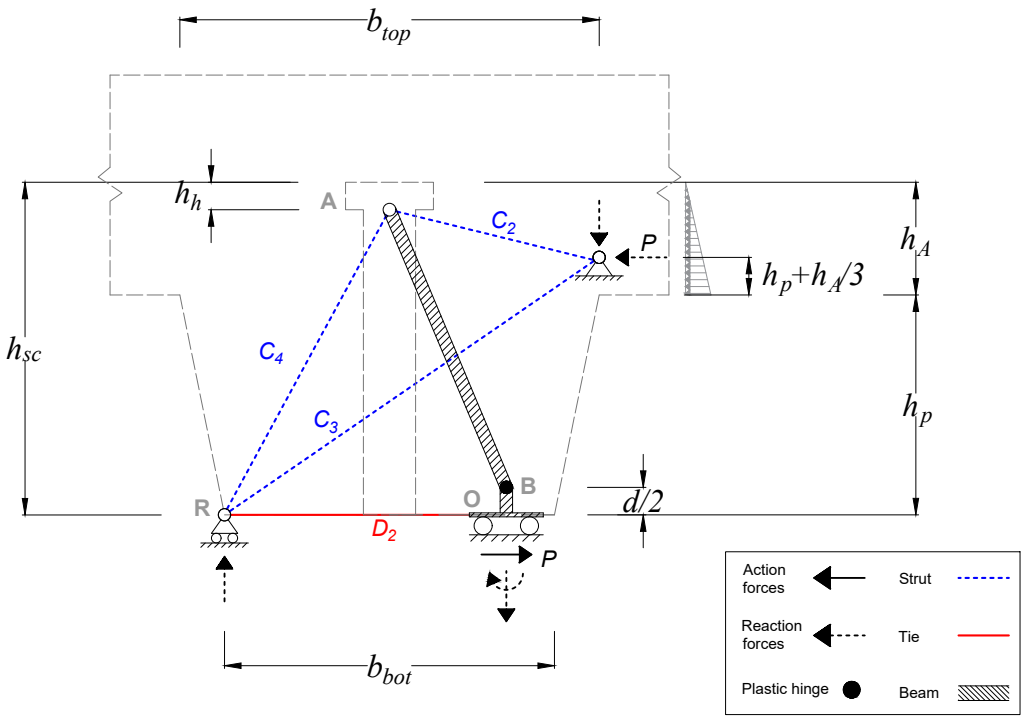

FIGURE 7.15: Strut and tie model at large displacements

7.3.2 Static analysis and assumptions

The strut and tie model (STM) shown in Figure 7.15 is a development of the system presented in phase 2. Owing to the progressive damage of the front side of the concrete rib, the load in the strut C_1 was considered negligible. From a static analysis, the system consist of 6 elements ($N = 6$) with 5 external restrains. Assuming that the tie element D_2 is yielded and considering the bottom plastic hinge at the node B, the internally restrained DoFs are 13 and the resulting degree of static indeterminacy n_s is given by:

$$n_s = (13 + 5) - 3 \cdot 6 = 0 \tag{7.42}$$

Considering that all the kinematic constraints are necessary, the current system is statically determined under the assumptions made and the internal forces can be calculated by means of equilibrium equations.

7.3.3 Equilibrium equations

Because the stud undergoes high slip displacements in Phase 3, it was assumed that the deformed shape of the connector affects significantly the equilibrium of the system. Hence, the deformations of the stud were taken into account in the equilibrium equations of the system, as can be seen in Figure 7.16, assuming an arbitrary slip value s.

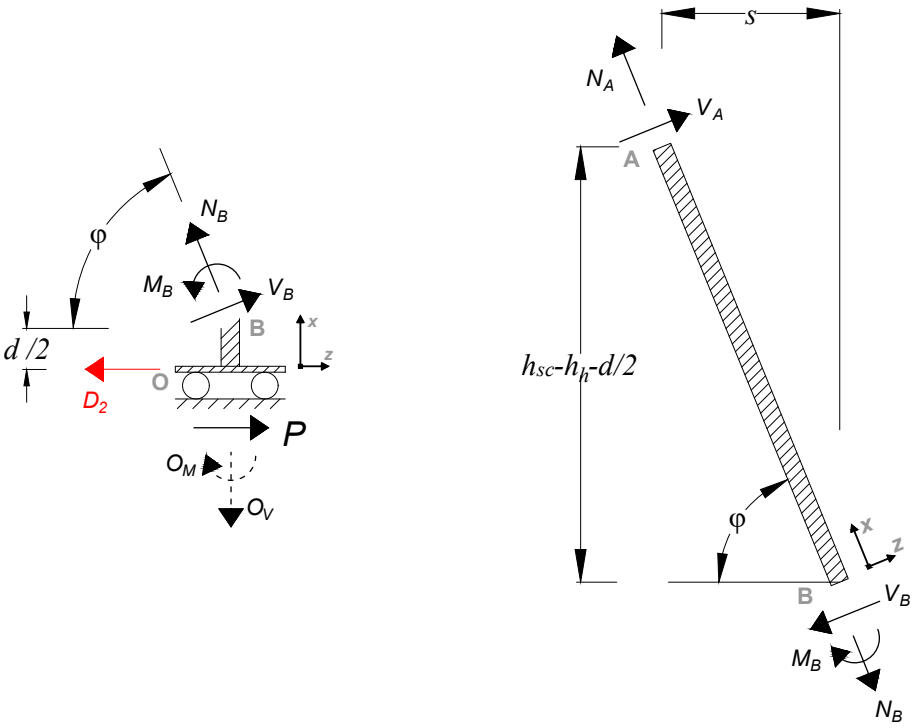

(a) (b)

FIGURE 7.16: Internal forces and reaction forces of the segment (a) BO and (b) AB of the strut and tie model

First, from the horizontal equilibrium equation of the element OB, see Figure 7.16a, the following relationship can be found:

$$V_B \sin\ \phi - N_B cos\ \phi + P - D_2 = 0 \tag{7.43}$$

From Eq.(7.43), the shear force V_B is:

$$V_B = N_B cot\ \phi + \frac{D_2 - P}{\sin \phi} \tag{7.44}$$

As shown in Figure 7.15, it was assumed that the head of the connector does not translate but it rotates around the bottom part of the head (node A). Therefore, the vertical distance between the point A and B was taken as $(h_{sc} - h_h - d/2)$, as displayed in Figure 7.16b. From the rotational equilibrium equation around the node A, the

following expression can be obtained:

$$-M_B - V_B \cdot \sqrt{(h_{sc} - h_h - d/2)^2 + s^2} = 0 \tag{7.45}$$

Thus, the shear force V_B can be written as:

$$V_B = -\frac{M_B}{\sqrt{(h_{sc} - h_h - d/2)^2 + s^2}} \tag{7.46}$$

The combination of Eq.(7.44) and Eq.(7.46) gives the expression:

$$-\frac{M_B}{\sqrt{(h_{sc} - h_h - d/2)^2 + s^2}} = N_B cot\ \phi + \frac{D_2 - P}{\sin\ \phi} \tag{7.47}$$

By solving Eq.(7.47), the final expression of the load P is obtained:

$$P = \frac{M_B \sin\ \phi}{\sqrt{(h_{sc} - h_h - d/2)^2 + s^2}} + N_B \cos\ \phi + D_2 \tag{7.48}$$

Whilst the value of D_2 can be taken as in the previous phase, the tensile force N_B is unknown. In order to extrapolate the capacity of the STM, this force was limited according to a failure criterion which is described in the next section.

7.3.4 Condition of failure

The failure criterion was defined in the stud shank at the node B considering the interaction between the axial force N_B, the shear force V_B and the bending moment M_B. However, it was assumed that the shear does not interact with the axial force as the shear stresses develop mostly in the centre of the cross-section. Therefore, the failure of the STM occurs when the bending moment at node B reaches the reduced bending resistance $M_{pl,N}(N/N_{pl})$ accounting for the influence of the axial force N. To calculate the analytical M-N interaction curve, the axial stress distribution was determined in accordance with rigid-plastic theory applied to a circular cross-section, as visualized in Figure 7.17.

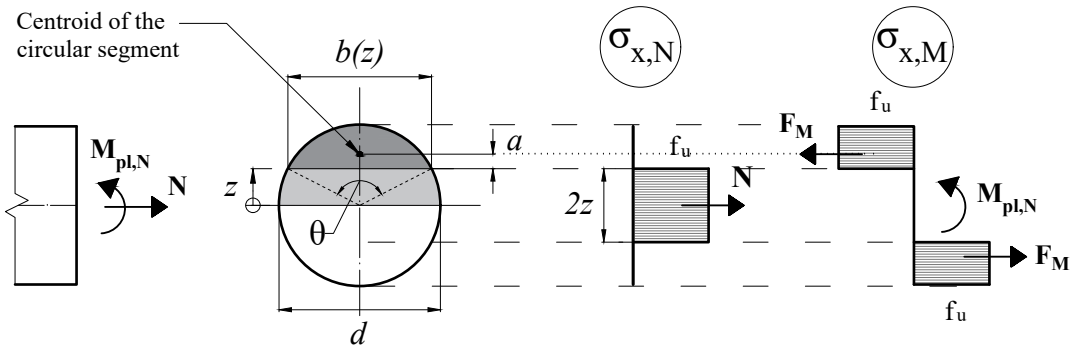

FIGURE 7.17: Axial stress distribution due to axial force N and bending moment M in a circular cross-section according to rigid-plastic theory

First, given a certain value of z, the respective axial force $N(z)$ and bending moment $M(z)$ can be calculated. Considering that the height of the area considered is equal

to $2z$, the axial force $N(z)$ is defined as:

$$N(z) = 2\int_0^z f_u \cdot b(z^\star)dz^\star \tag{7.49}$$

Where $z^\star$ is a the geometrical coordinate used for the integration of the function from 0 to z. The width $b(z^\star)$ is given by:

$$b(z^\star) = 2\sqrt{\frac{d^2}{4} - (z^\star)^2} \tag{7.50}$$

By using this expression of $b(z^\star)$ in Eq.(7.49), the integral can be written as:

$$N(z) = f_u d^2 \int_0^z \frac{2}{d}\sqrt{1 - \left(\frac{2}{d}z^\star\right)^2}\, dz^\star \tag{7.51}$$

The integral in Eq.(7.51) can be solved analytically and the resulting axial force is equal to:

$$N(z) = f_u d^2 \left[\frac{1}{2}\arcsin\left(\frac{2}{d}z\right) + \frac{z}{d}\sqrt{1 - \left(\frac{2}{d}z\right)^2}\right] \tag{7.52}$$

With reference to Figure 7.17, the corresponding plastic bending moment is:

$$M_{pl,N}(z) = F_M \cdot (2a + 2z) \tag{7.53}$$

With:

$$F_M(z) = \frac{N_{pl} - N(z)}{2} \tag{7.54}$$

The position of the centroid of the circular segment indicated in Figure 7.17 can be found via the variable a which is given by:

$$a = \frac{2d\sin^3\left(\frac{\theta}{2}\right)}{3(\theta - \sin\theta)} \tag{7.55}$$

With:

$$\theta = 2\arccos\left(\frac{2}{d}z\right) \tag{7.56}$$

By substituting the definition of the variables F_M and a in Eq.(7.53), the following expression can be found:

$$\frac{M_{pl,N}}{M_{pl}} = \frac{1}{M_{pl}}\frac{(N_{pl} - N(z))}{2}\frac{2d\sin^3\theta\left(\frac{\theta}{2}\right)}{3(\theta - \sin\theta)} \tag{7.57}$$

The domain defined by Eq.(7.57) was plotted in Figure 7.18 and compared with the simplified parabolic relationship proposed by EN 1993-1-1 (BSI, 2005) in Eq.(7.58):

$$\frac{M_{pl,N}}{M_{pl}} = 1 - \left(\frac{N}{N_{pl}}\right)^2 \tag{7.58}$$

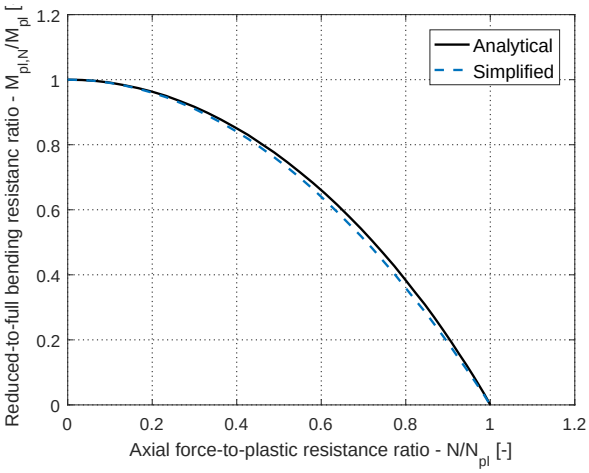

FIGURE 7.18: Analytical and simplified bending moment-axial force interaction diagram for circular cross-section

As seen in Figure 7.18, the analytical M-N curve of Eq.(7.57) is almost equal to the expression in Eq.(7.58). Hence, the simplified M-N interaction plot was considered in the next steps. In order to define the condition of failure, the axial force acting at node B is required. For this purpose, further to the numerical investigations in Chapter 5, a few more simulations were carried out up to higher displacements. Considering the simulation CP12A (see Table 5.4 for details), the axial force-to-plastic resistance ratio of the cross section of the stud N_B/N_{pl} as well as the inclination angle ϕ is finally plotted in Figure 7.19 as a function of the slip s. The results indicate that the ratio N_B/N_{pl} at a slip of 20-25 mm is almost 0.3 while the inclination angle of the stud θ deviates significantly from the initial value of $\pi/2$. However, although the rupture of the connector can limit the resistance of the system in this phase, the fracture of the stud material was not implemented in the FE model.

Using the simplified M-N plot relationship given in Eq.(7.58), the axial force at the node B $N_B = 0.3N_{pl}$ delivers a value of the bending resistance $M_B = 0.91M_{pl}$, as shown in Figure 7.20. In accordance with the failure criterion assumed, the values of N_B and M_B can be finally implemented in Eq.(7.48) to calculate the respective capacity of the STM P_3.

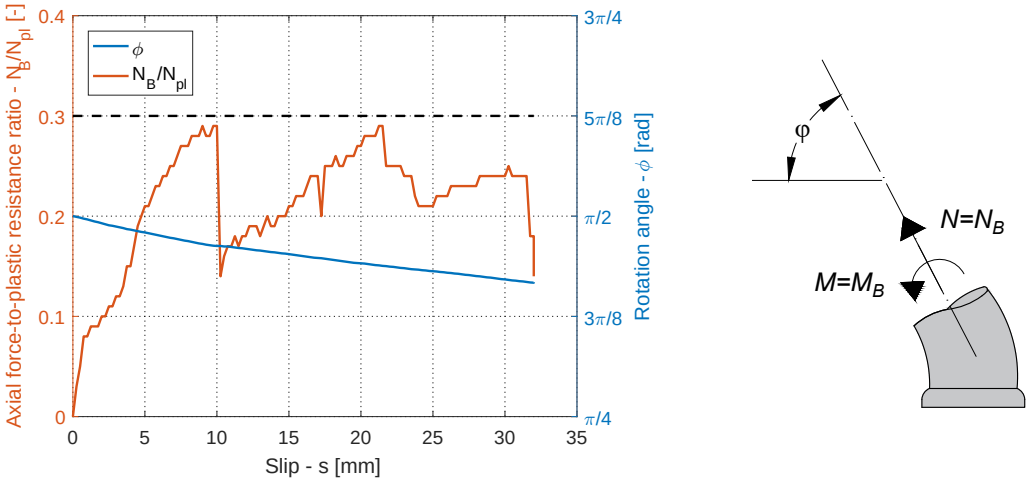

FIGURE 7.19: Tensile force-to-plastic resistance ratio observed at node B from the simulation CP12A

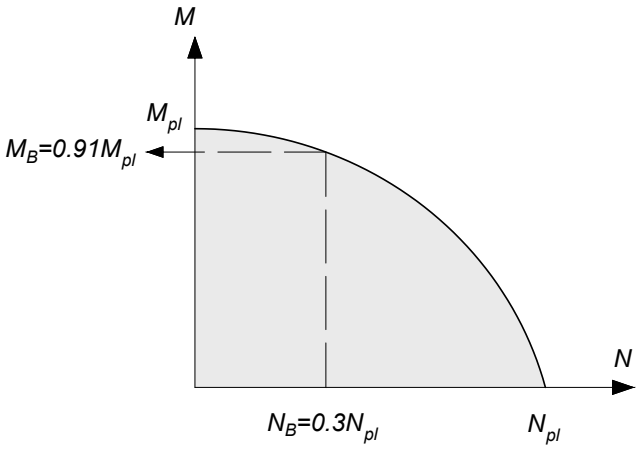

FIGURE 7.20: Bending moment-axial force interaction diagram considered for the cross-section of the stud at node B

7.3.5 Resistance function

From the outcomes of the previous section, the following expression of the resistance of the shear connection in phase 3 was derived:

$$P_3 = \frac{0.91(f_u d^3/6)\ \sin\phi}{\sqrt{(h_{sc} - h_h - d/2)^2 + s^2}} + 0.3 f_u \frac{\pi d^2}{4} \cos\phi + k_w f_{yp} \pi t d \tag{7.59}$$

$\frac{0.91(f_u d^3/6)\ \sin\phi}{\sqrt{(h_{sc}-h_h-d/2)^2+s^2}}$	Component (S1)	Stud in bending at bottom location
$0.3 f_u \frac{\pi d^2}{4} \cos\phi$	Component (ST)	Stud in tension
$k_w f_{yp} \pi t d$	Component (D2)	Steel sheeting in tension

With:

$$\phi = \arctan\left(\frac{h_{sc} - h_h - d/2}{s}\right) \tag{7.60}$$

Where:

f_c	is the compressive strength of concrete
f_u	is the ultimate tensile strength of the stud material
f_{yp}	is the yield strength of the material of the sheeting
t	is the thickness of the steel sheeting
s	is the slip of the shear connection
h_h	is the height of the stud head

7.4 Transition between the mechanical models

As already indicated in Section 6.4, the transition between the three main phases occurs in a smooth manner owing to the gradual concrete cone crack propagation (between first and second phases) and the local damage of the rib (between second and third phases). Based on the mechanical models presented in the previous section, three different resistance values were derived analytically in Eqs. (7.8), (7.32) and (7.59) respectively. These values represent three points of the load-slip curve observed in push-out tests at different slip displacements, as shown in Figure 7.21.

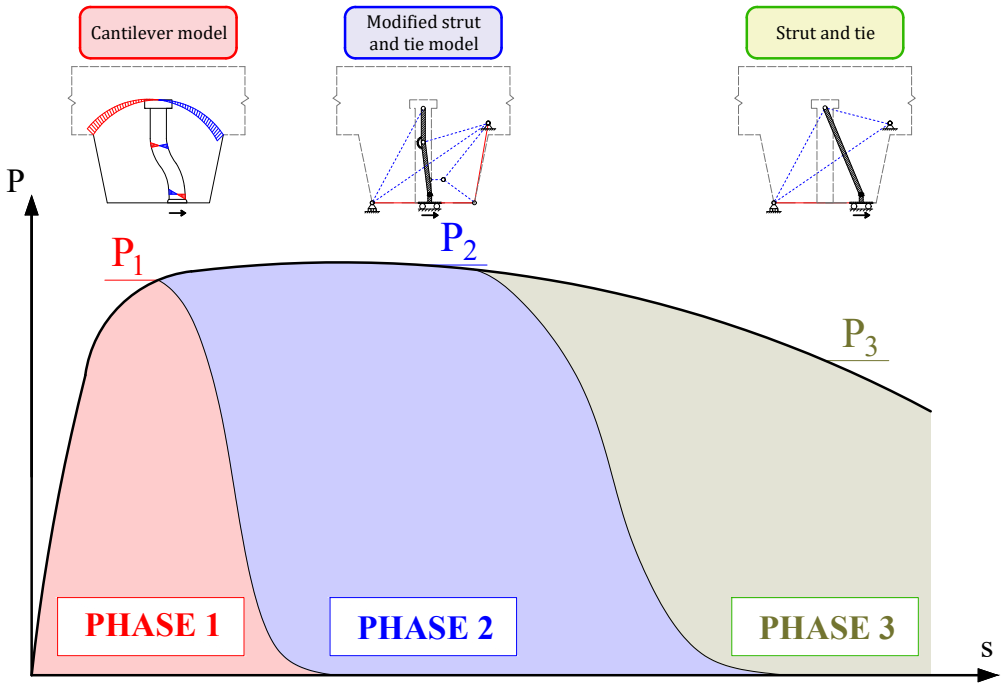

FIGURE 7.21: Transition between the proposed mechanical models at different slip displacements

7.5 Comparison with push-out tests

To check the suitability of the mechanical models proposed in this chapter, the three resistance values P_1, P_2 and P_3 were compared with the experimental load-slip curve of the conducted push-out tests presented in Chapter 4 as well as with the tests of the research project DISCCO (Lawson et al., 2017). As done with past design models in Chapter 2, tests with transversal load were not included in this evaluation. In consideration of the transition between the phases, it was assumed that these three analytical values of the resistance fall within the slip intervals of 1-3, 3-10 and 24-25 mm, respectively. In parallel, the respective experimental values of the resistance $P_{e,i}$ were defined for each phase i as follows:

$$P_{e,1} = \max_{s\in(1,3)\ mm} P_e(s) \tag{7.61}$$

$$P_{e,2} = \max_{s\in(3,10)\ mm} P_e(s) \tag{7.62}$$

$$P_{e,3} = \max_{s\in(24,25)\ mm} P_e(s) \tag{7.63}$$

The experimental and analytical resistance values shown in Figure 7.22 refer to the test CP12C-1 where a good agreement between the analytical and experimental load-slip curve can be seen.

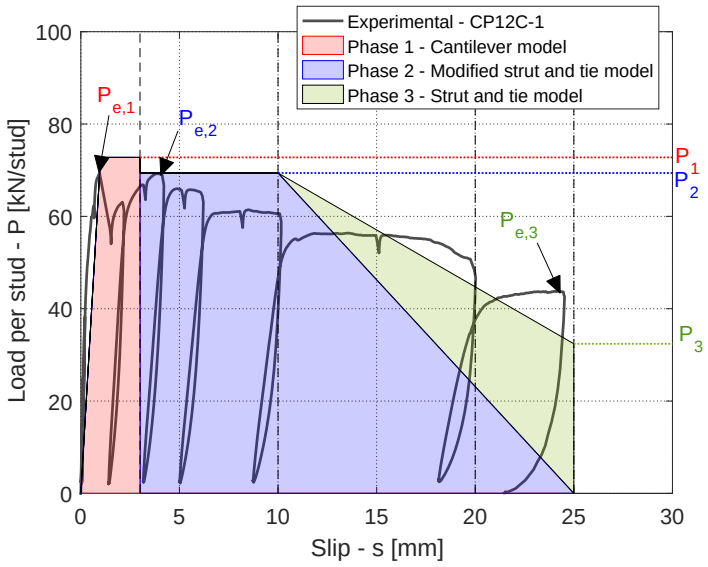

FIGURE 7.22: Comparison between experimental load-slip curve of the specimen CP12C-1 and analytically predicted values of the resistance

The three values P_1, P_2 and P_3 were finally compared with the corresponding experimental values $P_{e,1}$, $P_{e,2}$ and $P_{e,3}$ for each test and the results are visualized in Figure 7.23. Only the series CP12B was not considered because the mechanical models are limited to conventionally reinforced specimens where the effect of the waveform bars is not included. All the details are given in Table 7.2.

TABLE 7.2: Analytical prediction and experimental values of the load of the tests presented in Chapter 4 and DISCCO tests (Lawson et al., 2017)

Test	Analytical			Experimental			Ratio		
	P_1 [kN]	P_2 [kN]	P_3 [kN]	$P_{e,1}$ [kN]	$P_{e,2}$ [kN]	$P_{e,3}$ [kN]	$P_1/P_{e,1}$ [-]	$P_2/P_{e,2}$ [-]	$P_3/P_{e,3}$ [-]
CP12A-1	70.81	67.23	33.79	67.82	68.31	40.32	1.04	0.98	0.84
CP12A-2	71.24	67.70	33.79	63.71	65.25	41.03	1.12	1.04	0.82
CP12A-3	71.80	68.32	33.79	67.19	69.48	43.81	1.07	0.98	0.77
CP12C-1	72.77	69.39	33.79	69.27	69.24	43.81	1.05	1.00	0.77
CP12C-2	72.92	69.57	33.79	73.46	75.53	34.92	0.99	0.92	0.97
CP12C-3	73.19	69.87	33.79	70.09	-	-	1.04	-	-
CP14A-1	74.69	71.57	33.79	-	-	-	-	-	-
CP14A-2	74.89	71.80	33.79	68.71	72.35	48.72	1.09	0.99	0.69
CP14A-3	75.15	72.10	33.79	75.24	82.47	45.88	1.00	0.87	0.74
CP14B-1	75.38	72.37	33.79	80.60	85.46	48.44	0.94	0.85	0.70
CP14B-2	75.48	72.47	33.79	78.48	80.45	50.51	0.96	0.90	0.67
CP14B-3	75.61	72.63	33.79	83.19	88.70	-	0.91	0.82	-
CP14C-1	78.51	79.14	40.64	-	-	-	-	-	-
CP14C-2	78.55	79.18	40.64	67.58	85.39	45.83	1.16	0.93	0.89
CP14C-3	78.58	79.22	40.64	72.06	85.08	50.02	1.09	0.93	0.81
CP14D-1	76.14	76.88	28.03	78.17	84.17	58.02	0.97	0.91	0.48
CP14D-2	76.32	77.04	28.03	86.89	87.31	-	0.88	0.88	-
CP14D-3	76.63	77.33	28.03	85.19	85.07	-	0.90	0.91	-
NR1-1 (Lawson et al., 2017)	78.55	84.08	32.01	79.07	78.11	48.53	0.99	1.08	0.66
1-08-1 (Lawson et al., 2017)	46.42	56.43	32.57	45.51	53.43	36.68	1.02	1.06	0.89
1-08-2 (Lawson et al., 2017)	46.44	56.46	32.56	46.21	45.07	-	1.01	1.25	-
3-01-3 (Lawson et al., 2017)	46.28	55.61	32.44	52.78	45.48	28.38	0.88	1.22	1.14
1-03-1 (Lawson et al., 2017)	99.17	93.64	36.90	76.00	91.25	-	1.30	1.03	-
1-03-2 (Lawson et al., 2017)	99.99	94.02	37.04	93.13	93.88	-	1.07	1.00	-
1-03-3 (Lawson et al., 2017)	100.36	94.62	36.99	97.13	96.50	-	1.03	0.98	-
2-01-1 (Lawson et al., 2017)	75.16	77.65	33.44	65.25	64.50	-	1.15	1.20	
2-01-2 (Lawson et al., 2017)	75.30	77.78	33.44	70.13	70.13	-	1.07	1.11	-
2-01-3 (Lawson et al., 2017)	74.78	77.40	33.42	74.13	74.88	-	1.01	1.03	-
2-02-1 (Lawson et al., 2017)	74.12	77.03	33.36	66.13	69.88	-	1.12	1.10	-
2-03-1 (Lawson et al., 2017)	69.68	69.85	27.37	57.63	61.63	-	1.21	1.13	-
2-04-1 (Lawson et al., 2017)	61.58	59.90	33.58	64.81	68.38	-	0.95	0.88	-
2-05-1 (Lawson et al., 2017)	61.59	59.85	33.53	58.88	65.63	-	1.05	0.91	-
2-05-2 (Lawson et al., 2017)	60.90	59.09	33.44	69.31	71.06	-	0.88	0.83	-
2-05-3 (Lawson et al., 2017)	61.20	59.37	33.44	60.56	67.06	-	1.01	0.89	0.73
2-06-1 (Lawson et al., 2017)	98.25	91.97	37.08	83.50	89.38	-	1.18	1.03	-
2-06-2 (Lawson et al., 2017)	97.89	91.59	37.08	93.13	104.50	-	1.05	0.88	0.47
2-06-3 (Lawson et al., 2017)	98.60	92.36	37.08	96.50	96.50	-	1.02	0.96	-
2-07-1 (Lawson et al., 2017)	102.44	96.33	37.17	95.38	114.63	-	1.07	0.84	-
2-07-2 (Lawson et al., 2017)	102.53	96.74	37.08	106.25	112.38	-	0.97	0.86	-
2-07-3 (Lawson et al., 2017)	102.33	96.51	37.08	101.25	114.00	-	1.01	0.85	-
2-08-1 (Lawson et al., 2017)	73.96	73.88	27.34	59.13	67.88	-	1.25	1.09	-
3-03-1 (Lawson et al., 2017)	112.34	115.31	35.92	86.75	96.00	-	1.29	1.20	-
3-04-1 (Lawson et al., 2017)	91.43	110.31	29.06	112.88	112.88	-	0.81	0.98	-
3-05-1 (Lawson et al., 2017)	86.79	86.33	35.93	89.56	96.00	-	0.97	0.90	-
3-06-1 (Lawson et al., 2017)	86.54	86.13	35.94	78.50	94.88	-	1.10	0.91	-
3-07-1 (Lawson et al., 2017)	70.42	80.53	29.05	99.00	103.88	-	0.71	0.78	-
3-08-1 (Lawson et al., 2017)	70.83	81.15	29.09	105.50	111.00	-	0.67	0.73	-
3-09-1 (Lawson et al., 2017)	109.34	137.11	37.06	126.13	128.50	-	0.87	1.07	-
3-10-1 (Lawson et al., 2017)	108.57	135.58	37.22	117.38	130.25	-	0.93	1.04	-
						Mean	**1.02**	**0.97**	**0.77**
						CV	**12.6%**	**12.3%**	**20.5%**

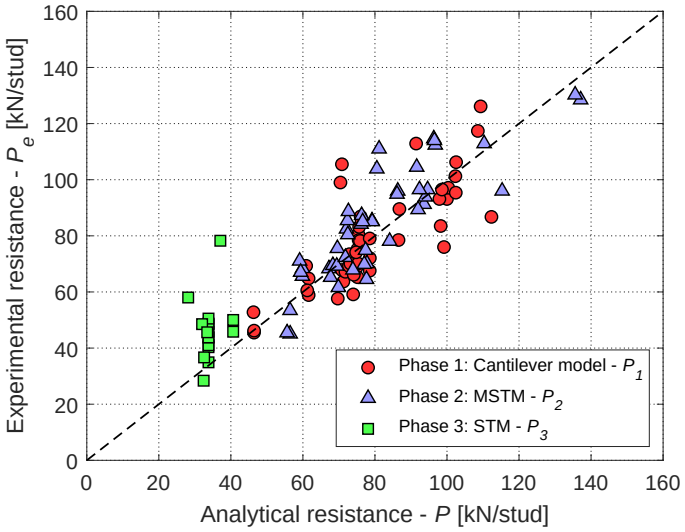

FIGURE 7.23: Comparison between analytical and experimental resistance of the push-out tests for each phase

In the first 2 phases, the test values are well predicted with a coefficient of variation (CV) of ca. 12%. However, in Phase 3, CV increases up to 20.5% while the mean value 0.77 indicates that the strut and tie model underestimates the resistance of the shear connection at large displacements. This might be caused by the bearing stresses of the concrete along the stud which were totally neglected. Although the first two models can be potentially used to determine the actual load bearing resistance of the shear connection, they might not be suitable for all the configurations in the database. For example, the modified strut and tie model may not reflect the actual failure modes when the studs are placed in favourable position or the embedment length is limited, as already discussed in Section 6.6. Therefore, to assess the field of application of each resistance function, reliability analyses were carried out and presented in the next chapter in accordance with the standard procedure of EN 1990.

Chapter 8

Calibration of the design equations

The field of application of the proposed mechanical based equations for the prediction of the resistance of studs in profiled steel sheeting was assessed via the statistical procedure of EN 1990 (BSI, 2002) on the representative database of push-out tests defined in Section 2.4.1. The results given in Chapter 4 were also added to the database resulting in a total of 260 experimental tests. As already mentioned, the strut and tie model of Phase 3 focuses on the behaviour at large displacements which is not always reached by the shear connection. Therefore, only the resistance functions of phase 1 and 2 were considered in this chapter for predicting the shear capacity of the connection. Unlike in Section 7.5 where the analytical resistances P_1 and P_2 were compared with test load values $P_{e,1}$ and $P_{e,2}$ in the respective phase, the performance of these proposed models are evaluated in this chapter against the experimental resistance r_e defined as the maximum load per connector within a slip of 6 mm. The same approach was employed for the statistical evaluation of past design models in Section 2.4.

The reliability analyses shown in the following sections were also performed including tests with $f_{cm} < 24$ MPa and the results are summarized in Appendix C.2.

8.1 Cantilever model

As proposed by CEN/TC250/SC4 (2020) for the revised version of EN 1994-1-1, a further limitation on the resistance function in Eq.(7.8) was included. Similarly to current EN 1994-1-1 design equations (BSI, 2004b), the capacity was assumed to be limited by the failure of the shank of the stud subjected to shear and tension using a factor 0.58. Therefore, the final expression of the theoretical resistance function is:

$$r_{t,Cant} = \min\{r_{t1,Cant}, r_{t2,Cant}\} \tag{8.1}$$

and

$$r_{t1,Cant} = 0.58 f_u \frac{\pi d^2}{4} \tag{8.2}$$

$$r_{t2,Cant} = C \cdot k_u \cdot \left(\frac{f_{ct} W}{n_r h_p} + \frac{n_y f_u d^3/6}{0.82 h_p - d/2} \right) \tag{8.3}$$

Unlike previous design models, Eq.(8.3) requires the tensile strength of concrete f_{ct} which is generally not directly measured. For evaluating the mean value of the tensile strength of the concrete f_{ctm} used in the statistical evaluation, the following relationship proposed by EN 1992-1-1 (BSI, 2004a) was adopted:

$$f_{ctm} = 0.3(f_{cm}\ [\text{MPa}] - 8)^{2/3}\ [\text{MPa}] \quad \text{for concrete strength classes} \leq \text{C50/C60} \tag{8.4}$$

Where:

f_{cm} is the mean measured cylindeer compressive strength of concrete

8.1.1 Full representative database

The statistical performance of the cantilever model was first assessed individually for Eqs.(8.2) and (8.3) considering the entire representative database. The results of the reliability analyses are shown graphically in Figure 8.1 including the key statistical properties. As can be seen, Eq.(8.2) delivers a partial safety factor of 1.198 and a coefficient of variation of 0.143. Comparable results are obtained for Eq.(8.3) with a partial safety factor of 1.26 and a slightly higher coefficient of variation equal to 0.166. However, the dispersion of Eq.(8.3) is negatively influenced by the uncertainty of the concrete related variables, such as the tensile strength f_{ct}. On the basis of the results obtained,the use of the partial safety factor $\gamma_V = 1.25$ leads to overestimation of the design resistance by only 0.8% and it can therefore be used for determining the design resistance of studs. Notwithstanding the suitability of the equations within a large scope of application, the design model was also analysed against different subsets in the next section to check if all the design variables were properly considered and how the equations may be further optimized in the future.

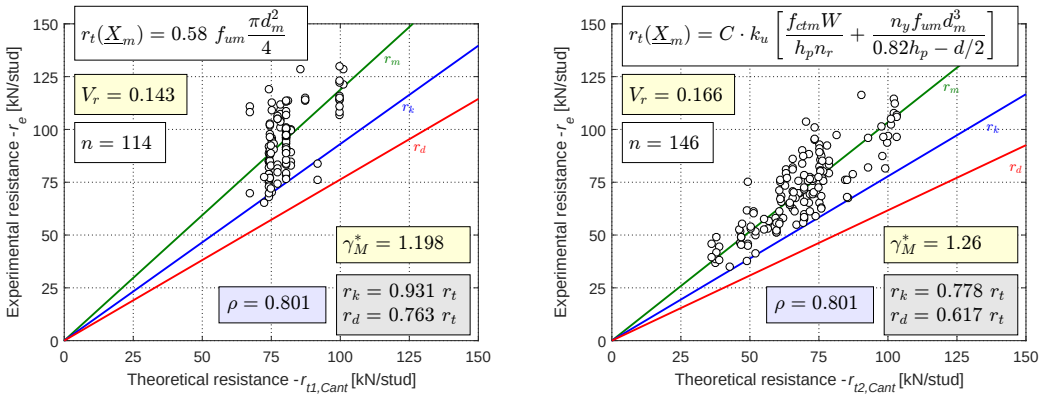

(a) (b)

FIGURE 8.1: Comparison between experimental and theoretical resistance according to the cantilever design model proposed the entire representative database

8.1.2 Evaluation of the field of application

The representative push-out test database was split in different subsets as a function of the following variables: position of stud in the trough, type of welding, number of studs per rib and emebedment length $(h_{sc} - h_p)$. The reliability analysis was undertaken for each subset and the results are summarized in Table 8.1.

TABLE 8.1: Results of the statistical evaluation of the cantilever design model for the resistance of studs in profiled steel sheeting for different subsets

	Mid		Staggered		Favourable		Unfavourable	
	Eq.(8.2)	Eq.(8.3)	Eq.(8.2)	Eq.(8.3)	Eq.(8.2)	Eq.(8.3)	Eq.(8.2)	Eq.(8.3)
n	85	90	4	15	24	14	1	27
ρ	0.842		0.772		0.684		0.528	
b	1.190	1.031	1.068	1.040	1.186	0.980	1.609	1.073
V_r	0.121	0.144	0.109	0.197	0.198	0.171	-	0.205
γ_M^*	1.141	1.199	2.355	1.484	1.537	1.377	-	1.377
	Through-deck		Pre-punched		Open trough		Re-entrant	
	Eq.(8.2)	Eq.(8.3)	Eq.(8.2)	Eq.(8.3)	Eq.(8.2)	Eq.(8.3)	Eq.(8.2)	Eq.(8.3)
n	84	83	30	63	77	129	37	17
ρ	0.732		0.896		0.788		0.689	
b	1.200	1.052	1.161	1.016	1.156	1.025	1.247	1.080
V_r	0.149	0.181	0.122	0.145	0.147	0.168	0.114	0.140
γ_M^*	1.236	1.303	1.196	1.224	1.275	1.280	1.077	1.149
	$n_r = 1$		$n_r = 2$		$h_{sc} - h_p < 2d$		$h_{sc} - h_p \geq 2d$	
	Eq.(8.2)	Eq.(8.3)	Eq.(8.2)	Eq.(8.3)	Eq.(8.2)	Eq.(8.3)	Eq.(8.2)	Eq.(8.3)
n	104	89	10	57	14	43	100	103
ρ	0.768		0.843		0.844		0.781	
b	1.202	1.045	1.034	1.013	1.172	1.107	1.190	1.013
V_r	0.136	0.165	0.155	0.167	0.154	0.181	0.142	0.156
γ_M^*	1.161	1.265	1.709	1.294	1.403	1.258	1.193	1.244

Both Eq.(8.2) and Eq.(8.3) show better performance when the studs are placed in the middle of the trough: ρ reaches the value 0.842 and the coefficient of variation V_r is equal to 0.121 and 0.144, respectively. In the other three cases (staggered, favourable and unfavourable position), the dispersion of the data increases with a coefficient of variation V_r ranging between 0.17 and 0.20. However, it could be argued that the higher scatter is caused by the reduced size of the population (not more than 30 tests for each equation) while the mean correction factor b remains stable. Compared to studs in pre-punched holes, the coefficient of variation V_r increases significantly in both equations when through-deck welded studs are considered. Furthermore, the linear correlation coefficient reduces from 0.896 to 0.732. From these results, it seems that the correction factor k_u which takes into account the effect of the welding should be refined in future studies. On the other hand, the number of studs as well as the shape of the profiles do not significantly affect the performance of the design model. Whilst EN 1994-1-1 rules is not applicable to configurations with anchorage length $(h_{sc} - h_p)$ lower than $2d$, the cantilever design model proposed shows good performance within this subset. Although V_r exceeded 0.18, the application of Eq.(8.3) delivers $\gamma_M^* = 1.258$ on the basis of 43 push-out tests. From the statistical performance of the model, a partial safety factor γ_V of 1.25 was finally recommended and the field of application coincides with the entire representative database of 260 tests.

8.1.3 Design proposal

In consideration of the results discussed in the previous sections, the proposed design resistance is given by:

$$P_{Rd,Cant} = \min\{P_{Rd1,Cant}, P_{Rd2,Cant}\} \tag{8.5}$$

and

$$P_{Rd1,Cant} = \left(0.58 f_{u,nom} \frac{\pi d^2}{4}\right) \cdot \frac{1}{\gamma_V} \tag{8.6}$$

$$P_{Rd2,Cant} = \left[C \cdot k_u \cdot \left(\frac{f_{ctk} W}{n_r h_p} + \frac{n_y f_{u,nom} d^3/6}{0.82 h_p - d/2}\right)\right] \cdot \frac{1}{\gamma_V} \tag{8.7}$$

With:

$$\gamma_V = 1.25$$

Where:

$f_{u,nom}$ is the specified ultimate tensile strength of stud material, but not higher than 450 MPa in computation

f_{ctk} is the characteristic tensile strength of the concrete according to EN 1992-1-1 (BSI, 2004a)

The scope of the application of the design proposal is defined by the following limitations:

- 19 mm $\leq d \leq$ 22 mm for studs in pre-punched profiled sheeting
- 19 mm $\leq d <$ 20 mm for through-deck welded studs
- 70 mm $\leq h_{sc} \leq$ 200 mm
- 40 mm $\leq h_p \leq$ 136 mm
- 40 mm $\leq b_{bot} \leq$ 160 mm
- 101 mm $\leq b_{top} \leq$ 240 mm
- 0.6 mm $\leq t \leq$ 1.2 mm
- Concrete strength class between C20/25 and C50/60

8.2 Modified strut and tie model

The analytical resistance of the modified strut and tie model was derived in Section 7.2 and the resulting theoretical resistance function is given by:

$$r_{t,MSTM} = k_s k_n (1.2 f_c \cdot d \cdot k \cdot w) \cdot \zeta + \frac{n_y f_u d^3/6}{h_s - d/2} + k_w \cdot f_{yp} \pi t d \tag{8.8}$$

8.2.1 Full representative database

The reliability analysis of Eq.(8.8) was initially carried out against the entire representative database and the results are illustrated in Figure 8.2. A good correlation between the prediction of Eq.(8.8) and experimental value of the resistance was found with $\rho = 0.856$. The coefficient of variation V_r is 0.155 while the corrected partial safety factor γ_M^* is 1.303. Although the resistance function in Eq.(8.8) can be used to predict the design resistance with a partial safety factor γ_V of 1.30 within the limits of the entire database, further evaluations are presented in the next section to assess the most appropriate field of application of Eq.(8.8).

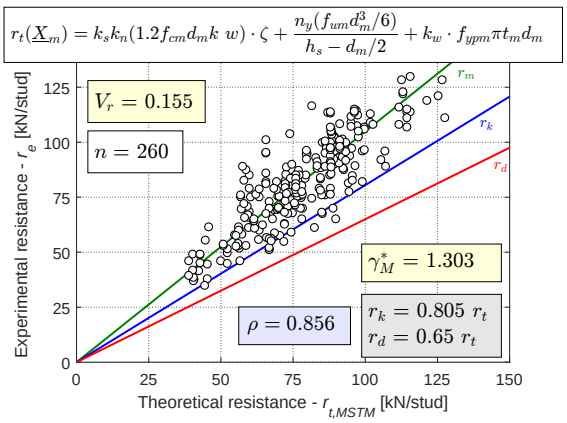

FIGURE 8.2: Comparison between experimental and theoretical resistance according to the MSTM proposed in the entire representative database

8.2.2 Evaluation of the field of application

As done for the cantilever model, the resistance function in Eq.(8.8) was compared with the experimental values of the resistance in different subsets. The results are summarized in Table 8.2.

By analysing subsets with different eccentric position of the stud, the design model performs efficiently when the connector is placed in the middle of the trough. In this case, a correlation coefficient ρ of 0.904 was found with a coefficient of variation V_r of only 0.131. Conversely, the prediction of the resistance of studs placed in favourable or unfavourable position is less satisfactory with a coefficient of variation of ca. 18%. In these cases, other type of failure take place decreasing the accuracy of the mechanical model proposed. The resistance function is therefore not optimized when the studs are eccentrically welded and the influence of some key parameters might have been ignored or not properly considered. Thus, further investigations are recommended to improve the model for such configurations. As can be seen in Table 8.2, the prediction of the resistance of through-deck welded studs delivers a coefficient of variation V_r of 0.163 and a correlation coefficient ρ of 0.792 . For studs placed in pre-punched sheeting, V_r reduces to 0.140 while ρ is equal to 0.926. However, it is thought that this difference is directly related to the position of the stud in the trough as in most of the configurations using through-deck welding, the connectors are welded in favourable or unfavourable position. It is also suggested to improve the performance of Eq.(8.8) when two studs per rib are employed by refining the factor k_n. Unlike in the cantilever model, a relationship between the embedment length and the performance of the design modified strut and tie model was found.

TABLE 8.2: Results of the statistical evaluation of the MSTM for the resistance of studs in profiled steel sheeting for different subsets

	Mid	Staggered	Favourable	Unfavourable
n	175	19	38	28
ρ	0.904	0.806	0.776	0.646
b	1.053	1.219	0.982	1.045
V_r	0.131	0.165	0.182	0.188
γ_M^*	1.206	1.175	1.472	1.461
	Through-deck	**Pre-punched**	**Open trough**	**Re-entrant**
n	167	93	206	54
ρ	0.792	0.926	0.820	0.831
b	1.054	1.040	1.043	1.069
V_r	0.163	0.140	0.162	0.124
γ_M^*	1.338	1.238	1.344	1.144
	$n_r = 1$	$n_r = 2$	$h_{sc} - h_p < 2d$	$\boldsymbol{h_{sc} - h_p \geq 2d}$
n	193	67	57	**203**
ρ	0.842	0.768	0.742	**0.873**
b	1.048	1.053	1.060	**1.046**
V_r	0.147	0.178	0.191	**0.144**
γ_M^*	1.276	1.378	1.432	**1.264**

Based on the evaluation of 57 tests with anchorage length $(h_{sc} - h_p)$ lower than $2d$, V_r increases up to 0.191. The resistance of the remaining 203 tests is more accurately predicted. The statistical analysis of this subset delivers $V_r = 0.144$ and $\rho = 0.873$ resulting in a corrected partial safety factor $\gamma_M^* = 1.264$. This indicates that the design model is more efficient for headed stud shear connections where $(h_{sc} - h_p)$ is not lower than $2d$ and the respective results are plotted in Figure 8.3.

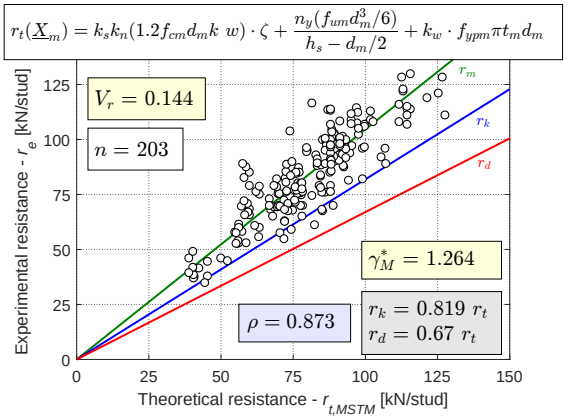

FIGURE 8.3: Comparison between experimental and theoretical resistance according to the MSTM in the proposed field of application

In the interest of harmonization with the Eurocode design rules for other type of steel

connections, a partial safety factor of 1.25 was proposed in this subset, even though it is ca. 1% higher than the target value. Finally, the limitation $(h_{sc} - h_p) \geq 2d$ was considered to define the scope of the design model.

8.2.3 Design proposal

On the basis of the reliability analyses performed, the design resistance of headed stud shear connection in profiled steel sheeting according to the modified strut and tie model is equal to:

$$P_{Rd,MSTM} = \left[k_s k_n (1.2 f_{ck} dk \cdot w) \cdot \zeta + \frac{n_y f_{u,nom} d^3/6}{h_s - d/2} + k_w f_{yp,nom} \pi t d\right] \frac{1}{\gamma_V} \quad (8.9)$$

With:

$$\gamma_V = 1.25$$

Where:

$f_{u,nom}$ is the specified ultimate tensile strength of stud material, but not higher than 450 MPa in computation

$f_{yp,nom}$ is the guaranteed minimum proof strength of the sheeting

In addition to the limits given by the database considered, a minimum anchorage length of $2d$ is recommended. Therefore, Eq.(8.9) is applicable if the shear connection satisfy the following conditions:

- $h_{sc} - h_p \geq 2d$
- 19 mm $\leq d \leq$ 22 mm for studs in pre-punched profiled sheeting
- 19 mm $\leq d <$ 20 mm for through-deck welded studs
- 70 mm $\leq h_{sc} \leq$ 200 mm
- 40 mm $\leq h_p \leq$ 136 mm
- 40 mm $\leq b_{bot} \leq$ 160 mm
- 101 mm $\leq b_{top} \leq$ 240 mm
- 0.6 mm $\leq t \leq$ 1.2 mm
- Concrete strength class between C20/25 and C50/60

8.3 Considerations on the new design proposals

The two design models derived in Chapter 7 were calibrated according to EN 1990 standard procedure. The statistical performance of these design models in the proposed field of application is summarized in Figure 8.4.

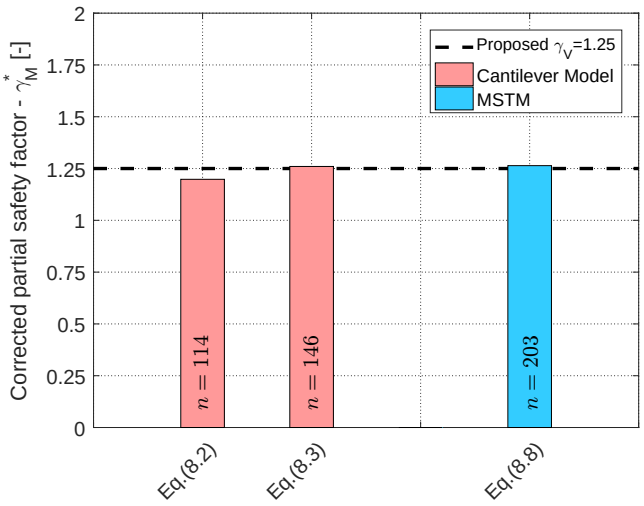

	Cantilever model		MSTM
	Eq.(8.2)	Eq.(8.3)	Eq.(8.8)
n	114	146	203
ρ	0.801		0.873
b	1.188	1.034	1.046
V_r	0.143	0.166	0.144
γ_M^*	1.198	1.260	1.264
γ_V	1.25	1.25	1.25

FIGURE 8.4: Results of the statistical evaluation of the design models proposed in the field of application

It can be concluded that the cantilever design model is able to predict appropriately the resistance of 260 push-out tests of the representative database. However, this design model requires the use two equations in combination with several empirical-based correction factors. On the other hand, although the scope of the modified strut and tie design model reduces to 203 tests, the correlation coefficient ρ increases from 0.801 to 0.873. Also, MSTM requires only one equation to calculate the design resistance. However, it is not optimized for studs welded in favourable or unfavourable position where other types of failure may prematurely occur. The advantages and disadvantages of the design models are listed in Table 8.3.

TABLE 8.3: Advantages and disadvantages of the new proposed design models for the resistance of studs in profiled steel sheeting

Design model	Advantages	Disadvantages
Cantilever model	+ Wide scope of application	- Several correction factors required - Two equations
Modified strut and tie model	+ Only one equation + High correlation with test results	- Not recommended in case of reduced anchorage length - Not optimized for eccentrical position of the studs in the trough

Chapter 9

Conclusions

The work presented in this thesis analysed the behaviour of headed stud shear connections employed in composite beams using profiled steel sheeting with the aim of supporting the practical application of these solutions as well as the development of new optimized products. Although numerous studies have been performed in the last decades on this topic, it is difficult to develop a reliable and safe design model for predicting the resistance of these shear connections due to the wide variety of geometrical and mechanical parameters involved. In particular, for steel sheeting with slender troughs, the failure modes change significantly. To address these issues, experimental and numerical investigations were undertaken and presented in this thesis in order to have a comprehensive understanding of the load bearing mechanisms and the resistance components activated in the connection. These outcomes were finally used to develop mechanical based models and the respective analytical equations to calibrate the corresponding design resistance for practical use.

The summary of this work is provided in Section 9.1 while Section 9.2 gives an outlook on the future research.

9.1 Summary

First, a large **experimental study** of 21 full scale push-out tests on headed stud shear connections was carried out and the results were discussed. All the configurations used a modern 58 mm high profiled steel sheeting with relatively narrow ribs (average width of 81.5 mm) transverse to the direction of the beam. From a general evaluation of the entire set of tests, all the specimens behaved ductile reaching a peak load at ca. 1-6 mm slip followed by a smooth load reduction. After the initiation of the concrete cone crack observed at the edge of the trough, all the configurations experienced rib punching failure at around 3-6 mm slip displacement. At higher displacements (20-25 mm slip), the concrete cones are pulled out owing to the increasing tensile forces in the connector. For longer studs, this failure occurred together with the rupture of the shank of the connector. By comparing the results of different test series, the influence of the following parameters was investigated: recess, waveform rebars, welding type, position of the wire mesh, length of the headed stud and slab depth. It was found that the 200 mm wide recess applied at the base of the specimen has a minor impact on the performance of the shear connection. The addition of the waveform reinforcement bars increased the resistance by 26% as well as the ductility. The position of the wire mesh (20 mm or 40 mm above the rib) did not show an important impact on the behaviour of 100 mm high studs. It was confirmed that the length of the stud affects positively the resistance of the connector while the slab depth showed a negligible influence on the shear connection. Further

to the evaluation of the aforementioned variables, several push-out tests were intentionally stopped at 2, 6 and 25 mm slip and cut longitudinally to identify the main resistance mechanisms.

In parallel, a **non-linear 3D FE model** was developed to further investigate the crack pattern observed in the concrete rib as well as the bending deformation of the studs. The FE model was validated against the conducted push-out tests where a good agreement was found in terms of resistance and ductility. From the visualization of the **stress and damage pattern** in the concrete, the main directions where the load spreads were preliminarily identified. Also, a large parametric study was performed to assess the influence of the geometry and the slip on the bending behaviour of the stud connector in detail. Specifically, the location and the degree of activation of the **plastic hinges** were extracted using a stress-based method. It was observed that, owing to the local crushing of the concrete caused by the high bearing stresses, the upper plastic hinge moves towards the stud head. The second plastic hinge (i.e. double curvature) may be partially or fully activated depending on the rotational restraint provided by the slab.

Based on the outcomes of the conducted tests together with the numerical simulations performed, three **load bearing mechanisms** were distinguished. In the first stage (Phase 1), the concrete rib remains undamaged until the first crack appears at the edge of the trough and the moment acting on the rib reached the elastic bending resistance of the so called "**concrete cone**". By increasing the slip displacement, the forces redistribute and the rib locally crushes in proximity of the stud (Phase 2) leading to **rib punching**. This is a ductile type of failure mode which normally appears when the width of the concrete in front of the stud is relatively small. The crushing of the rib occurs gradually while the centre of stiffness moves towards the slab. Finally, at large displacements (Phase 3), the bending component of the stud reduces and more load is transferred via tensile stresses as a result of non linear geometric effects. The front part of the concrete rib is fully damaged and, for larger displacements, **concrete pull-out** or **stud rupture** occurs. However, the sequence of resistance mechanisms might not be valid if the anchorage length of the stud is not sufficient to prevent the premature rotation of the rib leading to pull-out. Similar considerations apply to cases when the stud connector is placed on the favourable side of the trough. In both cases, the bearing resistance of the concrete cover in front of the stud might not be fully exploited.

In consideration of the resistance components activated in the three phases, the corresponding mechanical models were developed for predicting the load bearing capacity of the shear connection. In the first phase, the concrete rib was modelled as a linear elastic cantilever element in combination with the stud that develops a double plastic curvature. This **cantilever model** was analysed in accordance with Euler-Bernoulli beam theory assuming that the capacity of the shear connection is limited by the elastic bending resistance of the concrete cone (Phase 1). Whilst the concrete cone cracks propagate, the resistance mechanism changes and the load bearing capacity of the shear connection is limited by rib punching. At this stage (Phase 2), the redistributed internal forces in the concrete rib were considered as an equivalent system of struts. These elements were combined with the stud and the steel sheeting which were modelled as beam and tie elements, respectively. The resulting structural system was called **modified strut and tie model** (MSTM). An analogy between the typical failure mode in RC corbels and rib punching in headed stud shear connections was used to estimate the resistance of the system. At higher displacements

(Phase 3) it was assumed that the bearing stresses in the concrete are negligible while the tensile component of the stud becomes predominant. At this point, the modified strut and tie model develops into the **strut and tie model** (STM) where the resistance is governed by the pulling forces in the stud. Based on the load-slip curves of the push tests performed, the prediction of the three proposed mechanical models were consistently compared with the experimental resistance for each phase. Only the first two models were considered for the calibration of the design resistance as they focus on the behaviour of the connection in the first 10 mm slip whereas phase 3 might not always be reached.

The cantilever model and MSTM were statistically evaluated against the representative push-out test database in accordance with the standard procedure of EN 1990 (BSI, 2002). The field of application of the two proposed **design models** was determined by checking their statistical performance for different subsets. It was found that the cantilever model can be used to predict the design resistance of the studs within the limits defined by the entire representative database ($n = 260$) with a partial safety factor γ_V of 1.25. In this case, a coefficient of variation V_r of ca. 15% was obtained while the correlation coefficient ρ was 0.801. On the other hand, the MSTM delivers optimal values of the design resistance when the embedment length is not smaller than $2d$ ($n = 203$). By considering the tests falling within this domain, the coefficient of variation V_r is 14.4%, the correlation coefficient ρ reaches 0.873 and the partial safety factor γ_V can be safely taken as 1.25.

9.2 Outlook

In the conducted push-out tests, the profiled steel sheeting has relatively narrow troughs that can accommodate only studs in mid position. However, when the sheeting does not allow the central placement of the connector, the studs are placed alternately on the two sides of the trough (favourable and unfavourable position) along the length of the span, as recommended by EN 1994-1-1 (BSI, 2004b). In these cases, as already highlighted by past experimental studies, the mechanical performance as well as the failure modes of the shear connection change significantly. It is therefore recommended to study the evolution of the damage in such configurations by longitudinally cut the specimens, especially at low displacements, as done in the current experimental work. This would help to identify the key resistance components that govern the capacity of the connection and to establish reliable mechanical models.

As in the experimental campaign, the numerical study focused only on centrally placed stud while eccentrical positions were not considered. Again, to fill this knowledge gap, the presented FE model could be further extended to cover these cases allowing for a better estimation of the position and "number" of the plastic hinges in the connector. In parallel, the distribution of the bearing stresses in the concrete rib could be also analysed in the transversal direction in order to have a more precise evaluation of the effective depth of the strut elements used for the development of strut and tie models.

Further to the analytical approaches proposed to predict the shear connection resistance, the presented modified strut and tie model (MSTM) could be also used in combination with different assumptions to reproduce other types of failure which were not accounted in this contribution. For example, in consideration of the lower

statistical performance for cases with reduced embedment length, it could be of interest to include a concrete pull-out failure condition. A more accurate representation of these cases can potentially extend the scope of application of the design equations supporting the development of novel products.

Publications related to the thesis

During the time spent for this dissertation, the following papers related to this dissertation were published:

C. Odenbreit et al. (2018). "New mechanical model to predict the load bearing resistance of shear connectors with modern forms of profiled sheeting". In: *13th International Conference on Steel, Space and Composite Structures*. Perth. URL: http://hdl.handle.net/10993/35328

V. Vigneri et al. (2018). "Numerical evaluation of the plastic hinges developed in headed stud shear connectors in composite beams with profiled steel sheeting". In: *Proceedings of the 12th international conference on Advances in Steel-Concrete Composite Structures*. Valencia: ASCC18. URL: http://hdl.handle.net/10251/107874

V. Vigneri et al. (2019a). "Numerical evaluation of the plastic hinges developed in headed stud shear connectors in composite beams with profiled steel sheeting". In: *Structures*. DOI: 10.1016/j.istruc.2019.03.017. URL: http://hdl.handle.net/10993/40638

C. Odenbreit et al. (2019). "Equations to predict the shear connection capacity of composite beams with slender profiled steel sheeting". In: *Proceedings of the 9th International Conference on Steel and Aluminium Structures (ICSAS 2019)*. Bradford. URL: http://hdl.handle.net/10993/40549

V. Vigneri et al. (2019b). "Different load-bearing mechanisms in headed stud shear connections in composite beams with profiled steel sheeting". In: *ce/papers* 3.3-4, pp. 231–236. DOI: https://doi.org/10.1002/cepa.1050. URL: http://hdl.handle.net/10993/40640

V. Vigneri et al. (2019c). "Different load bearing mechanisms in headed stud shear connectors for composite beams with profiled steel sheeting". In: *Steel Construction* 12.3, 184–190. DOI: 10.1002/stco.201900019. URL: http://hdl.handle.net/10993/40640

V. Vigneri et al. (2021). "Modified strut and tie model of headed stud shear connectors in open trough profiled sheeting for predicting the post-cracking load bearing resistance". In: *Proceedings of Eurosteel 2020-2021*. [Accepted for publication]

Bibliography

AISC (2005). *Specification for structural steel buildings: ANSI/AISC 360-05*. Chicago (IL). DOI: 10.4224/40001245.

Amadio, C. et al. (2017). "Refined numerical modelling for the structural assessment of steel-concrete composite beam-to-column joints under seismic loads". In: *Engineering Structures* 138, 394–409. DOI: 10.1016/j.engstruct.2017.02.037.

An, L. and K. Cederwall (1996). "Push-out tests on studs in high strength and normal strength concrete". In: *Journal of Constructional Steel Research* 36.1, 15–29.

ArcelorMittal-Construction (2015). *Technical datasheet Cofraplus® 60 - Composite floor decking*. URL: https://construction.arcelormittal.com/.

A.S.C Steel Deck (2018). *Composite deck and non-composite deck for floor and roof deck applications*. URL: https://ascsd.com/files/FloorDeck.pdf.

Bijlaard, F., G. Sedlacek, and J. Stark (1988). *Procedure for the determination of design resistance from tests*. Tech. rep. TNO report: BI-87-112. Delft.

Birtel, V. and P. Mark (2006). *Parameterised Finite Element Modelling of RC Beam Shear Failure*. Abaqus users: conference.

Bode, H. and R. Künzel (1987). "Steifigkeit und Verformbarkeit von Verbundmittelnim Hochbau". In: *International symposium - Composite steel concrete structures*. Bratislava.

— (1999). *Anwendung der Durchschweißtechnik im Verbundbau. 3. überarbeitete Auflage – Forschungsbericht*. Kaiserslautern.

BSI (2002). *EN 1990: 2002 Eurocode - Basis of structural design*. London. DOI: 10.3403/02612036.

— (2004a). *EN 1992-1-1: 2004 Eurocode 2 - Design of concrete structures Part 1-1: General rules and rules for buildings*. London. DOI: 10.3403/03178016.

— (2004b). *EN 1994-1-1: 2004 Eurocode 4 - Design of composite steel and concrete structures Part 1-1: General rules and rules for buildings*. London. DOI: 10.3403/03221508.

— (2005). *EN 1993-1-1: 2004 Eurocode 3 - Design of steel structures Part 1-1: General rules and rules for buildings*. London. DOI: 10.3403/03270565.

Bullo, S. and R. Di Marco (1995). "Effects of high-performance concrete on stud shear connector behaviour". In: *Proceedings of Nordie Steel Construction Conference. Malmö*.

Cashell, K. and N. Baddoo (2014). "Experimental assessment of ferritic stainless steel composite slabs". In: *Composite Construction in Steel and Concrete VII*, pp. 300–313.

CEN (1998). *ENV 1993-1-1:1992/A2:1998*.

CEN/TC250/SC4 (2020). *CEN/TC250/SC4 N2143: Shear resistance of headed stud connectors welded within the ribs of profiled sheets – Proposed design model considerations (Annex B)*.

Chapman, J. (1964). "The behaviour of composite beams in steel and concrete". In: *Struct. Engr* 42, pp. 115–125.

Chapman, J. and S Balakrishnan (1964). "Experiments on composite beams". In: *The Structural Engineer* 42.11, pp. 369–383.

Cornelissen, H., D. Hordijk, and H. Reinhardt (1986). "Experimental determination of crack softening characteristics of normalweight and lightweight concrete". In: *HERON* 31.2, 45–56.

C.S.T.B. (2015). *Document Technique d'Application 3/15-800 - Cofraplus 60*. Champs sur Marne: CSTB. URL: http://www.cstb.fr/pdf/atec/GS03-D/AD150800.pdf.

Dallam, L. N. (1968). "High strength bolt shear connectors-pushout tests". In: *Journal Proceedings*. Vol. 65. 9, pp. 767–769.

Döinghaus, P. (2001). *Zum Zusammenwirken hochfester Baustoffe in Verbundträgern*. de. Aachen: Aachen University.

Eggert, F. (2019). "Einfluss der Verdübelung auf das Trag- und Verformungsverhalten von Verbundträgern mit und ohne Profilblech". de. Ph.D. Dissertation. Stuttgart Universität, Stuttgart.

El-Lobody, E. and D. Lam (2002). "Modelling of headed stud in steel-precast composite beams". In: *Steel and Composite Structures* 2.5, 355–378. DOI: 10.12989/scs.2002.2.5.355.

Ernst, S. (2006). *Factors affecting the behaviour of the shear connection of steel-concrete composite beams*. University of Western Sydney. URL: http://handle.uws.edu.au:8081/1959.7/32633.

Feldmann, M. (2007). *Untersuchungen zum Trag-und Verformungsverhalten von Verbundmitteln unter ruhender und nichtruhender Belastung bei Verwendung hochfester Werkstoffe: Forschungsvorhaben P 621*. de.

FIB (2010). *Model Code for Concrete Structures 2010*. DOI: 10.1002/9783433604090.

Grant, J. A., J. W. Fisher, and R. G. Slutter (1977). "Composite beams with formed steel deck". In: *Engineering Journal* 14.1. URL: https://www.aisc.org/Composite-Beams-with-Formed-Steel-Deck.

Hanswille, G. and M. Porsch (2007). *Zur Festlegung der Tragfähigkeit von Kopfbolzendübeln in Vollbetonplatten in DIN 18000-5 und EN 1994-1-1*. de.

Hanswille, G., M. Porsch, and C. Üstündag (2006). *Versuchsbericht über die Durchführung von 77 Push-Out-Versuchen. Forschungsprojekt: Modellierung von Schädigungsmechanismen zur Beurteilung der Lebensdauer von Verbundkonstruktionen aus Stahl und Beton*. de. Institut für Konstruktiven Ingenieurbau.

Hanswille, G. et al. (1998). "Experimentelle Untersuchungen zur Tragfähigkeit von Kopfbolzendübeln mit großen Schaftdurchmessern". de. In: *Stahlbau* 67.7, 555–560.

Hawkins, N. M. and D. Mitchell (1984). "Seismic response of composite shear connections". In: *Journal of Structural Engineering* 110.9, pp. 2120–2136. DOI: 10.1061/(ASCE)0733-9445(1984)110:9(2120).

Hicks, S. J. (1997). "Longitudinal shear resistance of steel and concrete composite beams". Ph.D. Dissertation. Cambridge: University of Cambridge, Department of Engineering. URL: https://www.repository.cam.ac.uk/handle/1810/252318.

— (2007). "Resistance and ductility of shear connection: Full-scale beam and push tests". In: *Proceedings of the sixth International Conference on Steel and Aluminium Structures*.

— (2009). "Strength and Ductility of Headed Stud Connectors Welded in Modern Profiled Steel Sheeting". In: *Structural Engineering International* 4, 415–419. DOI: 10.2749/101686609789846975.

— (2017). "Design shear resistance of headed studs embedded in solid slabs and encasements". In: *Journal of Constructional Steel Research* 139, 339–352. DOI: 10.1016/j.jcsr.2017.09.018.

Hicks, S. J. and A. L. Smith (2014). "Stud shear connectors in composite beams that support slabs with profiled steel sheeting". In: *Structural Engineering International* 24.2, pp. 246–253. DOI: 10.2749/101686614X13830790993122.

Hicks, S. J. and R. E. McConnel (1997). "The shear resistance of headed studs used with profiled steel sheeting". In: *Composite construction in steel and concrete III*. ASCE, pp. 325–338.

Hiragi, H. et al. (1981). "Static strength of stud shear connectors in SRC structures". In: *Transactions of the Japan Concrete Institute* 3, 453–460.

Huo, J. et al. (2019). "Experimental study on impact behaviour of stud shear connectors in composite beams with profiled steel sheeting". In: *Journal of Constructional Steel Research* 161, pp. 436–449. DOI: 10.1016/j.jcsr.2018.04.029.

Hwang, S., W. Lu, and H. Lee (2000). "Shear Strength Prediction for Reinforced Concrete Corbels". In: *ACI Strucutral Journal* 97.4, 543–552.

ISE/109 (2006). *EN 10143:2006 Continuously hot-dip coated steel sheet and strip. Tolerances on dimensions and shape*.

ISO/TC164/SC1 (2019). *ISO 6892-1:2019 Metallic materials — Tensile testing — Part 1: Method of test at room temperature*. URL: https://www.iso.org/standard/78322.html.

ISO/TC44/SC10 (2017). *ISO 13918:2017 Welding — Studs and ceramic ferrules for arc stud welding*. URL: https://www.iso.org/standard/67251.html.

ISO/TC98/SC2 (1997). *ISO 12491:1997 Statistical methods for quality control of building materials and components*. URL: https://www.iso.org/standard/2644.html.

Jayas, B. S. and M. U. Hosain (1987). *Behaviour of headed studs in composite beams: push-out tests*. DOI: 10.1139/188-032.

Jenisch, F. M. (2000). "Einflüsse des profilierten Betongurtes und der Querbiegung auf das Tragverhalten von Verbundträgern". de. Ph.D. Dissertation. Kaiserslautern: Universität Kaiserslautern. URL: https://elib.uni-stuttgart.de/bitstream/11682/10416/3/2019_04_22_Eggert_Dissertation_2019.pdf.

Jähring, A. (2007). "Zum Tragverhalten von Kopfbolzendübeln in hochfestem Beton". de. Ph.D. Dissertation. München: Technischen Universität München. URL: https://d-nb.info/992784522/34.

Johnson, R. P. and H Yuan (1998). "Models and design rules for stud shear connectors in trough of profiled sheeting". In: *Proceedings of the Institution of Civil Engineers-Structures and Buildings* 128.3, pp. 252–263. DOI: 10.1680/istbu.1998.30459.

Kemp, A. and P. Trinchero (1997). "Horizontal shear failures around connectors used with steel decking". In: *Composite Construction in Steel and Concrete III*. ASCE, pp. 104–118.

Konrad, M. (2011). *Tragverhalten von Kopfbolzen in Verbundträgern bei senkrecht spannenden Trapezprofilblechen, Stuttgart: Institut für Konstruktion und Entwurf, Stahl- Holz- und Verbundbau*. de. Universität Stuttgart. URL: http://elib.uni-stuttgart.de/handle/11682/383.

Lam, D. (1998). "Composite steel beams using precast concrete hollow core floor slabs". PhD thesis. University of Nottingham.

Lawson, M. et al. (2017). *Development of improved shear connection rules in composite beams - Final Report*. DOI: 10.2777/923858.

Lawson, R., J. Lim, and S. Popo-Ola (2013). "Pull-out forces in shear connectors in composite beams with large web openings". In: *Journal of Constructional Steel Research* 87, pp. 48 –59. DOI: https://doi.org/10.1016/j.jcsr.2013.03.025.

Lee, P. G., C. S. Shim, and S. P. Chang (2005). "Static and fatigue behavior of large stud shear connectors for steel–concrete composite bridges". In: *Journal of constructional steel research* 61.9, 1270–1285. DOI: 10.1016/j.jcsr.2005.01.007.

Leonhardt, F. et al. (1987). "Neues, vorteilhaftes Verbundmittel für Stahlverbund-Tragwerke mit hoher Dauerfestigkeit." In: *Beton-und Stahlbetonbau* 82.12, pp. 325–331.

Lim, O. K. et al. (2020). "Fire performance of headed shear studs in profiled steel sheeting". In: *Journal of Constructional Steel Research* 164, p. 105791. ISSN: 0143-974X. DOI: 10.1016/j.jcsr.2019.105791.

Lloyd, R. and H. D. Wright (1990). "Shear connection between composite slabs and steel beams". In: *Journal of constructional steel research* 15.4, 255–285. DOI: 10.1016/0143-974X(90)90050-Q.

Lungershausen (1988). "Zur Schubtragfähigkeit von Kopfbolzendübeln". de. Ph.D. Dissertation. Ruhr universität bochum.

Lyons, J. C. (1994). *Strength of welded shear studs*. Virginia Polytechinic Institute. URL: http://hdl.handle.net/10919/42990.

Mainstone, R. and J. Menzies (1967). "Static and fatigue tests on push-out specimens". In: *Concrete* 1.9, 291–302.

Maleki, S. and S. Bagheri (2008). "Behavior of channel shear connectors, Part I: Experimental study". In: *Journal of Constructional Steel Research* 64.12, pp. 1333–1340.

Menzies, J. B. (1971). "CP 117 and shear connectors in steel-concrete composite beams made with normal-density or lightweight concrete". In: *Structural Engineer*.

Mottram, J. T. and R. P. Johnson (1990). "Push tests on studs welded through profiled steel sheeting". In: *The Structural Engineer*.

Nellinger, S. (2015). "On the behaviour of shear stud connections in composite beams with deep decking". Ph.D. Dissertation. Luxembourg. URL: http://hdl.handle.net/10993/24468.

Nellinger, S. et al. (2017). "Influence of transverse loading onto push-out tests with deep steel decking". In: *Journal of Constructional Steel Research* 128, 335–353. DOI: 10.1016/j.jcsr.2016.08.021.

NRC (2005). *National Building Code of Canada*. DOI: 10.4224/40001245.

Odenbreit, C., V. Vigneri, and D. Lam (2019). "Equations to predict the shear connection capacity of composite beams with slender profiled steel sheeting". In: *Proceedings of the 9th International Conference on Steel and Aluminium Structures (ICSAS 2019)*. Bradford. URL: http://hdl.handle.net/10993/40549.

Odenbreit, C. et al. (2018). "New mechanical model to predict the load bearing resistance of shear connectors with modern forms of profiled sheeting". In: *13th International Conference on Steel, Space and Composite Structures*. Perth. URL: http://hdl.handle.net/10993/35328.

Oehlers, D. J. (1981). *Results of tests on 101 push specimens and 4 composite T-beams*. Warwick: University of Warwick, Department of Engineering.

Oehlers, D. J. and R. P. Johnson (1987). "The strength of stud shear connections in composite beams". In: *The Structural Engineer* 65.2, pp. 44–48. URL: https://www.istructe.org/journal/volumes/volume-65-(published-in-1987)/issue-14/the-strength-of-stud-shear-connections-in-composit/.

Ollgaard, J. G., R. G. Slutter, and J. W. Fisher (1971). "Shear strength of stud connectors in lightweight and normal weight concrete". In: *AISC Engineering Journal*, 71–10. URL: https://preserve.lehigh.edu/engr-civil-environmental-fritz-lab-reports/2010.

Pavlović, M. et al. (2013). "Bolted shear connectors vs. headed studs behaviour in push-out tests". In: *Journal of Constructional Steel Research* 88, pp. 134 –149. DOI: https://doi.org/10.1016/j.jcsr.2013.05.003.

Popovics, S. (1973). "A numerical approach to the complete stress-strain curve of concrete". In: *Cement and concrete research* 3, 583–599. DOI: 10.1016/0008-8846(73)90096-3.

Qureshi, J. (2010). "Finite element modelling of steel-concrete composite structures". Ph.D. Dissertation. PhD Thesis, Leeds. URL: https://ethos.bl.uk/OrderDetails.do?uin=uk.bl.ethos.535124.

Qureshi, J., D. Lam, and J. Ye (2011). "Effect of Shear Connector Spacing and Layout on the Shear Connector Capacity in Composite Beams". In: *Journal of Constructional Steel Research* 67.4, 706–719. DOI: 10.1016/j.jcsr.2010.11.009.

Rambo-Roddenberry, M. D. (2002). "Behaviour and strength of welded stud shear connectors". PhD Dissertation. Virginia polytechnic institute. URL: http://hdl.handle.net/10919/26989.

Robinson, H. (1988). *Multiple stud shear connections in deep ribbed metal deck*. DOI: 10.1139/188-076.

Roik, K. and K. E. Bürkner (1980). "Untersuchungen des Trägerverbundes unter Verwendung von Stahltrapezprofilen mit einer Höhe> 80 mm". de. In: *Bochum: Studiengesellschaft für Anwendungstechnik von Eisen und Stahl e. V*, – 40.

— (1981). "Beitrag zur Tragfähigkeit von Kopfbolzendübeln in Verbundträgern mit Stahlprofilblechen". de. In: *Bauingenieur* 56.3.

Roik, K. and G. Hanswille (1983). "Beitrag zur Bestimmung der Tragfähigkeit von Kopfbolzendübeln". de. In: *Stahlbau* 52.10.

Roik, K and G Hanswille (1987). "Zur Dauerfestigkeit von Kopfbolzendübeln bei Verbundträgern". In: *Bauingenieur* 62.

Roik, K., G. Hanwille, and A. Cunze-O. Lanna (1988). *Report on Eurocode 4 - Clause 6.6.2 Stud connectors*. Tech. rep. Report EC4/8/88. Ruhr Universität Bochum.

Roik, K. and H. Lungershausen (1988). *Verbundträger mit Stahltrapezprofilblechen mit Rippenhöhen > 80 mm / Studiengesellschaft für Anwendungstechnik von Eisen und Stahl e. V.* de. Tech. rep.

Russo, G. et al. (2006). "Reinforced Concrete Corbels — Shear Strength Model and Design Formula". In: *ACI Structura Journal* 103.1, 3–10.

Sattler, K. (1962). *Betrachtungen uber neue Verdubelungen im Verbundbau*. de. Vol. 37. 1, pp. 1–8.

Shen, M. (2014). "Structural behaviour of shear connection in composite structures under complex loading conditions". Ph.D. Dissertation. Hong Kong Polytechnic University, Hong Kong. URL: https://theses.lib.polyu.edu.hk/handle/200/7398.

Shen, M. H. and K. F. Chung (2017). "Structural behaviour of stud shear connections with solid and composite slabs under co-existing shear and tension forces". In: *Structures* 9. DOI: 10.1016/j.istruc.2016.09.011.

Simulia, D. S. (2014). *Abaqus Analysis User's Guide v6.14*. fr.

Slutter, R. G. and G. C. Driscoll (1963). "Flexural strength of steel and concrete composite beams". In: *Journal of the Structural Division* 91.2.

Smith, A. L. and G. H. Couchman (2010). "Strength and ductility of headed stud shear connectors in profiled steel sheeting". In: *Journal of Constructional Steel Research* 66, 748–754. DOI: 10.1016/j.jcsr.2010.01.005.

Spremic, M. et al. (2018). "FE validation of the equivalent diameter calculation model for grouped headed studs". In: *Steel and Composite Structures* 26.3, 375–386. DOI: 10.12989/scs.2018.26.3.375.

Stark, J. W. and B. W. Hove (1991). *TNO Report BI-91-163: Statistical analysis of push-out tests on stud connectors in composite steel and concrete structures*. Delft: TNO Building and Cconstruction Research.

Sublett, C. N. (1992). "Strength of welded headed studs in ribbed metal deck on composite joists". M.SC. thesis. Virginia Polytechnic Institute. URL: http://hdl.handle.net/10919/45303.

Sun, Q. et al. (2019). "Monotonic and cyclic behavior of headed steel stud anchors welded through profiled steel deck". In: *Journal of Constructional Steel Research* 157, pp. 121–131. DOI: 10.1016/j.jcsr.2019.01.022.

Thorenfeldt, E., A. Tomaszewicz, and J. J. Jensen (1987). "Mechanical properties of high strength concrete and application in design". In: *Symposium on Utilization of High-strength Concrete*. Trondheim.

Varrette, S. et al. (2014). "Management of an Academic HPC Cluster: The UL Experience". In: *Proc. of the 2014 Intl. Conf. on High Performance Computing & Simulation (HPCS 2014)*. Bologna, Italy: IEEE, pp. 959–967.

Viest, I. M. (1956). "Investigation of stud shear connectors for composite concrete and steel T-beams". In: *Journal Proceedings* 52.4, 875–892.

Viest, I. M. (1951). *Full-scale tests of channel shear connectors and composite t-beams*. Tech. rep. University of Illinois at Urbana Champaign, College of Engineering.

Vigneri, V., C. Odenbreit, and M. Braun (2018). "Numerical evaluation of the plastic hinges developed in headed stud shear connectors in composite beams with profiled steel sheeting". In: *Proceedings of the 12th international conference on Advances in Steel-Concrete Composite Structures*. Valencia: ASCC18. URL: http://hdl.handle.net/10251/107874.

— (2019a). "Numerical evaluation of the plastic hinges developed in headed stud shear connectors in composite beams with profiled steel sheeting". In: *Structures*. DOI: 10.1016/j.istruc.2019.03.017. URL: http://hdl.handle.net/10993/40638.

Vigneri, V. et al. (2021). "Modified strut and tie model of headed stud shear connectors in open trough profiled sheeting for predicting the post-cracking load bearing resistance". In: *Proceedings of Eurosteel 2020-2021*. [Accepted for publication].

Vigneri, V., C. Odenbreit, and D. Lam (2019b). "Different load-bearing mechanisms in headed stud shear connections in composite beams with profiled steel sheeting". In: *ce/papers* 3.3-4, pp. 231–236. DOI: https://doi.org/10.1002/cepa.1050. URL: http://hdl.handle.net/10993/40640.

— (2019c). "Different load bearing mechanisms in headed stud shear connectors for composite beams with profiled steel sheeting". In: *Steel Construction* 12.3, 184–190. DOI: 10.1002/stco.201900019. URL: http://hdl.handle.net/10993/40640.

Wang, Q. et al. (2011). "Experimental study on stud shear connectors with large diameter and high strength". In: *International Conference on Electric Technology and Civil Engineering (ICETCE*, 340–343. DOI: 10.1109/ICETCE.2011.5776113.

Xue, D. et al. (2012). "Static behavior of multi-stud shear connectors for steel-concrete composite bridge". In: *Journal of Constructional Steel Research* 74, 1–7. DOI: https://doi.org/10.1016/j.jcsr.2011.09.017.

Yamamoto, M. and S. Nakamura (1962). "The study on shear connectors". In: *The Public Works Research Institute, Construction Ministry Japan* 5.

Yuan, H. (1996). *The resistance of stud shear connectors with profiled sheeting*. University of Warwick. URL: http://webcat.warwick.ac.uk/record=b1402883~S1.

Zellner, W. (1988). "Recent designs of composite bridges and a new type of shear connectors". In: *Composite Construction in Steel and Concrete*.

Zhang, P. C. et al. (2008). "Friction-Based Sliding Between Steel and Steel, Steel and Concrete, and Wood and Stone". In: *The 14th World Conference on Earthquake Engineering*. Beijing.

Appendix A

Details on the standard procedure of EN1990 for resistance models

This appendix presents the standard evaluation procedure of a design model for the resistance of headed studs in profiled steel sheeting according to EN 1990 (BSI, 2002) Annex D. Such procedure aims to derive the design resistance from the theoretical model via a statistical calibration of the respective resistance functions against representative experimental results. All the steps and the data are defined in the next sections, from Section A.1 to A.10.

A.1 Step 1: Definition of the resistance function

The theoretical resistance of the design model r_t is represented by the analytical function $g_{rt}(\underline{X})$ covering all the relevant independent mechanical and geometrical variables $\underline{X}$.

$$r_t = g_{rt}(\underline{X}) \tag{A.1}$$

A.2 Step 2: Correlation with experimental values

To preliminary check the suitability of the design model, the theoretical resistance function using mean values $g_{rt}(\underline{X}_m)$ is compared with experimental resistance values r_e. Specifically, the mean values of the mechanical properties were taken as mean measured values. If the geometrical properties were not measured, the mean values were considered as a function of the nominal values. A detailed list of the mean values of the basic variables is given in Table A.1 including the values of the coefficient of variation. As suggested by Bijlaard et al. (1988), the suitability of the design model should be preliminarily checked by calculating the coefficient of correlation ρ defined in Eq.(A.2). If this the correlation is sufficient, the design model is suitable to predict the experimental resistance.

$$\rho = \frac{\sum_{i=1}^{n} r_{e,i} r_{t,i} - n\overline{r}_e\overline{r}_t}{(n-1)\sigma_{r_e}\sigma_{r_t}} \tag{A.2}$$

With:

$$\overline{r}_e = \frac{1}{n}\sum_{i=1}^{n} r_{e,i} \tag{A.3}$$

$$\overline{r}_t = \frac{1}{n}\sum_{i=1}^{n} r_{t,i} \tag{A.4}$$

Where n is the sample size (i.e. number of tests considered).

A.3 Step 3: Estimate the mean correction factor b

The probabilistic model of the resistance r can be represented by:

$$r_t = b r_t \delta \tag{A.5}$$

Where δ is the error term and b is the mean correction factor calculated as the "Least Squares" best-fit to the slope:

$$b = \frac{\sum_{i=1}^{n} r_{e,i} r_{t,i}}{\sum_{i=1}^{n} {r_{t,i}}^2} \tag{A.6}$$

A.4 Step 4: Estimate the coefficient of variation of the errors V_δ

The error term δ_i for each experimental value $r_{e,i}$ should be determined from:

$$\delta_i = \frac{r_{e,i}}{b \cdot r_{t,i}} \tag{A.7}$$

To calculate an estimated value of the coefficient of variation V_δ of the error term, the following paameter should be firstly defined:

$$\Delta_i = \ln \delta_i \tag{A.8}$$

The estimated value of the mean for the expected value of Δ should be determined from:

$$\overline{\Delta} = \frac{1}{n}\sum_{i=1}^{n} \Delta_i \tag{A.9}$$

The estimated value of the variance should be calculated from:

$$s_\Delta^2 = \frac{1}{n-1}\sum_{i=1}^{n} (\Delta_i - \overline{\Delta}) \tag{A.10}$$

Finally, for the coefficient of variation of the error terms V_δ, the following expression can be used:

$$V_\delta^2 = e^{s_\Delta^2} - 1 \tag{A.11}$$

A.5 Step 5: Compatibility analysis

To determine which variables have more influence on the scatter, the test results can be split into subsets with respect to these parameters. This would allow to identify the variables which are not adequately represented in the resistance functions.

A.6 Step 6: Coefficient of variation of the basic variables V_X

From the push-out test database, there is not sufficient information about the actual variability of the basic variables X_i. Therefore, the coefficient of variation $V_{X,i}$ of these parameters needs to be determined by prior knowledge. The mean value and the coefficient of variation for each basic variables were chosen according to several scientific sources and they are given in Table A.1. All the basic variables are assumed to be normally distributed. The subscript "meas" defines the mean measured value of the variable while "nom" indicates nominal values. Based on the tensile test results on the sheeting material shown in Table D.3, the minimum guaranteed proof strength $R_{p0.2,min}$ (ISE/109, 2006) was considered as the design value of the yield strength f_{yp} using the fractile factor $k_{d,\infty} = 3.04$. The coefficient of variation was conservatively taken as 3%.

TABLE A.1: Mean and coefficient of variation of the basic variables $\underline{X}$

Basic variables $\underline{X}$	**Mean value $\underline{X}_m$**	**Coefficient of Variation V_X**	**References**
f_c	$f_{c,meas}$	$8/1.64 f_{cm}$ [MPa]	BSI (2004a), Hicks (2017) Smith and Couchman (2010)
f_u	$f_{u,meas}$	0.05	Roik et al. (1988)
f_{yp}	$R_{p0.2,min}/(1 - k_{d,\infty} V_{f_{yp}})$	0.03	Table D.3
d	$d_{nom} - 0.2$ mm	$8/1.64 d_m$ [mm]	ISO/TC44/SC10 (2017) Hicks (2017)
h_{sc}	$h_{sc,meas}$	0.01	Nellinger (2015)
h_p	$h_{p,nom}$	$2/1.64 h_{pm}$ [mm]	C.S.T.B. (2015) A.S.C Steel Deck (2018)
b_{top}	$b_{top,nom}$	0.05	Nellinger (2015)
b_{bot}	$b_{bot,nom}$	0.05	Nellinger (2015)
t	t_{nom}	$0.12/1.64 t_m$ [mm]	(ISE/109, 2006)
e_t	$e_{t,nom}$	0.10	Nellinger (2015)
e_L	$e_{L,nom}$	0.10	Nellinger (2015)

Some of the geometrical basic variables are shown in Figure A.1 while the others are:

f_c	is the compressive strength of the concrete
f_u	is the ultimate tensile strength of the stud material
f_{yp}	is the yield strength of the sheeting material
t	is the thickness of the steel sheeting
e_t	is the transversal spacing between the studs in the rib

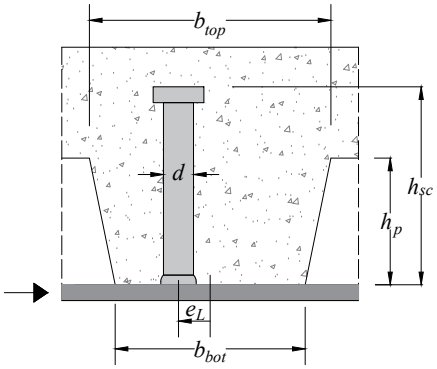

FIGURE A.1: Geometrical dimensions of headed stud shear connections with profiled sheeting

A.7 Step 7: Characteristic value of the resistance r_k

If V_δ and $V_{X,i}$ are relatively small, the following approximation can be used to determine the coefficient of variation of the resistance function V_r:

$$V_r = V_\delta^2 + V_{rt}^2 \tag{A.12}$$

V_{rt} indicates the coefficient of variation of the theoretical resistance r_t from uncertainties in the basic variables $\underline{X}$. Because of the complexity of the resistance functions r_t presented in this work, the coefficient of variation V_{rt} was estimated by randomly extracting values of the basic variables according to their statistical distribution defined by the data given in Table A.1. This computational method is named as "Monte-Carlo simulations".

The characteristic resistance r_k should be calculated from Eq.(A.13).

$$r_k = b \cdot g_{rt}(\underline{X}_m) \cdot \exp(-k_\infty \alpha_{rt} Q_{rt} - k_n \alpha_\delta Q_\delta - 0.5Q^2) \tag{A.13}$$

With:

$$Q_\delta = \sqrt{\ln(V_\delta^2 + 1)} \tag{A.14}$$

$$Q_{rt} = \sqrt{\ln(V_{rt}^2 + 1)} \tag{A.15}$$

$$Q = \sqrt{\ln(V_r^2 + 1)} \tag{A.16}$$

$$\alpha_\delta = \frac{Q_\delta}{Q} \tag{A.17}$$

$$\alpha_{rt} = \frac{Q_{rt}}{Q} \tag{A.18}$$

The fractile factors k were calculated for an unknown coefficient of variation because there is no prior knowledge of the variability of the design model against test results. Therefore, the fractile factor k for a probability p and a sample size n is calculated in accordance with ISO/TC98/SC2 (1997):

$$k(p, n) = t_p(\nu) \cdot \left(1 + \frac{1}{n}\right)^{0.5} \tag{A.19}$$

Where $t_p(\nu)$ is the fractile factor of the t-distribution for the probability p and number of degrees of freedom $\nu = n - 1$. For the calculation of the characteristic value of the resistance, the fractile factors k_n and k_∞ were calculated for a probability $p = 5\%$ which refer to n and infinity test results, respectively.

A.8 Step 8: Design value of the resistance r_d

Similarly to what has been done for the determination of the characteristic value r_k in Section A.7, the design value of the resistance r_d is given by:

$$r_d = b \cdot g_{rt}(\underline{X}_m) \cdot \exp(-k_{d,\infty}\alpha_{rt}Q_{rt} - k_{d,n}\alpha_\delta Q_\delta - 0.5Q^2) \tag{A.20}$$

Where $k_{d,n}$ and $k_{d,\infty}$ define the fractile factors of a normal distribution with a probability of 0.1% for a finite and infinite sample size, respectively.

From the definition given in EN 1990 (BSI, 2002), the partial safety factor relative to the resistance function considered γ_M is equal to:

$$\gamma_M = \frac{r_k}{r_d} \tag{A.21}$$

However, EN 1990 (BSI, 2002) does not explicitly provide further information on the assessment of the partial safety factor if the resistance functions use nominal value of the basic variables. Hence, on the basis of the Annex Z of ENV1993-1-1:1992/A2:1998 (CEN, 1998), two additional steps are included in the procedure.

A.9 Step 9: Corrected partial safety factor $\gamma_M{}^*$

Unlike in the statistical procedure detailed in the previous steps, the mean value of the variables is not always available in the actual design situations. Therefore, the final design resistance is based on the nominal resistance r_n that uses the nominal values of the variables given in Table A.2.

On the basis of a past research on the strength of the stud material (Roik et al., 1988), the nominal value of f_u was assumed to be smaller than the characteristic value corresponding to a fractile factor of 2 (instead of 1.64).

TABLE A.2: Nominal values of the basic variables $\underline{X_n}$

Basic variables $\underline{X}$	**Nominal value** $\underline{X_n}$
f_c	f_{ck}
f_u	$f_{um}(1-2V_{f_u}) \leq f_{u,lim}$ [a]
f_{yp}	$R_{p0.2,min}$ [b]
d	d_{nom}
h_{sc}	l_2 [c] (-5 mm for through deck welding)
h_p	$h_{p,nom}$
b_{top}	$b_{top,nom}$
b_{bot}	$b_{bot,nom}$
t	t_{nom}
e_L	$e_{L,nom}$
e_t	$e_{t,nom}$

[a] $f_{u,lim}$ is taken as 450 MPa or 500 MPa but it may be defined differently.
[b] $R_{p0.2,min}$ is the minimum proof strength of sheeting material (ISE/109, 2006)
[c] l_2 is length of the stud after welding defined in ISO 13918 (ISO/TC44/SC10, 2017).

In order to calculate the partial safety factor related to the nominal resistance r_n, the nominal to characteristic resistance ratio k_c is determined by Eq.(A.22) for each single test. The average value is finally considered to determine the corrected partial safety factor γ_M^* in Eq.(A.23).

$$k_c = \frac{r_n}{r_k} = \frac{g_{rt}(X_n)}{r_k} \tag{A.22}$$

$$\gamma_M^* = \frac{r_n}{r_d} = k_c \cdot \gamma_M \tag{A.23}$$

A.10 Step 10: Final choice of the partial safety factor

The partial safety factor is chosen according to the application considered. For example, in case of headed stud shear connection, it is suggested to adopt a value of $\gamma_V = 1.25$ as recommended in the design of other types of steel connections when the failure is governed by fracture of bolts or welds.

Therefore, the design resistance can be written as follows:

$$r_d = r_n \cdot \frac{1}{\gamma_M^*} = \frac{r_n}{\gamma_V}\left(\frac{\gamma_V}{\gamma_M^*}\right) \tag{A.24}$$

A good calibration of the design model is ensured when the corrected partial safety factor γ_M^* is equal or close to the target γ_V. In this case, the proposed design resistance P_{Rd} is given by the expression:

$$P_{Rd} = r_n \cdot \frac{1}{\gamma_V} \tag{A.25}$$

To ease the visualization of the statistical procedure described in the previous section, the log-normal distribution of the theoretical resistance function r_t is plotted in Figure A.2 where the mean, characteristic, nominal and design value of the resistance are also indicated.

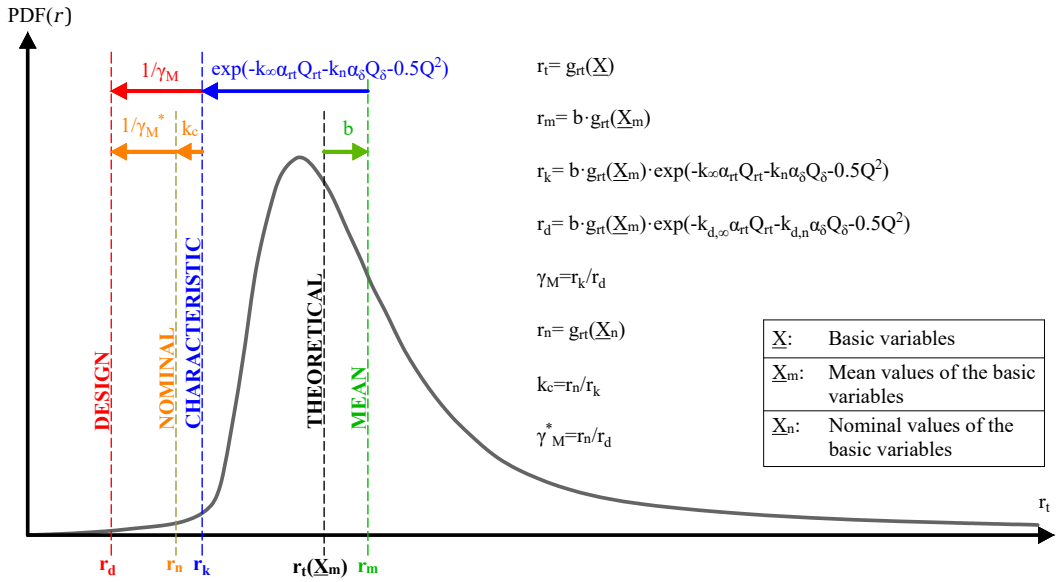

FIGURE A.2: Overview of the resistance values of the design model according to the statistical evaluation of EN 1990 (BSI, 2002)

Appendix B

Database of push-out tests

B.1 Headed studs in solid slabs

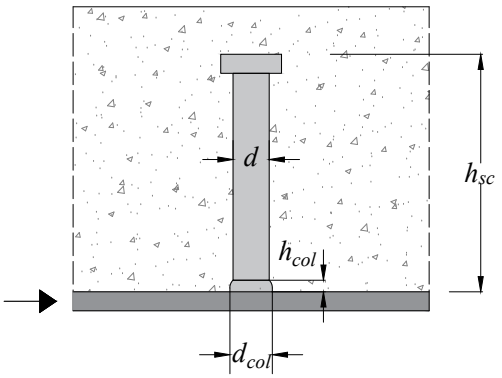

FIGURE B.1: Geometrical dimensions of headed stud shear connectors in solid slabs

TABLE B.1: Database of representative push-out tests on headed studs in solid slabs

i	Source	Test	d_{nom} [mm]	h_{scm} [mm]	d_{col} [mm]	h_{col} [mm]	f_{cm} [N/mm²]	E_{cm} [N/mm²]	f_{um} [N/mm²]	P_e [kN/stud]
1	Yamamoto and Nakamura (1962)	D1/1	16.0	100	21.0	4.5	30.2	30650	580	99.00
2	Yamamoto and Nakamura (1962)	D1/2	16.0	100	21.0	4.5	30.2	30650	580	94.00
3	Yamamoto and Nakamura (1962)	D2/1	19.0	99.9	23.0	6.0	30.2	30650	500	123.00
4	Yamamoto and Nakamura (1962)	D2/2	19.0	99.9	23.0	6.0	30.2	30650	500	128.80
5	Yamamoto and Nakamura (1962)	D2/3	19.0	99.9	23.0	6.0	30.2	30650	500	126.50
6	Yamamoto and Nakamura (1962)	D3/1	22.0	99.9	29.0	6.0	30.2	30650	548	148.50
7	Yamamoto and Nakamura (1962)	D3/2	22.0	99.9	29.0	6.0	30.2	30650	548	148.00
8	Yamamoto and Nakamura (1962)	D3/3	22.0	99.9	29.0	6.0	30.2	30650	548	146.80
9	Mainstone and Menzies (1967)	S3	19.1	101.6	23.0	6.0	29.0	30279	600	96.20
10	Mainstone and Menzies (1967)	S4	19.1	101.6	23.0	6.0	28.3	30058	600	100.10
11	Mainstone and Menzies (1967)	S5	19.1	101.6	23.0	6.0	27.7	29865	600	106.70
12	Mainstone and Menzies (1967)	S6	19.1	101.6	23.0	6.0	27.7	29865	600	126.20
13	Mainstone and Menzies (1967)	S8	19.1	101.6	23.0	6.0	30.7	30801	600	121.40
14	Mainstone and Menzies (1967)	S11	19.1	101.6	23.0	6.0	29.6	30466	600	112.70
15	Mainstone and Menzies (1967)	S16	19.1	101.6	23.0	6.0	31.3	30980	600	115.00
16	Mainstone and Menzies (1967)	S19	19.1	101.6	23.0	6.0	32.0	31187	600	115.00
17	Mainstone and Menzies (1967)	S22	19.1	101.6	23.0	6.0	34.7	31954	600	106.90
18	Mainstone and Menzies (1967)	S26	19.1	101.6	23.0	6.0	24.9	28926	600	99.10
19	Mainstone and Menzies (1967)	S29	19.1	101.6	23.0	6.0	27.1	29670	600	104.10
20	Ollgaard et al. (1971)	1-A	19.1	76.2	23.0	6.0	35.7	32227	499	132.90
21	Ollgaard et al. (1971)	2-A	19.1	76.2	23.0	6.0	35.7	32227	499	147.40
22	Ollgaard et al. (1971)	3-A	19.1	76.2	23.0	6.0	35.7	32227	499	138.80
23	Ollgaard et al. (1971)	1-LA	19.1	76.2	23.0	6.0	25.6	29167	499	111.10
24	Ollgaard et al. (1971)	2-LA	19.1	76.2	23.0	6.0	25.6	29167	499	120.20
25	Ollgaard et al. (1971)	3-LA	19.1	76.2	23.0	6.0	25.6	29167	499	112.00
26	Ollgaard et al. (1971)	1-SA	15.9	76.2	17.0	3.0	28.2	30026	493	88.50
27	Ollgaard et al. (1971)	2-SA	15.9	76.2	17.0	3.0	28.2	30026	493	94.40

Continue on the next page

Table B.1 - *continued from previous page*

i	Source	Test	d_{nom} [mm]	h_{scm} [mm]	d_{col} [mm]	h_{col} [mm]	f_{cm} [N/mm²]	E_{cm} [N/mm²]	f_{um} [N/mm²]	P_e [kN/stud]
28	Ollgaard et al. (1971)	3-SA	15.9	76.2	17.0	3.0	28.2	30026	493	90.30
29	Ollgaard et al. (1971)	1-B	19.1	76.2	23.0	6.0	33.6	31646	499	124.30
30	Ollgaard et al. (1971)	2-B	19.1	76.2	23.0	6.0	33.6	31646	499	115.20
31	Ollgaard et al. (1971)	3-B	19.1	76.2	23.0	6.0	33.6	31646	499	115.20
32	Ollgaard et al. (1971)	1-LB	19.1	76.2	23.0	6.0	18.8	26587	499	83.00
33	Ollgaard et al. (1971)	2-LB	19.1	76.2	23.0	6.0	18.8	26587	499	82.10
34	Ollgaard et al. (1971)	3-LB	19.1	76.2	23.0	6.0	18.8	26587	499	78.50
35	Ollgaard et al. (1971)	1-SB	15.9	76.2	17.0	6.0	28.3	30058	493	82.60
36	Ollgaard et al. (1971)	2-SB	15.9	76.2	17.0	6.0	28.3	30058	493	76.70
37	Ollgaard et al. (1971)	3-SB	15.9	76.2	17.0	6.0	28.3	30058	493	85.30
38	Ollgaard et al. (1971)	1-2B	19.1	76.2	23.0	6.0	33.6	31646	499	118.40
39	Ollgaard et al. (1971)	2-2B	19.1	76.2	23.0	6.0	33.6	31646	499	115.70
40	Ollgaard et al. (1971)	3-2B	19.1	76.2	23.0	6.0	33.6	31646	499	113.40
41	Menzies (1971)	P1	19.1	101.6	23.0	6.0	16.6	25617	600	97.50
42	Menzies (1971)	P2	19.1	101.6	23.0	6.0	16.6	25617	600	96.50
43	Menzies (1971)	P3	19.1	101.6	23.0	6.0	16.6	25617	600	97.00
44	Menzies (1971)	P4	19.1	101.6	23.0	6.0	40.8	33544	600	127.00
45	Menzies (1971)	P5	19.1	101.6	23.0	6.0	40.8	33544	600	127.00
46	Menzies (1971)	P6	19.1	101.6	23.0	6.0	40.8	33544	600	127.00
47	Oehlers (1981)	RSs1	19.0	99.5	25.9	5.0	27.0	29637	620	135.00
48	Oehlers (1981)	RSs2	19.0	99.5	25.9	5.0	27.0	29637	620	133.00
49	Oehlers (1981)	RSs3	19.0	99.5	25.9	5.0	21.8	27795	620	122.00
50	Oehlers (1981)	RSs4	19.0	99.5	25.9	5.0	21.8	27795	620	131.00
51	Oehlers (1981)	RSs5	19.0	99.5	25.9	5.0	25.5	29133	620	133.00
52	Oehlers (1981)	RSs6	19.0	99.5	25.9	5.0	25.5	29133	620	142.00
53	Hiragi et al. (1981)	2A	19.0	69.9	23.0	5.0	40.3	33421	485	141.00
54	Hiragi et al. (1981)	3A	19.0	99.9	23.0	5.0	39.1	33119	485	166.00
55	Hiragi et al. (1981)	4A	19.0	99.9	23.0	5.0	47.1	35021	485	160.00

Continue on the next page

Table B.1 - *continued from previous page*

i	Source	Test	d_{nom} [mm]	h_{scm} [mm]	d_{col} [mm]	h_{col} [mm]	f_{cm} [N/mm²]	E_{cm} [N/mm²]	f_{um} [N/mm²]	P_e [kN/stud]
56	Hiragi et al. (1981)	5A	19.0	99.9	23.0	5.0	57.5	37181	485	172.00
57	Roik and Hanswille (1983)	T1/1	19.0	100	24.3	5.0	36.7	32495	460	144.50
58	Roik and Hanswille (1983)	T1/2	19.0	100	24.3	5.0	36.7	32495	460	147.80
59	Roik and Hanswille (1983)	T1/3	19.0	100	24.3	5.0	36.7	32495	460	135.50
60	Roik and Hanswille (1983)	T1/4	19.0	100	24.3	5.0	38.3	32914	460	148.90
61	Roik and Hanswille (1983)	T1/5	19.0	100	24.3	5.0	38.3	32914	460	137.80
62	Roik and Hanswille (1983)	T2/1	22.0	100	29.0	5.0	36.3	32389	472	170.10
63	Roik and Hanswille (1983)	T2/2	22.0	100	29.0	5.0	36.3	32389	472	168.10
64	Roik and Hanswille (1983)	T2/3	22.0	100	29.0	5.0	36.3	32389	472	165.90
65	Roik and Hanswille (1983)	T2/4	22.0	100	29.0	5.0	36.3	32389	472	170.60
66	Roik and Hanswille (1983)	T2/5	22.0	100	29.0	5.0	36.3	32389	472	168.80
67	Roik and Hanswille (1983)	T3/1	19.0	100	24.3	5.0	44.7	34483	460	148.90
68	Roik and Hanswille (1983)	T3/2	19.0	100	24.3	5.0	44.7	34483	460	145.10
69	Roik and Hanswille (1983)	T4/1	19.0	100	24.3	5.0	44.7	34483	460	137.30
70	Roik and Hanswille (1983)	T4/2	19.0	100	24.3	5.0	44.7	34483	460	133.60
71	Roik and Hanswille (1983)	T4/3	19.0	100	24.3	5.0	44.7	34483	460	137.60
72	Roik and Hanswille (1983)	T5/1	22.0	100	29.0	5.0	59.0	37477	472	176.30
73	Roik and Hanswille (1983)	T5/2	22.0	100	29.0	5.0	59.0	37477	472	177.50
74	Roik and Hanswille (1983)	T6/1	22.0	100	29.0	5.0	57.4	37152	472	166.60
75	Roik and Hanswille (1983)	T6/2	22.0	100	29.0	5.0	57.4	37152	472	159.90
76	Roik and Hanswille (1983)	T6/3	22.0	100	29.0	5.0	57.4	37152	472	177.90
77	Hicks (1997)	6-25-2S-TRB	19.0	95	23.0	6.0	31.9	31166	456	94.50
78	Hicks (1997)	6-25-4S-ORB2	19.0	95	23.0	6.0	32.0	31187	456	90.39
79	Hicks (1997)	6-25-4S-FB1	19.0	95	23.0	6.0	35.1	32064	456	107.33
80	Hicks (1997)	6-25-4S-FB2	19.0	95	23.0	6.0	32.0	31187	456	118.11
81	Rambo-Roddenberry (2002)	Test 22	19.1	101.6	23.0	6.0	42.1	33852	447	104.93
82	Rambo-Roddenberry (2002)	Test 23	19.1	101.6	23.0	6.0	42.1	33852	447	118.63

Continue on the next page

Table B.1 - *continued from previous page*

i	Source	Test	d_{nom} [mm]	h_{scm} [mm]	d_{col} [mm]	h_{col} [mm]	f_{cm} [N/mm²]	E_{cm} [N/mm²]	f_{um} [N/mm²]	P_e [kN/stud]
83	Rambo-Roddenberry (2002)	Test 24	19.1	101.6	23.0	6.0	42.1	33852	447	119.17
84	An and Cederwall (1996)	NSC11	19.0	75	23.9	4.5	30.8	30822	519	115.00
85	An and Cederwall (1996)	NSC12	19.0	75	23.9	4.5	30.8	30822	519	111.50
86	An and Cederwall (1996)	NSC21	19.0	75	23.9	4.5	30.8	30822	519	120.80
87	An and Cederwall (1996)	NSC22	19.0	75	23.9	4.5	31.8	31125	519	119.10
88	An and Cederwall (1996)	HSC11	19.0	75	23.9	4.5	86.1	41970	519	156.80
89	An and Cederwall (1996)	HSC12	19.0	75	23.9	4.5	81.3	41246	519	158.60
90	An and Cederwall (1996)	HSC21	19.0	75	23.9	4.5	81.3	41246	519	151.90
91	An and Cederwall (1996)	HSC22	19.0	75	23.9	4.5	91.2	42705	519	161.00
92	Feldmann (2007)	K-22 1/3	22.0	98.2	29.0	6.7	110.2	45191	546	253.41
93	Feldmann (2007)	K-22 2/3	22.0	97.9	29.4	6.8	111.0	45289	546	243.28
94	Feldmann (2007)	K-22 3/3	22.0	97.9	29.3	6.9	111.0	45289	546	249.44
95	Feldmann (2007)	RK-22 1	22.0	98.2	29.8	8.0	110.8	45267	456	239.80
96	Feldmann (2007)	A0-22 1/3	22.0	97.9	29.8	7.3	102.5	44216	546	269.94
97	Feldmann (2007)	A0-22 2/3	22.0	97.6	30.2	7.7	104.7	44498	546	247.78
98	Feldmann (2007)	A0-22 3/3	22.0	98.6	29.8	6.0	104.7	44498	546	252.45
99	Feldmann (2007)	A3-25 1/3	25.0	99.6	32.0	8.6	106.3	44708	554	318.90
100	Feldmann (2007)	A3-25 2/3	25.0	99.7	31.6	8.2	106.3	44708	554	312.76
101	Feldmann (2007)	A3-25 3/3	25.0	99.7	31.8	7.9	105.1	44549	554	310.19
102	Feldmann (2007)	S-19 1/3	19.0	76.6	23.3	5.1	106.8	44771	537	133.75
103	Feldmann (2007)	S-19 2/3	19.0	76.6	24.1	5.1	106.8	44771	537	138.25
104	Feldmann (2007)	S-19 3/3	19.0	75.3	24.8	3.7	106.8	44771	537	143.26
105	Feldmann (2007)	S-22 1/3	22.0	98.6	29.0	7.1	106.8	44771	546	201.32
106	Feldmann (2007)	S-22 2/3	22.0	99.4	29.6	5.1	106.8	44771	546	188.51
107	Feldmann (2007)	S-22 3/3	22.0	98.3	30.4	7.7	106.8	44771	546	207.03
108	Feldmann (2007)	A2-19_w 1/3	19.0	77.5	29.8	5.3	105.4	44587	537	211.15
109	Feldmann (2007)	A2-19_w 2/3	19.0	77.2	29.6	5.4	108.1	44927	537	208.74
110	Feldmann (2007)	A2-19_w 3/3	19.0	77.3	29.7	5.1	108.1	44927	537	200.75

Continue on the next page

Table B.1 - *continued from previous page*

i	Source	Test	d_{nom} [mm]	h_{scm} [mm]	d_{col} [mm]	h_{col} [mm]	f_{cm} [N/mm²]	E_{cm} [N/mm²]	f_{um} [N/mm²]	P_e [kN/stud]
111	Feldmann (2007)	S-19_w 1/3	19.0	76.6	29.6	5.0	106.8	44771	537	160.28
112	Feldmann (2007)	S-19_w 2/3	19.0	76.6	30.5	4.8	106.8	44771	537	149.06
113	Feldmann (2007)	S-19_w 3/3	19.0	75.3	29.1	4.9	106.8	44771	537	150.77
114	Viest (1956)	4A2	12.7	101.6	25.4	3.0	33.1	31502	487	64.05
115	Viest (1956)	4B2	12.7	101.6	25.4	3.0	37.8	32792	487	61.83
116	Viest (1956)	5A2	15.9	100.1	28.7	3.0	32.7	31378	488	105.87
117	Viest (1956)	5B2	15.9	100.1	28.7	3.0	36.6	32477	469	100.08
118	Viest (1956)	6A2	19.1	99.1	31.8	6.0	33.4	31576	436	142.34
119	Viest (1956)	6B2	19.1	99.1	31.8	6.0	36.5	32453	482	144.57
120	Viest (1956)	6A4	19.1	101.6	31.8	6.0	29.0	30267	485	94.30
121	Viest (1956)	6B4	19.1	103.6	31.8	6.0	28.1	29994	467	100.08
122	Viest (1956)	8A2	25.4	101.1	38.1	7.0	32.4	31306	478	186.83
123	Viest (1956)	8B2	25.4	100.8	38.1	7.0	36.5	32432	507	200.17
124	Viest (1956)	10A2	31.8	97.5	44.5	7.0	27.5	29797	440	222.41
125	Viest (1956)	10B2	31.8	100.1	44.5	7.0	30.2	30637	439	211.29
126	Wang et al. (2011)	SS-1/1	22.0	200	29.0	6.0	58.6	37385	465	236.50
127	Wang et al. (2011)	SS-1/2	22.0	200	29.0	6.0	58.6	37385	465	236.50
128	Wang et al. (2011)	SS-1/3	22.0	200	29.0	6.0	58.6	37385	465	236.50
129	Wang et al. (2011)	SS-2/1	22.0	200	29.0	6.0	58.6	37385	675	272.70
130	Wang et al. (2011)	SS-2/2	22.0	200	29.0	6.0	58.6	37385	675	272.70
131	Wang et al. (2011)	SS-2/3	22.0	200	29.0	6.0	58.6	37385	675	272.70
132	Wang et al. (2011)	SS-3/1	25.0	200	31.0	7.0	58.6	37385	485	269.00
133	Wang et al. (2011)	SS-3/2	25.0	200	31.0	7.0	58.6	37385	485	269.00
134	Wang et al. (2011)	SS-3/3	25.0	200	31.0	7.0	58.6	37385	485	269.00
135	Wang et al. (2011)	SS-4/1	30.0	200	35.0	8.0	58.6	37385	430	330.10
136	Wang et al. (2011)	SS-4/2	30.0	200	35.0	8.0	58.6	37385	430	330.10
137	Wang et al. (2011)	SS-4/3	30.0	200	35.0	8.0	58.6	37385	430	330.10

Continue on the next page

Table B.1 - *continued from previous page*

i	Source	Test	d_{nom} [mm]	h_{scm} [mm]	d_{col} [mm]	h_{col} [mm]	f_{cm} [N/mm²]	E_{cm} [N/mm²]	f_{um} [N/mm²]	P_e [kN/stud]
138	Hanswille et al. (1998)	I/1	25.0	125	31.8	7.7	23.7	28500	464	179.50
139	Hanswille et al. (1998)	I/2	25.0	125	31.8	7.7	23.7	28500	464	183.00
140	Hanswille et al. (1998)	I/3	25.0	125	31.8	7.7	23.7	28500	464	180.40
141	Hanswille et al. (1998)	I/4	25.0	125	31.8	7.7	23.7	28500	464	183.10
142	Hanswille et al. (1998)	I/5	25.0	125	31.8	7.7	23.7	28500	464	178.60
143	Hanswille et al. (1998)	II/1	25.0	125	31.8	7.7	41.3	33667	464	233.00
144	Hanswille et al. (1998)	II/2	25.0	125	31.8	7.7	41.3	33667	464	238.00
145	Hanswille et al. (1998)	II/3	25.0	125	31.8	7.7	41.3	33667	464	234.90
146	Hanswille et al. (1998)	II/4	25.0	125	31.8	7.7	41.3	33667	464	234.50
147	Hanswille et al. (1998)	II/5	25.0	125	31.8	7.7	41.3	33667	464	232.80
148	Bullo and Di Marco (1995)	6019A	19.0	75	23.0	6.0	49.4	35526	495	148.30
149	Bullo and Di Marco (1995)	6019B	19.0	75	23.0	6.0	49.4	35526	495	147.55
150	Bullo and Di Marco (1995)	6019C	19.0	75	23.0	6.0	49.4	35526	495	163.10
151	Bullo and Di Marco (1995)	6025A	25.0	120	31.0	7.0	49.4	35526	495	189.05
152	Bullo and Di Marco (1995)	6025B	25.0	120	31.0	7.0	49.4	35526	495	256.20
153	Bullo and Di Marco (1995)	6025C	25.0	120	31.0	7.0	49.4	35526	495	252.65
154	Bullo and Di Marco (1995)	8019A	19.0	75	23.0	6.0	78.4	40805	495	203.60
155	Bullo and Di Marco (1995)	8019B	19.0	75	23.0	6.0	78.4	40805	495	191.00
156	Bullo and Di Marco (1995)	8019C	19.0	75	23.0	6.0	78.4	40805	495	180.85
157	Bullo and Di Marco (1995)	8025A	25.0	120	31.0	7.0	78.4	40805	495	250.00
158	Bullo and Di Marco (1995)	8025B	25.0	120	31.0	7.0	78.4	40805	495	293.15
159	Bullo and Di Marco (1995)	8025C	25.0	120	31.0	7.0	78.4	40805	495	199.70
160	Döinghaus (2001)	Serie 1/1	19.0	80	23.0	4.0	89.1	42403	550	140.40
161	Döinghaus (2001)	Serie 1/2	19.0	80	23.0	4.0	89.1	42403	550	139.80
162	Döinghaus (2001)	Serie 1/3	19.0	80	23.0	4.0	89.1	42403	550	146.90
163	Döinghaus (2001)	Serie 2/1	22.0	100	27.0	6.0	91.2	42704	530	197.20
164	Döinghaus (2001)	Serie 2/2	22.0	100	27.0	6.0	91.2	42704	530	190.90
165	Döinghaus (2001)	Serie 2/3	22.0	100	27.0	6.0	91.2	42704	530	200.70

Continue on the next page

Table B.1 - *continued from previous page*

i	Source	Test	d_{nom} [mm]	h_{scm} [mm]	d_{col} [mm]	h_{col} [mm]	f_{cm} [N/mm²]	E_{cm} [N/mm²]	f_{um} [N/mm²]	P_e [kN/stud]
166	Döinghaus (2001)	Serie 3/1	25.0	120	31.0	6.0	92.2	42832	450	226.00
167	Döinghaus (2001)	Serie 3/2	25.0	120	31.0	6.0	92.2	42832	450	237.30
168	Döinghaus (2001)	Serie 3/3	25.0	120	31.0	6.0	92.2	42832	450	226.90
169	Döinghaus (2001)	Serie 9/1	19.0	80	23.0	4.0	93.5	43015	557	183.90
170	Döinghaus (2001)	Serie 9/2	19.0	80	23.0	4.0	93.5	43015	557	168.20
171	Döinghaus (2001)	Serie 10/1	22.0	105.6	27.0	6.0	93.8	43061	531	246.60
172	Döinghaus (2001)	Serie 10/2	22.0	105.6	27.0	6.0	93.8	43061	531	244.00
173	Döinghaus (2001)	Serie 10/3	22.0	105.6	27.0	6.0	93.8	43061	531	235.50
174	Döinghaus (2001)	Serie 11/1	19.0	80	23.0	4.0	69.7	39397	557	171.20
175	Döinghaus (2001)	Serie 11/2	19.0	80	23.0	4.0	69.7	39397	557	162.50
176	Döinghaus (2001)	Serie 11/3	19.0	80	23.0	4.0	69.7	39397	557	155.20
177	Döinghaus (2001)	Serie 12/1	22.0	100	27.0	6.0	69.7	39397	531	216.10
178	Döinghaus (2001)	Serie 12/2	22.0	100	27.0	6.0	69.7	39397	531	211.00
179	Döinghaus (2001)	Serie 12/3	22.0	100	27.0	6.0	69.7	39397	531	218.20
180	Döinghaus (2001)	Serie 13/1	25.0	120	31.0	6.0	71.4	39670	452	210.90
181	Döinghaus (2001)	Serie 13/2	25.0	120	31.0	6.0	71.4	39670	452	225.10
182	Döinghaus (2001)	Serie 13/3	25.0	120	31.0	6.0	71.4	39670	452	254.40
183	Döinghaus (2001)	Serie 25/1	22.0	100	27.0	6.0	85.6	41895	554	240.50
184	Döinghaus (2001)	Serie 25/2	22.0	100	27.0	6.0	85.6	41895	554	235.00
185	Döinghaus (2001)	Serie 25/3	22.0	100	27.0	6.0	85.6	41895	554	216.30
186	Eggert (2019)	1-01 P1	19.0	125	23.0	4.0	44.2	34350	474	157.94
187	Eggert (2019)	1-01 P2	19.0	125	23.0	4.0	44.3	34390	474	169.00
188	Eggert (2019)	1-01 P3	19.0	125	23.0	4.0	44.8	34504	474	168.69
189	Eggert (2019)	1-02-1 P1	22.0	125	27.0	4.0	45.6	34673	526	215.31
190	Eggert (2019)	1-02-1 P2	22.0	125	27.0	6.0	45.5	34662	526	216.75
191	Eggert (2019)	1-02-1 P3	22.0	125	27.0	6.0	44.2	34368	526	218.43
192	Eggert (2019)	1-02-2 P1	22.0	125	27.0	6.0	46.2	34824	526	206.81
193	Eggert (2019)	1-02-2 P2	22.0	125	27.0	6.0	45.8	34718	526	211.56

Continue on the next page

Table B.1 - *continued from previous page*

i	Source	Test	d_{nom} [mm]	h_{scm} [mm]	d_{col} [mm]	h_{col} [mm]	f_{cm} [N/mm²]	E_{cm} [N/mm²]	f_{um} [N/mm²]	P_e [kN/stud]
194	Eggert (2019)	1-02-2 P3	22.0	125	27.0	6.0	45.4	34628	526	208.68
195	Sattler (1962)	Test 1	19.0	75	23.0	4.0	44.3	34388	392	98.10
196	Sattler (1962)	Test 2	19.0	75	23.0	4.0	29.2	30348	392	86.33
197	Sattler (1962)	Test 3	19.0	75	23.0	4.0	46.1	34796	392	122.63
198	Sattler (1962)	Test 4	19.0	75	23.0	4.0	47.6	35123	392	116.49
199	Lee et al. (2005)	ST25-B1	25.0	142	31.0	7.0	45.3	34614	426	176.40
200	Lee et al. (2005)	ST25-B2	25.0	142	31.0	7.0	45.3	34614	426	176.70
201	Lee et al. (2005)	ST25-B3	25.0	142	31.0	7.0	45.3	34614	426	187.30
202	Lee et al. (2005)	ST27-C1	27.0	141	32.5	8.0	53.0	36283	426	208.20
203	Lee et al. (2005)	ST27-C2	27.0	141	32.5	8.0	53.0	36283	426	238.50
204	Lee et al. (2005)	ST27-C3	27.0	141	32.5	8.0	53.0	36283	426	186.90
205	Lee et al. (2005)	ST30-C1	30.0	141	35.0	8.0	53.0	36283	426	222.80
206	Lee et al. (2005)	ST30-C2	30.0	141	35.0	8.0	53.0	36283	426	240.00
207	Lee et al. (2005)	ST30-C3	30.0	141	35.0	8.0	53.0	36283	426	234.00
208	Xue et al. (2012)	SD-1	22.0	200	29.0	6.0	55.7	36828	475	208.80
209	Xue et al. (2012)	MD-1	22.0	200	29.0	6.0	55.7	36828	475	189.50
210	Xue et al. (2012)	MD-2	22.0	200	29.0	6.0	55.7	36828	475	181.20
211	Xue et al. (2012)	MD-3	22.0	200	29.0	6.0	55.7	36828	475	194.70
212	Xue et al. (2012)	MD-4	22.0	200	29.0	6.0	55.7	36828	475	185.40
213	Jähring (2007)	KI5.1	19.0	125	23.0	5.7	45.4	34637	580	156.50
214	Jähring (2007)	KI5.2	19.0	125	23.0	5.7	47.5	35110	580	166.38
215	Jähring (2007)	KI5.8	19.0	125	23.0	5.7	47.7	35154	580	163.75
216	Jähring (2007)	KI3.2	22.0	125	29.0	5.9	46.3	34842	549	205.50
217	Jähring (2007)	KI3.7	22.0	125	29.0	5.9	44.9	34522	549	205.00
218	Jähring (2007)	KI1.8	22.0	125	29.0	5.9	48.3	35286	549	186.88
219	Jähring (2007)	KI1.9	22.0	125	29.0	5.9	48.3	35286	549	177.75
220	Jähring (2007)	KI1.5	25.0	125	31.0	6.1	45.2	34591	568	241.13

Continue on the next page

Table B.1 - *continued from previous page*

i	Source	Test	d_{nom} [mm]	h_{scm} [mm]	d_{col} [mm]	h_{col} [mm]	f_{cm} [N/mm²]	E_{cm} [N/mm²]	f_{um} [N/mm²]	P_e [kN/stud]
221	Jähring (2007)	KI1.7	25.0	125	31.0	6.1	46.1	34796	568	239.38
222	Jähring (2007)	KI5.3	19.0	125	23.0	5.7	79.1	40914	580	170.38
223	Jähring (2007)	KI5.4	19.0	125	23.0	5.7	76.1	40443	580	188.25
224	Jähring (2007)	KI5.5	19.0	125	23.0	5.7	76.5	40506	580	181.75
225	Jähring (2007)	KI5.6	19.0	125	23.0	5.7	78.9	40883	580	160.88
226	Jähring (2007)	KI5.7	19.0	125	23.0	5.7	80.6	41146	580	168.88
227	Jähring (2007)	KI5.9	19.0	125	23.0	5.7	80.4	41115	580	189.50
228	Jähring (2007)	KI3.1	22.0	125	29.0	5.9	79.7	41007	549	231.13
229	Jähring (2007)	KI3.3	22.0	125	29.0	5.9	79.7	41007	549	221.75
230	Jähring (2007)	KI3.8	22.0	125	29.0	5.9	78.9	40883	549	228.25
231	Jähring (2007)	KI3.9	22.0	125	29.0	5.9	80.8	41176	549	220.50
232	Jähring (2007)	KI5.10	22.0	125	29.0	5.9	81.4	41268	549	216.38
233	Jähring (2007)	KI6.9	22.0	125	29.0	5.9	77.8	40711	549	233.00
234	Jähring (2007)	KI3.5	22.0	125	29.0	5.9	85.9	41939	549	213.88
235	Jähring (2007)	KI3.6	22.0	125	29.0	5.9	86.0	41954	549	218.00
236	Jähring (2007)	KI1.1	25.0	125	31.0	6.1	80.0	41053	568	280.88
237	Jähring (2007)	KI1.4	25.0	125	31.0	6.1	80.3	41100	568	286.75
238	Jähring (2007)	KI6.8	25.0	125	31.0	6.1	78.8	40868	568	284.00
239	Jähring (2007)	KI3.4	22.0	125	29.0	5.9	112.7	45499	549	219.50
240	Jähring (2007)	KI6.6	22.0	125	29.0	5.9	107.8	44896	549	226.38
241	Jähring (2007)	KI6.10	22.0	125	29.0	5.9	112.1	45426	549	205.13
242	Jähring (2007)	KI1.2	25.0	125	31.0	6.1	104.0	44415	568	265.63
243	Jähring (2007)	KI1.3	25.0	125	31.0	6.1	106.2	44695	568	278.50
244	Jähring (2007)	KI1.6	25.0	125	31.0	6.1	105.1	44556	568	285.13
245	Jähring (2007)	KII2.9	22.0	125	29.0	5.9	105.1	44556	549	198.00
246	Jähring (2007)	KII6.4	22.0	125	29.0	5.9	105.1	44556	549	196.59
247	Jähring (2007)	KII6.1	22.0	125	29.0	5.9	105.1	44556	549	226.00
248	Jähring (2007)	KII6.3	22.0	125	29.0	5.9	105.1	44556	549	216.00
249	Jähring (2007)	KII6.2	22.0	125	29.0	5.9	105.1	44556	549	217.58

Continue on the next page

Table B.1 - *continued from previous page*

i	Source	Test	d_{nom} [mm]	h_{scm} [mm]	d_{col} [mm]	h_{col} [mm]	f_{cm} [N/mm²]	E_{cm} [N/mm²]	f_{um} [N/mm²]	P_e [kN/stud]
250	Jähring (2007)	KII6.5	22.0	125	29.0	5.9	105.1	44556	549	221.50
251	Jähring (2007)	KIII5.11	22.0	125	29.0	5.9	105.1	44556	549	197.50
252	Jähring (2007)	KIII7.1	22.0	125	29.0	5.9	105.1	44556	549	197.00
253	Jähring (2007)	KIII7.5	22.0	125	29.0	5.9	105.1	44556	549	185.00
254	Jähring (2007)	KIII7.2	22.0	125	29.0	5.9	105.1	44556	549	212.25
255	Jähring (2007)	KIII7.6	22.0	125	29.0	5.9	105.1	44556	549	222.50
256	Jähring (2007)	KIII7.7	22.0	125	29.0	5.9	105.1	44556	549	217.00
257	Jähring (2007)	KIII6.11	22.0	125	29.0	5.9	105.1	44556	549	225.25
258	Jähring (2007)	KIII7.3	22.0	125	29.0	5.9	105.1	44556	549	221.75
259	Jähring (2007)	KIII7.4	22.0	125	29.0	5.9	105.1	44556	549	219.75
260	Hanswille et al. (2006)	S1-1a	22.0	125	29.0	6.0	44.2	34360	528	191.30
261	Hanswille et al. (2006)	S1-1b	22.0	125	29.0	6.0	49.0	35439	528	211.30
262	Hanswille et al. (2006)	S1-1c	22.0	125	29.0	6.0	49.7	35590	528	213.00
263	Hanswille et al. (2006)	S2-1a	22.0	125	29.0	6.0	44.7	34476	528	201.30
264	Hanswille et al. (2006)	S2-1b	22.0	125	29.0	6.0	42.8	34030	528	173.30
265	Hanswille et al. (2006)	S2-1c	22.0	125	29.0	6.0	42.8	34030	528	175.30
266	Hanswille et al. (2006)	S3-1a	22.0	125	29.0	6.0	56.2	36927	528	216.00
267	Hanswille et al. (2006)	S3-1b	22.0	125	29.0	6.0	53.9	36467	528	200.60
268	Hanswille et al. (2006)	S3-1c	22.0	125	29.0	6.0	53.9	36467	528	201.00
269	Hanswille et al. (2006)	S4-1a	22.0	125	29.0	6.0	43.4	34172	528	186.80
270	Hanswille et al. (2006)	S4-1b	22.0	125	29.0	6.0	43.4	34172	528	176.50
271	Hanswille et al. (2006)	S4-1c	22.0	125	29.0	6.0	43.4	34172	528	179.10
272	Hanswille et al. (2006)	S5-1a	22.0	125	29.0	6.0	42.9	34053	528	184.60
273	Hanswille et al. (2006)	S5-1b	22.0	125	29.0	6.0	42.9	34053	528	186.80
274	Hanswille et al. (2006)	S5-1c	22.0	125	29.0	6.0	45.8	34728	528	196.00

B.2 Headed studs in profiled steel sheeting transverse to the beam

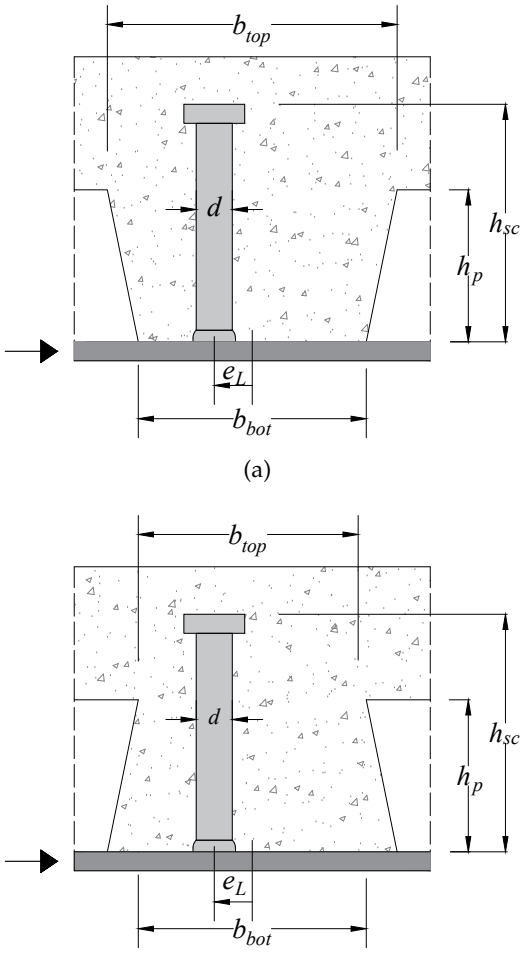

FIGURE B.2: Geometrical dimensions of headed stud shear connectors in (a) open trough and (b) re-entrant profiled sheeting

TABLE B.2: Database of representative push-out tests on headed studs in composite slabs with transverse profiled steel sheeting

i	Source	Test	n_r [-]	Pos. [-]	Welding [-]	e_t [mm]	e_L [mm]	d_{nom} [mm]	h_{scm} [mm]	t [mm]	Sheeting [-]	h_p [mm]	b_{top} [mm]	b_{bot} [mm]	f_{cm} [N/mm²]	f_{um} [N/mm²]	TL [N]	P_e [kN/stud]	LI [-]
1	Lawson et al. (2017)	NR1-1	1	M	T	0	0	19	121.3	0.9	Comflor 80	80	155	120	44.1	551	0	79.07	D
2	Lawson et al. (2017)	1-08-1	2	M	T	100	0	19	117.4	0.9	Comflor 80	80	155	120	42.2	551	Weak	51.84	D
3	Lawson et al. (2017)	1-08-2	2	M	T	100	0	19	117.5	0.9	Comflor 80	80	155	120	42.2	551	Weak	46.21	D
4	Lawson et al. (2017)	3-01-3	2	M	T	100	0	19	118.3	0.9	Comflor 80	80	155	120	40.4	551	0	52.78	D
5	Lawson et al. (2017)	1-03-1	1	M	O	0	0	22	123.3	0.89	Cofraplus 60	58	101	62	41.0	514	0	81.50	D
6	Lawson et al. (2017)	1-03-2	1	M	O	0	0	22	122.5	0.89	Cofraplus 60	58	101	62	42.5	514	0	93.88	D
7	Lawson et al. (2017)	1-03-3	1	M	O	0	0	22	122.8	0.89	Cofraplus 60	58	101	62	42.9	514	0	97.13	D
8	Lawson et al. (2017)	2-01-1	1	M	T	0	0	19	121.8	0.89	Cofraplus 60	58	101	62	42.4	467	0	65.25	D
9	Lawson et al. (2017)	2-01-2	1	M	T	0	0	19	121.8	0.89	Cofraplus 60	58	101	62	42.6	467	0	70.13	D
10	Lawson et al. (2017)	2-01-3	1	M	T	0	0	19	122	0.89	Cofraplus 60	58	101	62	41.8	467	0	74.88	D
11	Lawson et al. (2017)	2-02-1	1	M	T	0	0	19	122.5	0.89	Cofraplus 60	58	101	62	40.7	467	0	69.88	D
12	Lawson et al. (2017)	2-03-1	1	M	O	0	0	19	121.8	0.89	Cofraplus 60	58	101	62	39.7	467	0	57.63	D
13	Lawson et al. (2017)	2-04-1	2	M	T	100	0	19	120.6	0.89	Cofraplus 60	58	101	62	40.3	467	0	68.38	D
14	Lawson et al. (2017)	2-05-1	2	M	T	100	0	19	121	0.89	Cofraplus 60	58	101	62	40.2	467	0	65.63	D
15	Lawson et al. (2017)	2-05-2	2	M	T	100	0	19	121.8	0.89	Cofraplus 60	58	101	62	38.6	467	0	71.06	D
16	Lawson et al. (2017)	2-05-3	2	M	T	100	0	19	121.8	0.89	Cofraplus 60	58	101	62	39.2	467	0	67.06	D
17	Lawson et al. (2017)	2-06-1	1	M	O	0	0	22	122.3	0.89	Cofraplus 60	58	101	62	40.1	514	0	87.50	D
18	Lawson et al. (2017)	2-06-2	1	M	O	0	0	22	122.3	0.89	Cofraplus 60	58	101	62	39.6	514	0	101.60	D
19	Lawson et al. (2017)	2-06-3	1	M	O	0	0	22	122.3	0.89	Cofraplus 60	58	101	62	40.6	514	0	96.50	D
20	Lawson et al. (2017)	2-07-1	1	M	O	0	0	22	121.8	0.89	Cofraplus 60	58	101	62	46.4	514	0	114.60	D
21	Lawson et al. (2017)	2-07-2	1	M	O	0	0	22	122.3	0.89	Cofraplus 60	58	101	62	46.3	514	0	112.40	D
22	Lawson et al. (2017)	2-07-3	1	M	O	0	0	22	122.3	0.89	Cofraplus 60	58	101	62	46.0	514	0	107.60	D
23	Lawson et al. (2017)	2-08-1	1	M	O	0	0	19	122	0.89	Cofraplus 60	58	101	62	45.8	467	0	59.10	D
24	Lawson et al. (2017)	3-03-1	1	M	T	0	0	19	122	1	Cofrastra 56	56	110	137	39.9	467	0	96.00	D
25	Lawson et al. (2017)	3-04-1	1	M	O	0	0	19	122.3	1	Cofrastra 56	56	110	137	41.0	467	0	112.90	D
26	Lawson et al. (2017)	3-05-1	2	M	T	100	0	19	121.9	1	Cofrastra 56	56	110	137	39.7	467	0	95.10	D
27	Lawson et al. (2017)	3-06-1	2	M	T	100	0	19	121.8	1	Cofrastra 56	56	110	137	39.5	467	0	94.60	D
28	Lawson et al. (2017)	3-07-1	2	M	O	100	0	19	122.4	1	Cofrastra 56	56	110	137	40.7	467	0	103.90	D
29	Lawson et al. (2017)	3-08-1	1	M	O	100	0	19	122	1	Cofrastra 56	56	110	137	41.3	467	0	109.10	D
30	Lawson et al. (2017)	3-09-1	1	M	O	0	0	22	123.3	1	Cofrastra 56	56	110	137	40.7	467	0	128.50	D
31	Lawson et al. (2017)	3-10-1	1	M	O	0	0	22	122.3	1	Cofrastra 56	56	110	137	40.5	467	0	121.25	D
32	Ernst (2006)	S3	2	S	T	80	-30	19	95	0.6	KF 70	55	193	136	33.9	460	0	75.00	D
33	Ernst (2006)	S5	2	F	T	120	30	19	95	0.6	KF 70	55	193	136	36.2	460	0	68.00	D
34	Ernst (2006)	SR1	1	F	T	0	30	19	95	1	KF 70	55	193	136	28.4	460	0	92.00	D
35	Ernst (2006)	SR2	1	F	T	0	30	19	95	0.6	KF 70	55	193	136	41.0	460	0	89.00	D
36	Ernst (2006)	SR3	1	F	T	0	30	19	95	1	KF 70	55	193	136	41.0	460	0	119.00	D
37	Ernst (2006)	SR13	2	F	O	80	30	19	130	1	KF 70	55	193	136	38.2	417	0	70.00	D
38	Ernst (2006)	S01	1	F	T	0	30	19	125	0.75	KF 70	55	193	136	48.2	417	0	111.00	D

LEGEND: M: Mid Position F: Favourable position U: Unfavourable position S: Staggered position T: Through deck welding O: Pre-punched holes *TL:* Transversal load *LI:* Load introduction

Continue on the next page

Table B.2 - *continued from previous page*

i	Source	Test	n_r [-]	Pos. [-]	Welding [-]	e_t [mm]	e_L [mm]	d_{nom} [mm]	h_{scm} [mm]	t [mm]	Sheeting [-]	h_p [mm]	b_{top} [mm]	b_{bot} [mm]	f_{cm} [N/mm²]	f_{um} [N/mm²]	TL [N]	P_e [kN/stud]	LI [-]
39	Ernst (2006)	S02	1	U	T	0	-30	19	125	0.75	KF 70	55	193	136	48.5	417	0	108.00	D
40	Ernst (2006)	SW1	1	M	O	0	0	19	127	0.75	Lysaght W-Dek	78	212	143	29.6	509	0	100.00	D
41	Ernst (2006)	SW2	1	M	O	0	0	19	127	0.75	Lysaght W-Dek	78	212	143	30.7	509	0	99.70	D
42	Ernst (2006)	SWR6	2	M	O	80	0	19	127	1	Lysaght W-Dek	78	212	143	32.9	509	0	69.70	D
43	Ernst (2006)	SWR7	2	M	O	80	0	19	127	1	Lysaght W-Dek	78	212	143	32.6	509	0	75.50	D
44	Ernst (2006)	SDM1	2	S	O	80	-35	19	127	0.75	Lysaght W-Dek	78	212	143	31.2	550	0	69.80	D
45	Ernst (2006)	SDM3	2	S	O	80	-35	19	127	0.75	Lysaght W-Dek	78	212	143	33.0	550	0	65.90	D
46	Roik and Bürkner (1981)	1.1	1	M	O	0	0	19	125	0.75	n.a.	60	153	101	28.2	460	0	83.80	U
47	Roik and Bürkner (1981)	1.2	1	M	O	0	0	19	125	0.75	n.a.	60	153	101	28.2	460	0	90.00	U
48	Roik and Bürkner (1981)	2.1	1	M	O	0	0	19	100	0.75	n.a.	60	153	101	22.2	460	0	73.80	U
49	Roik and Bürkner (1981)	2.2	1	M	O	0	0	19	100	0.75	n.a.	60	153	101	22.4	460	0	60.00	U
50	Roik and Bürkner (1981)	3.1	1	M	O	0	0	19	125	0.75	n.a.	80	143	89	28.3	460	0	53.00	U
51	Roik and Bürkner (1981)	3.2	1	M	O	0	0	19	125	0.75	n.a.	80	143	89	27.8	460	0	54.00	U
52	Roik and Bürkner (1981)	4.1	2	M	O	80	0	19	125	0.75	n.a.	60	153	101	23.7	460	0	69.50	U
53	Roik and Bürkner (1981)	4.2	2	S	T	80	-25	19	120	0.75	n.a.	60	153	101	23.7	460	0	74.50	U
54	Roik and Bürkner (1981)	5.1	2	S	T	80	-25	19	95	0.75	n.a.	60	153	101	26.3	460	0	61.50	U
55	Roik and Bürkner (1981)	5.2	2	S	T	80	-25	19	95	0.75	n.a.	60	153	101	24.1	460	0	55.50	U
56	Roik and Bürkner (1981)	6.1	2	S	T	80	-25	19	120	0.75	n.a.	80	143	89	33.9	460	0	41.50	U
57	Roik and Bürkner (1981)	6.2	2	S	T	80	-25	19	120	0.75	n.a.	80	143	89	30.1	460	0	37.50	U
58	Roik and Bürkner (1981)	7.1	1	F	T	0	25	19	95	0.75	n.a.	60	153	101	24.0	460	0	74.00	U
59	Roik and Bürkner (1981)	7.2	1	F	T	0	25	19	95	0.75	n.a.	60	153	101	24.0	460	0	78.00	U
60	Roik and Bürkner (1981)	8.1	1	U	T	0	-25	19	95	0.75	n.a.	60	153	101	24.0	460	0	79.00	U
61	Roik and Bürkner (1981)	8.2	1	U	T	0	-25	19	95	0.75	n.a.	60	153	101	28.3	460	0	75.00	U
62	Roik and Bürkner (1980)	1.1	1	M	O	0	0	19	150	0.75	n.a.	106	110	40	26.8	460	0	37.00	U
63	Roik and Bürkner (1980)	1.2	1	M	O	0	0	19	150	0.75	n.a.	106	110	40	26.8	460	0	38.50	U
64	Roik and Bürkner (1980)	2.1	1	M	O	0	0	19	175	0.75	n.a.	106	110	40	24.7	460	0	44.50	U
65	Roik and Bürkner (1980)	2.2	1	M	O	0	0	19	175	0.75	n.a.	106	110	40	24.7	460	0	38.00	U
66	Roik and Bürkner (1980)	3.1	1	M	O	0	0	19	150	0.75	n.a.	106	210	140	31.1	460	0	82.00	U
67	Roik and Bürkner (1980)	3.2	1	M	O	0	0	19	150	0.75	n.a.	106	210	140	31.1	460	0	78.50	U
68	Roik and Bürkner (1980)	4.2	1	M	O	0	0	19	175	0.75	n.a.	106	210	140	33.4	460	0	76.00	U
69	Roik and Bürkner (1980)	5.1	1	M	O	0	0	19	175	0.75	n.a.	125	120	40	26.9	460	0	42.00	U
70	Roik and Bürkner (1980)	5.2	1	M	O	0	0	19	175	0.75	n.a.	125	120	40	26.9	460	0	49.00	U
71	Roik and Bürkner (1980)	6.1	1	M	O	0	0	19	175	0.75	n.a.	125	120	40	24.7	460	0	39.50	U
72	Roik and Bürkner (1980)	6.2	1	M	O	0	0	19	175	0.75	n.a.	125	120	40	24.7	460	0	46.00	U
73	Roik and Bürkner (1980)	7.1	1	M	O	0	0	19	175	0.75	n.a.	125	210	130	31.6	460	0	73.00	U
74	Roik and Bürkner (1980)	7.2	1	M	O	0	0	19	175	0.75	n.a.	125	210	130	31.6	460	0	70.00	U
75	Roik and Bürkner (1980)	8.1	1	M	O	0	0	19	175	0.75	n.a.	125	210	130	25.1	460	0	79.00	U
76	Roik and Bürkner (1980)	8.2	1	M	O	0	0	19	175	0.75	n.a.	125	210	130	25.1	460	0	85.00	U
77	Roik and Bürkner (1980)	11.1	1	M	O	0	0	19	175	0.75	n.a.	106	210	140	24.8	460	0	84.50	U

LEGEND: M: Mid Position F: Favourable position U: Unfavourable position S: Staggered position T: Through deck welding O: Pre-punched holes *TL:* Transversal load *LI:* Load introduction

Continue on the next page

Table B.2 - *continued from previous page*

i	Source	Test	n_r [-]	Pos. [-]	Welding [-]	e_t [mm]	e_L [mm]	d_{nom} [mm]	h_{scm} [mm]	t [mm]	Sheeting [-]	h_p [mm]	b_{top} [mm]	b_{bot} [mm]	f_{cm} [N/mm²]	f_{um} [N/mm²]	TL [N]	P_e [kN/stud]	LI [-]
78	Roik and Bürkner (1980)	11.2	1	M	O	0	0	19	175	0.75	n.a.	106	210	140	24.8	460	0	85.00	U
79	Roik and Bürkner (1980)	12.1	2	M	O	80	0	19	175	0.75	n.a.	106	210	140	23.6	460	0	73.75	U
80	Roik and Bürkner (1980)	13.1	1	M	O	0	0	22	175	0.75	n.a.	106	210	140	26.9	460	0	82.00	U
81	Roik and Bürkner (1980)	13.2	1	M	O	0	0	22	175	0.75	n.a.	106	210	140	26.9	460	0	96.00	U
82	Roik and Bürkner (1980)	10.1	2	M	O	100	0	22	175	0.75	n.a.	106	210	140	19.6	460	0	67.50	U
83	Roik and Bürkner (1980)	10.2	2	M	O	100	0	22	175	0.75	n.a.	106	210	140	19.6	460	0	72.50	U
84	Roik and Bürkner (1980)	16.1	1	M	O	0	0	19	175	0.75	n.a.	125	210	130	33.1	460	0	79.00	U
85	Roik and Bürkner (1980)	16.2	1	M	O	0	0	19	175	0.75	n.a.	125	120	40	33.1	460	0	35.00	U
86	Roik and Lungershausen (1988)	B11	1	M	O	0	0	19	175	0.75	n.a.	110	129	40	33.3	530	0	53.00	U
87	Roik and Lungershausen (1988)	B12	1	M	O	0	0	19	175	0.75	n.a.	136	137	40	33.3	530	0	46.00	U
88	Roik and Lungershausen (1988)	A1	1	M	O	0	0	22	200	0.75	n.a.	136	137	40	37.3	530	0	55.00	U
89	Roik and Lungershausen (1988)	A2	2	M	O	80	0	22	200	0.75	n.a.	136	137	40	37.3	530	0	45.00	U
90	Konrad (2011)	V1-TK-2f	2	F	T	80	29.75	19	145	0.75	ThyssenKrupp T85.1	83	240	119	31.6	570	0	83.63	D
91	Konrad (2011)	V2-TK-2f	2	F	T	80	29.75	19	145	0.75	ThyssenKrupp T85.1	83	240	119	30.3	570	0	76.25	D
92	Konrad (2011)	V3-TK-2u	2	U	T	80	-29.75	19	145	0.75	ThyssenKrupp T85.1	83	240	119	31.6	570	0	55.75	D
93	Konrad (2011)	V4-TK-2u	2	U	T	80	-29.75	19	145	0.75	ThyssenKrupp T85.1	83	240	119	31.8	570	0	60.00	D
94	Konrad (2011)	V5-TK-2a	2	S	T	80	-29.75	19	145	0.75	ThyssenKrupp T85.1	83	240	119	30.3	570	0	76.25	D
95	Konrad (2011)	V6-TK-2a	2	S	T	80	-29.75	19	145	0.75	ThyssenKrupp T85.1	83	240	119	31.8	570	0	78.75	D
96	Konrad (2011)	V7-Co-1f	1	F	T	0	21.75	19	95	1	Cofrastra 70	73	124	87	33.7	532	0	92.50	D
97	Konrad (2011)	V8-Co-1f	1	F	T	0	21.75	19	120	1	Cofrastra 70	73	124	87	33.7	570	0	116.50	D
98	Konrad (2011)	V10-Co-1u	1	U	T	0	-21.75	19	95	1	Cofrastra 70	73	124	87	34.2	532	0	56.75	D
99	Konrad (2011)	V12-Co-1u	1	U	T	0	-21.75	19	145	1	Cofrastra 70	73	124	87	32.5	570	0	61.25	D
100	Konrad (2011)	V13-Hoe-1m	1	M	T	0	0	19	70	0.75	Holorib 51	51	113	135	32.7	551	0	88.50	D
101	Konrad (2011)	V14-Hoe-1m	1	M	T	0	0	19	95	0.75	Holorib 51	51	113	135	32.7	532	0	97.25	D
102	Konrad (2011)	V16-Hoe-1f	1	F	T	0	33.75	19	95	0.75	Holorib 51	51	113	135	37.5	532	0	128.50	D
103	Konrad (2011)	V17-Hoe-2a	2	S	T	80	-33.75	19	95	0.75	Holorib 51	51	113	135	35.1	532	0	87.50	D
104	Bode and Künzel (1999)	SH0-1	1	M	O	0	0	19	100	1	Holorib 51	51	114	138	27.5	463	0	75.50	U
105	Bode and Künzel (1999)	SH0-2	1	M	O	0	0	19	100	1	Holorib 51	51	114	138	28.0	463	0	77.60	U
106	Bode and Künzel (1999)	SH0-3	1	M	O	0	0	19	100	1	Holorib 51	51	114	138	28.9	463	0	76.40	U
107	Bode and Künzel (1999)	SH1-1	1	M	T	0	0	19	95	1	Holorib 51	51	114	138	27.5	463	0	88.10	U
108	Bode and Künzel (1999)	SH1-2	1	M	T	0	0	19	95	1	Holorib 51	51	114	138	28.6	463	0	88.40	U
109	Bode and Künzel (1999)	SH1-3	1	M	T	0	0	19	95	1	Holorib 51	51	114	138	30.2	463	0	97.60	U
110	Bode and Künzel (1999)	SH2-1	1	M	T	0	0	19	95	1	Holorib 51	51	114	138	32.6	463	0	101.80	U
111	Bode and Künzel (1999)	SH2-2	1	M	T	0	0	19	95	1	Holorib 51	51	114	138	32.5	463	0	102.80	U
112	Bode and Künzel (1999)	SH2-3	1	M	T	0	0	19	95	1	Holorib 51	51	114	138	32.5	463	0	102.20	U
113	Bode and Künzel (1999)	CS0-1	1	M	O	0	0	19	95	0.88	Cofrastra150/40	40	104	124	25.3	463	0	77.10	U
114	Bode and Künzel (1999)	CS0-2	1	M	O	0	0	19	95	0.88	Cofrastra150/40	40	104	124	26.0	463	0	77.10	U
115	Bode and Künzel (1999)	CS0-3	1	M	O	0	0	19	95	0.88	Cofrastra150/40	40	104	124	29.0	463	0	96.30	U
116	Bode and Künzel (1999)	CS1-1	1	M	T	0	0	19	100	0.88	Cofrastra150/40	40	104	124	28.4	463	0	90.20	U

LEGEND: M: Mid Position F: Favourable position U: Unfavourable position S: Staggered position T: Through deck welding O: Pre-punched holes *TL:* Transversal load *LI:* Load introduction

Continue on the next page

Table B.2 - *continued from previous page*

i	Source	Test	n_r [-]	Pos. [-]	Welding [-]	e_t [mm]	e_L [mm]	d_{nom} [mm]	h_{scm} [mm]	t [mm]	Sheeting [-]	h_p [mm]	b_{top} [mm]	b_{bot} [mm]	f_{cm} [N/mm²]	f_{um} [N/mm²]	TL [N]	P_e [kN/stud]	LI [-]
117	Bode and Künzel (1999)	CS1-2	1	M	T	0	0	19	100	0.88	Cofrastra150/40	40	104	124	27.0	463	0	85.10	U
118	Bode and Künzel (1999)	CS1-3	1	M	T	0	0	19	100	0.88	Cofrastra150/40	40	104	124	30.8	463	0	88.30	U
119	Bode and Künzel (1987)	H1	1	M	O	0	0	22	100	0.75	Holorib 51	51	114	138	38.3	460	0	114.00	U
120	Bode and Künzel (1987)	H2	1	M	O	0	0	22	100	0.75	Holorib 51	51	114	138	38.3	460	0	107.00	U
121	Bode and Künzel (1987)	H11	1	M	O	0	0	22	100	0.75	Holorib 51	51	114	138	36.5	460	0	108.00	U
122	Bode and Künzel (1987)	H13	1	M	O	0	0	22	100	0.75	Holorib 51	51	114	138	36.5	460	0	116.00	U
123	Bode and Künzel (1987)	H3	1	M	O	0	0	22	100	0.75	Holorib 51	51	114	138	39.1	460	0	114.00	U
124	Bode and Künzel (1987)	H4	1	M	O	0	0	22	100	0.75	Holorib 51	51	114	138	39.1	460	0	130.00	U
125	Bode and Künzel (1987)	H5	1	M	O	0	0	22	100	0.75	Holorib 51	51	114	138	38.3	460	0	111.00	U
126	Bode and Künzel (1987)	H6	1	M	O	0	0	22	100	0.75	Holorib 51	51	114	138	38.3	460	0	115.00	U
127	Bode and Künzel (1987)	H7	1	M	O	0	0	22	100	0.75	Holorib 51	51	114	138	37.4	460	0	122.00	U
128	Bode and Künzel (1987)	H8	1	M	O	0	0	22	100	0.75	Holorib 51	51	114	138	37.4	460	0	123.00	U
129	Bode and Künzel (1987)	D1	2	M	O	100	0	22	125	0.75	Holorib 51	51	114	138	35.9	550	0	107.00	U
130	Bode and Künzel (1987)	D2	2	M	O	100	0	22	125	0.75	Holorib 51	51	114	138	35.9	550	0	96.50	U
131	Bode and Künzel (1987)	D3	2	M	O	100	0	22	125	0.75	Holorib 51	51	114	138	35.9	550	0	106.00	U
132	Bode and Künzel (1987)	D4	2	M	O	100	0	22	125	0.75	Holorib 51	51	114	138	34.0	550	0	102.50	U
133	Bode and Künzel (1987)	D5	2	M	O	100	0	22	125	0.75	Holorib 51	51	114	138	34.0	550	0	105.00	U
134	**cashell2013a**	1-B	1	M	T	0	0	19	95	0.75	Cofraplus 60	58	101	62	44.4	488	0	58.68	D
135	**cashell2013a**	2-A	1	M	T	0	0	19	95	0.75	Cofraplus 60	58	101	62	37.5	488	0	62.43	D
136	**cashell2013a**	2-B	1	M	T	0	0	19	95	0.75	Cofraplus 60	58	101	62	29.6	488	0	61.30	D
137	**cashell2013a**	2-C	1	M	T	0	0	19	95	0.75	Cofraplus 60	58	101	62	39.3	488	0	67.73	D
138	**cashell2013a**	3-A	1	M	O	0	0	19	100	0.75	Cofraplus 60	58	101	62	30.1	488	0	57.92	D
139	**cashell2013a**	3-B	1	M	O	0	0	19	100	0.75	Cofraplus 60	58	101	62	41.3	488	0	61.05	D
140	**cashell2013a**	3-C	1	M	O	0	0	19	100	0.75	Cofraplus 60	58	101	62	34.3	488	0	58.10	D
141	Yuan (1996)	G1F-1	1	F	T	0	32.5	19	120	1.2	Multideck 80	80	180	100	28.4	472	0	93.10	D
142	Yuan (1996)	G1F-2	1	F	T	0	32.5	19	120	1.2	Multideck 80	80	180	100	28.4	472	0	90.60	D
143	Yuan (1996)	G2C-1	1	M	T	0	0	19	120	0.9	PMF CF70	55	188	136	22.1	472	0	88.60	D
144	Yuan (1996)	G2C-2	1	M	T	0	0	19	120	0.9	PMF CF70	55	188	136	22.1	472	0	88.00	D
145	Yuan (1996)	G5U-1	1	U	T	0	-37.5	19	120	1.2	Multideck 80	80	180	100	28.4	472	0	70.90	D
146	Yuan (1996)	G5U-2	1	U	T	0	-37.5	19	120	1.2	Multideck 80	80	180	100	28.4	472	0	67.50	D
147	Yuan (1996)	G6U-1	1	U	T	0	-30	19	95	0.9	PMF CF60	60	185	155	17.8	486	0	51.30	D
148	Yuan (1996)	G6U-2	1	U	T	0	-30	19	95	0.9	PMF CF60	60	185	155	17.8	486	0	53.80	D
149	Yuan (1996)	G7D-1	2	S	T	0	-26.5	19	95	0.9	PMF CF60	60	185	155	26.2	486	0	49.80	D
150	Yuan (1996)	G7D-2	2	S	T	0	-26.5	19	95	0.9	PMF CF60	60	185	155	26.2	486	0	51.60	D
151	Yuan (1996)	G8D-1	2	S	T	0	-32.5	19	120	1.2	Multideck 80	80	180	100	26.2	472	0	61.40	D
152	Yuan (1996)	G8D-2	2	S	T	0	-32.5	19	120	1.2	Multideck 80	80	180	100	26.2	472	0	60.10	D
153	Hicks (2009)	Test 1	1	F	T	0	35.5	19	95	0.9	Kingspan MD60-V2	60	181	119	20.4	514	0	84.68	D
154	Hicks (2009)	Test 2	1	F	T	0	35.5	19	95	0.9	Kingspan MD60-V2	60	181	119	20.4	514	0	88.96	D

LEGEND: M: Mid Position F: Favourable position U: Unfavourable position S: Staggered position T: Through deck welding O: Pre-punched holes *TL:* Transversal load *LI:* Load introduction

Continue on the next page

Table B.2 - *continued from previous page*

i	Source	Test	n_r [-]	Pos. [-]	Welding [-]	e_t [mm]	e_L [mm]	d_{nom} [mm]	h_{scm} [mm]	t [mm]	Sheeting [-]	h_p [mm]	b_{top} [mm]	b_{bot} [mm]	f_{cm} [N/mm²]	f_{um} [N/mm²]	TL [N]	P_e [kN/stud]	LI [-]
155	Hicks (2009)	Test 3	1	F	T	0	35.5	19	95	0.9	Kingspan MD60-V2	60	181	119	20.4	514	0	88.72	D
156	Hicks (2009)	Test 4	2	F	T	146	35.5	19	95	0.9	Kingspan MD60-V2	60	181	119	20.4	514	0	51.21	D
157	Hicks (2009)	Test 5	2	F	T	146	35.5	19	95	0.9	Kingspan MD60-V2	60	181	119	20.4	514	0	54.45	D
158	Hicks (2009)	Test 6	2	F	T	146	35.5	19	95	0.9	Kingspan MD60-V2	60	181	119	20.4	514	0	61.30	D
159	Mottram and Johnson (1990)	H25-1A	1	M	T	0	0	19	95	1.2	Holorib 51	51	112	138	19.3	486	0	93.77	D
160	Mottram and Johnson (1990)	H25-1B	1	M	T	0	0	19	95	1.2	Holorib 51	51	112	138	19.3	486	0	95.55	D
161	Mottram and Johnson (1990)	H25-1C	1	M	T	0	0	19	95	1.2	Holorib 51	51	112	138	19.3	486	0	92.87	D
162	Mottram and Johnson (1990)	H30-1A	1	M	T	0	0	19	95	1.2	Holorib 51	51	112	138	27.6	486	0	104.48	D
163	Mottram and Johnson (1990)	H30-1B	1	M	T	0	0	19	95	1.2	Holorib 51	51	112	138	27.6	486	0	100.91	D
164	Mottram and Johnson (1990)	H30-1C	1	M	T	0	0	19	95	1.2	Holorib 51	51	112	138	27.6	486	0	103.59	D
165	Mottram and Johnson (1990)	H40-1A	1	M	T	0	0	19	95	1.2	Holorib 51	51	112	138	33.2	486	0	108.95	D
166	Mottram and Johnson (1990)	H40-1B	1	M	T	0	0	19	95	1.2	Holorib 51	51	112	138	33.2	486	0	107.16	D
167	Mottram and Johnson (1990)	H40-1C	1	M	T	0	0	19	95	1.2	Holorib 51	51	112	138	33.2	486	0	111.63	D
168	Mottram and Johnson (1990)	H30-2-50A	2	M	T	50	0	19	98.9	1.2	Holorib 51	51	112	138	25.9	486	0	71.44	D
169	Mottram and Johnson (1990)	H30-2-50B	2	M	T	50	0	19	98.6	1.2	Holorib 51	51	112	138	25.9	486	0	72.33	D
170	Mottram and Johnson (1990)	H30-2-50C	2	M	T	50	0	19	98.9	1.2	Holorib 51	51	112	138	25.9	486	0	78.58	D
171	Mottram and Johnson (1990)	H30-2-76A	2	M	T	76	0	19	98.1	1.2	Holorib 51	51	112	138	28.0	504	0	80.37	D
172	Mottram and Johnson (1990)	H30-2-76B	2	M	T	76	0	19	97.9	1.2	Holorib 51	51	112	138	28.0	504	0	77.69	D
173	Mottram and Johnson (1990)	R30-1-UA	1	U	T	0	-44	19	96	1.2	Ribdeck	60	155	115	26.9	542	0	73.23	D
174	Mottram and Johnson (1990)	R30-1-UB	1	U	T	0	-44	19	96.4	1.2	Ribdeck	60	155	115	26.9	542	0	81.26	D
175	Mottram and Johnson (1990)	R30-1-UC	1	U	T	0	-44	19	96.8	1.2	Ribdeck	60	155	115	26.9	542	0	79.48	D
176	Mottram and Johnson (1990)	R30-1-FA	1	F	T	0	44	19	95.6	1.2	Ribdeck	60	155	115	27.7	542	0	113.41	D
177	Mottram and Johnson (1990)	R30-1-FB	1	F	T	0	44	19	95.3	1.2	Ribdeck	60	155	115	27.7	542	0	115.20	D
178	Mottram and Johnson (1990)	R30-1-FC	1	F	T	0	44	19	96.5	1.2	Ribdeck	60	155	115	27.7	542	0	114.30	D
179	Mottram and Johnson (1990)	R30-2-SA	2	S	T	66	-44	19	96.5	1.2	Ribdeck	60	155	115	26.3	504	0	75.01	D
180	Mottram and Johnson (1990)	R30-2-SB	2	S	T	66	-44	19	96.3	1.2	Ribdeck	60	155	115	26.3	504	0	75.91	D
181	Mottram and Johnson (1990)	R30-1-DA	1	U	T	0	-44	19	121.3	1.2	Ribdeck	60	155	115	29.4	542	0	92.87	D
182	Mottram and Johnson (1990)	R30-1-DB	1	U	T	0	-44	19	121.8	1.2	Ribdeck	60	155	115	29.4	542	0	91.09	D
183	Mottram and Johnson (1990)	R30-1-DC	1	U	T	0	-44	19	121.8	1.2	Ribdeck	60	155	115	29.4	542	0	89.30	D
184	Mottram and Johnson (1990)	H30-1-P	1	M	T	0	0	19	97.3	1.2	Holorib 51	51	112	138	25.6	504	0	113.41	D
185	Jayas and Hosain (1987)	JDT-8	1	F	T	0	46	19	122	1	Robertson QL Lock-rib	76	184	121	24.4	480	0	74.50	L
186	Hicks (2007)	E60-01	1	F	T	0	27.5	19	95	0.87	Ribdeck E60	60	180	110	32.3	450	0	65.15	U
187	Hicks (2007)	E60-04	1	F	T	0	27.5	19	95	0.87	Ribdeck E60	60	180	110	36.1	450	0	77.64	U
188	Hicks (2007)	E60-07u	1	U	T	0	-27.5	19	95	0.87	Ribdeck E60	60	180	110	31.6	450	0	77.12	U
189	Hicks (2007)	E80-06u	1	U	T	0	-33.75	19	120	1.19	n.a.	80.5	185	135	34.2	450	0	76.59	U
190	Hicks (2007)	CF70-08	1	U	T	0	-34	19	95	0.92	KF 70	55	188	136	35.8	559	0	67.71	U
191	Hicks (2007)	CF70-09	1	U	T	0	-34	19	95	0.92	KF 70	55	188	136	35.5	559	0	68.14	U
192	Hicks (2007)	CF70-10	1	U	T	0	-34	19	95	0.92	KF 70	55	188	136	35.5	559	0	76.02	U

LEGEND: M: Mid Position F: Favourable position U: Unfavourable position S: Staggered position T: Through deck welding O: Pre-punched holes *TL:* Transversal load *LI:* Load introduction

Continue on the next page

Table B.2 - *continued from previous page*

i	Source	Test	n_r [-]	Pos. [-]	Welding [-]	e_t [mm]	e_L [mm]	d_{nom} [mm]	h_{scm} [mm]	t [mm]	Sheeting [-]	h_p [mm]	b_{top} [mm]	b_{bot} [mm]	f_{cm} [N/mm²]	f_{um} [N/mm²]	TL [N]	P_e [kN/stud]	LI [-]
193	Hicks (2007)	TR60-12	1	U	T	0	-33.21	19	95	0.9	TR60 +	60	175	133	35.6	450	0	70.32	U
194	Hicks (1997)	1-TA25-1F-FB	1	F	T	0	42.5	19	95	1.2	n.a.	50	180	140	25.2	465	0	92.45	U
195	Hicks (1997)	1-TA25-2S-FB	2	S	T	191	-42.5	19	95	1.2	n.a.	50	180	140	26.2	465	0	72.10	U
196	Hicks (1997)	2-TA25-2S-FB	2	S	T	191	-42.5	19	95	1.2	n.a.	50	180	140	23.6	465	0	75.53	U
197	Hicks (1997)	1-TA25-1F-FB	1	F	T	0	42.5	19	95	1.2	n.a.	50	180	140	23.3	465	0	115.59	U
198	Hicks (1997)	1-TA25-2S-FB	2	S	T	191	-42.5	19	95	1.2	n.a.	50	180	140	23.3	465	0	76.02	U
199	Hicks (1997)	2-TA25-2S-FB	2	S	T	191	-42.5	19	95	1.2	n.a.	50	180	140	25.3	465	0	88.93	U
200	Hicks (1997)	1-TA-25-2S-FB	2	S	T	191	-42.5	19	95	1.2	n.a.	50	180	140	26.2	465	0	82.77	U
201	Hicks (1997)	2-TA-25-2S-FB	2	S	T	191	-42.5	19	95	1.2	n.a.	50	180	140	23.6	465	0	111.79	U
202	Wuppertal (U.R.)	1	1	M	T	0	0	19	95	1	Holorib 51	51	114	138	19.5	463	0	88.10	U
203	Wuppertal (U.R.)	2	1	M	T	0	0	19	95	1	Holorib 51	51	114	138	20.6	463	0	88.40	U
204	Wuppertal (U.R.)	3	1	M	T	0	0	19	95	1	Holorib 51	51	114	138	22.3	463	0	97.60	U
205	Wuppertal (U.R.)	4	1	M	T	0	0	19	95	0.88	Cofrastra 40	40	104	124	20.5	463	0	90.20	U
206	Wuppertal (U.R.)	5	1	M	T	0	0	19	95	0.88	Cofrastra 40	40	104	124	19.0	463	0	85.10	U
207	Wuppertal (U.R.)	6	1	M	T	0	0	19	95	0.88	Cofrastra 40	40	104	124	22.9	463	0	88.30	U
208	Robinson (1988)	Q1-A	1	M	T	0	0	19	111	1	Robertson QL Lock-rib	76	184	121	28.0	480	0	83.55	L
209	Robinson (1988)	Q1-B	1	M	T	0	0	19	111	1	Robertson QL Lock-rib	76	184	121	28.0	480	0	81.35	L
210	Robinson (1988)	Q1-C	1	M	T	0	0	19	111	1	Robertson QL Lock-rib	76	184	121	28.0	480	0	79.75	L
211	Robinson (1988)	Q2-A	2	M	T	102	0	19	111	1	Robertson QL Lock-rib	76	184	121	28.0	480	0	53.20	L
212	Robinson (1988)	Q2-B	2	M	T	102	0	19	111	1	Robertson QL Lock-rib	76	184	121	28.0	480	0	53.78	L
213	Robinson (1988)	T1-A	1	F	T	0	38.25	19	111	1	Westeel T-30V	76	203	160	28.0	480	0	106.40	L
214	Robinson (1988)	T1-B	1	F	T	0	38.25	19	111	1	Westeel T-30V	76	203	160	28.0	480	0	104.85	L
215	Robinson (1988)	T1-C	1	F	T	0	38.25	19	111	1	Westeel T-30V	76	203	160	28.0	480	0	105.15	L
216	Robinson (1988)	R1-A	1	M	T	0	0	19	86	1	Robertson QL Span-rib	51	114.5	89	28.0	480	0	82.00	L
217	Robinson (1988)	R1-B	1	M	T	0	0	19	86	1	Robertson QL Span-rib	51	114.5	89	28.0	480	0	81.10	L
218	Robinson (1988)	R1-C	1	M	T	0	0	19	86	1	Robertson QL Span-rib	51	114.5	89	28.0	480	0	86.00	L
219	Robinson (1988)	TV2-A	1	U	T	0	-52.75	19	111	1	Westeel T-30V	76	203	160	28.0	480	0	95.00	L
220	Robinson (1988)	TV2-B	1	U	T	0	-52.75	19	111	1	Westeel T-30V	76	203	160	28.0	480	0	95.45	L
221	Robinson (1988)	TV2-C	1	U	T	0	-52.75	19	111	1	Westeel T-30V	76	203	160	28.0	480	0	101.10	L
222	Robinson (1988)	T2-A	2	F	T	102	52.75	19	111	1	Westeel T-30V	76	203	160	28.0	480	0	64.30	L
223	Robinson (1988)	T2-B	2	F	T	102	52.75	19	111	1	Westeel T-30V	76	203	160	28.0	480	0	64.23	L
224	Robinson (1988)	T2-C	2	F	T	102	52.75	19	111	1	Westeel T-30V	76	203	160	28.0	480	0	65.23	L
225	Robinson (1988)	TV3-A	2	U	T	102	-52.75	19	111	1	Westeel T-30V	76	203	160	28.0	480	0	45.25	L
226	Robinson (1988)	TV3-B	2	U	T	102	-52.75	19	111	1	Westeel T-30V	76	203	160	28.0	480	0	48.83	L
227	Robinson (1988)	TV3-C	2	U	T	102	-52.75	19	111	1	Westeel T-30V	76	203	160	28.0	480	0	49.10	L
228	Hicks and Smith (2014)	Test 1	2	F	T	105.8	35.5	19	95	0.9	Kingspan MD60-V2	60	181	119	31.7	509	0	51.24	D
229	Hicks and Smith (2014)	Test 2	2	F	T	105.8	35.5	19	95	0.9	Kingspan MD60-V2	60	181	119	31.7	509	0	51.39	D
230	Hicks and Smith (2014)	Test 3	2	F	T	105.8	35.5	19	95	0.9	Kingspan MD60-V2	60	181	119	32.4	509	0	56.30	D

LEGEND: M: Mid Position F: Favourable position U: Unfavourable position S: Staggered position T: Through deck welding O: Pre-punched holes *TL:* Transversal load *LI:* Load introduction

Continue on the next page

Table B.2 - *continued from previous page*

i	Source	Test	n_r [-]	Pos. [-]	Welding [-]	e_t [mm]	e_L [mm]	d_{nom} [mm]	h_{scm} [mm]	t [mm]	Sheeting [-]	h_p [mm]	b_{top} [mm]	b_{bot} [mm]	f_{cm} [N/mm²]	f_{um} [N/mm²]	TL [N]	P_e [kN/stud]	LI [-]
231	Hicks and Smith (2014)	Test 4 (N.R.)	2	F	T	105.8	35.5	19	95	0.9	Kingspan MD60-V2	60	181	119	31.7	509	0	55.99	D
232	Hicks and Smith (2014)	Test 5 (N.R.)	2	F	T	105.8	35.5	19	95	0.9	Kingspan MD60-V2	60	181	119	31.7	509	0	52.12	D
233	Hicks and Smith (2014)	Test 6 (N.R.)	2	F	T	105.8	35.5	19	95	0.9	Kingspan MD60-V2	60	181	119	32.4	509	0	55.18	D
234	Hicks and Smith (2014)	Test 7 (N.R.)	1	F	T	0	35.5	19	95	0.9	Kingspan MD60-V2	60	181	119	31.7	509	0	84.76	D
235	Hicks and Smith (2014)	Test 8 (N.R.)	1	F	T	0	35.5	19	95	0.9	Kingspan MD60-V2	60	181	119	31.7	509	0	82.71	D
236	Hicks and Smith (2014)	Test 9 (N.R.)	1	F	T	0	35.5	19	95	0.9	Kingspan MD60-V2	60	181	119	32.4	509	0	89.33	D
237	Lloyd and Wright (1990)	S1-1	1	M	T	0	0	19	95	1.2	SCI generic profile	50	175	125	35.8	500	0	96.30	D
238	Lloyd and Wright (1990)	S1-2	1	M	T	0	0	19	95	1.2	SCI generic profile	50	175	125	35.8	500	0	96.20	D
239	Lloyd and Wright (1990)	S1-3	1	M	T	0	0	19	95	1.2	SCI generic profile	50	175	125	35.8	500	0	93.30	D
240	Lloyd and Wright (1990)	S2-1	1	M	T	0	0	19	95	1.2	SCI generic profile	50	175	125	28.2	500	0	83.30	D
241	Lloyd and Wright (1990)	S2-2	1	M	T	0	0	19	95	1.2	SCI generic profile	50	175	125	28.2	500	0	83.80	D
242	Lloyd and Wright (1990)	S2-3	1	M	T	0	0	19	95	1.2	SCI generic profile	50	175	125	28.2	500	0	78.30	D
243	Lloyd and Wright (1990)	S3-1	1	M	T	0	0	19	95	1.2	SCI generic profile	50	175	125	31.6	500	0	79.20	D
244	Lloyd and Wright (1990)	S3-2	1	M	T	0	0	19	95	1.2	SCI generic profile	50	175	125	31.6	500	0	100.00	D
245	Lloyd and Wright (1990)	S3-3	1	M	T	0	0	19	95	1.2	SCI generic profile	50	175	125	31.6	500	0	90.50	D
246	Lloyd and Wright (1990)	S4-1	1	M	T	0	0	19	95	1.2	SCI generic profile	50	175	125	37.0	500	0	95.80	D
247	Lloyd and Wright (1990)	S4-2	1	M	T	0	0	19	95	1.2	SCI generic profile	50	175	125	37.0	500	0	91.70	D
248	Lloyd and Wright (1990)	S4-3	1	M	T	0	0	19	95	1.2	SCI generic profile	50	175	125	37.0	500	0	100.00	D
249	Lloyd and Wright (1990)	S5-1	1	M	T	0	0	19	95	1.2	SCI generic profile	50	175	125	34.9	500	0	100.20	D
250	Lloyd and Wright (1990)	S5-2	1	M	T	0	0	19	95	1.2	SCI generic profile	50	175	125	34.9	500	0	108.50	D
251	Lloyd and Wright (1990)	S5-3	1	M	T	0	0	19	95	1.2	SCI generic profile	50	175	125	34.9	500	0	100.00	D
252	Lloyd and Wright (1990)	S6-1	1	M	T	0	0	19	95	1.2	SCI generic profile	50	175	125	35.0	500	0	97.30	D
253	Lloyd and Wright (1990)	S6-2	1	M	T	0	0	19	95	1.2	SCI generic profile	50	175	125	35.0	500	0	101.00	D
254	Lloyd and Wright (1990)	S6-3	1	M	T	0	0	19	95	1.2	SCI generic profile	50	175	125	35.0	500	0	98.00	D
255	Lloyd and Wright (1990)	S7-1	1	M	T	0	0	19	95	1.2	SCI generic profile	50	175	125	29.8	500	0	100.50	D
256	Lloyd and Wright (1990)	S7-2	1	M	T	0	0	19	95	1.2	SCI generic profile	50	175	125	29.8	500	0	95.00	D
257	Lloyd and Wright (1990)	S7-3	1	M	T	0	0	19	95	1.2	SCI generic profile	50	175	125	29.8	500	0	89.20	D
258	Lloyd and Wright (1990)	S8-1	1	M	T	0	0	19	95	1.2	SCI generic profile	50	175	125	31.7	500	0	76.50	D
259	Lloyd and Wright (1990)	S8-2	1	M	T	0	0	19	95	1.2	SCI generic profile	50	175	125	31.7	500	0	94.00	D
260	Lloyd and Wright (1990)	S8-3	1	M	T	0	0	19	95	1.2	SCI generic profile	50	175	125	31.7	500	0	91.30	D
261	Lloyd and Wright (1990)	S9-1	1	M	T	0	0	19	95	1.2	SCI generic profile	50	175	125	31.8	500	0	85.70	D
262	Lloyd and Wright (1990)	S9-2	1	M	T	0	0	19	95	1.2	SCI generic profile	50	175	125	31.8	500	0	90.70	D
263	Lloyd and Wright (1990)	S9-3	1	M	T	0	0	19	95	1.2	SCI generic profile	50	175	125	31.8	500	0	88.70	D
264	Lloyd and Wright (1990)	S10-1	1	M	T	0	0	19	95	1.2	SCI generic profile	50	175	125	31.7	500	0	96.70	D
265	Lloyd and Wright (1990)	S10-2	1	M	T	0	0	19	95	1.2	SCI generic profile	50	175	125	31.7	500	0	97.50	D
266	Lloyd and Wright (1990)	S10-3	1	M	T	0	0	19	95	1.2	SCI generic profile	50	175	125	31.7	500	0	97.50	D
267	Lloyd and Wright (1990)	A1-1	1	M	T	0	0	19	95	1.2	Alphalok	50	180	140	30.8	500	0	113.30	D
268	Lloyd and Wright (1990)	A1-2	1	M	T	0	0	19	95	1.2	Alphalok	50	180	140	30.8	500	0	107.00	D
269	Lloyd and Wright (1990)	A1-3	1	M	T	0	0	19	95	1.2	Alphalok	50	180	140	30.8	500	0	113.80	D

LEGEND: M: Mid Position F: Favourable position U: Unfavourable position S: Staggered position T: Through deck welding O: Pre-punched holes *TL:* Transversal load *LI:* Load introduction

Continue on the next page

Table B.2 - *continued from previous page*

i	Source	Test	n_r [-]	Pos. [-]	Welding [-]	e_t [mm]	e_L [mm]	d_{nom} [mm]	h_{scm} [mm]	t [mm]	Sheeting [-]	h_p [mm]	b_{top} [mm]	b_{bot} [mm]	f_{cm} [N/mm²]	f_{um} [N/mm²]	TL [N]	P_e [kN/stud]	LI [-]
270	Shen and Chung (2017)	SCFr-1	2	F	T	76	30	19	95	1	n.a.	50	130	90	37.2	500	0	63.00	D
271	Shen and Chung (2017)	SCFr-2	2	F	T	76	30	19	95	1	n.a.	50	130	90	37.2	500	0	68.30	D
272	Shen and Chung (2017)	SCFr-3	2	F	T	76	30	19	95	1	n.a.	50	130	90	37.2	500	0	62.70	D
273	Shen and Chung (2017)	SCUr-07	2	U	T	76	-30	19	95	1	n.a.	50	130	90	37.4	500	0	52.80	D
274	Shen and Chung (2017)	SCUr-08	2	U	T	76	-30	19	95	1	n.a.	50	130	90	37.4	500	0	57.60	D

LEGEND: M: Mid Position F: Favourable position U: Unfavourable position S: Staggered position T: Through deck welding O: Pre-punched holes *TL:* Transversal load *LI:* Load introduction

Appendix C

Statistical evaluation of the design models of headed studs in profiled steel sheeting including tests with low strength concrete

C.1 Previous design models

In addition to the reliability analysis of the design models for the prediction of the resistance of studs in profiled steel sheeting given in Section 2.4, the evaluations were performed including tests with low strength concrete (f_{cm}<24 MPa). The results of the analyses are provided below in Table C.1 and Table C.2, considering the entire database and the respective field of application, respectively.

TABLE C.1: Statistical evaluation of the design models for the resistance of studs in profiled steel sheeting in the whole representative database including tests with f_{cm} <24 MPa

	EN 1994-1-1 (2004b) Eq. (2.20)	EN 1994-1-1 (2004b) Eq. (2.21)	Lungershausen (1988) Eq. (2.27)	Lloyd and Wright (1990) Eq. (2.31)
n	71	203	274	274
ρ	0.696		0.757	0.412
b	0.999	1.075	1.370	1.080
V_r	0.242	0.312	0.186	0.316
γ_M^*	2.032	2.129	1.193	2.350
γ_V	1.25	1.25	1.20	-

	Johnson and Yuan (1998) Eq. (2.35)	Eq. (2.36)	Eq. (2.37)	Eq. (2.38)	Konrad (2011) Eq. (2.41)	Eq. (2.42)
n	129	67	23	55	1	273
ρ	0.730				0.786	
b	0.987	1.033	1.213	1.491	1.106	1.132
V_r	0.211	0.187	0.304	0.236	-	0.208
γ_M^*	1.712	1.560	2.103	1.295	-	1.448
γ_V	1.25	1.25	1.25	1.25	1.25	1.25

TABLE C.2: Statistical evaluation of the previous design models for the resistance of studs in profiled steel sheeting in the field of application including tests with f_{cm}<24 MPa

	EN 1994-1-1 (2004b) Eq. (2.20)	EN 1994-1-1 (2004b) Eq. (2.21)	Lungershausen (1988) Eq. (2.27)	Lloyd and Wright (1990) Eq. (2.31)
n	59	119	193	33
ρ	0.596		0.750	0.584
b	1.006	1.046	1.359	1.060
V_r	0.222	0.212	0.165	0.095
γ_M^*	1.902	1.627	1.128	1.242
γ_V	1.25	1.25	1.20	-

	Johnson and Yuan (1998) Eq. (2.35)	Eq. (2.36)	Eq. (2.37)	Eq. (2.38)	Konrad (2011) Eq. (2.41)	Eq. (2.42)
n	113	66	13	23	1	223
ρ	0.664				0.749	
b	0.987	1.031	1.223	1.528	1.106	1.137
V_r	0.210	0.188	0.353	0.199	-	0.193
γ_M^*	1.708	1.565	2.949	1.162	-	1.374
γ_V	1.25	1.25	1.25	1.25	1.25	1.25

C.2 Proposed design models

Similarly to the results shown in the previous section, the two proposed design models (cantilever and modified strut and tie model) were statistically analysed against the test database including tests with f_{cm}<24 MPa. The summary of the analyses is given in Table C.3, for the entire database and the corresponding field of application.

TABLE C.3: Statistical evaluation of the new proposed design models for the resistance of studs in profiled steel sheeting in the field of application including tests with f_{cm}<24 MPa

	Full database			Field of application		
	Cantilever model Eq.(8.2)	Eq.(8.3)	MSTM Eq.(8.8)	Cantilever model Eq.(8.2)	Eq.(8.3)	MSTM Eq.(8.8)
n	123	170	293	123	170	225
ρ	0.789		0.832	0.789		0.840
b	1.191	1.058	1.063	1.191	1.058	1.064
V_r	0.145	0.183	0.165	0.145	0.183	0.158
γ_M^*	1.201	1.310	1.325	1.201	1.310	1.297
γ_V	1.25	1.25	1.25	1.25	1.25	1.25

Appendix D

Data of conducted tests

D.1 Tests on materials

D.1.1 Concrete

For each concrete mixture, 150 mm cube and 150x300 mm cylinder samples were prepared and air-cured alongside the push-out tests in accordance with EN 1994-1-1 B.2 (BSI, 2004b) to assess the compressive strength. The results of the cylinder tests are plotted in Figure D.1 while the details are given in Table D.1.

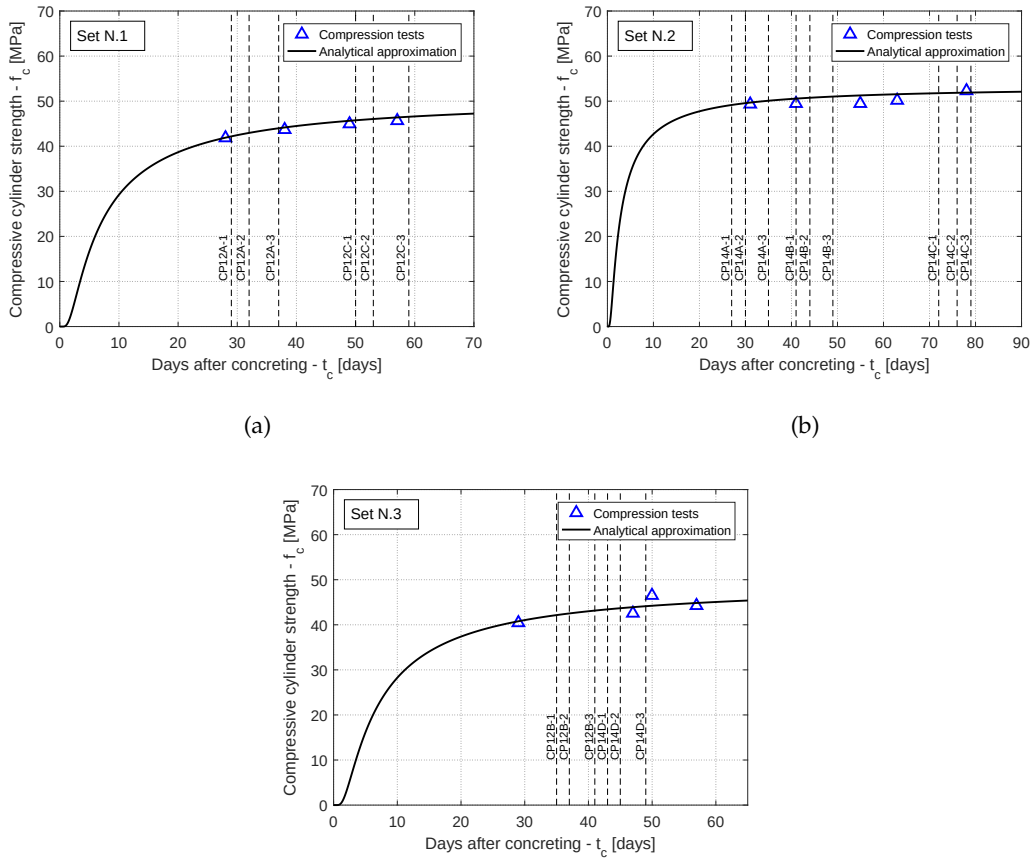

FIGURE D.1: Analytical approximation of the compressive strength at various ages in accordance with EN 1992-1-1 BSI, 2004a

TABLE D.1: Data of the compression tests on concrete cylinder specimens

		Crosshead speed equal to 0.6 MPa/s			
Date	Specimen	f_c [MPa]	Mean [MPa]	D [-]	t_c[a] [days]
17-06-19	Z-8	41.5		-0.9%	
17-06-19	Z-2	43.0	41.9	2.7%	28
17-06-19	Z-12	41.1		-1.7%	
27-06-19	Z-1	44.9		2.6%	
27-06-19	Z-3	43.0	43.7	-1.8%	38
27-06-19	Z-7	43.4		-0.8%	
08-07-19	Z-5	44.6		-0.8%	
08-07-19	Z-6	44.7	45.0	-0.7%	49
08-07-19	Z-13	45.7		1.6%	
16-07-19	Z-4	49.1		7.4%	
16-07-19	Z-14	43.3	45.7	-5.4%	57
16-07-19	Z-15	44.8		-2.0%	
25-10-19	Z-1	49.0		-0.7%	
25-10-19	Z-2	49.0	49.3	-0.7%	31
25-10-19	Z-3	50.0		1.3%	
04-11-19	Z-4	49.3		-0.3%	
04-11-19	Z-5	48.8	49.4	-1.3%	41
04-11-19	Z-6	50.2		1.7%	
18-11-19	Z-7	48.9		-1.2%	
18-11-19	Z-8	50.3	49.5	1.6%	55
18-11-19	Z-9	49.3		-0.5%	
26-11-19	Z-10	51.8		3.2%	
26-11-19	Z-11	48.5	50.2	-3.2%	63
26-11-19	Z-12	50.1		0.0%	
11-12-19	Z-13	52.3		0.0%	
11-12-19	Z-14	52.9	52.3	1.1%	78
11-12-19	Z-15	51.8		-1.0%	
16-07-20	Z-1	40.1		-1.1%	
16-07-20	Z-2	39.8	40.5	-1.9%	29
16-07-20	Z-3	41.8		3.0%	
03-08-20	Z-4	42.7		0.5%	
03-08-20	Z-5	43.0	42.5	1.3%	47
03-08-20	Z-6	41.7		-1.8%	
06-08-20	Z-10	49.1		5.6%	
06-08-20	Z-11	45.3	46.5	-2.5%	50
06-08-20	Z-12	45.0		-3.1%	
13-08-20	Z-13	44.5		0.5%	
13-08-20	Z-14	43.6	44.3	-1.6%	57
13-08-20	Z-15	44.8		1.2%	

[a] t_c: Days after concreting

D.1.2 Stud material

The stud material properties are important for the assessment of the behaviour of the shear connection in the push-out tests. Therefore, 10 tensile test specimens were machined out of 100 mm and 125 mm long studs in compliance with ISO 6892-1 (ISO/TC164/SC1, 2019), as shown in Figure D.2. The test results are given in Table D.2.

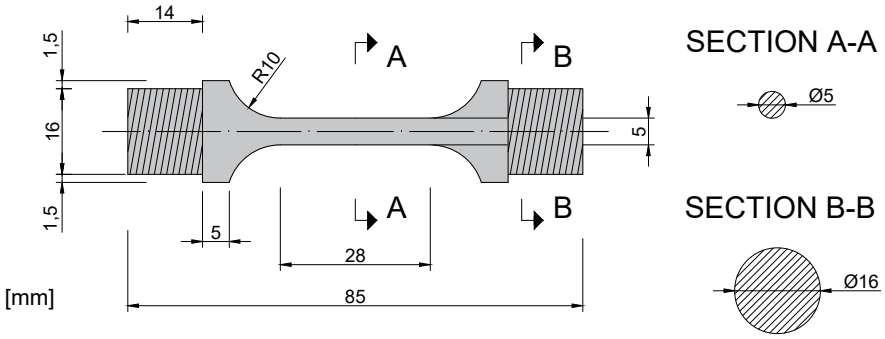

FIGURE D.2: Geometry of the machined specimen of for the determination of the stud material properties

TABLE D.2: Data of the tensile tests on the stud material

Crosshead speed equal to 0.3 mm/min

	Specimen	Diameter [mm]	S_o[a] [mm^2]	$A\%$[b] [%]	F_{max} [kN]	$R_{p0.2}$[c] [MPa]	R_m[d] [MPa]	E[e] [MPa]
Köco stud 19x100 mm	S1	4.976	19.45	19.5	11.1	491	573	202963
	S2	4.985	19.52	23.0	11.1	491	570	204259
	S3	4.970	19.40	19.5	10.2	445	525	204549
	S4	4.984	19.51	18.0	11.2	489	572	207723
	S5	4.980	19.48	24.0	11.0	487	567	197395
	S6	4.997	19.61	19.0	9.8	425	499	204710
					Mean:	471.3	551.0	203600
					CV:	5.6%	5.2%	1.5%
Köco stud 19x125 mm	L1	4.965	19.36	26.0	9.8	409	504	203825
	L2	5.003	19.66	31.0	9.5	386	481	211910
	L3	4.974	19.43	25.0	10.1	419	518	199515
	L4	4.962	19.34	27.0	9.7	408	503	219500
	L5	5.001	19.65	29.0	9.8	399	497	212028
	L6	4.999	19.63	25.5	10.3	423	523	192942
					Mean:	407.3	504.3	206620
					CV:	3.0%	2.7%	4.3%

[a] S_o: Original cross-sectional area of the parallel length
[b] $A\%$: Elongation after fracture
[c] $R_{p0.2}$: Yield strength at 0.2% plastic strain
[d] R_m: Mechanical strength
[e] E: Modulus of elasticity

D.1.3 Sheeting material

The properties of the sheeting material was assessed through tensile tests performed in compliance with ISO 6892-1 (ISO/TC164/SC1, 2019). The geometrical dimensions of the respective dog bone test specimen is shown in Figure D.3 while the results of the tests are provided in Table D.3.

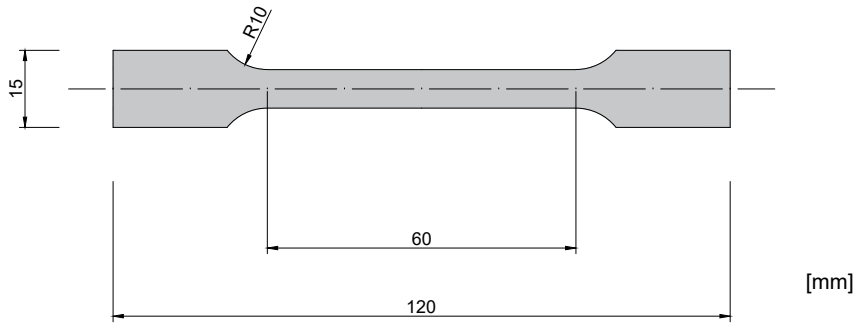

FIGURE D.3: Geometry of the machined specimen of for the determination of the material properties of the sheeting

TABLE D.3: Data of the tensile tests on the material of the profiled steel sheeting

Crosshead speed equal to 2.0 mm/min

	Specimen	Width [mm]	Thickness [mm]	S_0 [mm^2]	$A\%$ [%]	F_{max} [kN]	R_{eH}[a] [MPa]	R_{eL}[b] [MPa]	R_m [MPa]	E [MPa]
Cofraplus 60	SH01	7.487	0.847	6.34	28.5	2.5	384	359	399	194 714
	SH02	7.491	0.852	6.38	30.0	2.5	376	345	393	184 359
	SH03	7.482	0.844	6.31	26.5	2.5	391	358	399	190 407
	SH04	7.483	0.844	6.32	28.0	2.5	387	359	397	197 966
	SH05	7.486	0.844	6.32	28.0	2.5	389	360	400	192 525
	SH06	7.487	0.841	6.30	25.5	2.5	383	361	403	186 851
						Mean:	385.0	357.0	398.5	191137
						CV:	1.3%	1.5%	0.8%	2.4%

[a] R_{eH}: Upper yield point
[b] R_{eL}: Lower yield point

D.2 Push-out tests

SPECIMEN CP12A-1

STEEL BEAM

Profile	Length	Steel grade
HE 260 B	900 mm	S355

STEEL DECK

Product	Yield strength	Welding type
ArcelorMittal Cofraplus 60 P	385.0 MPa	Pre-punched holes

Thickness	Height
0.88 mm	58 mm

Top width	Bottom width
101 mm	62 mm

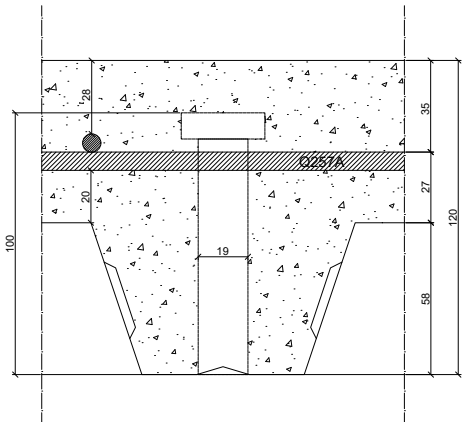

HEADED STUDS

Length as welded	Diameter
98 mm	19 mm

Position	Ultimate strength
Centered	551.0 MPa

REINFORCEMENT MESH

Type	Position
B 500 A	20 mm above the deck | Below the head of the stud

CONCRETE SLAB

Dimensions	Depth	Recess	Cylinder strength
900x680 mm	120 mm	No	42.2 MPa

TEST RESULTS

Peak load	Load at 6 mm slip	Failure mode(s)
68.3 kN/stud	67.4 kN/stud	Rib punching, Concrete pull-out

NOTE

-

SPECIMEN CP12A-1

LOAD-SLIP CURVE

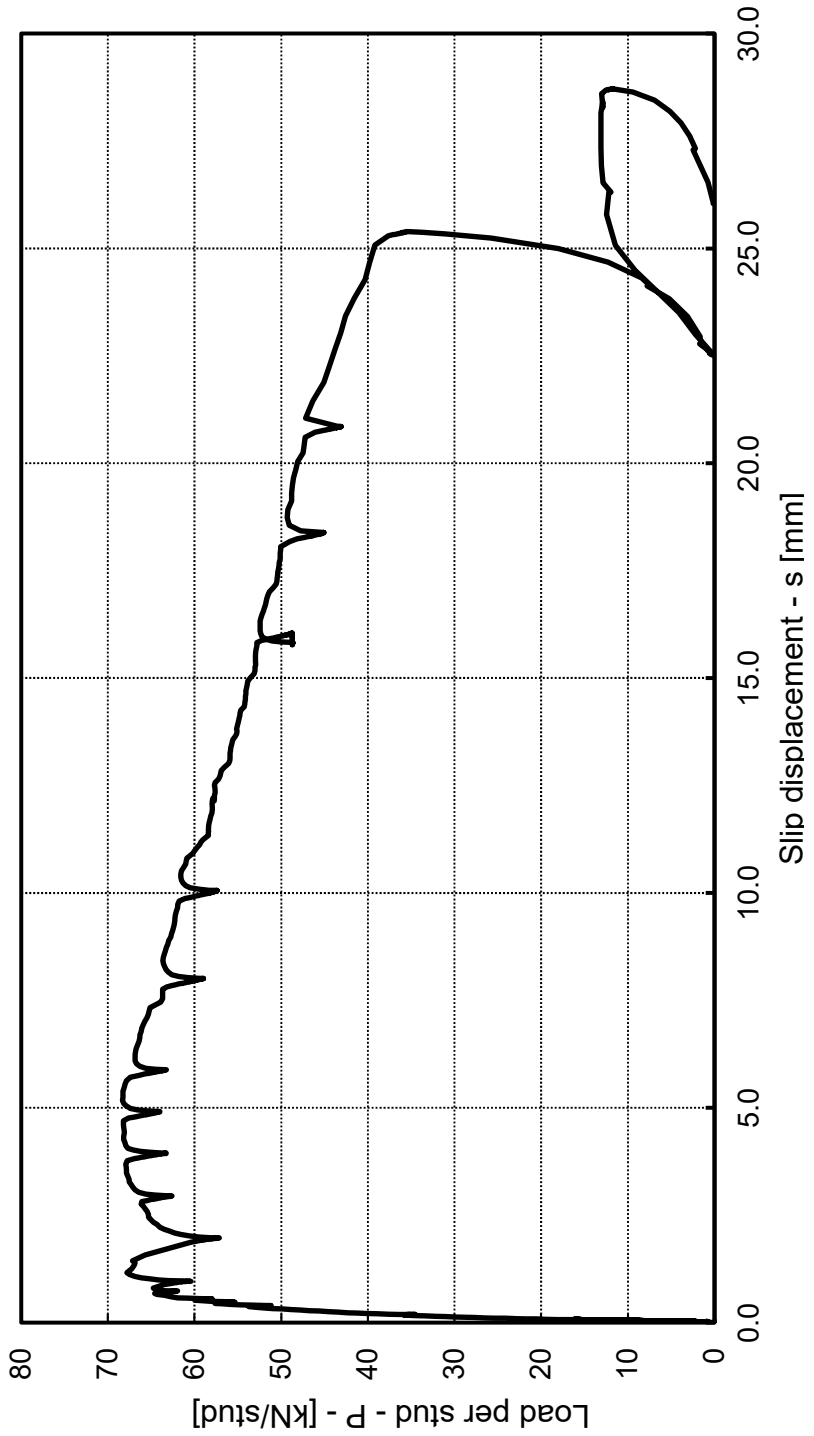

SPECIMEN CP12A-2

STEEL BEAM

Profile	Length	Steel grade
HE 260 B	900 mm	S355

STEEL DECK

Product	Yield strength	Welding type
ArcelorMittal Cofraplus 60 P	385.0 MPa	Pre-punched holes

Thickness	Height
0.88 mm	58 mm

Top width	Bottom width
101 mm	62 mm

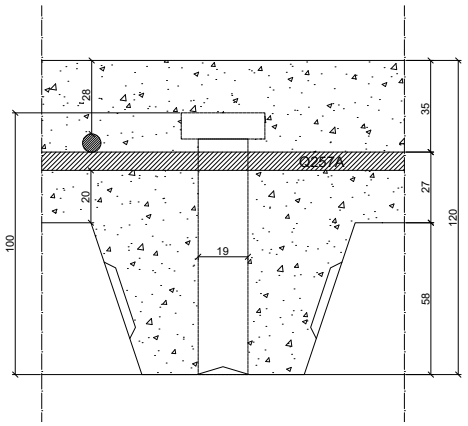

HEADED STUDS

Length as welded	Diameter
98 mm	19 mm

Position	Ultimate strength
Centered	551.0 MPa

REINFORCEMENT MESH

Type	Position
B 500 A	20 mm above the deck | Below the head of the stud

CONCRETE SLAB

Dimensions	Depth	Recess	Cylinder strength
900x680 mm	120 mm	No	42.9 MPa

TEST RESULTS

Peak load	Load at 6 mm slip	Failure mode(s)
65.3 kN/stud	63.4 kN/stud	Rib punching, Concrete pull-out

NOTE

-

SPECIMEN CP12A-2

LOAD-SLIP CURVE

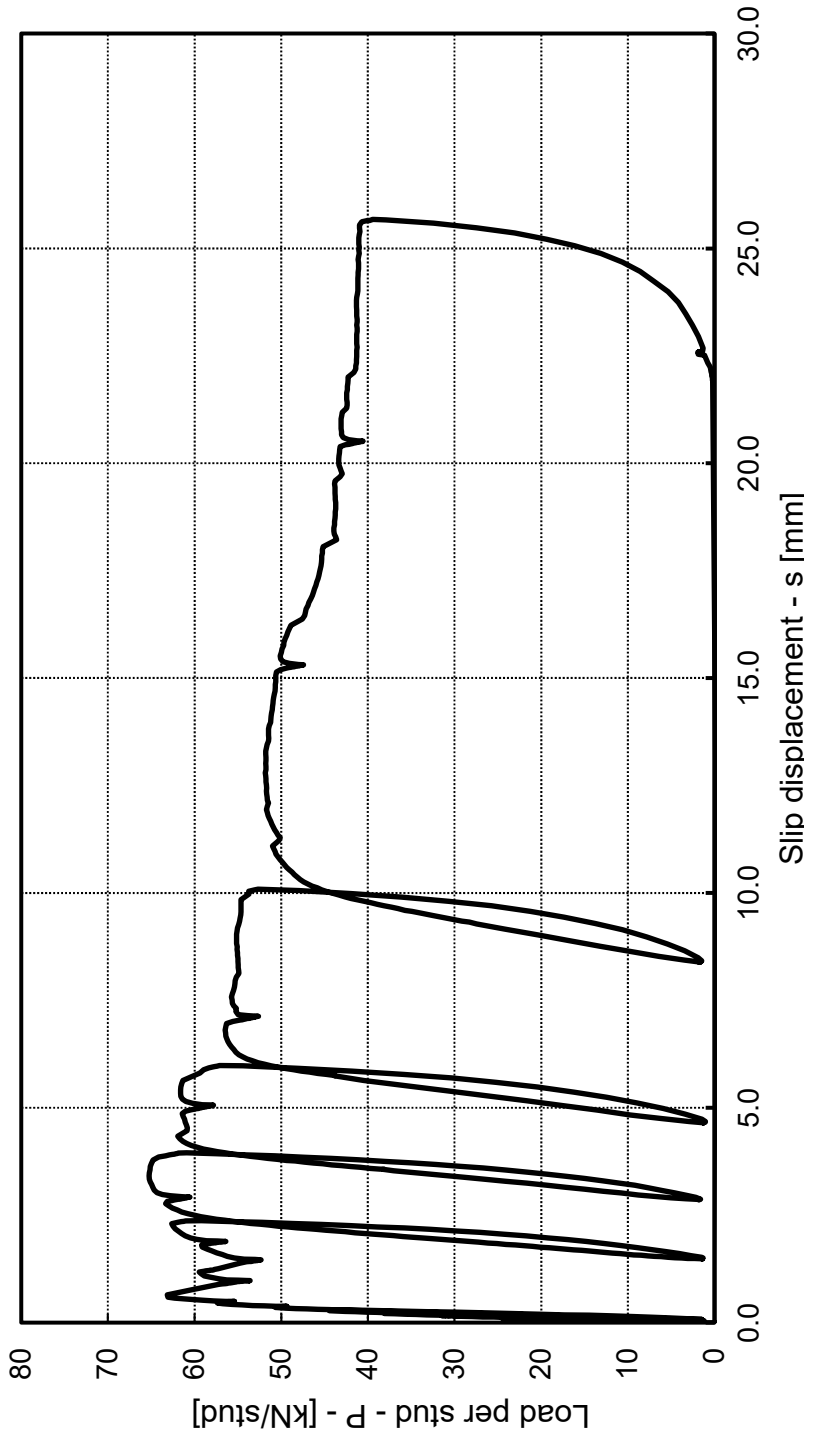

SPECIMEN CP12A-3

STEEL BEAM

Profile	Length	Steel grade
HE 260 B	900 mm	S355

STEEL DECK

Product	Yield strength	Welding type
ArcelorMittal Cofraplus 60 P	385.0 MPa	Pre-punched holes

Thickness	Height
0.88 mm	58 mm

Top width	Bottom width
101 mm	62 mm

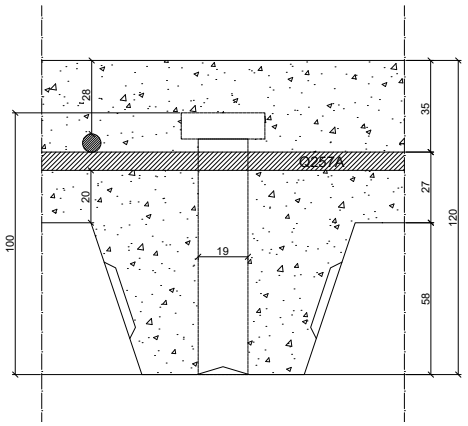

HEADED STUDS

Length	Diameter
98 mm	19 mm

Position	Ultimate strength
Centered	551.0 MPa

REINFORCEMENT MESH

Type	Position
B 500 A	20 mm above the deck | Below the head of the stud

CONCRETE SLAB

Dimensions	Depth	Recess	Cylinder strength
900x680 mm	120 mm	No	44.0 MPa

TEST RESULTS

Peak load	Load at 6 mm slip	Failure mode(s)
69.5 kN/stud	60.1 kN/stud	Rib punching, Concrete pull-out

NOTE

-

SPECIMEN CP12A-3

LOAD-SLIP CURVE

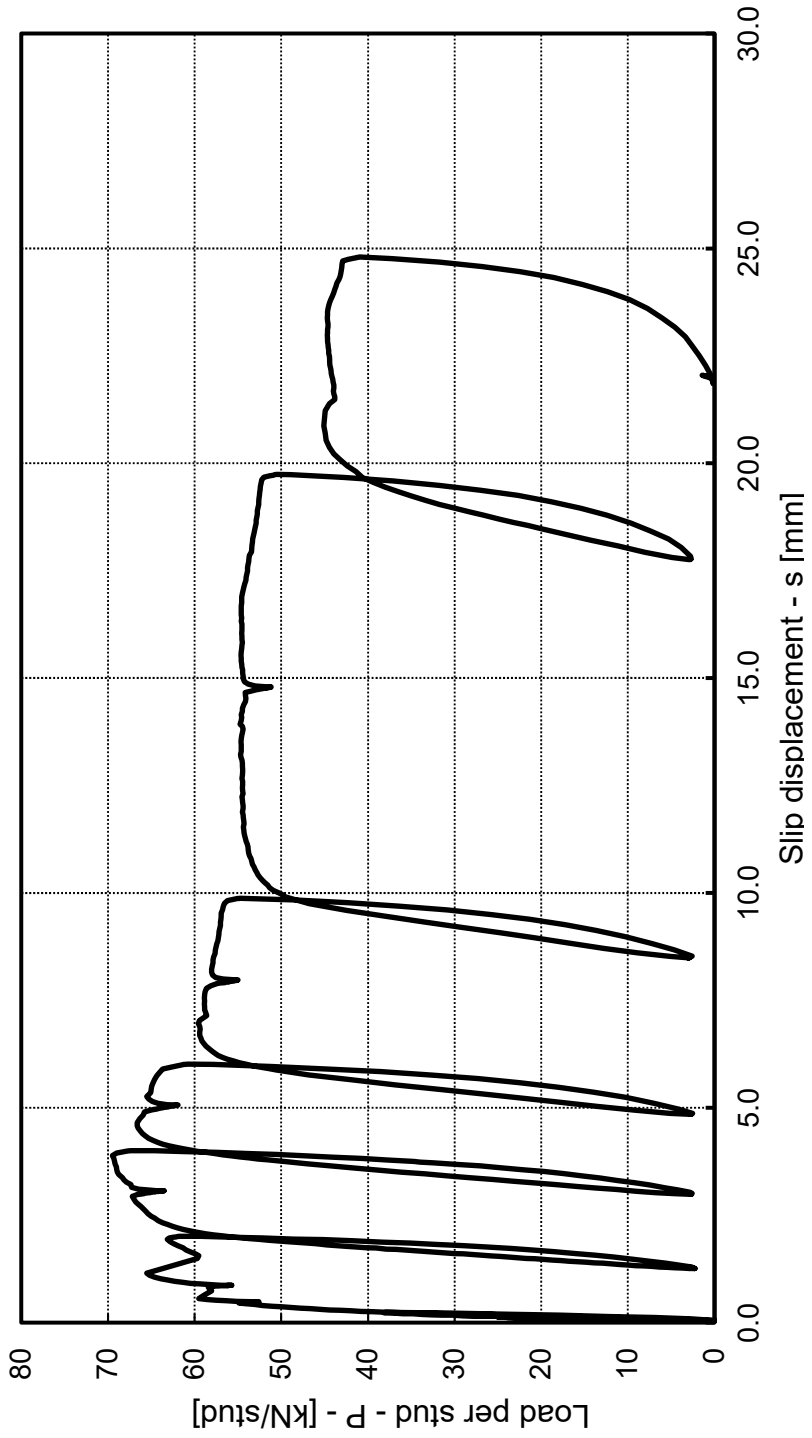

SPECIMEN CP12B-1

STEEL BEAM

Profile	Length	Steel grade
HE 260 B	900 mm	S355

STEEL DECK

Product	Yield strength	Welding type
ArcelorMittal Cofraplus 60 P	385.0 MPa	Pre-punched holes

Thickness	Height
0.88 mm	58 mm

Top width	Bottom width
101 mm	62 mm

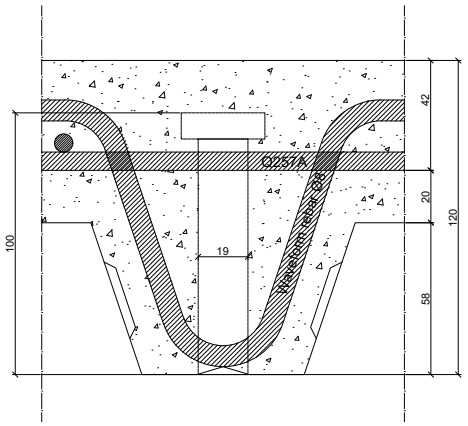

HEADED STUDS

Length as welded	Diameter
98 mm	19 mm

Position	Ultimate strength
Centered	551.0 MPa

REINFORCEMENT MESH

Type	Position
B 500 A	20 mm above the deck | Below the head of the stud

CONCRETE SLAB

Dimensions	Depth	Recess	Cylinder strength
900x680 mm	120 mm	No	42.2 MPa

TEST RESULTS

Peak load	Load at 6 mm slip	Failure mode(s)
81.3 kN/stud	77.0 kN/stud	Rib punching, Concrete pull-out

NOTE

-

SPECIMEN CP12B-1

LOAD-SLIP CURVE

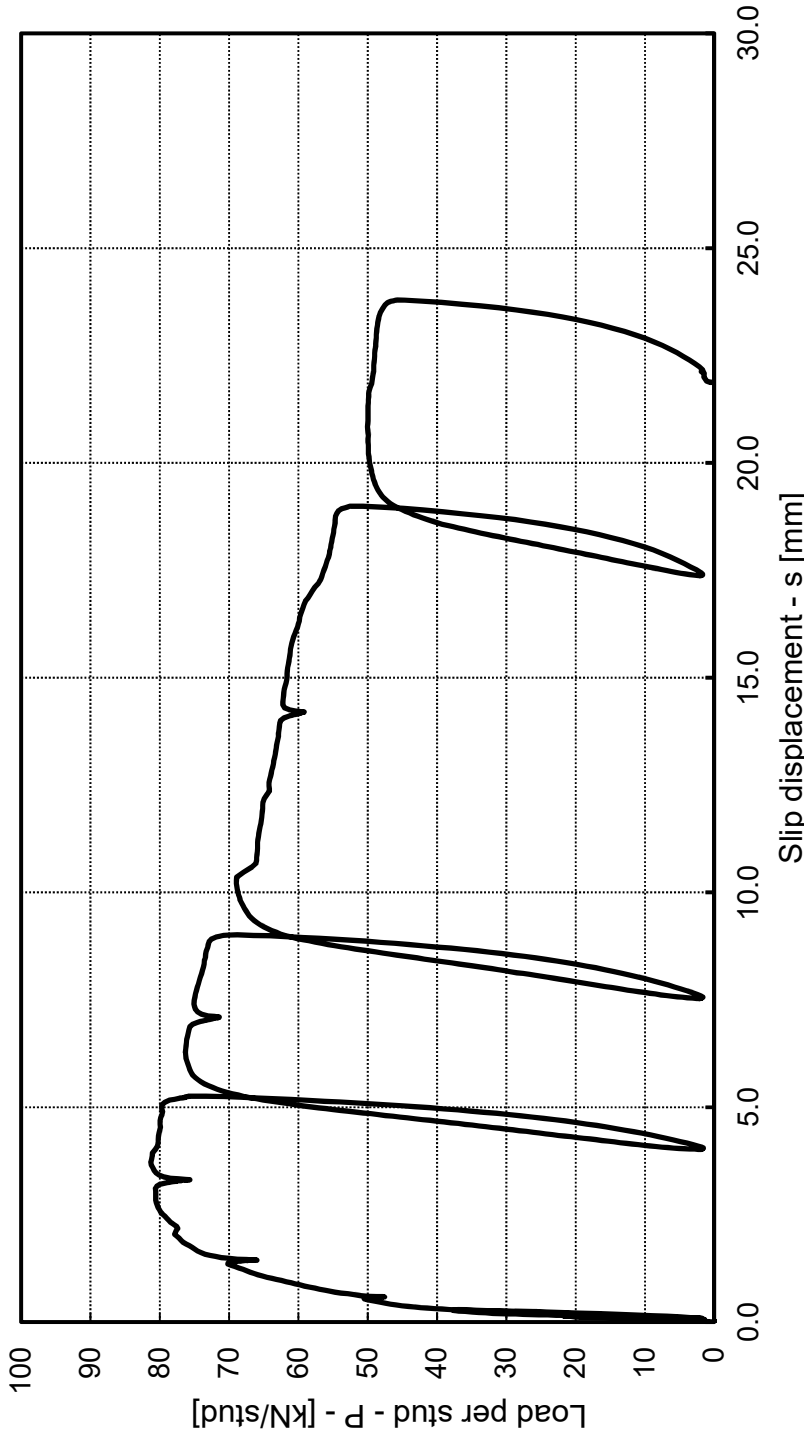

SPECIMEN CP12B-2

STEEL BEAM

Profile	Length	Steel grade
HE 260 B	900 mm	S355

STEEL DECK

Product	Yield strength	Welding type
ArcelorMittal Cofraplus 60 P	385.0 MPa	Pre-punched holes

Thickness	Height
0.88 mm	58 mm

Top width	Bottom width
101 mm	62 mm

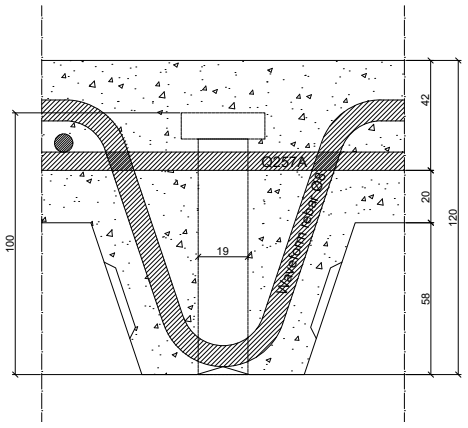

HEADED STUDS

Length as welded	Diameter
98 mm	19 mm

Position	Ultimate strength
Centered	551.0 MPa

REINFORCEMENT MESH

Type	Position
B 500 A	20 mm above the deck | Below the head of the stud

CONCRETE SLAB

Dimensions	Depth	Recess	Cylinder strength
900x680 mm	120 mm	No	42.6 MPa

TEST RESULTS

Peak load	Load at 6 mm slip	Failure mode(s)
83.7 kN/stud	80.3 kN/stud	Rib punching, Concrete pull-out

NOTE

-

SPECIMEN CP12B-2

LOAD-SLIP CURVE

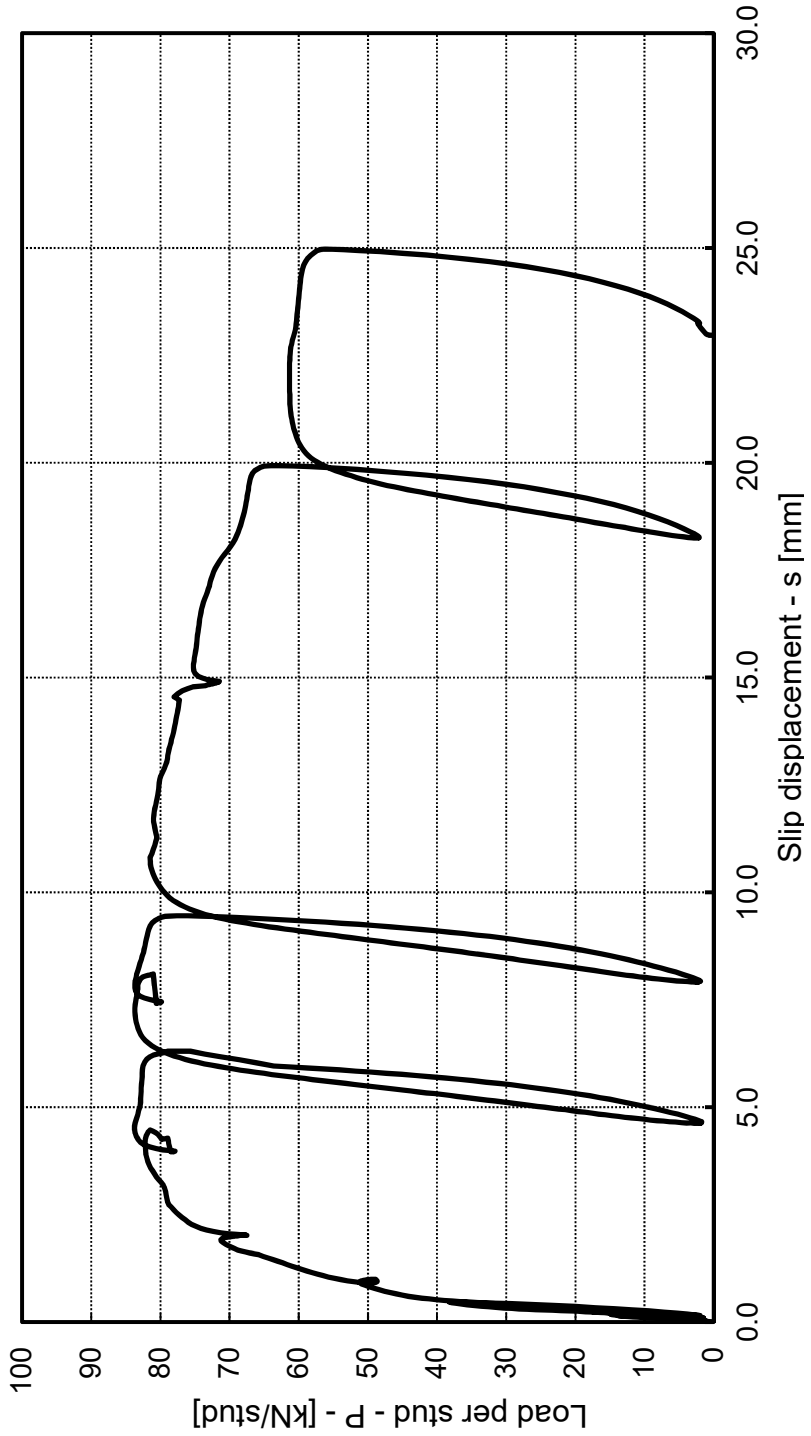

SPECIMEN CP12B-3

STEEL BEAM

Profile	Length	Steel grade
HE 260 B	900 mm	S355

STEEL DECK

Product	Yield strength	Welding type
ArcelorMittal Cofraplus 60 P	385.0 MPa	Pre-punched holes

Thickness	Height
0.88 mm	58 mm

Top width	Bottom width
101 mm	62 mm

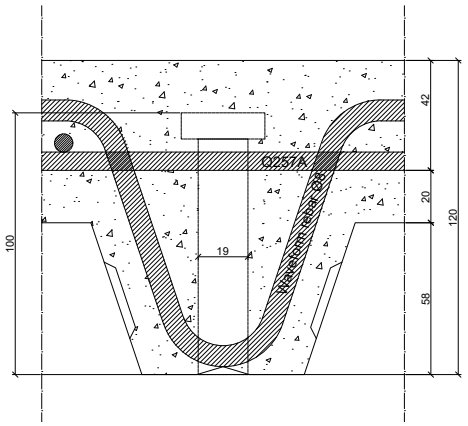

HEADED STUDS

Length	Diameter
98 mm	19 mm

Position	Ultimate strength
Centered	551.0 MPa

REINFORCEMENT MESH

Type	Position
B 500 A	20 mm above the deck | Below the head of the stud

CONCRETE SLAB

Dimensions	Depth	Recess	Cylinder strength
900x680 mm	120 mm	No	43.2 MPa

TEST RESULTS

Peak load	Load at 6 mm slip	Failure mode(s)
90.7 kN/stud	80.1 kN/stud	Rib punching, Concrete pull-out

NOTE

-

SPECIMEN CP12B-3

LOAD-SLIP CURVE

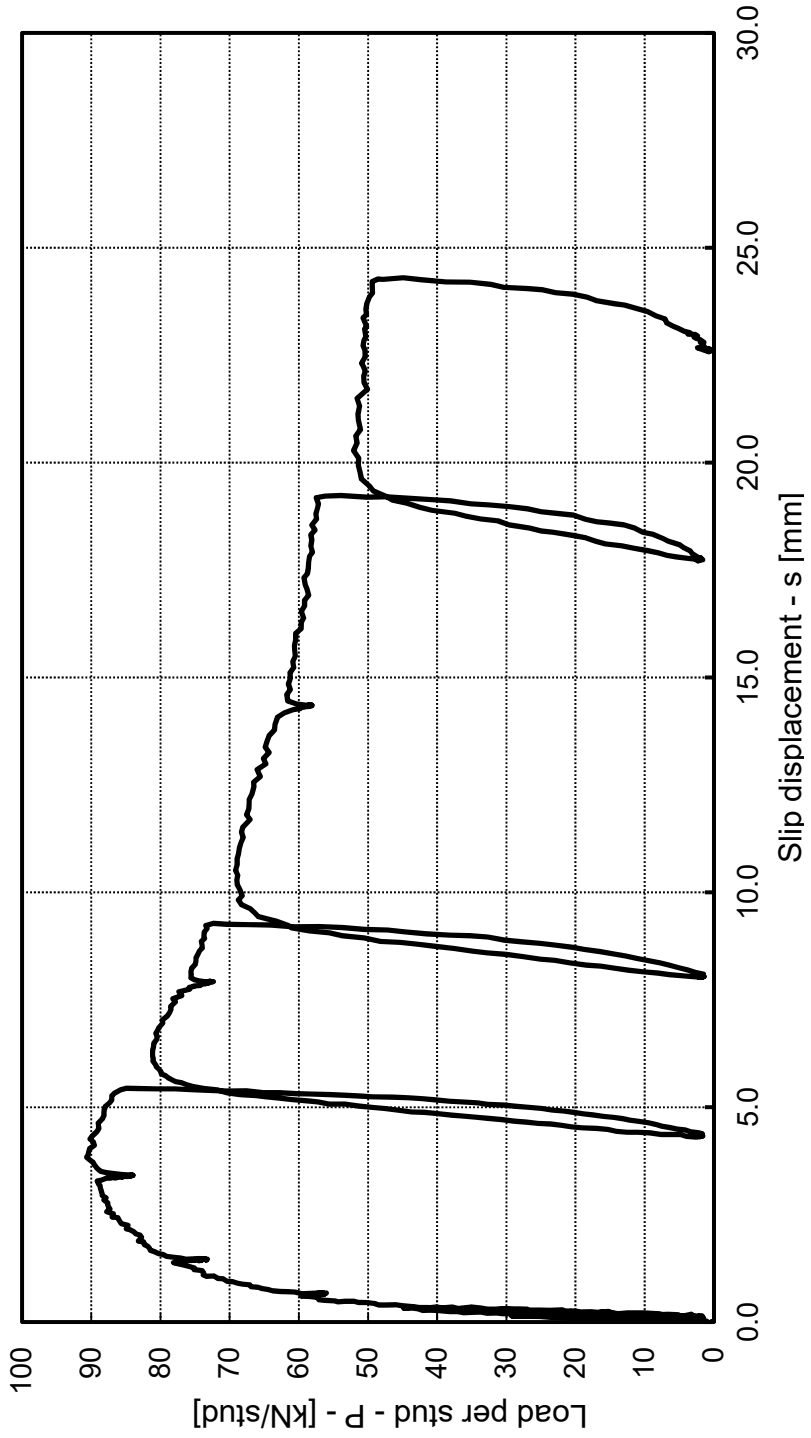

SPECIMEN CP12C-1

STEEL BEAM

Profile	Length	Steel grade
HE 260 B	900 mm	S355

STEEL DECK

Product	Yield strength	Welding type
ArcelorMittal Cofraplus 60 P	385.0 MPa	Pre-punched holes

Thickness	Height
0.88 mm	58 mm

Top width	Bottom width
101 mm	62 mm

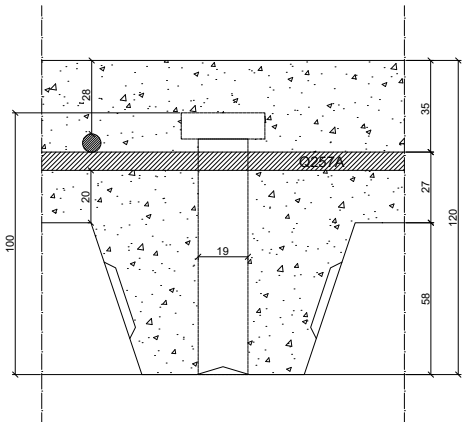

HEADED STUDS

Length as welded	Diameter
98 mm	19 mm

Position	Ultimate strength
Centered	551.0 MPa

REINFORCEMENT MESH

Type	Position
B 500 A	20 mm above the deck | Below the head of the stud

CONCRETE SLAB

Dimensions	Depth	Recess	Cylinder strength
900x680 mm	120 mm	Yes	45.7 MPa

TEST RESULTS

Peak load	Load at 6 mm slip	Failure mode(s)
69.3 kN/stud	65.3 kN/stud	Rib punching, Concrete pull-out

NOTE

-

SPECIMEN CP12C-1

LOAD-SLIP CURVE

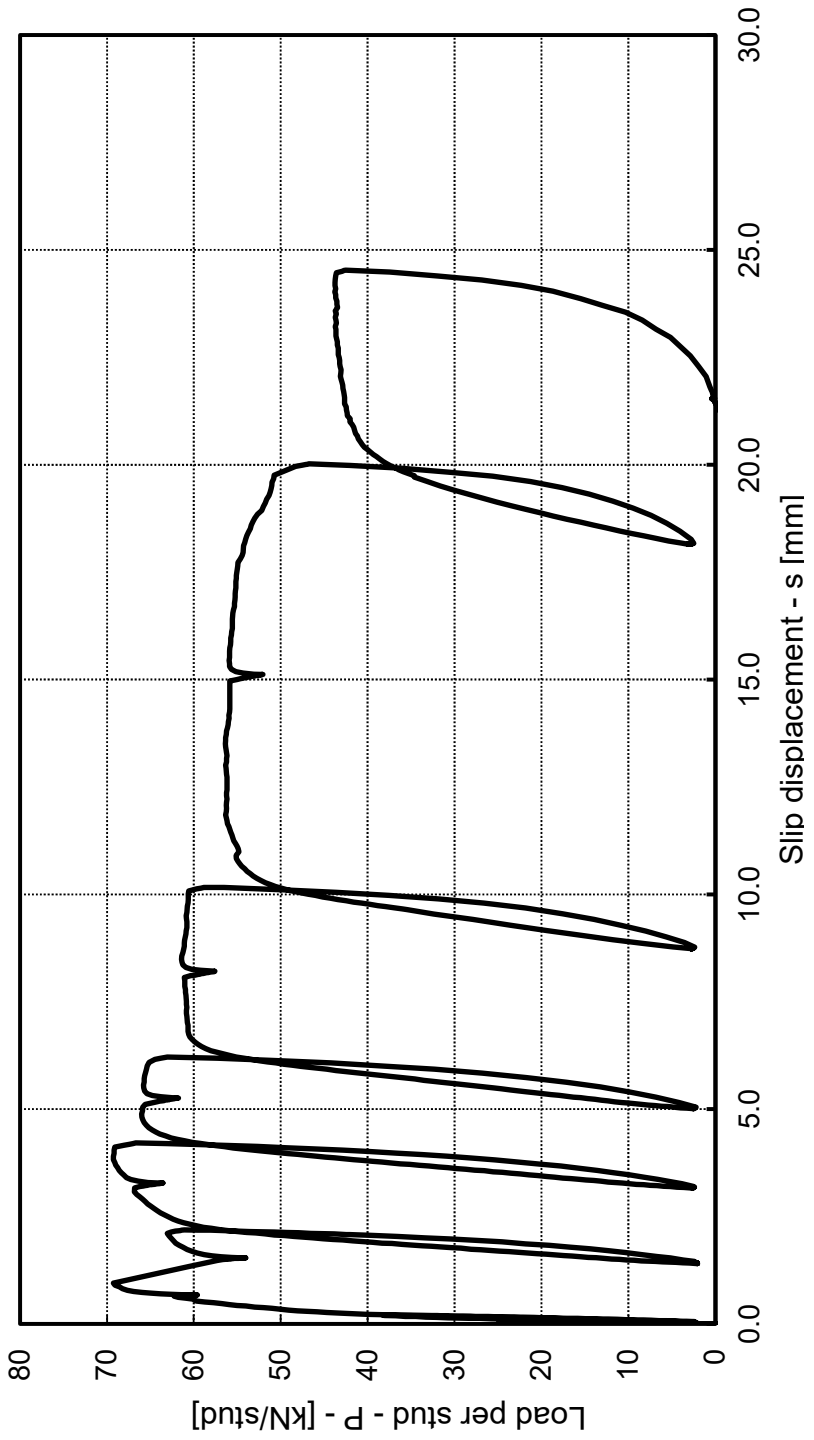

SPECIMEN CP12C-2

STEEL BEAM

Profile	Length	Steel grade
HE 260 B	900 mm	S355

STEEL DECK

Product	Yield strength	Welding type
ArcelorMittal Cofraplus 60 P	385.0 MPa	Pre-punched holes

Thickness	Height
0.88 mm	58 mm

Top width	Bottom width
101 mm	62 mm

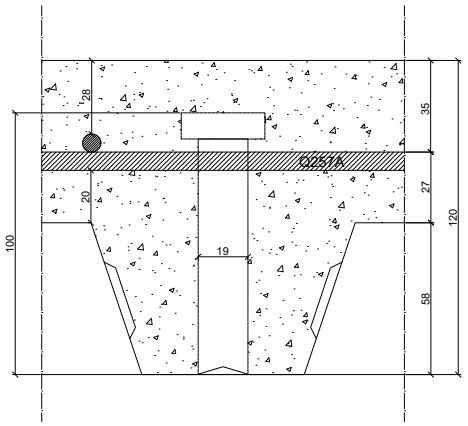

HEADED STUDS

Length as welded	Diameter
98 mm	19 mm

Position	Ultimate strength
Centered	551.0 MPa

REINFORCEMENT MESH

Type	Position
B 500 A	20 mm above the deck | Below the head of the stud

CONCRETE SLAB

Dimensions	Depth	Recess	Cylinder strength
900x680 mm	120 mm	Yes	46.0 MPa

TEST RESULTS

Peak load	Load at 6 mm slip	Failure mode(s)
75.5 kN/stud	69.1 kN/stud	Rib punching, Concrete pull-out

NOTE

-

SPECIMEN CP12C-2

LOAD-SLIP CURVE

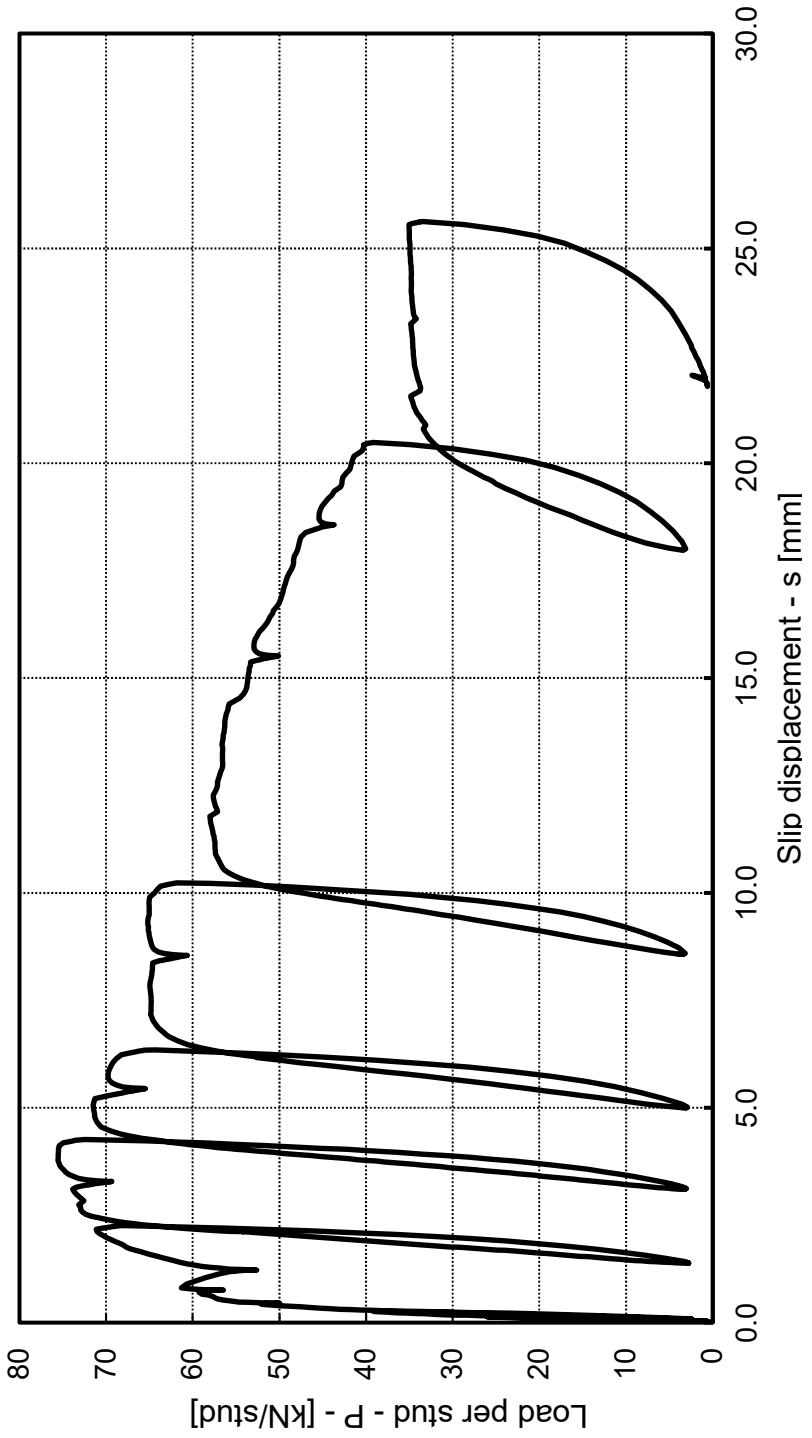

SPECIMEN CP12C-3

STEEL BEAM

Profile	Length	Steel grade
HE 260 B	900 mm	S355

STEEL DECK

Product	Yield strength	Welding type
ArcelorMittal Cofraplus 60 P	385.0 MPa	Pre-punched holes

Thickness	Height
0.88 mm	58 mm

Top width	Bottom width
101 mm	62 mm

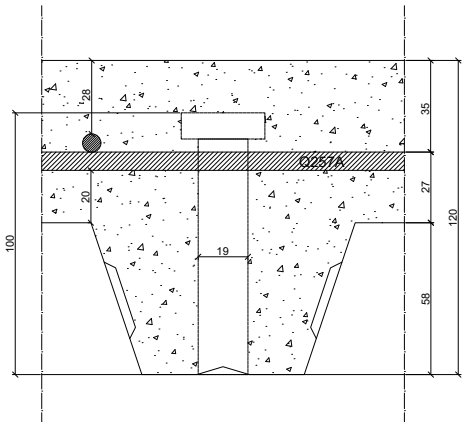

HEADED STUDS

Length as welded	Diameter
98 mm	19 mm

Position	Ultimate strength
Centered	551.0 MPa

REINFORCEMENT MESH

Type	Position
B 500 A	20 mm above the deck | Below the head of the stud

CONCRETE SLAB

Dimensions	Depth	Recess	Cylinder strength
900x680 mm	120 mm	Yes	46.5 MPa

TEST RESULTS

Peak load	Load at 6 mm slip	Failure mode(s)
70.1 kN/stud	-	-

NOTE

The test was intentionally stopped at a slip of ca. 2 mm

SPECIMEN CP12C-3

LOAD-SLIP CURVE

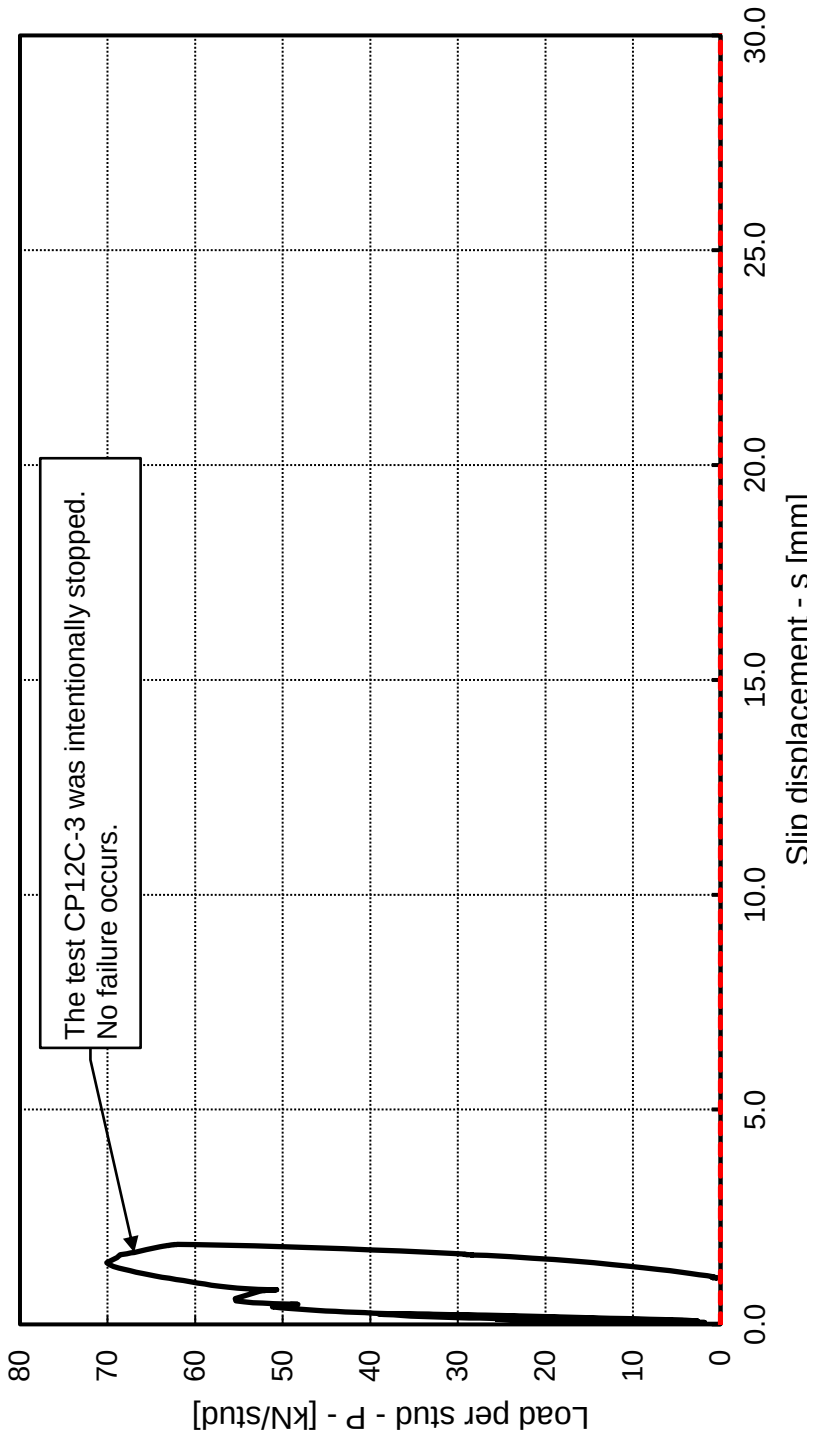

SPECIMEN CP14A-1

STEEL BEAM

Profile	Length	Steel grade
HE 260 B	900 mm	S355

STEEL DECK

Product	Yield strength	Welding type
ArcelorMittal Cofraplus 60 P	385.0 MPa	Pre-punched holes

Thickness	Height
0.88 mm	58 mm

Top width	Bottom width
101 mm	62 mm

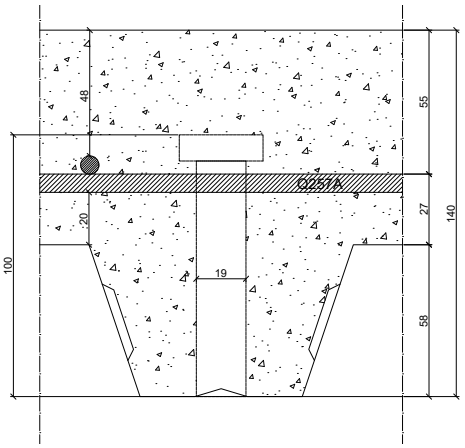

HEADED STUDS

Length as welded	Diameter
98 mm	19 mm

Position	Ultimate strength
Centered	551.0 MPa

REINFORCEMENT MESH

Type	Position
B 500 A	20 mm above the deck | Below the head of the stud

CONCRETE SLAB

Dimensions	Depth	Recess	Cylinder strength
900x680 mm	140 mm	No	49.3 MPa

TEST RESULTS

Peak load	Load at 6 mm slip	Failure mode(s)
85.7 kN/stud	70.6 kN/stud	Rib punching, Concrete pull-out

NOTE

This specimen was accidentally loaded at high displacement rate up to 5 mm slip

SPECIMEN CP14A-1

LOAD-SLIP CURVE

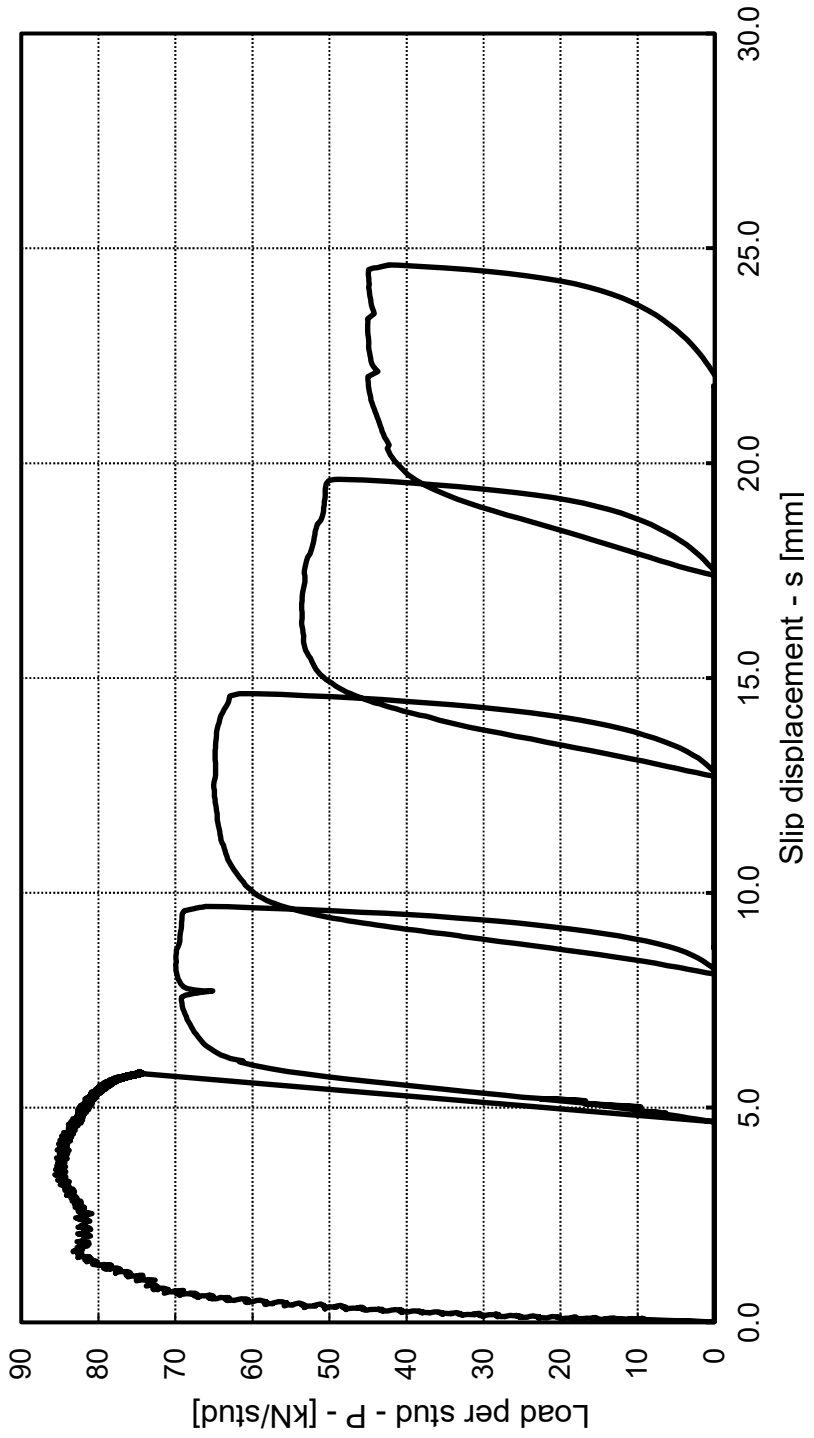

SPECIMEN CP14A-2

STEEL BEAM

Profile	Length	Steel grade
HE 260 B	900 mm	S355

STEEL DECK

Product	Yield strength	Welding type
ArcelorMittal Cofraplus 60 P	385.0 MPa	Pre-punched holes

Thickness	Height
0.88 mm	58 mm

Top width	Bottom width
101 mm	62 mm

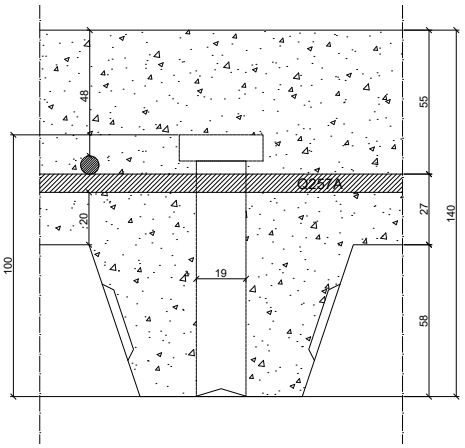

HEADED STUDS

Length as welded	Diameter
98 mm	19 mm

Position	Ultimate strength
Centered	551.0 MPa

REINFORCEMENT MESH

Type	Position
B 500 A	20 mm above the deck | Below the head of the stud

CONCRETE SLAB

Dimensions	Depth	Recess	Cylinder strength
900x680 mm	140 mm	No	49.7 MPa

TEST RESULTS

Peak load	Load at 6 mm slip	Failure mode(s)
72.4 kN/stud	67.4 kN/stud	Rib punching, Concrete pull-out

NOTE

-

SPECIMEN CP14A-2

LOAD-SLIP CURVE

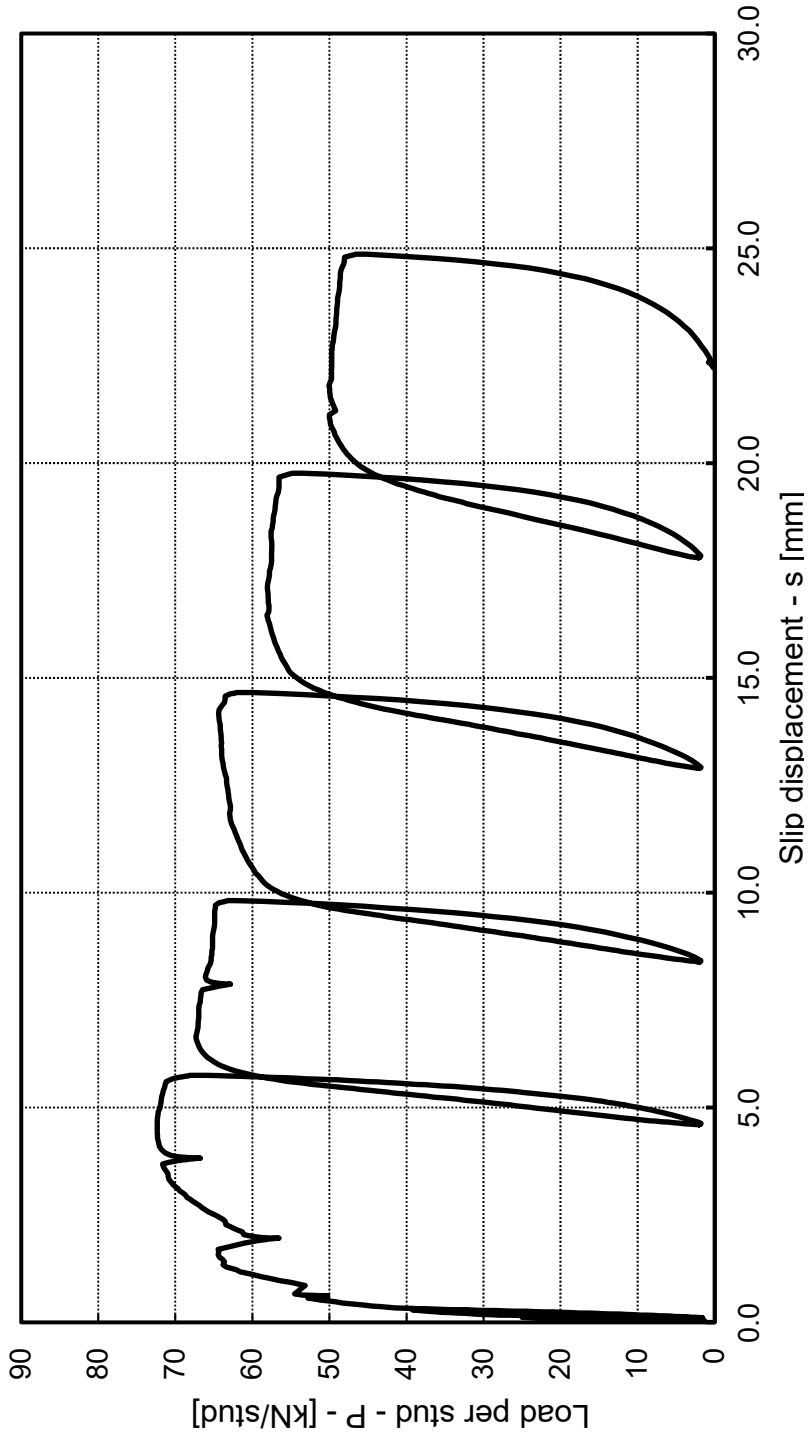

SPECIMEN CP14A-3

STEEL BEAM

Profile	Length	Steel grade
HE 260 B	900 mm	S355

STEEL DECK

Product	Yield strength	Welding type
ArcelorMittal Cofraplus 60 P	385. MPa	Pre-punched holes

Thickness	Height
0.88 mm	58 mm

Top width	Bottom width
101 mm	62 mm

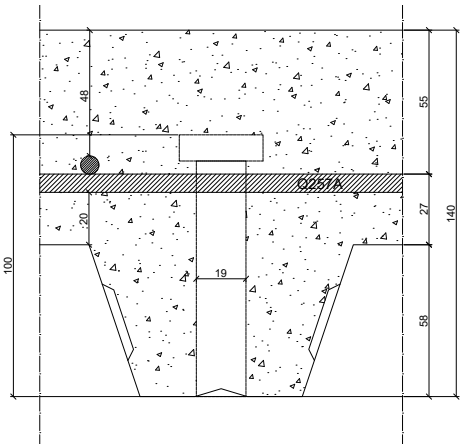

HEADED STUDS

Length as welded	Diameter
98 mm	19 mm

Position	Ultimate strength
Centered	551.0 MPa

REINFORCEMENT MESH

Type	Position
B 500 A	20 mm above the deck | Below the head of the stud

CONCRETE SLAB

Dimensions	Depth	Recess	Cylinder strength
900x680 mm	140 mm	No	50.2 MPa

TEST RESULTS

Peak load	Load at 6 mm slip	Failure mode(s)
82.5 kN/stud	80.3 kN/stud	Rib punching, Concrete pull-out

NOTE

-

SPECIMEN CP14A-3

LOAD-SLIP CURVE

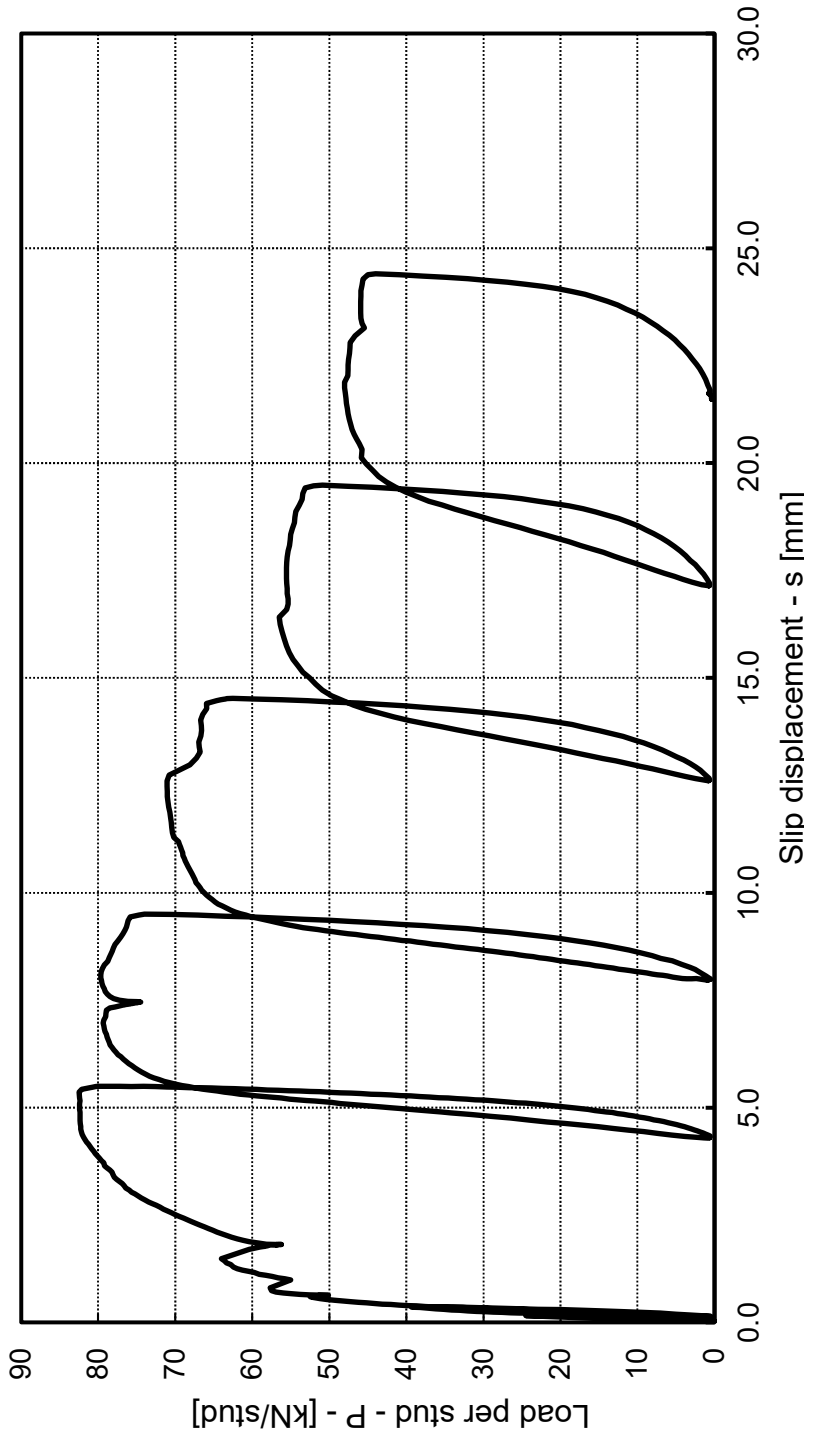

SPECIMEN CP14B-1

STEEL BEAM

Profile	Length	Steel grade
HE 260 B	900 mm	S355

STEEL DECK

Product	Yield strength	Welding type
ArcelorMittal Cofraplus 60 P	385.0 MPa	Pre-punched holes

Thickness	Height
0.88 mm	58 mm

Top width	Bottom width
101 mm	62 mm

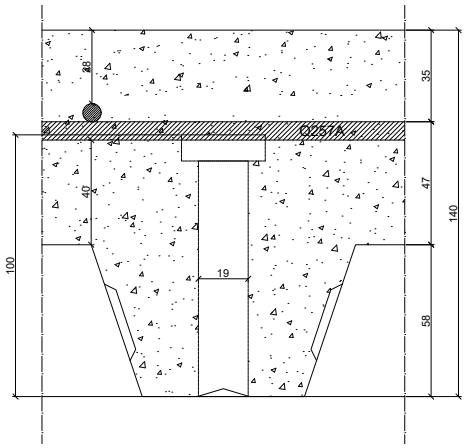

HEADED STUDS

Length as welded	Diameter
98 mm	19 mm

Position	Ultimate strength
Centered	551.0 MPa

REINFORCEMENT MESH

Type	Position
B 500 A	40 mm above the deck | Above the head of the stud

CONCRETE SLAB

Dimensions	Depth	Recess	Cylinder strength
900x680 mm	140 mm	No	50.7 MPa

TEST RESULTS

Peak load	Load at 6 mm slip	Failure mode(s)
85.5 kN/stud	79.2 kN/stud	Rib punching, Concrete pull-out

NOTE

-

SPECIMEN CP14B-1

LOAD-SLIP CURVE

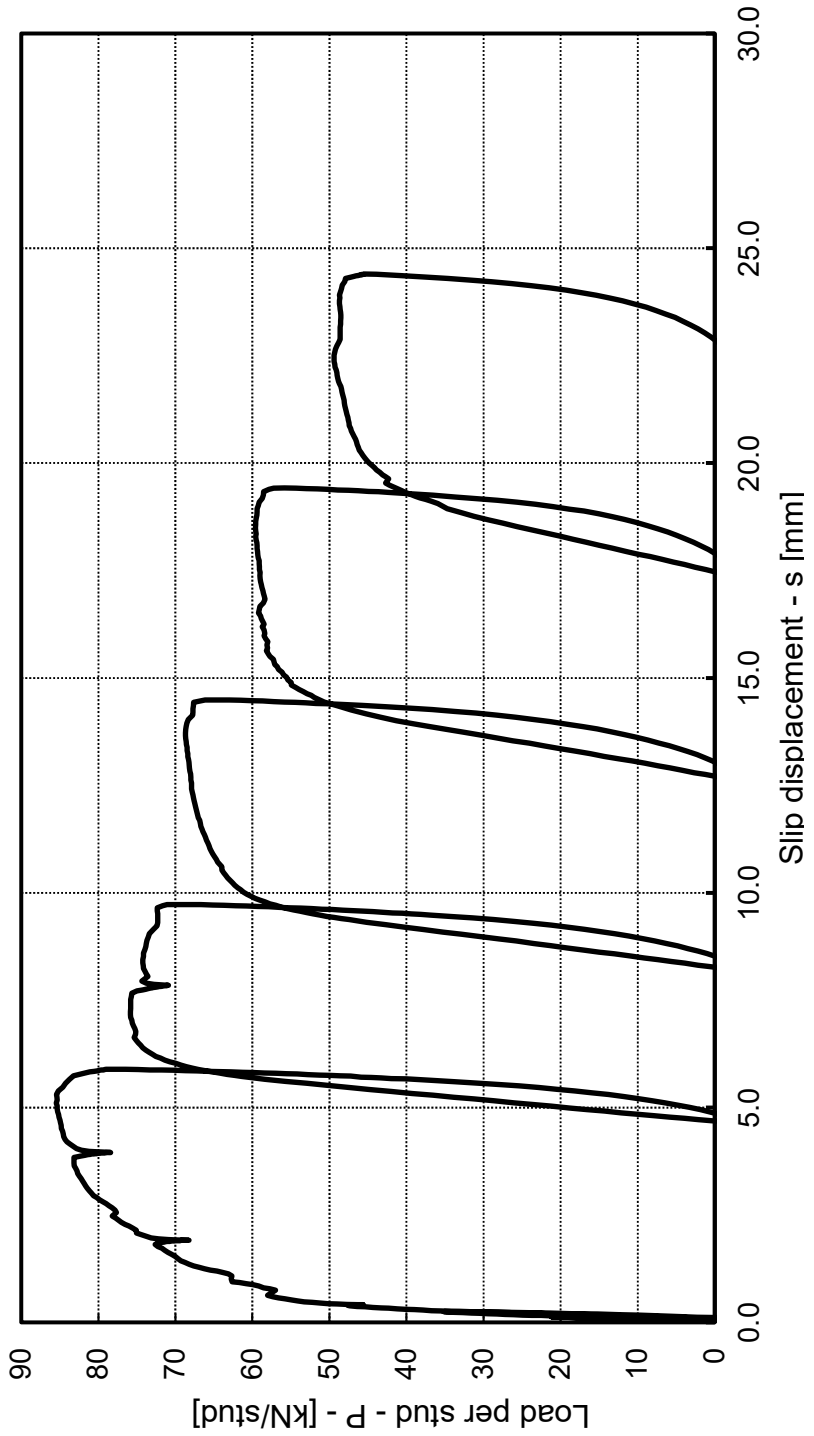

SPECIMEN CP14B-2

STEEL BEAM

Profile	Length	Steel grade
HE 260 B	900 mm	S355

STEEL DECK

Product	Yield strength	Welding type
ArcelorMittal Cofraplus 60 P	385.0 MPa	Pre-punched holes

Thickness	Height
0.88 mm	58 mm

Top width	Bottom width
101 mm	62 mm

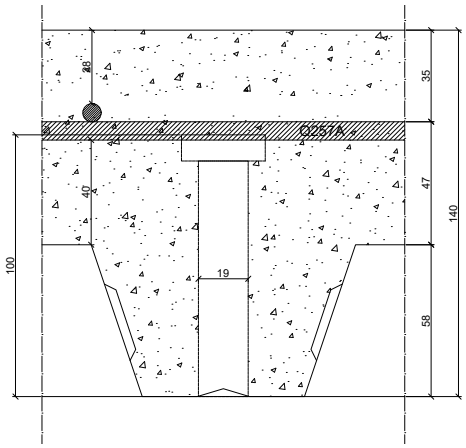

HEADED STUDS

Length as welded	Diameter
98 mm	19 mm

Position	Ultimate strength
Centered	551.0 MPa

REINFORCEMENT MESH

Type	Position
B 500 A	40 mm above the deck | Above the head of the stud

CONCRETE SLAB

Dimensions	Depth	Recess	Cylinder strength
900x680 mm	140 mm	No	50.8 MPa

TEST RESULTS

Peak load	Load at 6 mm slip	Failure mode(s)
74.0 kN/stud	72.3 kN/stud	Rib punching, Concrete pull-out

NOTE

-

SPECIMEN CP14B-2

LOAD-SLIP CURVE

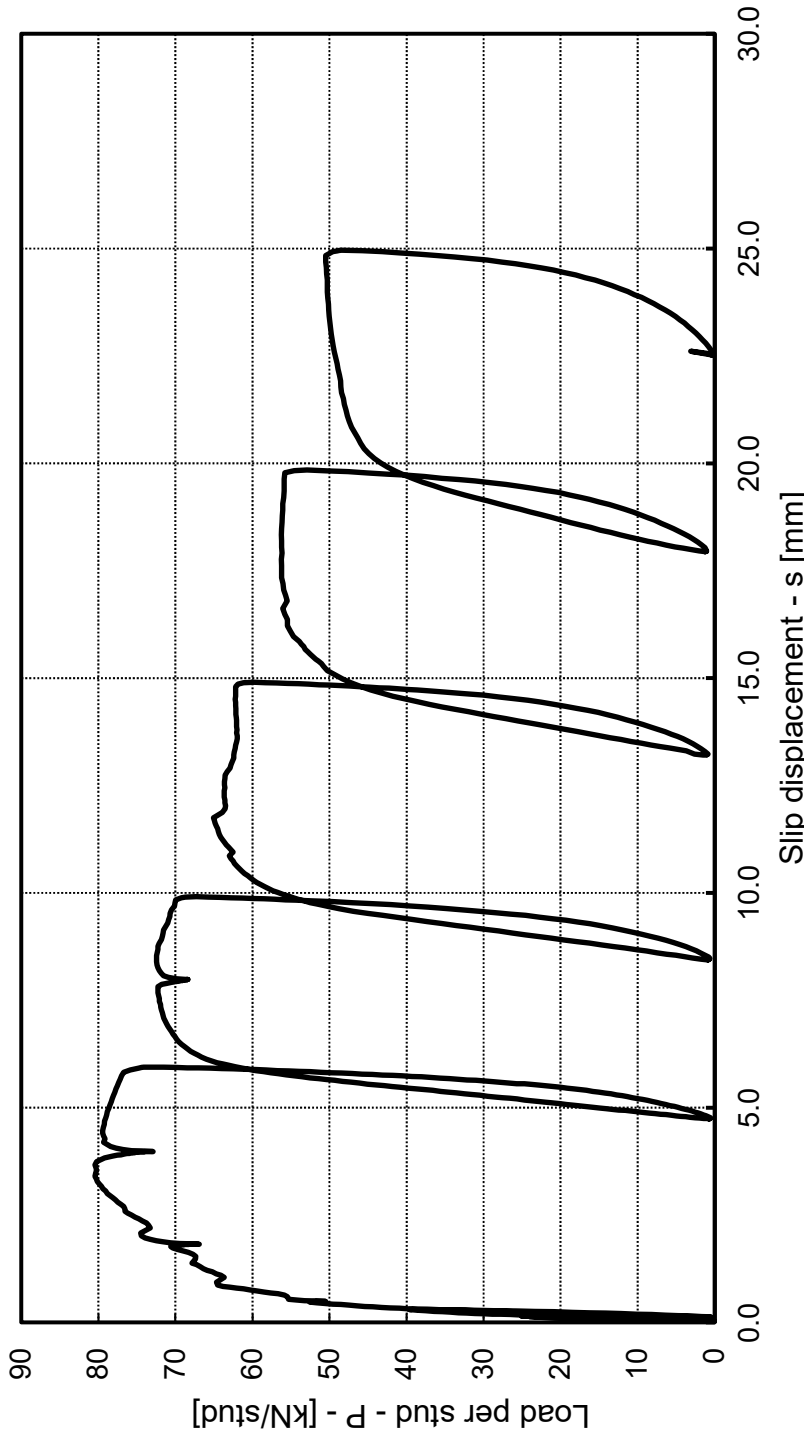

SPECIMEN CP14B-3

STEEL BEAM

Profile	Length	Steel grade
HE 260 B	900 mm	S355

STEEL DECK

Product	Yield strength	Welding type
ArcelorMittal Cofraplus 60 P	385.0 MPa	Pre-punched holes

Thickness	Height
0.88 mm	58 mm

Top width	Bottom width
101 mm	62 mm

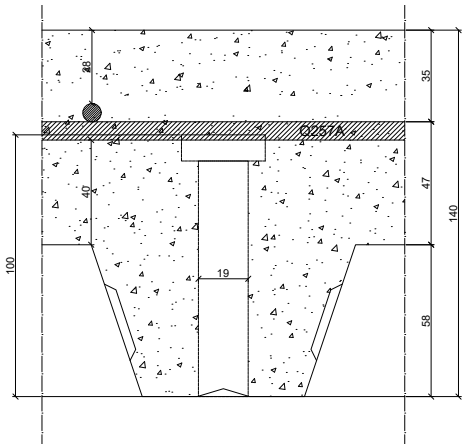

HEADED STUDS

Length as welded	Diameter
98 mm	19 mm

Position	Ultimate strength
Centered	551.0 MPa

REINFORCEMENT MESH

Type	Position
B 500 A	40 mm above the deck | Above the head of the stud

CONCRETE SLAB

Dimensions	Depth	Recess	Cylinder strength
900x680 mm	140 mm	No	51.1 MPa

TEST RESULTS

Peak load	Load at 6 mm slip	Failure mode(s)
88.7 kN/stud	-	Rib punching

NOTE

The test was intentionally stopped at a slip of ca. 6 mm

SPECIMEN CP14B-3

LOAD-SLIP CURVE

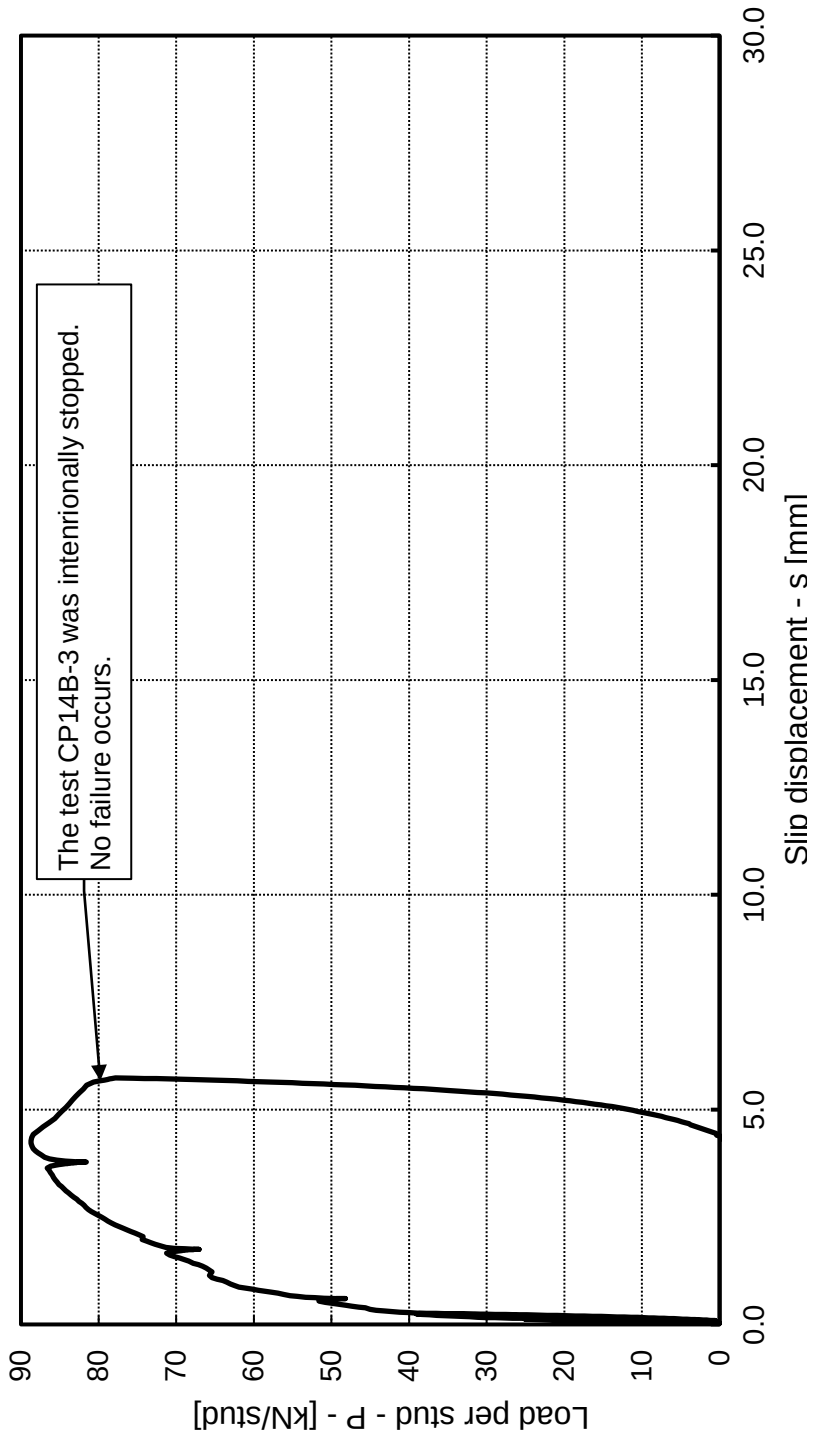

SPECIMEN CP14C-1

STEEL BEAM

Profile	Length	Steel grade
HE 260 B	900 mm	S355

STEEL DECK

Product	Yield strength	Welding type
ArcelorMittal Cofraplus 60 C	385.0 MPa	Through-deck welding

Thickness	Height
0.88 mm	58 mm

Top width	Bottom width
101 mm	62 mm

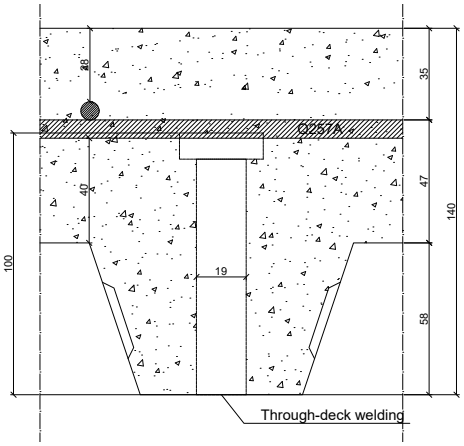

HEADED STUDS

Length as welded	Diameter
94 mm	19 mm

Position	Ultimate strength
Centered	551.0 MPa

REINFORCEMENT MESH

Type	Position
B 500 A	40 mm above the deck | Above the head of the stud

CONCRETE SLAB

Dimensions	Depth	Recess	Cylinder strength
900x680 mm	140 mm	No	51.8 MPa

TEST RESULTS

Peak load	Load at 6 mm slip	Failure mode(s)
68.4 kN/stud	66.4 kN/stud	Rib punching, Concrete pull-out

NOTE

One of the stud was poorly welded

SPECIMEN CP14C-1

LOAD-SLIP CURVE

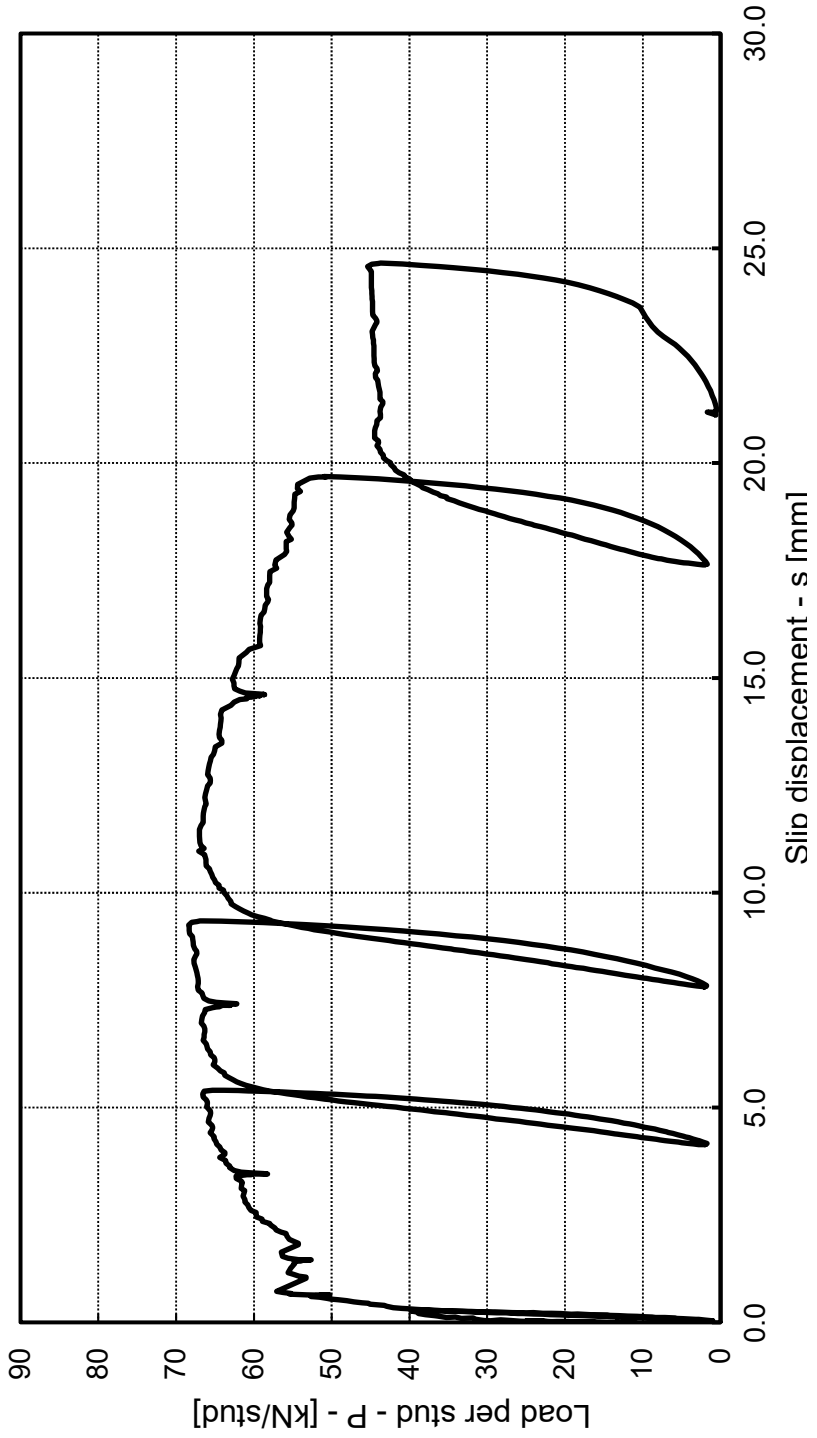

SPECIMEN CP14C-2

STEEL BEAM

Profile	Length	Steel grade
HE 260 B	900 mm	S355

STEEL DECK

Product	Yield strength	Welding type
ArcelorMittal Cofraplus 60 C	385.0 MPa	Through-deck welding

Thickness	Height
0.88 mm	58 mm

Top width	Bottom width
101 mm	62 mm

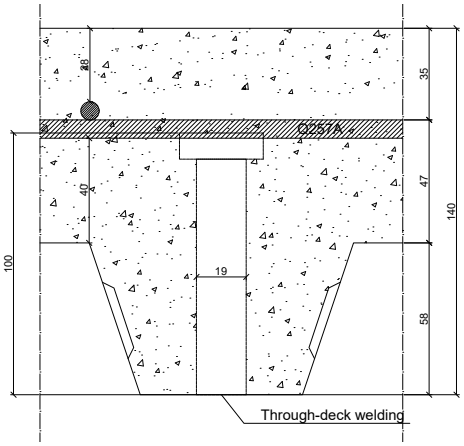

HEADED STUDS

Length as welded	Diameter
94 mm	19 mm

Position	Ultimate strength
Centered	551.0 MPa

REINFORCEMENT MESH

Type	Position
B 500 A	40 mm above the deck | Above the head of the stud

CONCRETE SLAB

Dimensions	Depth	Recess	Cylinder strength
900x680 mm	140 mm	No	51.9 MPa

TEST RESULTS

Peak load	Load at 6 mm slip	Failure mode(s)
85.4 kN/stud	82.6 kN/stud	Rib punching, Concrete pull-out

NOTE

-

SPECIMEN CP14C-2

LOAD-SLIP CURVE

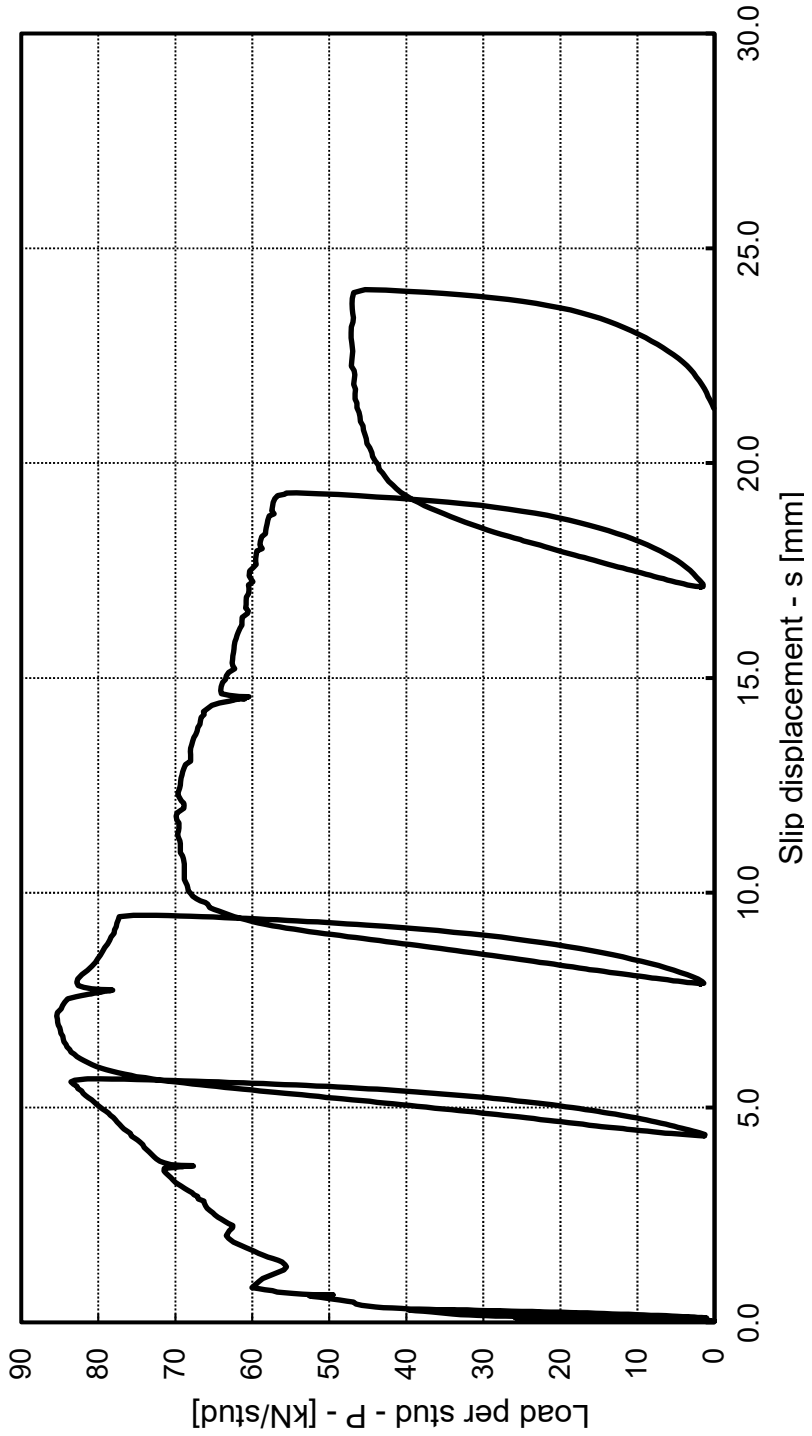

SPECIMEN CP14C-3

STEEL BEAM

Profile	Length	Steel grade
HE 260 B	900 mm	S355

STEEL DECK

Product	Yield strength	Welding type
ArcelorMittal Cofraplus 60 C	385.0 MPa	Through-deck welding

Thickness	Height
0.88 mm	58 mm

Top width	Bottom width
101 mm	62 mm

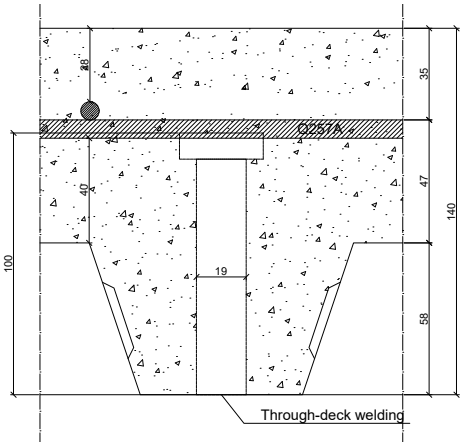

HEADED STUDS

Length as welded	Diameter
94 mm	19 mm

Position	Ultimate strength
Centered	551.0 MPa

REINFORCEMENT MESH

Type	Position
B 500 A	40 mm above the deck | Above the head of the stud

CONCRETE SLAB

Dimensions	Depth	Recess	Cylinder strength
900x680 mm	140 mm	No	52.0 MPa

TEST RESULTS

Peak load	Load at 6 mm slip	Failure mode(s)
85.1 kN/stud	77.5 kN/stud	Rib punching, Concrete pull-out

NOTE

-

SPECIMEN CP14C-3

LOAD-SLIP CURVE

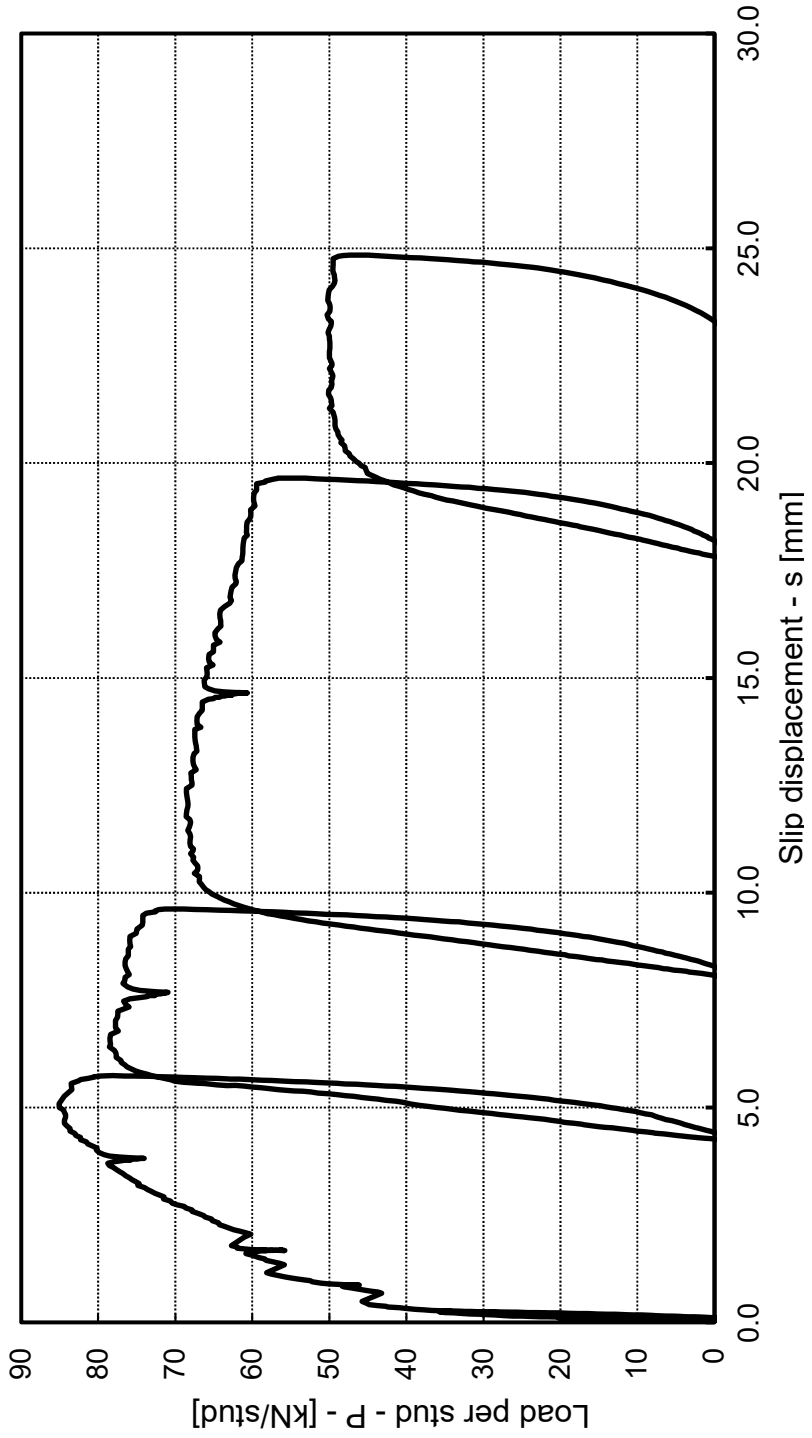

SPECIMEN CP14D-1

STEEL BEAM

Profile	Length	Steel grade
HE 260 B	900 mm	S355

STEEL DECK

Product	Yield strength	Welding type
ArcelorMittal Cofraplus 60 P	385.0 MPa	Pre-punched holes

Thickness	Height
0.88 mm	58 mm

Top width	Bottom width
101 mm	62 mm

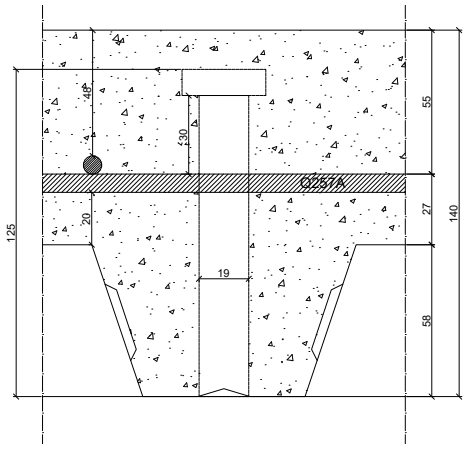

HEADED STUDS

Length as welded	Diameter
124 mm	19 mm

Position	Ultimate strength
Centered	504.3 MPa

REINFORCEMENT MESH

Type	Position
B 500 A	20 mm above the deck | Below the head of the stud

CONCRETE SLAB

Dimensions	Depth	Recess	Cylinder strength
900x680 mm	140 mm	No	43.5 MPa

TEST RESULTS

Peak load	Load at 6 mm slip	Failure mode(s)
84.2 kN/stud	80.3 kN/stud	Rib punching, Concrete pull-out, Stud rupture

NOTE

-

SPECIMEN CP14D-1

LOAD-SLIP CURVE

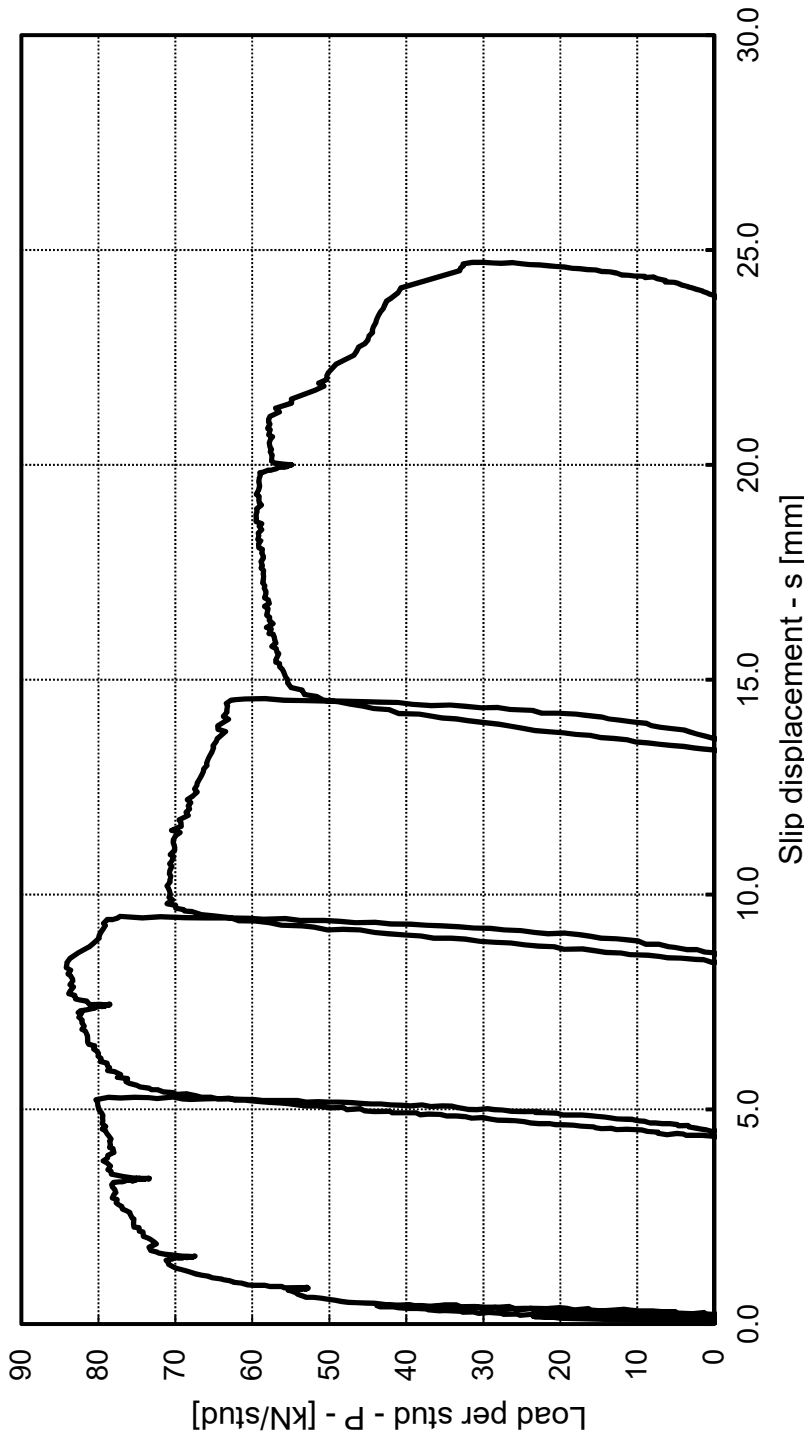

SPECIMEN CP14D-2

STEEL BEAM

Profile	Length	Steel grade
HE 260 B	900 mm	S355

STEEL DECK

Product	Yield strength	Welding type
ArcelorMittal Cofraplus 60 P	385.0 MPa	Pre-punched holes

Thickness	Height
0.88 mm	58 mm

Top width	Bottom width
101 mm	62 mm

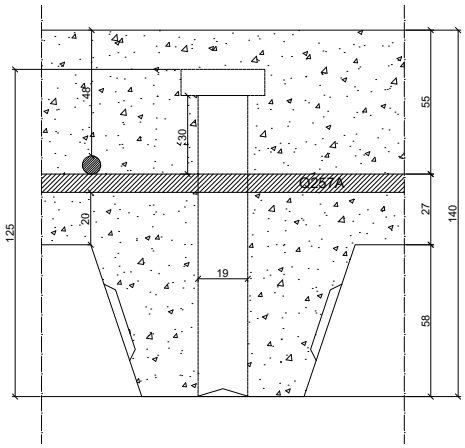

HEADED STUDS

Length as welded	Diameter
124 mm	19 mm

Position	Ultimate strength
Centered	504.3 MPa

REINFORCEMENT MESH

Type	Position
B 500 A	20 mm above the deck | Below the head of the stud

CONCRETE SLAB

Dimensions	Depth	Recess	Cylinder strength
900x680 mm	140 mm	No	43.7 MPa

TEST RESULTS

Peak load	Load at 6 mm slip	Failure mode(s)
87.3 kN/stud	78.4 kN/stud	Rib punching, Concrete pull-out, Stud rupture

NOTE

-

SPECIMEN CP14D-2

LOAD-SLIP CURVE

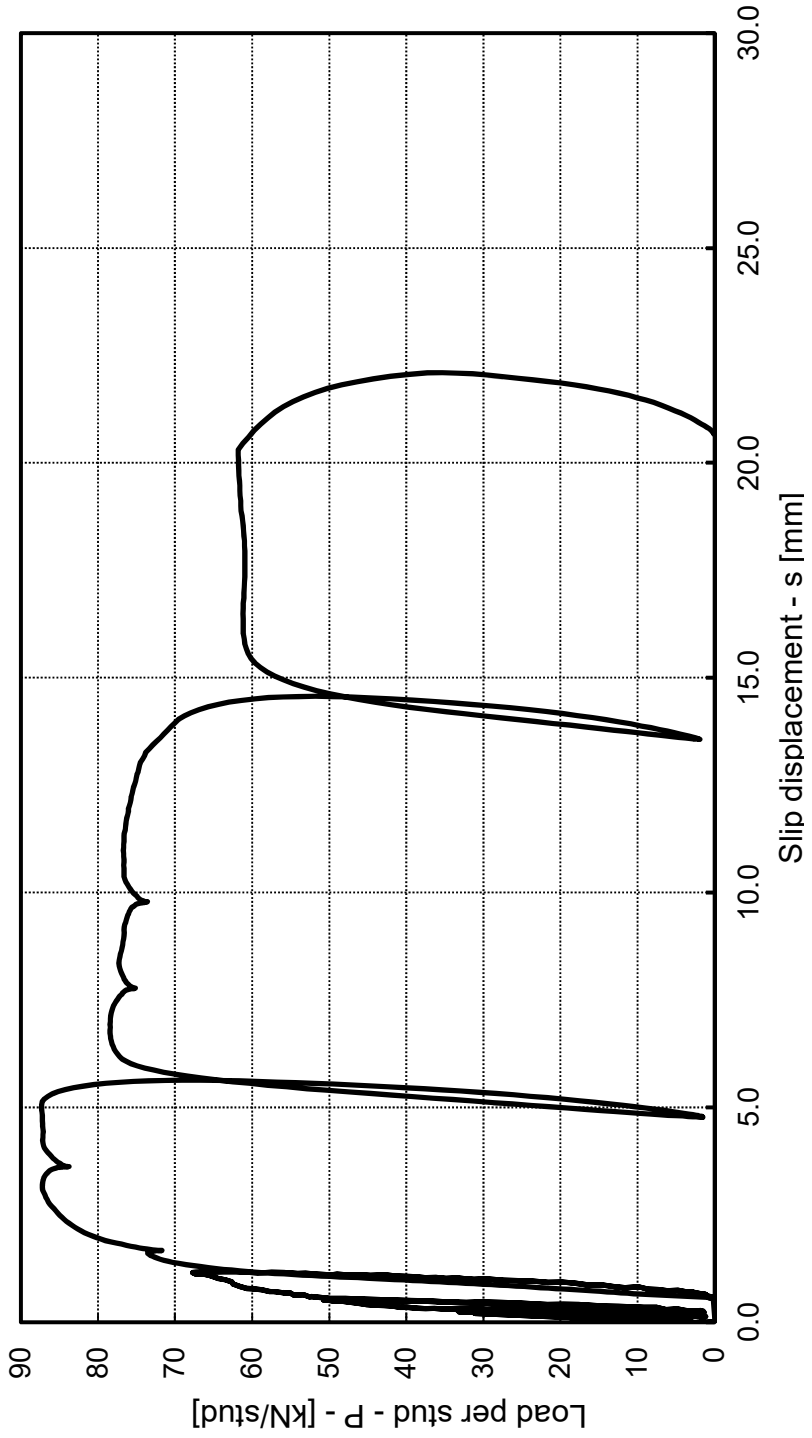

SPECIMEN CP14D-3

STEEL BEAM

Profile	Length	Steel grade
HE 260 B	900 mm	S355

STEEL DECK

Product	Yield strength	Welding type
ArcelorMittal Cofraplus 60 P	385.0 MPa	Pre-punched holes

Thickness	Height
0.88 mm	58 mm

Top width	Bottom width
101 mm	62 mm

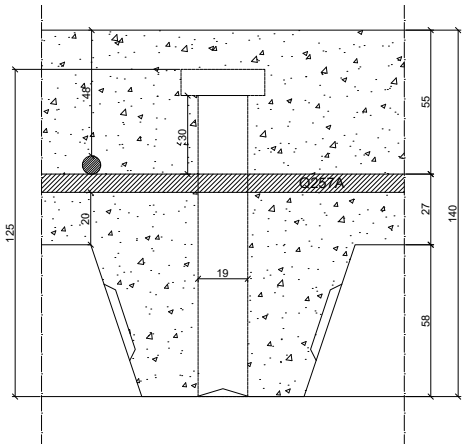

HEADED STUDS

Length as welded	Diameter
124 mm	19 mm

Position	Ultimate strength
Centered	504.3 MPa

REINFORCEMENT MESH

Type	Position
B 500 A	20 mm above the deck | Below the head of the stud

CONCRETE SLAB

Dimensions	Depth	Recess	Cylinder strength
900x680 mm	140 mm	No	44.2 MPa

TEST RESULTS

Peak load	Load at 6 mm slip	Failure mode(s)
85.2 kN/stud	72.6 kN/stud	Rib punching, Concrete pull-out, Stud rupture

NOTE

-

SPECIMEN CP14D-3

LOAD-SLIP CURVE